Molecular Recognition and Co-Crystallization of Methylated and Halogenated Fragments of Danicalipin A by Enantiopure Alleno-Acetylenic Cage Receptors

Supporting Information

Cornelius Gropp[†], Stefan Fischer[†], Tamara Husch[‡], Nils Trapp[†], Erick M. Carreira*[,†] and François Diederich*[,†]

Experimental Section

S1. Materials and Methods

Chemicals: Chemicals for guest binding studies and for crystallization experiments were used without prior purification (ABCR, Acros, Sigma Aldrich, Fluka, TCI). AACs $(P)_4$- and $(M)_4$-**1** were synthesized following the reported procedure.[1] Corresponding ^{1}H, ^{13}C, and ^{19}F NMR spectra are attached for AAC $(P)_4$-**1** and the synthesized guest molecules. All compounds were purchased in their racemic form or in their enantiomerically pure form, where indicated.

^{1}H NMR spectra were recorded on a *Gemini 400* (400 MHz, ^{1}H) instrument at 298 K. Chemical shifts (δ_H) are quoted in parts per million (ppm), referenced to the residual solvent peak ($CDCl_3$, δ_H 7.226). Coupling constants (J) are reported to the nearest 0.5 Hz. Multiplicities are reported as follows: s = singlet, d = doublet, t = triplet, q = quartet, m = multiplet, or as a combination of them. Coupling constants J are given in Hertz (Hz).

^{13}C NMR spectra were recorded on a *Bruker DRX 400* (100 MHz, ^{13}C) spectrometer. Chemical shifts (δ_C) are quoted in ppm referenced to the appropriate solvent peak ($CDCl_3$, δ 77.0 ppm).

1D and 2D NMR spectra of the host–guest complexes were recorded on a *Bruker AVIII 600 Ultra Shell* spectrometer equipped with a *Prodigy Cryo Probe* (600 MHz for ^{1}H; 150 MHz for ^{13}C).

Isothermal Titration Calorimetry (ITC) was performed on a MicroCal VP-ITC calorimeter. 25 Portions of 10 µL "guest"-solution were added to a "host"-solution at intervals of 240 s. The power (P) that was consumed to keep the sample temperature at 303 K was monitored. The heat of dilution of "guest"-solution added to pure solvent (n-octane) was measured and subtracted. The MicroCal Origin 5.0 software was used for data treatment.[2]

Electronic Circular Dichroism **(ECD)** spectra were recorded on a *JASCO Corp. J-715, Rev. 1.00 instrument*. The spectra were measured in a quartz cuvette (1 cm) at 293 K. The absorption wavelength is reported in nm with the molar extinction coefficient $\Delta\varepsilon$ ($dm^3\ mol^{-1}\ cm^{-1}$).

Infrared spectra (IR) were recorded on a *Perkin-Elmer 1600 FT-IR spectrometer (ATR, Golden State)*. Only selected absorbances (υ_{max}) are reported. The samples are reported as absorption

maxima in cm^{-1} with corresponding relative intensities described as sh (shoulder), s (strong), m (medium), and w (weak).

Optical Rotation was recorded on a Perkin-Elmer 1600 FT-IR spectrometer 241 polarimeter.

High Resolution Mass spectra **(HR-MS)** measurements were performed by the MS service at the Laboratory of Organic Chemistry of ETH Zurich. EI-MS: *Waters Micromass AutoSpe-Ultima spectrometer*; ESI-MS: *Bruker maXis spectrometer*. HR-MALDI: *Varian IonSpec* FT - ICR; Masses are reported in *m/z* units as the molecule ion M+, $[M + H]^+$, $[M + Na]^+$, $[M + K]^+$, with the corresponding intensities in %.

X-ray Intensity Data were measured on a Rigaku XtaLAB Synergy diffractometer equipped with a Dectris Pilatus 300K hybrid pixel array detector, using microfocus sealed-tube Cu-*K*α radiation with mirror optics (λ = 1.54184 Å) at the given temperature. Samples were mounted on MiTeGen Micromount Kapton sample holders in perfluoroalkylether oil. Collected data were processed with the CrysAlisPro[3] software package and corrected for absorption effects using the multi-scan or Gaussian method, or a combination thereof. Structures were solved and refined using the OLEX2[4] and SHELX[5] software packages. Generally, wherever relative occupancies (in %) within disordered regions are discussed, they are directly taken from the refined free variables. The authors are aware that this method can be rather unreliable due to a variety of reasons and hence for all purposes of discussion we assumed an error margin of +/– 5%. Additionally, care was taken not to over-restrain disorder of the guest molecules. Only soft similar distance restraints (SADI) and enhanced rigid bond restraints (RIGU) were applied in this region. Their usage was kept at the practicable minimum.
Supplementary data for the obtained X-ray co-crystal structures (CCDC 1914836–1914843) can be obtained free of charge from The Cambridge Crystallographic Data Centre, 12 Union Road, Cambridge CB2 1EZ, UK (fax: +44(1223)-336-033; e-mail: deposit@ccdc.cam.ac.uk), or online via https://www.ccdc.cam.ac.uk/getstructures. HKL data and refinement instructions, as well as applied restraints, are included with the deposited files.

S2. Synthetic Procedures

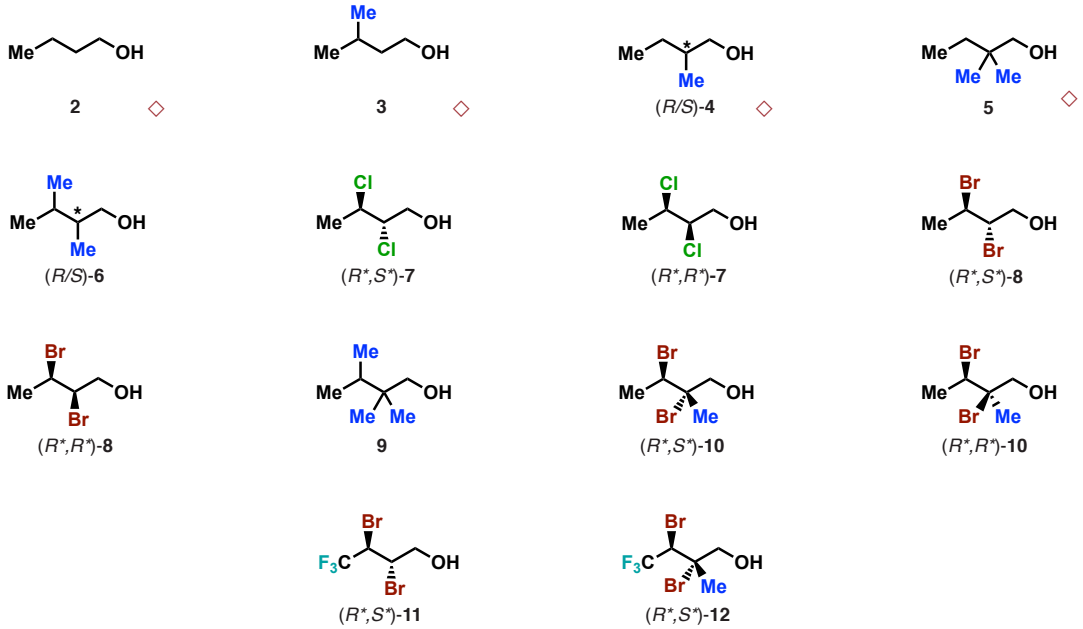

Figure S1. Guest molecules selected for complexation studies with enantiopure AACs $(P)_4$-**1** and $(M)_4$-**1**. Structures designated with a red square (◇) are commercially available. All other molecules were prepared in a racemic fashion following the procedures below.

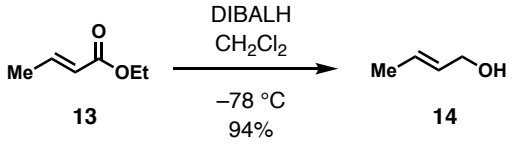

(*E*)-But-2-en-1-ol (14). Ethyl enoate **13** (5.1 mL, 48 mmol, 1.0 equiv) was dissolved in CH_2Cl_2 (43 mL) and cooled to 0 °C. DIBALH (1 M in CH_2Cl_2, 100 mL, 100 mmol, 2.1 equiv.) was added, and the mixture was stirred at 0 °C for 1 h. The mixture was quenched with the addition of MeOH (5 mL) at 0 °C and allowed to reach ambient temperature. After the addition of sat. aq. NaCl solution (50 mL) and Et_2O (50 mL), the mixture was filtered through a plug of Celite. The layers were separated, dried over Na_2SO_4 and concentrated under reduced pressure. Purification by flash column chromatography (SiO_2, Et_2O/pentane 1:1) afforded allylic alcohol **3** (3.2 g, 45 mmol, 94%) as a colorless liquid.

Reference spectrum: *Chem. Eur. J.* **2015**, *21*, 7408–7412.

^{1}H NMR (400 MHz, $CDCl_3$): δ 5.81-5.58 (m, 2H), 4.13-4.00 (m, 2H), 1.71 (dt, J = 4.7, 1.1 Hz, 3H) ppm.

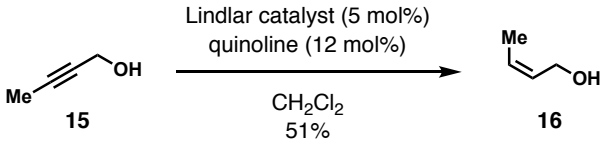

15 16

(*Z*)-But-2-en-1-ol (16). A mixture of alkyne **15** (2.9 g, 41 mmol, 1.0 equiv), quinoline (0.58 mL, 4.9 mmol, 0.12 equiv), and LINDLAR catalyst (5 wt% Pd, 4.3 g, 2.0 mmol, 0.05 equiv) in CH_2Cl_2 (50 mL) was stirred under a H_2 atmosphere for 1 week. The mixture was filtered through a plug of Celite and then concentrated under reduced pressure. Distillation (110 °C, 1 atm) afforded olefin **16** (1.5 g, 21 mmol, 51%) as a colorless liquid.

Reference spectrum: *Chem. Commun.* **2013**, *49*, 7037–7039.

^{1}H NMR (400 MHz, $CDCl_3$): δ 5.68-5.57 (m, 2H), 4.26-4.17 (m, 2H), 1.73-1.61 (m, 3H) ppm.

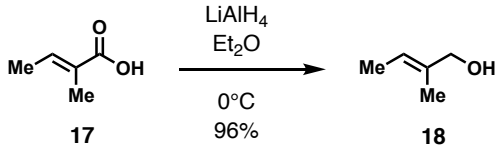

17 18

(*E*)-2-Methylbut-2-en-1-ol (18). Tiglic acid **17** (5.0 g, 50 mmol, 1.0 equiv) was added dropwise to a suspension of $LiAlH_4$ (3.8 g, 100 mmol, 2.0 equiv) in Et_2O (20 mL) at 0 °C. The suspension was allowed to reach ambient temperature over 16 h. After slow addition of NaOH (3 M, 20 mL) at 0 °C and Et_2O (100 mL), the mixture was filtered and concentrated under reduced pressure. Purification by flash column chromatography (SiO_2, Et_2O/pentane 1:1) afforded alcohol **7** (4.1 g, 48 mmol, 96%) as a colorless liquid.

Reference spectrum: *Tetrahedron* **2012**, *68*, 7280–7287.

^{1}H NMR (400 MHz, $CDCl_3$): δ 5.49 (qq, J = 6.7, 1.4 Hz, 1H), 3.99 (t, J = 1.2 Hz, 2H), 1.67 (t, J = 1.3 Hz, 3H), 1.62 (dq, J = 6.7, 1.2 Hz, 3H) ppm.

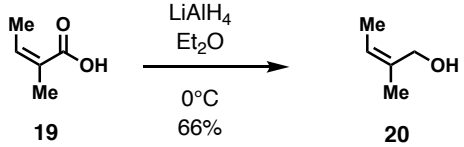

19 20

(*Z*)-2-Methylbut-2-en-1-ol (20). Angelic acid **19** (1.4 g, 14 mmol, 1.0 equiv) in Et_2O (5.8 mL) was added dropwise to a suspension of $LiAlH_4$ (1.4 g, 38 mmol, 2.7 equiv) in Et_2O (17 mL) at ambient temperature. After 2 h, NaOH (3 M, 20 mL) and Et_2O (20 mL) were added. Extraction with Et_2O (3 × 40 mL), drying over Na_2SO_4, filtration, and concentration under reduced pressure afforded the crude product. Purification by flash column chromatography (SiO_2, Et_2O/pentane 1:1) afforded alcohol **20** (790 mg, 9.2 mmol, 66%) as a colorless liquid.

Reference spectrum: *Org. Lett.* **2017**, *19*, 3703–3706.

^{1}H NMR (400 MHz, $CDCl_3$): δ 5.43-5.32 (m, 1H), 4.15 (d, J = 0.7 Hz, 2H), 1.78 (p, J = 1.5 Hz, 3H), 1.68-1.60 (m, 3H) ppm.

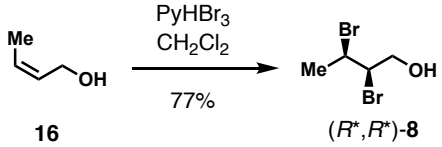

16 (*R**,*R**)-**8**

(2*R,3*R**)-2,3-Dibromobutan-1-ol ((±)-8).** Pyridinium tribromide (910 mg, 2.8 mmol, 1.2 equiv) was added to a solution of olefin **16** (170 mg, 2.4 mmol, 1.0 equiv) in CH_2Cl_2 (7 mL), and the mixture was stirred at ambient temperature for 20 min. After addition of Et_2O (5 mL) and sat. aq. $Na_2S_2O_3$ solution (10 mL), the layers were separated. The organic layer was washed with HCl (1 M), dried over Na_2SO_4, filtered, and concentrated under reduced pressure (30 min at 40 °C/250 mbar) to afford dibromide (±)-**8** (420 mg, 1.8 mmol, 77%) as a brown liquid. Separation of the enantiomers was performed by normal-phase HPLC. The product (200 mg) was dissolved (hexane/EtOH 97:3, 2 mL) and then divided into 4 sequential runs on a CHIRALPAK IB column (flow: 18 mL/min, eluent: hexane/EtOH 97:3). The runs were monitored at a wavelength of 220 nm. The fractions were collected and concentrated under reduced pressure (30 min at 40 °C/100 mbar) to afford (+)-**8** (64 mg, t_R = 16.07 min, e.r. = 99:1, white solid) and (–)-**8** (70 mg, t_R = 18.65 min, e.r. = 99:1, white solid).

TLC: R_f = 0.59 (EtOAc/hexane 3:7); ^{1}H NMR (400 MHz, $CDCl_3$): δ 4.49 (qd, J = 6.8, 3.0 Hz, 1H), 4.25 (ddd, J = 7.1, 5.5, 3.0 Hz, 1H), 4.03 (dd, J = 12.1, 5.5 Hz, 1H), 3.95 (dd, J = 12.1, 7.1 Hz, 1H), 1.98-1.89 (m, 1H), 1.81 (d, J = 6.8 Hz, 3H) ppm; ^{13}C NMR (101 MHz, $CDCl_3$): δ 65.3, 60.8, 49.0, 23.4 ppm; IR (UATR): ν 3369, 2926, 1449, 1380, 1232, 1054, 978, 844, 704, 552 cm^{-1}; Optical Rotation (+)-**8**: α_D^{23} +41.4 (c = 0.50, $CHCl_3$); Optical Rotation (–)-**8**: α_D^{23} –41.7 (c = 0.50, $CHCl_3$); HRMS (EI): exact mass calculated for $C_4H_8BrO^+$ [(*M*–Br)$^+$] 150.9753; found 150.9753.

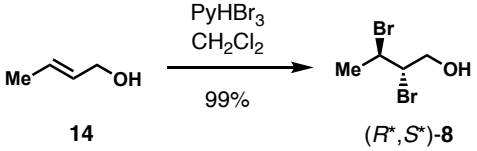

14 (*R**,*S**)-**8**

(2*S,3*R**)-2,3-Dibromobutan-1-ol ((±)-8).** Pyridinium tribromide (2.0 g, 6.2 mmol, 1.2 equiv) was added to a solution of olefin **3** (370 mg, 5.2 mmol, 1.0 equiv) in CH_2Cl_2 (15 mL), and the mixture was stirred at ambient temperature for 20 min. After addition of Et_2O (5 mL) and sat. aq. $Na_2S_2O_3$ solution (10 mL), the layers were separated. The organic layer was washed with HCl (1 M), dried over Na_2SO_4, filtered, and concentrated under reduced pressure

(30 min at 40 °C/250 mbar) to afford dibromide (±)-**8** (1.2 g, 5.1 mmol, 99%) as a brown liquid. Separation of the enantiomers was performed by normal-phase HPLC. The product (200 mg) was dissolved (hexane/EtOH 97:3, 2 mL) and then divided into 4 sequential runs on a CHIRALPAK IB column (flow: 18 mL/min, eluent: hexane/EtOH 97:3). The runs were monitored at a wavelength of 220 nm. The fractions were collected and concentrated under reduced pressure (30 min at 40 °C/100 mbar) to afford (–)-**8** (49 mg, t_R = 17.85 min, e.r. = 99:1, white solid) and (+)-**8** (37 mg, t_R = 19.48 min, e.r. = 99:1, white solid).

TLC: R_f = 0.59 (EtOAc/hexane 3:7); ^{1}H NMR (400 MHz, $CDCl_3$): δ 4.38 (dq, J = 9.4, 6.6 Hz, 1H), 4.25 (ddd, J = 9.4, 4.6, 3.6 Hz, 1H), 4.15-4.02 (m, 2H), 1.98 (t, J = 6.9 Hz, 1H), 1.91 (d, J = 6.6 Hz, 3H) ppm; ^{13}C NMR (101 MHz, $CDCl_3$): δ 66.3, 62.5, 47.8, 25.7 ppm; IR (UATR): ν 3370, 2932, 1451, 1380, 1202, 1155, 1101, 1065, 1009, 936, 545 cm^{-1}; Optical Rotation (–)-**8**: α_D^{23} –3.0 (c = 0.50, $CHCl_3$); Optical Rotation (+)-**8**: α_D^{23} +2.7 (c = 0.50, $CHCl_3$); HRMS (EI): exact mass calculated for $C_4H_7Br_2^+$ [(*M*–OH)$^+$] 212.8909; found 212.8909.

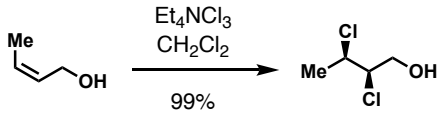

16 (*R**,*R**)-**7**

(2*R,3*R**)-2,3-Dichlorobutan-1-ol ((±)-7).** MIOSKOWSKI's reagent (2.6 g, 11 mmol, 1.2 equiv) was added to a solution of olefin **16** (400 mg, 5.6 mmol, 1.0 equiv) in CH_2Cl_2 (14 mL), and the mixture was stirred at ambient temperature for 20 min. After addition of sat. aq. $NaHCO_3$ solution (5 mL) and sat. aq. $Na_2S_2O_3$ solution (5 mL), the layers were separated and the crude product extracted with pentane (3 × 10 mL). The organic layer was dried over Na_2SO_4, filtered, and concentrated under reduced pressure (30 min at 40 °C/250 mbar) to afford dichloride **(±)-13** (780 mg, 5.5 mmol, 99%) as a yellow liquid. Purification was performed by normal-phase HPLC. The product (120 mg) was dissolved (hexane/EtOH 20:1, 1 mL) and then divided into 3 sequential runs on a CHIRALPAK IB column (flow: 18 mL/min, eluent: hexane/EtOH 20:1). The fractions were collected, monitored by thin-layer chromatography (SiO_2, EtOAc/hexane 3:7, $KMnO_4$), and concentrated under reduced pressure (30 min at 40 °C/120 mbar) to afford dichloride (±)-**7** (30 mg).

TLC: R_f = 0.54 (EtOAc/hexane 3:7); ^{1}H NMR (400 MHz, $CDCl_3$): δ 4.41 (qd, J = 6.7, 3.1 Hz, 1H), 4.12 (ddd, J = 6.9, 5.5, 3.2 Hz, 1H), 3.96 (dd, J = 11.9, 5.5 Hz, 1H), 3.88 (dd, J = 11.8, 6.9 Hz, 1H), 1.63 (d, J = 6.7 Hz, 3H) ppm; ^{13}C NMR (101 MHz, $CDCl_3$): δ 66.7, 64.4, 57.0,

21.9 ppm; IR (UATR): ν 3369, 2934, 1445, 1381, 1262, 1060, 982, 857, 755, 708, 656, 622, 518 cm^{-1}.

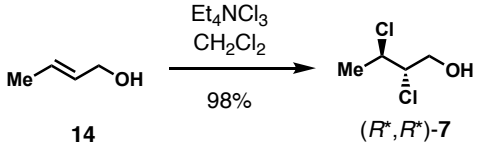

(2*S,3*R**)-2,3-Dichlorobutan-1-ol ((±)-7).** MIOSKOWSKI's reagent (2.6 g, 11 mmol, 1.2 equiv) was added to a solution of olefin **14** (390 mg, 5.5 mmol, 1.0 equiv) in CH_2Cl_2 (14 mL), and the mixture was stirred at ambient temperature for 20 min. After addition of sat. aq. $NaHCO_3$ solution (5 mL) and sat. aq. $Na_2S_2O_3$ solution (5 mL), the layers were separated and the crude product extracted with pentane (3 × 10 mL). The organic layer was dried over Na_2SO_4, filtered, and concentrated under reduced pressure (30 min at 40 °C/250 mbar) to afford dichloride (±)-**7** (760 mg, 5.3 mmol, 98%) as a yellow liquid. Purification was performed by normal-phase HPLC. The product (120 mg) was dissolved (hexane/EtOH 20:1, 1 mL) and then divided into 3 sequential runs on a CHIRALPAK IB column (flow: 18 mL/min, eluent: hexane/EtOH 20:1). The fractions were collected, monitored by thin-layer chromatography (SiO_2, EtOAc/hexane 3:7, $KMnO_4$), and concentrated under reduced pressure (30 min at 40 °C/120 mbar) to afford dichloride (±)-**7** (76 mg).

TLC: R_f = 0.54 (EtOAc/hexane 3:7); ^{1}H NMR (400 MHz, $CDCl_3$): δ 4.30-4.18 (m, 1H), 4.07-3.97 (m, 3H), 2.09-1.94 (m, 1H) ppm, 1.67 (d, J = 6.6 Hz, 3H); ^{13}C NMR (101 MHz, $CDCl_3$): δ 68.0, 64.6, 56.3, 22.7 ppm; IR (UATR): ν 3369, 2938, 1451, 1382, 1196, 1106, 1071, 1017, 948, 854, 751, 656 cm^{-1}.

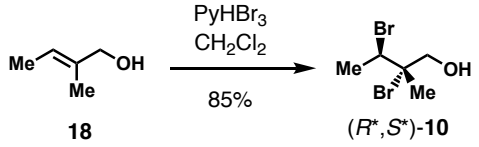

(2*S,3*R**)-2,3-Dibromo-2-methylbutan-1-ol ((±)-10).** Pyridinium tribromide (2.2 g, 7.0 mmol, 1.2 equiv) was added to a solution of olefin **18** (500 mg, 5.8 mmol, 1.0 equiv) in CH_2Cl_2 (17 mL), and the mixture was stirred at ambient temperature for 20 min. After addition of Et_2O (5 mL) and sat. aq. $Na_2S_2O_3$ solution (10 mL), the layers were separated. The organic layer was washed with HCl (1 M), dried over Na_2SO_4, filtered, and concentrated under reduced pressure (30 min at 40 °C/250 mbar) to afford the crude product. Purification by flash column chromatography (SiO_2, Et_2O/pentane 1:1) was followed by dilution of the product with MeCN

(2 mL), and filtration through a syringe filter and concentration under reduced pressure (20 min at 40 °C/120 mbar) afforded (±)-**10** (1.2 g, 4.9 mmol, 85%) as a grey solid. Further purification was performed by normal-phase HPLC. The product (100 mg) was dissolved (hexane/EtOH 97:3, 1 mL) and then divided into 2 sequential runs on a CHIRALPAK IB column (flow: 18 mL/min, eluent: hexane/EtOH 97:3). The runs were monitored at a wavelength of 220 nm. The fractions were collected and concentrated under reduced pressure (20 min at 40 °C/120 mbar) to afford (±)-**10** (75 mg, t_R = 10.7 min).

^{1}H NMR (400 MHz, $CDCl_3$): δ 4.68 (q, J = 6.8 Hz, 1H), 3.94 (d, J = 12.7 Hz, 1H), 3.82 (d, J = 12.7 Hz, 1H), 1.92 (d, J = 6.8 Hz, 3H), 1.77 (s, 3H) ppm; ^{13}C NMR (101 MHz, $CDCl_3$): δ 76.0, 72.0, 53.1, 22.9, 21.8 ppm; IR (UATR): ν 3378, 2979, 2934, 2872, 1451, 1379, 1214, 1160, 1063, 1025, 980, 963, 908, 803, 688, 615, 574, 537 cm^{-1}; HRMS (EI): exact mass calculated for $C_5H_{10}BrO^+$ [$(M–Br)^+$] 164.9910; found 164.9910.

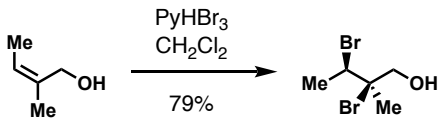

20 (*R**,*R**)-**10**

(2*R,3*R**)-2,3-Dibromo-2-methylbutan-1-ol ((±)-10).** Pyridinium tribromide (890 mg, 2.8 mmol, 1.2 equiv) was added to a solution of olefin **20** (200 mg, 2.3 mmol, 1.0 equiv) in CH_2Cl_2 (6.6 mL), and the mixture was stirred at ambient temperature for 20 min. After addition of Et_2O (5 mL) and sat. aq. $Na_2S_2O_3$ solution (10 mL), the layers were separated. The organic layer was washed with HCl (1 M), dried over Na_2SO_4, filtered, and concentrated under reduced pressure (30 min at 40 °C/250 mbar) to afford the crude product. Purification by flash column chromatography (SiO_2, Et_2O/pentane 1:4, then 1:1) afforded (±)-**10** (450 mg, 1.8 mmol, 79%) as a white solid. Further purification and separation of the enantiomers was performed by normal-phase HPLC. The product (200 mg) was dissolved (hexane/EtOH 97:3, 2 mL) and then divided into 4 sequential runs on a CHIRALPAK IB column (flow: 18 mL/min, eluent: hexane/EtOH 97:3). The runs were monitored at a wavelength of 220 nm. Two runs were performed to collect the racemate (80 mg) and two runs were used to separate the enantiomers: **(+)-10** (38 mg, t_R = 15.94 min, e.r. = 99:1, white solid) and **(–)-10** (34 mg, t_R = 17.79 min, e.r. = 99:1, white solid).

^{1}H NMR (400 MHz, $CDCl_3$): δ 4.44 (q, J = 6.8 Hz, 1H), 3.95-3.85 (m, 2H), 1.99 (td, J = 7.1, 0.8 Hz, 1H), 1.91-1.83 (m, 6H) ppm; ^{13}C NMR (101 MHz, $CDCl_3$): δ 74.5, 70.1, 56.1, 27.1, 23.0 ppm; IR (UATR): ν 3391, 2979, 2935, 2872, 1442, 1380, 1308, 1205, 1145, 1090, 1068,

1024, 976, 959, 908, 806, 733, 668, 637, 593, 562, 536, 514 cm^{-1}; Optical Rotation **(+)-10**: α_D^{23} +4.8 (c = 0.50, $CHCl_3$); Optical Rotation **(–)-10**: α_D^{23} –4.9 (c = 0.50, $CHCl_3$); HRMS (EI): exact mass calculated for $C_5H_{10}BrO^+$ [(M–Br)$^+$] 164.9910; found 164.9910.

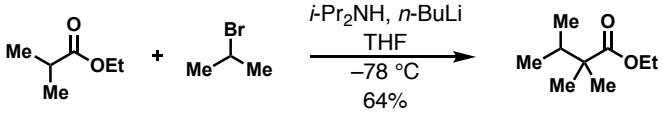

21 22 23

Ethyl 2,2,3-trimethylbutanoate (23). *n*-BuLi (1.6 M in hexane, 30 mL, 48 mmol, 1.3 equiv) was added at 0 °C to a solution of diisopropylamine (8.0 mL, 56 mmol, 1.5 equiv) in THF (45 mL), and the mixture was stirred at that temperature for 30 min. Ethyl isobutyrate **21** (5.0 mL, 37 mmol, 1.0 equiv) was added dropwise at –78 °C. The mixture was stirred at that temperature for 1 h. Subsequently, 2-bromopropane **22** (11 mL, 110 mmol, 3.0 equiv) was added dropwise to the mixture. The reaction mixture was allowed to reach ambient temperature over 48 h. After dilution with Et_2O (50 mL) and addition of sat. aq. NH_4Cl solution (30 mL), the layers were separated. The crude product was extracted with Et_2O (3 × 50 mL), dried over Na_2SO_4, filtered, and concentrated under reduced pressure. Distillation (155 °C, 1 atm) afforded product **23** (3.7 g, 24 mmol, 64%) as a colorless liquid.

^{1}H NMR (400 MHz, $CDCl_3$): δ 4.12 (q, J = 7.1 Hz, 2H), 1.97 (hept, J = 6.9 Hz, 1H), 1.24 (t, J = 7.1 Hz, 3H), 1.08 (s, 6H), 0.84 (d, J = 6.9 Hz, 6H) ppm; ^{13}C NMR (101 MHz, $CDCl_3$): δ 178.4, 60.2, 45.7, 35.0, 21.6 (2C), 17.7 (2C), 14.4 ppm; IR (UATR): ν 2967, 2879, 1727, 1465, 1383, 1371, 1334, 1264, 1221, 1158, 1131, 1097, 1065, 1027, 909, 857, 797, 775, 616, 517 cm^{-1}; HRMS (EI): exact mass calculated for $C_6H_{12}O_2^+$ [(M–C_3H_6)$^+$] 116.0837; found 116.0832.

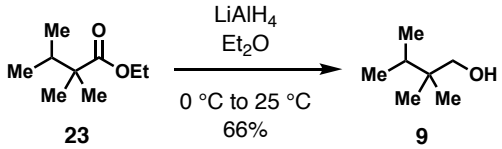

23 9

2,2,3-Trimethylbutan-1-ol (9). Ethyl enoate **23** (3.4 g, 21 mmol, 1.0 equiv) in Et_2O (4 mL) was added at 0 °C to a suspension of $LiAlH_4$ (1.8 g, 47 mmol, 2.2 equiv) in Et_2O (42 mL), and the mixture was allowed to reach ambient temperature over 18 h. After addition of NaOH (3 M, 10 mL) and Rochelle'salt solution (20 mL), the mixture was further diluted with Et_2O (20 mL). After stirring for 30 min, the layers were separated. The organic layer was dried over Na_2SO_4,

filtered, and concentrated under reduced pressure. Distillation (160 °C, 1 atm) afforded product **9** (1.6 g, 14 mmol, 66%) as a colorless liquid.

^{1}H NMR (400 MHz, $CDCl_3$): δ 3.38 (s, 2H), 1.63 (hept, J = 6.9 Hz, 1H), 1.34 (s, 1H), 0.86 (d, J = 6.9 Hz, 6H), 0.82 (s, 6H) ppm; ^{13}C NMR (101 MHz, $CDCl_3$): δ 71.2, 37.5, 32.7, 21.1 (2C), 17.5 (2C) ppm; IR (UATR): ν 3350, 2960, 2876, 1467, 1392, 1379, 1367, 1272, 1206, 1176, 1151, 1102, 1029, 967, 903, 844, 826, 571 cm^{-1}; HRMS (EI): exact mass calculated for $C_6H_{13}^+$ [(M–CH_3O)$^+$] 85.1012; found 85.1012.

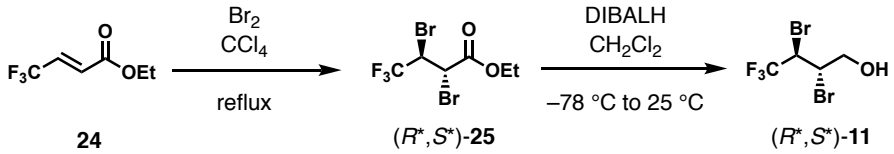

(2*S,3*R**)-2,3-Dibromo-4,4,4-trifluorobutan-1-ol (±)-11).** Br_2 (0.57 mL, 11 mmol, 1.1 equiv) was added to a solution of olefin **24** (1.69 g, 10.0 mmol, 1.0 equiv) in CCl_4 (30 mL), and the mixture was heated to reflux for 5 h. The solvent was removed under reduced pressure. The crude dibromide **(±)-25** was then dissolved in CH_2Cl_2 (20 mL) and cooled to –78 °C. DIBALH (1 M in CH_2Cl_2, 12 mL, 1.2 mmol, 1.2 equiv) was added and the reaction mixture was stirred at 0 °C for 40 min. The mixture was quenched with sat. aq. $Na_2S_2O_3$ solution and stirred for 2 h resulting in the crude product of **(±)-11** (2.62 g). Separation was performed by normal-phase HPLC. The product (500 mg) was dissolved (hexane/EtOH 97:3, 5 mL) and then divided into several sequential runs on a CHIRALPAK IB column (flow: 18 mL/min, eluent: hexane/EtOH 97:3). The runs were monitored at a wavelength of 220 nm. The fractions were collected and concentrated under reduced pressure (1 h at 30 °C/80-90 mbar) to afford 233 mg. TLC: R_f = 0.45 (EtOAc/hexane 3:7); ^{1}H NMR (400 MHz, $CDCl_3$): δ 4.67-4.60 (m, 1H), 4.39 (td, J = 6.1, 3.7 Hz, 1H), 4.14-4.03 (m, 2H) ppm; ^{13}C NMR (101 MHz, $CDCl_3$): δ 65.6, 50.3, 48.7 (q, J = 32.1) ppm; ^{19}F NMR (377 MHz, $CDCl_3$): –66.8 ppm.

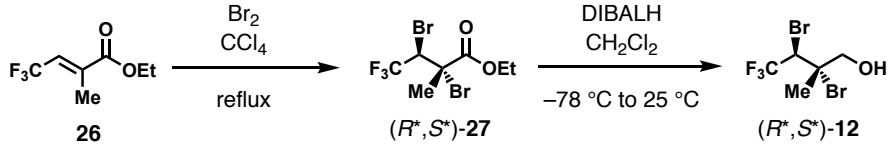

((2*R,3*R**)-2,3-Dibromo-4,4,4-trifluoro-2-methylbutan-1-ol (±)-12).** Br_2 (0.62 mL, 12 mmol, 2.2 equiv) was added to a solution of olefin **26** (1.0 g, 5.49 mmol, 1.0 equiv) in CCl_4 (17 mL), and the mixture was heated to reflux for 5 h. The solvent was removed under reduced pressure. The crude dibromide **(±)-27** was then dissolved in CH_2Cl_2 (11 mL) and cooled to 0 °C. DIBALH (1 M in CH_2Cl_2, 8.2 mL, 8.2 mmol, 1.5 equiv) was added and the reaction

mixture was stirred at 0 °C for 30 min. The mixture was quenched with sat. aq. $Na_2S_2O_3$ solution and stirred for 2 h resulting in the crude product of **(±)-12** (1.6 g). Purification was performed by normal-phase HPLC. The product (500 mg) was dissolved (hexane/EtOH 96:4, 5 mL) and then divided into several sequential runs on a CHIRALPAK IB column (flow: 18 mL/min, eluent: hexane/EtOH 96:4). The runs were monitored at a wavelength of 220 nm. The combined fractions were collected and concentrated under reduced pressure to afford 149 mg.

TLC: R_f = 0.48 (EtOAc/hexane 3:7); ^{1}H NMR (400 MHz, $CDCl_3$): δ 4.85 (q, J = 7.1, 1H), 3.91 (dd, J = 100.5, 12.6 Hz, 1H), 1.85 (br. s, 3H) ppm; ^{13}C NMR (101 MHz, $CDCl_3$): δ 72.4, 65.1, 52.1 (q, J = 30.4 Hz), 23.4 ppm; ^{19}F NMR (377 MHz, $CDCl_3$): –62.2 ppm.

S3. Methods for Solution Binding Studies

Preparation of solutions for ECD titrations: A solution of the AAC $(P)_4$- or $(M)_4$-**1**, referred to as "host", was prepared gravimetrically (~10 μM) in *n*-octane. The parent solution was used to prepare the stock solution of the varied component, referred to as "guest" (**2**–**12**). All studies were carried out under air atmosphere without drying of the solvents prior to use. Portions of the guest solution were added stepwise, and the ECD spectrum was recorded after each addition. During titration, the change in $\Delta\Delta\varepsilon$ (M^{-1} cm^{-1}) was followed at the maximum of the highest wavelength (302–306 nm).

Determination of the association constant: During ECD titrations, the change in $\Delta\varepsilon$ (M^{-1} cm^{-1}) was followed at the maximum intensity between 302–306 nm. The change in $\Delta\varepsilon$ (M^{-1} cm^{-1}) was plotted against the guest concentration and curve-fitted to a 1:1 binding isotherm.

The data was curve-fitted using the software IGOR Pro V6.12 according to the following equation.[6]

$$\Delta\delta = \frac{\Delta\delta_{sat}}{2}\left[\left(\frac{[G]_0}{[H]_0} + 1 + \frac{1}{K_a[H]_0}\right) - \sqrt{\left(\frac{[G]_0}{[H]_0} + 1 + \frac{1}{K_a[H]_0}\right)^2 + \frac{[G]_0}{[H]_0}}\right]$$

with $\Delta\delta = (\delta_{sat} - \delta_0)\frac{[C]}{[H]_0}$

where the following parameters were applied:

$\Delta\delta$	Change in relative shift ($\Delta\Delta\varepsilon$) to the free host
$\Delta\delta_{sat}$	Calculated change in chemical shift at saturation binding ($\Delta\Delta\varepsilon_{sat}$)

$[H]_0$	Constant host concentration (M)
$[G]$	Guest concentration (M)
K_a	Association constant (M^{-1})

The calculated fitting error for all measurements is given below each binding isotherm. All fitting errors are well within ±15% (K_a). Due to the preparation process of the solutions the actual error of the measurement was estimated to be higher than the actual fitting errors. The overall error in K_a is therefore estimated to be ±20%. The authors are well aware that the error value is likely to be overestimated.

Preparation of solutions for ITC titrations: A solution of the AAC $(P)_4$-**1** or $(M)_4$-**1**, referred to as "host", was prepared gravimetrically (~0.1 mM) in *n*-octane. The "guest" solution was prepared in concentrations between 1–10 mM depending on the order of magnitude of the expected binding constant. All studies were carried out under air atmosphere without drying of the solvents prior to use at 303 K.

From ITC experiments, the thermodynamic quantities of K_a, ΔG, ΔH, and ΔS were obtained.

S4. Titration Data and Binding Isotherms Obtained by ECD Spectroscopic Titrations

Butan-1-ol 2

Table S1. Experimental values for the determination of the association constant K_a of AAC $(P)_4$-**1** with butan-1-ol **2** in *n*-octane at 293 K.

	K_a M^{-1}	AAC $(P)_4$-**1** (μM)	$[\text{guest}]_{max}$ (mM)	guest equiv._{max}	$\Delta\Delta\varepsilon_{max}$ (M^{-1} cm^{-1})	$\Delta\Delta\varepsilon_{sat}$ (M^{-1} cm^{-1})
ECD	–	8.8	5.4	611.6	–	–

3-Methylbutan-1-ol 3

Table S2. Experimental values for the determination of the association constant K_a of AAC $(P)_4$-**1** with 3-methylbutan-1-ol **3** in *n*-octane at 293 K.

	K_a M^{-1}	AAC $(P)_4$-**1** (μM)	$[\text{guest}]_{max}$ (mM)	guest equiv._{max}	$\Delta\Delta\varepsilon_{max}$ (M^{-1} cm^{-1})	$\Delta\Delta\varepsilon_{sat}$ (M^{-1} cm^{-1})
ECD	$1.5 \cdot 10^3$	8.8	3.3	376.3	83.8	102.9

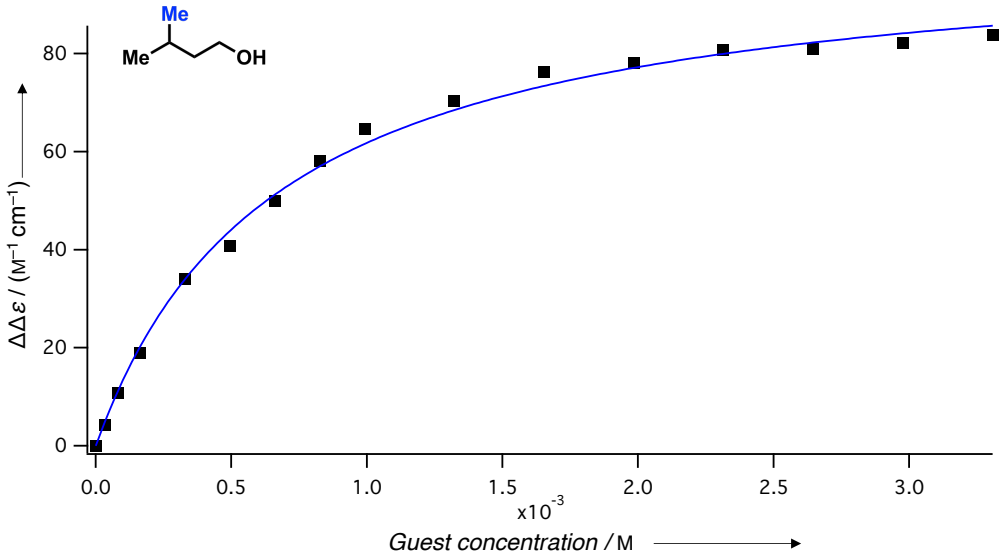

Figure S2. ECD binding isotherm of AAC $(P)_4$-**1** with 3-methylbutan-1-ol **3** in *n*-octane at 293 K. $K_a = 1.51 \cdot 10^3 \pm 0.09 \cdot 10^3$, $\Delta\Delta\varepsilon_{max} = 83.8$ M^{-1} cm^{-1}, $\Delta\Delta\varepsilon_{sat} = 102.9 \pm 1.9$ M^{-1} cm^{-1}.

(±)-2-Methylbutan-1-ol (*R*/*S*)-4

Table S3. Experimental values for the determination of the association constant K_a of AAC $(P)_4$-**1** with (±)-2-methylbutan-1-ol (*R*/*S*)-**4** in *n*-octane at 293 K.

	K_a	AAC $(P)_4$-**1**	$[guest]_{max}$	guest	$\Delta\Delta\varepsilon_{max}$	$\Delta\Delta\varepsilon_{sat}$
	M^{-1}	(μM)	(mM)	$equiv._{max}$	(M^{-1} cm^{-1})	(M^{-1} cm^{-1})
ECD	$2.3 \cdot 10^3$	9.6	3.1	326.7	64.1	76.4

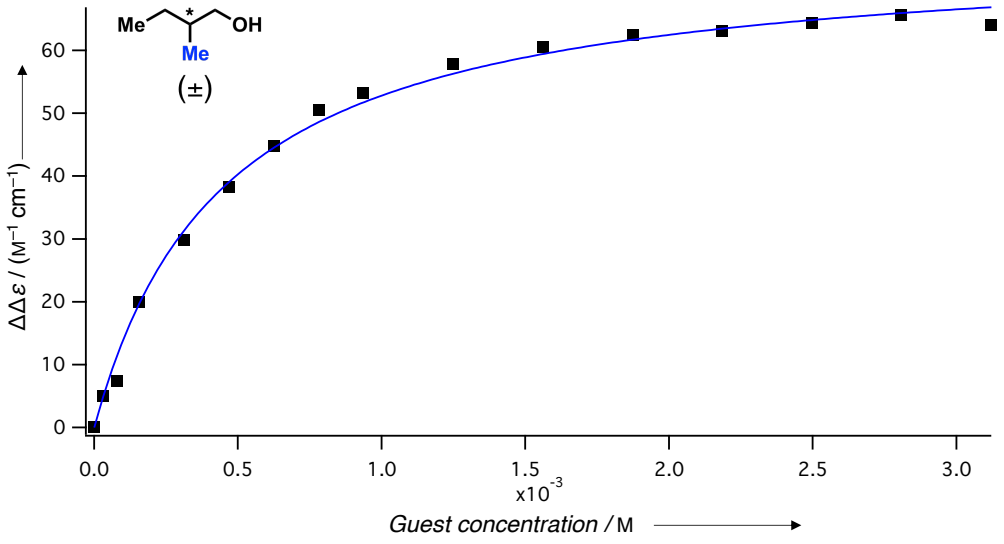

Figure S3. ECD binding isotherm of AAC $(P)_4$-**1** with (±)-2-methylbutan-1-ol (*R*/*S*)-**4** in *n*-octane at 293 K. $K_a = 2.26 \cdot 10^3 \pm 0.14 \cdot 10^3$, $\Delta\Delta\varepsilon_{max} = 64.1$ M^{-1} cm^{-1}, $\Delta\Delta\varepsilon_{sat} = 76.4 \pm 1.3$ M^{-1} cm^{-1}.

2,2-Dimethylbutan-1-ol 5

Table S4. Experimental values for the determination of the association constant K_a of AAC $(P)_4$-**1** with 2,2-dimethylbutan-1-ol **5** in *n*-octane at 293 K.

	K_a	AAC $(P)_4$-**1**	$[\text{guest}]_{max}$	guest	$\Delta\Delta\varepsilon_{max}$	$\Delta\Delta\varepsilon_{sat}$
	M^{-1}	(μM)	(mM)	equiv._{max}	(M^{-1} cm^{-1})	(M^{-1} cm^{-1})
ECD	$2.0 \cdot 10^4$	8.9	2.6	293.1	102.0	106.1

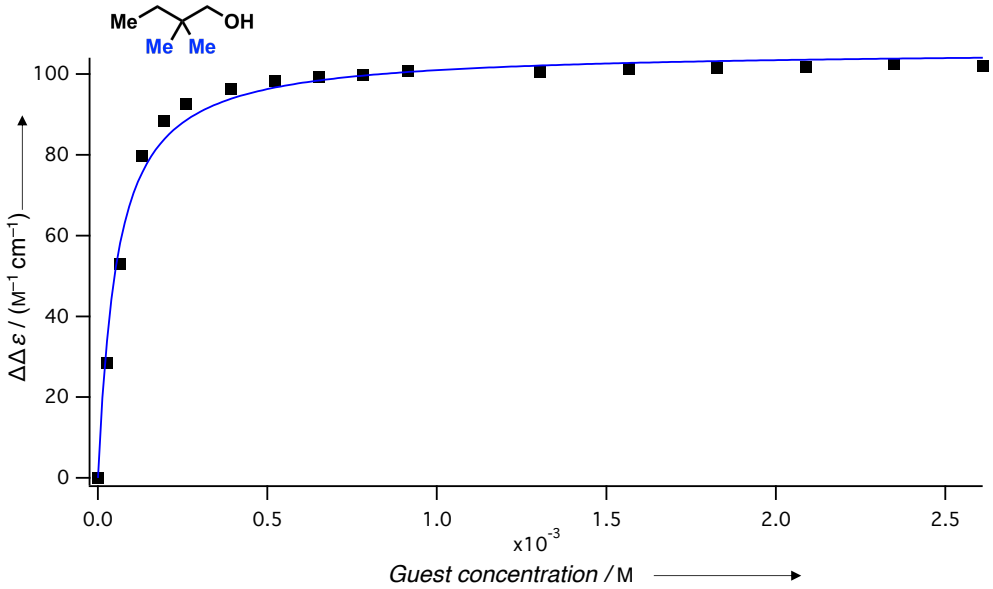

Figure S4. ECD binding isotherm of AAC $(P)_4$-**1** with 2,2-dimethylbutan-1-ol **5** in *n*-octane at 293 K. $K_a = 2.01 \cdot 10^4 \pm 0.16 \cdot 10^4$, $\Delta\Delta\varepsilon_{max} = 102.0$ M^{-1} cm^{-1}, $\Delta\Delta\varepsilon_{sat} = 106.1 \pm 1.1$ M^{-1} cm^{-1}.

(±)-2,3-Methylbutan-1-ol (*R*/*S*)-6

Table S5. Experimental values for the determination of the association constant K_a of AAC $(P)_4$-**1** with (±)-2,3-dimethylbutan-1-ol (*R*/*S*)-**6** in *n*-octane at 293 K.

	K_a	AAC $(P)_4$-**1**	$[\text{guest}]_{max}$	guest	$\Delta\Delta\varepsilon_{max}$	$\Delta\Delta\varepsilon_{sat}$
	M^{-1}	(μM)	(mM)	equiv._{max}	(M^{-1} cm^{-1})	(M^{-1} cm^{-1})
ECD	$9.9 \cdot 10^3$	9.1	1.4	156.1	59.4	65.5

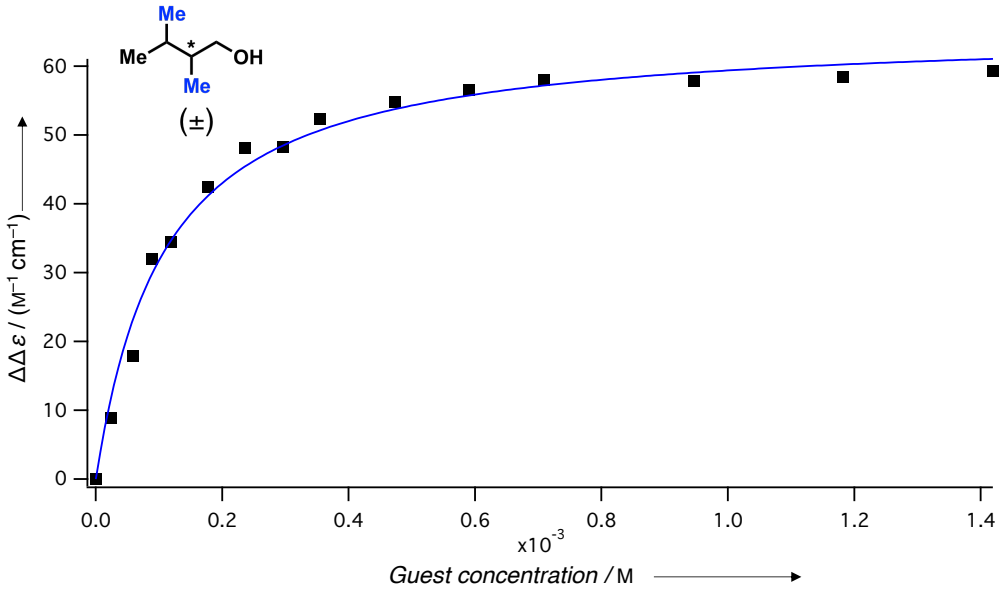

Figure S5. ECD binding isotherm of AAC $(P)_4$-**1** with (±)-2,3-dimethylbutan-1-ol (*R*/*S*)-**6** in *n*-octane at 293 K. $K_a = 9.88 \cdot 10^3 \pm 0.90 \cdot 10^3$, $\Delta\Delta\varepsilon_{max} = 59.4\ M^{-1}\ cm^{-1}$, $\Delta\Delta\varepsilon_{sat} = 65.5 \pm 1.4\ M^{-1}\ cm^{-1}$.

2,2,3-Trimethylbutan-1-ol 9

Table S6. Experimental values for the determination of the association constant K_a of AAC $(P)_4$-**1** with 2,2,3-trimethylbutan-1-ol **9** in *n*-octane at 293 K.

	K_a	AAC $(P)_4$-**1**	$[guest]_{max}$	guest	$\Delta\Delta\varepsilon_{max}$	$\Delta\Delta\varepsilon_{sat}$
	M^{-1}	(μM)	(mM)	equiv.$_{max}$	($M^{-1}\ cm^{-1}$)	($M^{-1}\ cm^{-1}$)
ECD	$6.9 \cdot 10^3$	8.8	1.4	161.7	81.3	93.5

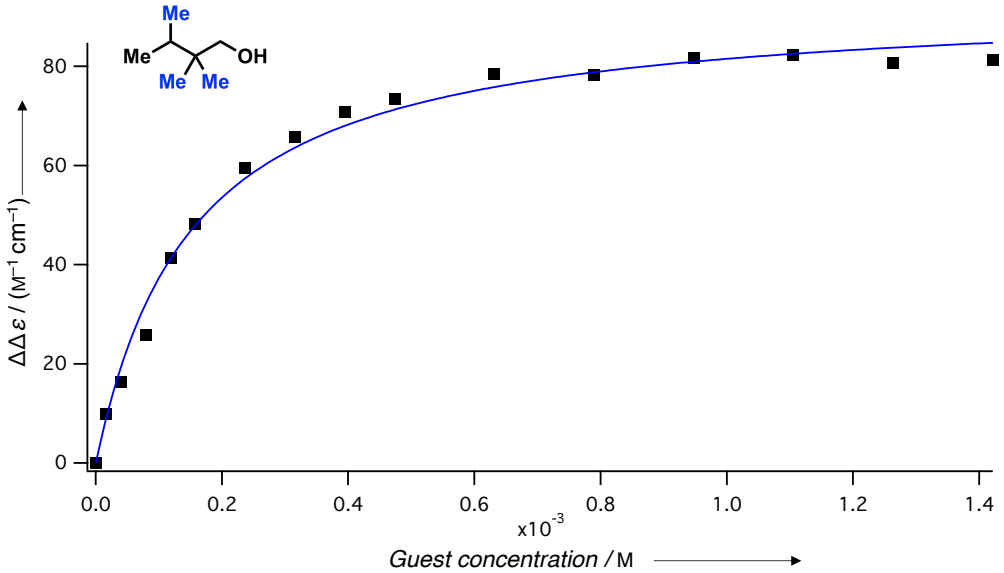

Figure S6. ECD binding isotherm of AAC $(P)_4$-**1** with 2,2,3-trimethylbutan-1-ol **9** in *n*-octane at 293 K. $K_a = 6.88 \cdot 10^3 \pm 0.54 \cdot 10^3$, $\Delta\Delta\varepsilon_{max} = 81.3\ M^{-1}\ cm^{-1}$, $\Delta\Delta\varepsilon_{sat} = 93.5 \pm 1.9\ M^{-1}\ cm^{-1}$.

(±)-(2*S**,3*R**)-2,3-Dichlorobutan-1-ol (*R**,*S**)-7

Table S7. Experimental values for the determination of the association constant K_a of AAC $(P)_4$-**1** with (±)-(2*S**,3*R**)-2,3-dichlorobutan-1-ol (*R**,*S**)-**7** in *n*-octane at 293 K.

	K_a	AAC $(P)_4$-**1**	$[\text{guest}]_{max}$	guest	$\Delta\Delta\varepsilon_{max}$	$\Delta\Delta\varepsilon_{sat}$
	M^{-1}	(μM)	(mM)	equiv._{max}	(M^{-1} cm^{-1})	(M^{-1} cm^{-1})
ECD	$1.5 \cdot 10^4$	8.8	0.7	79.4	65.6	74.8

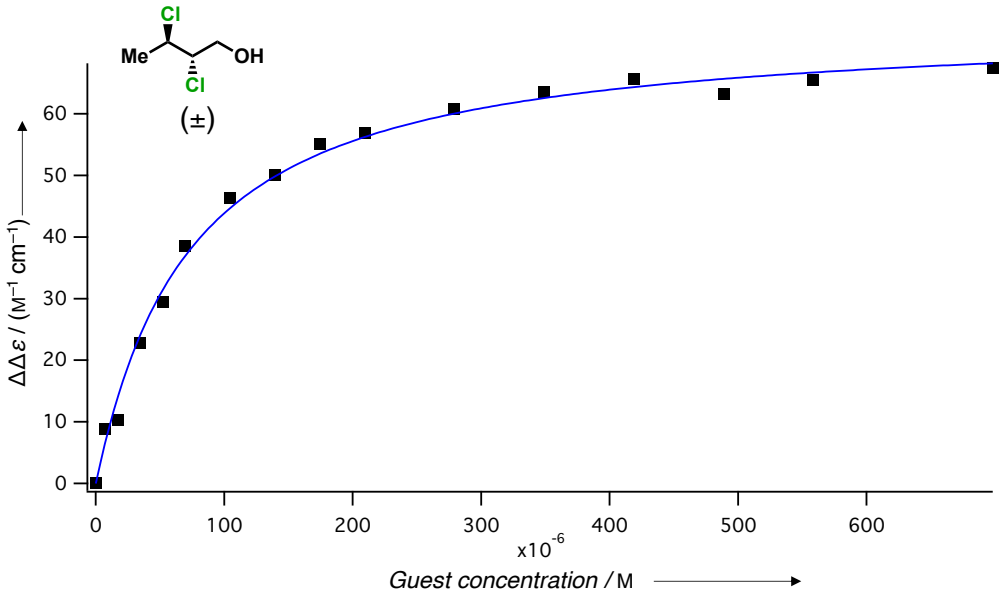

Figure S7. ECD binding isotherm of AAC $(P)_4$-**1** with (±)-(2*S**,3*R**)-2,3-dichlorobutan-1-ol (*R**,*S**)-**7** in *n*-octane at 293 K. $K_a = 1.50 \cdot 10^4 \pm 0.10 \cdot 10^4$, $\Delta\Delta\varepsilon_{max} = 65.6$ M^{-1} cm^{-1}, $\Delta\Delta\varepsilon_{sat} = 74.8 \pm 1.3$ M^{-1} cm^{-1}.

(±)-(2*R**,3*R**)-2,3-Dichlorobutan-1-ol (*R**,*R**)-7

Table S8. Experimental values for the determination of the association constant K_a of AAC $(P)_4$-**1** with (±)-(2*R**,3*R**)-2,3-dichlorobutan-1-ol (*R**,*R**)-**7** in *n*-octane at 293 K.

	K_a	AAC $(P)_4$-**1**	$[\text{guest}]_{max}$	guest	$\Delta\Delta\varepsilon_{max}$	$\Delta\Delta\varepsilon_{sat}$
	M^{-1}	(μM)	(mM)	equiv._{max}	(M^{-1} cm^{-1})	(M^{-1} cm^{-1})
ECD	$7.0 \cdot 10^4$	8.8	0.7	46.4	82.3	86.7

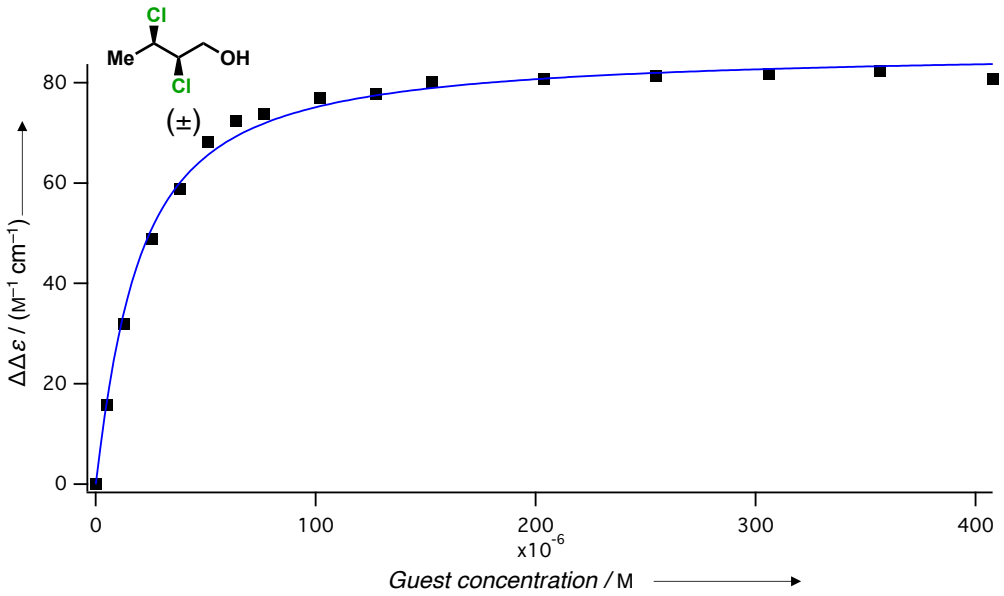

Figure S8. ECD binding isotherm of AAC $(P)_4$-**1** with (±)-(2*R**,3*R**)-2,3-dichlorobutan-1-ol (*R**,*R**)-**7** in *n*-octane at 293 K. $K_a = 7.02 \cdot 10^4 \pm 0.46 \cdot 10^4$, $\Delta\Delta\varepsilon_{max} = 82.3$ M^{-1} cm^{-1}, $\Delta\Delta\varepsilon_{sat} = 86.7 \pm 0.9$ M^{-1} cm^{-1}.

(±)-(2*S**,3*R**)-2,3-Dibromobutan-1-ol (*R**,*S**)-8

Table S9. Experimental values for the determination of the association constant K_a of AAC $(P)_4$-**1** with (±)-(2*S**,3*R**)-2,3-dibromobutan-1-ol (*R**,*S**)-**8** in *n*-octane at 293 K.

	K_a	AAC $(P)_4$-**1**	$[\text{guest}]_{max}$	guest	$\Delta\Delta\varepsilon_{max}$	$\Delta\Delta\varepsilon_{sat}$
	M^{-1}	(μM)	(mM)	equiv.$_{max}$	(M^{-1} cm^{-1})	(M^{-1} cm^{-1})
ECD	$7.6 \cdot 10^4$	9.7	0.5	53.0	102.6	107.0

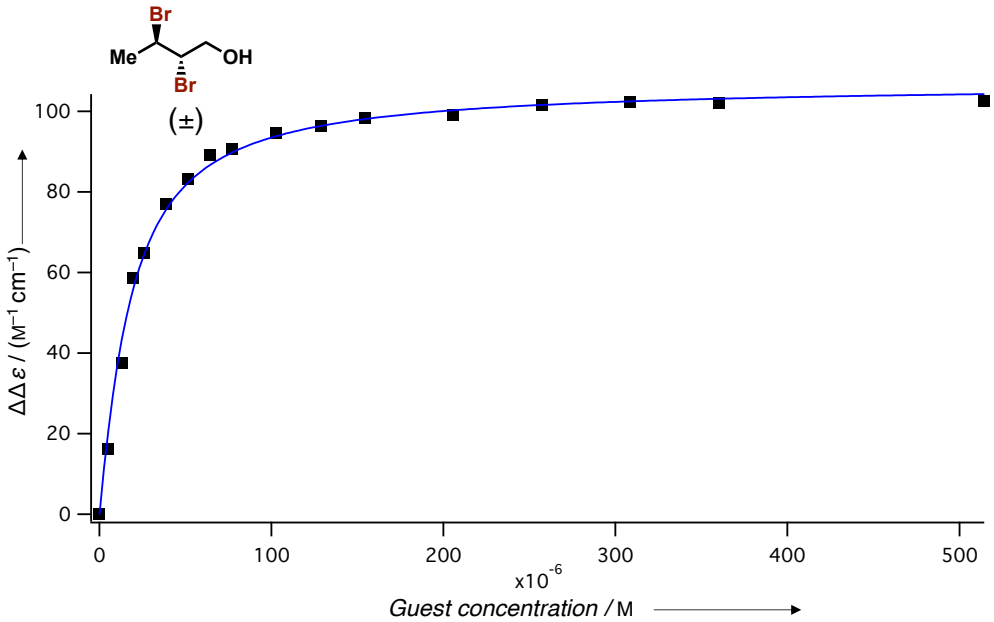

Figure S9. ECD binding isotherm of AAC $(P)_4$-**1** with (±)-(2*R**,3*R**)-2,3-dibromobutan-1-ol (*R**,*S**)-**8** in *n*-octane at 293 K. $K_a = 7.56 \cdot 10^4 \pm 0.47 \cdot 10^4$, $\Delta\Delta\varepsilon_{max} = 102.6$ M^{-1} cm^{-1}, $\Delta\Delta\varepsilon_{sat} = 107.0 \pm 1.1$ M^{-1} cm^{-1}.

(–)-(2*R*,3*S*)-2,3-Dibromobutan-1-ol (*R*,*S*)-8

Table S10. Experimental values for the determination of the association constant K_a of AAC $(P)_4$-**1** with (–)-(2*R*,3*S*)-2,3-dibromobutan-1-ol (*R*,*S*)-**8** in *n*-octane at 293 K.

	K_a	AAC $(P)_4$-**1**	$[\text{guest}]_{max}$	guest	$\Delta\Delta\varepsilon_{max}$	$\Delta\Delta\varepsilon_{sat}$
	M^{-1}	(μM)	(mM)	equiv._{max}	(M^{-1} cm^{-1})	(M^{-1} cm^{-1})
ECD	$6.1 \cdot 10^4$	9.5	0.5	36.1	80.6	86.3

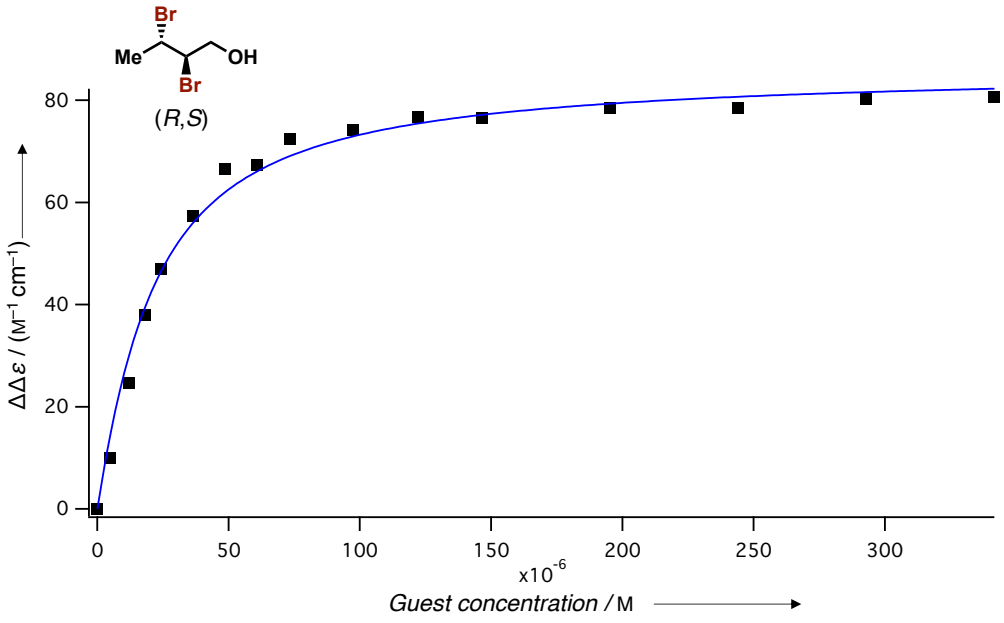

Figure S10. ECD binding isotherm of AAC $(P)_4$-**1** with (–)-(2*R*,3*S*)-2,3-dibromobutan-1-ol (*R*,*S*)-**8** in *n*-octane at 293 K. $K_a = 6.1 \cdot 10^4 \pm 0.56 \cdot 10^4$, $\Delta\Delta\varepsilon_{max} = 80.6$ M^{-1} cm^{-1}, $\Delta\Delta\varepsilon_{sat} = 86.3 \pm 1.5$ M^{-1} cm^{-1}.

(+)-(2*S*,3*R*)-2,3-Dibromobutan-1-ol (*S*,*R*)-**8**

Table S11. Experimental values for the determination of the association constant K_a of AAC $(P)_4$-**1** with (+)-(2*S*,3*R*)-2,3-dibromobutan-1-ol (*S*,*R*)-**8** in *n*-octane at 293 K.

	K_a	AAC $(P)_4$-**1**	$[\text{guest}]_{max}$	guest	$\Delta\Delta\varepsilon_{max}$	$\Delta\Delta\varepsilon_{sat}$
	M^{-1}	(μM)	(mM)	equiv._{max}	(M^{-1} cm^{-1})	(M^{-1} cm^{-1})
ECD	$6.0 \cdot 10^4$	9.5	0.4	38.2	74.7	76.5

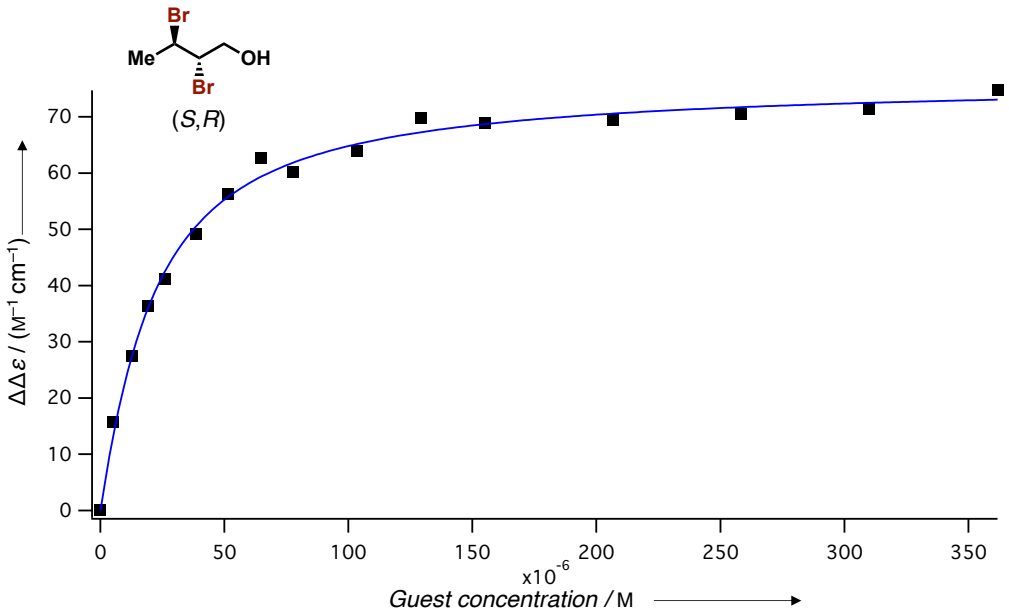

Figure S11. ECD binding isotherm of AAC $(P)_4$-**1** with (+)-(2*S*,3*R*)-2,3-dibromobutan-1-ol (*S*,*R*)-**8** in *n*-octane at 293 K. $K_a = 6.04 \cdot 10^4 \pm 0.37 \cdot 10^4$, $\Delta\Delta\varepsilon_{max} = 74.7$ M^{-1} cm^{-1}, $\Delta\Delta\varepsilon_{sat} = 76.5 \pm 0.9$ M^{-1} cm^{-1}.

(±)-(2*R**,3*R**)-2,3-Dibromobutan-1-ol (*R**,*R**)-**8**

Table S12. Experimental values for the determination of the association constant K_a of AAC $(P)_4$-**1** with (±)-(2*R**,3*R**)-2,3-dibromobutan-1-ol (*R**,*R**)-**8** in *n*-octane at 293 K.

	K_a	AAC $(P)_4$-**1**	$[\text{guest}]_{max}$	guest	$\Delta\Delta\varepsilon_{max}$	$\Delta\Delta\varepsilon_{sat}$
	M^{-1}	(μM)	(mM)	equiv._{max}	(M^{-1} cm^{-1})	(M^{-1} cm^{-1})
ECD	$3.8 \cdot 10^5$	8.6	0.2	24.0	88.7	89.4

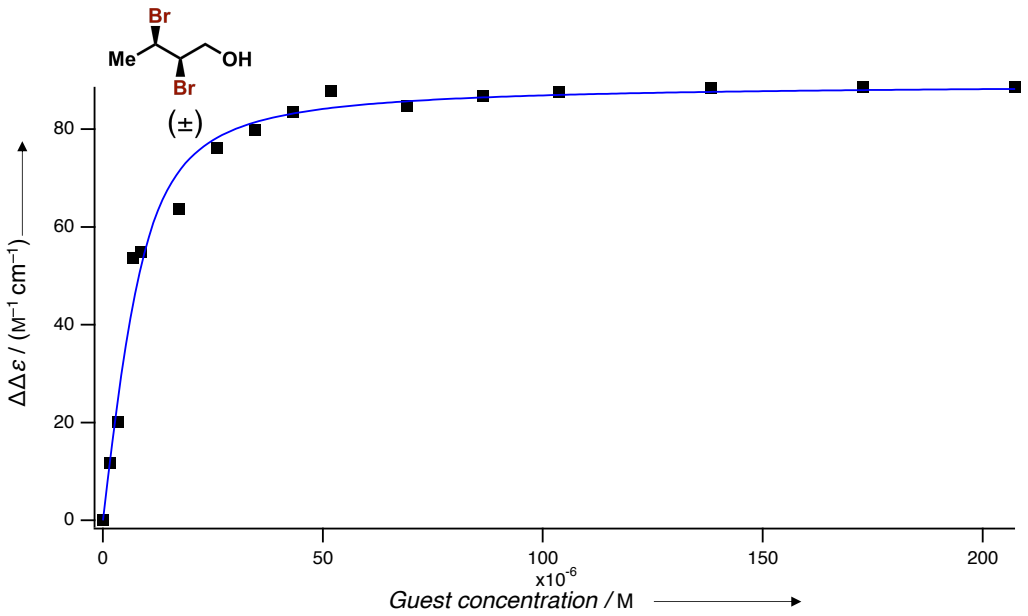

Figure S12. ECD binding isotherm of AAC $(P)_4$-**1** with (±)-(2*R**,3*R**)-2,3-dibromobutan-1-ol (*R**,*R**)-**8** in *n*-octane at 293 K. $K_a = 3.82 \cdot 10^5 \pm 0.73 \cdot 10^5$, $\Delta\Delta\varepsilon_{max} = 88.7$ M^{-1} cm^{-1}, $\Delta\Delta\varepsilon_{sat} = 89.4 \pm 1.6$ M^{-1} cm^{-1}.

(+)-(2*R*,3*R*)-2,3-Dibromobutan-1-ol (*R*,*R*)-8

Table S13. Experimental values for the determination of the association constant K_a of AAC $(P)_4$-**1** with (+)-(2*R*,3*R*)-2,3-dibromobutan-1-ol (*R*,*R*)-**8** in *n*-octane at 293 K.

	K_a	AAC $(P)_4$-**1**	$[\text{guest}]_{max}$	guest	$\Delta\Delta\varepsilon_{max}$	$\Delta\Delta\varepsilon_{sat}$
	M^{-1}	(μM)	(mM)	equiv.$_{max}$	(M^{-1} cm^{-1})	(M^{-1} cm^{-1})
ECD	$1.2 \cdot 10^6$	9.0	0.04	4.0	81.5	83.0

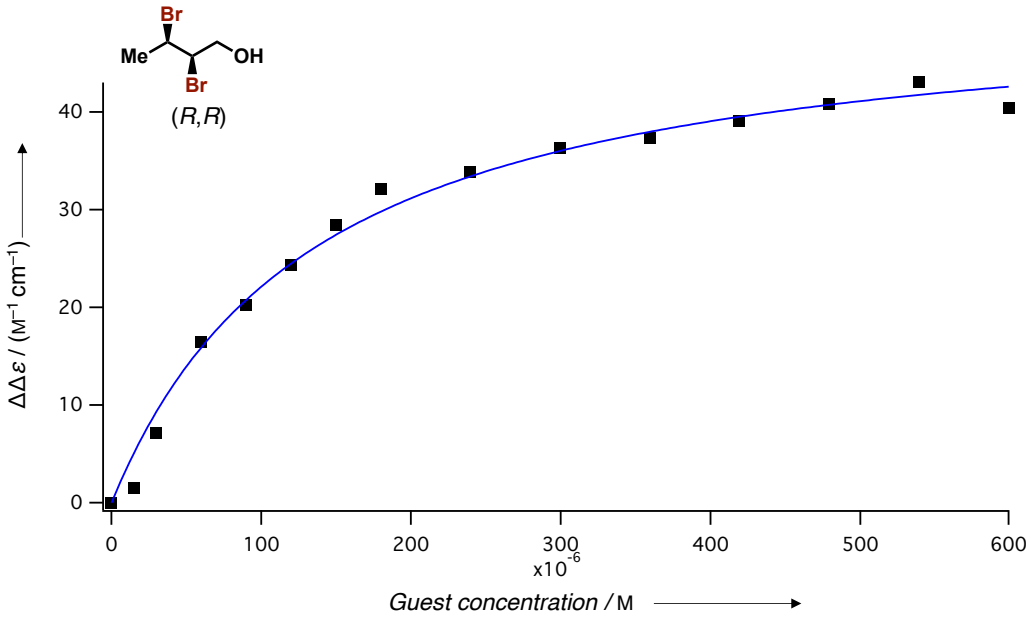

Figure S13. ECD binding isotherm of AAC $(P)_4$-**1** with (+)-(2*R*,3*R*)-2,3-dibromobutan-1-ol (*R*,*R*)-**8** in *n*-octane at 293 K. $K_a = 1.17 \cdot 10^6 \pm 0.18 \cdot 10^6$, $\Delta\Delta\varepsilon_{max} = 81.5$ M^{-1} cm^{-1}, $\Delta\Delta\varepsilon_{sat} = 83.0 \pm 1.2$ M^{-1} cm^{-1}.

(–)-(2*S*,3*S*)-2,3-Dibromobutan-1-ol (*S*,*S*)-8

Table S14. Experimental values for the determination of the association constant K_a of AAC $(P)_4$-**1** with (–)-(2*S*,3*S*)-2,3-dibromobutan-1-ol (*S*,*S*)-**8** in *n*-octane at 293 K.

	K_a	AAC $(P)_4$-**1**	$[\text{guest}]_{max}$	guest	$\Delta\Delta\varepsilon_{max}$	$\Delta\Delta\varepsilon_{sat}$
	M^{-1}	(μM)	(mM)	equiv._{max}	(M^{-1} cm^{-1})	(M^{-1} cm^{-1})
ECD	$2.8 \cdot 10^5$	9.0	0.03	3.7	65.3	74.9

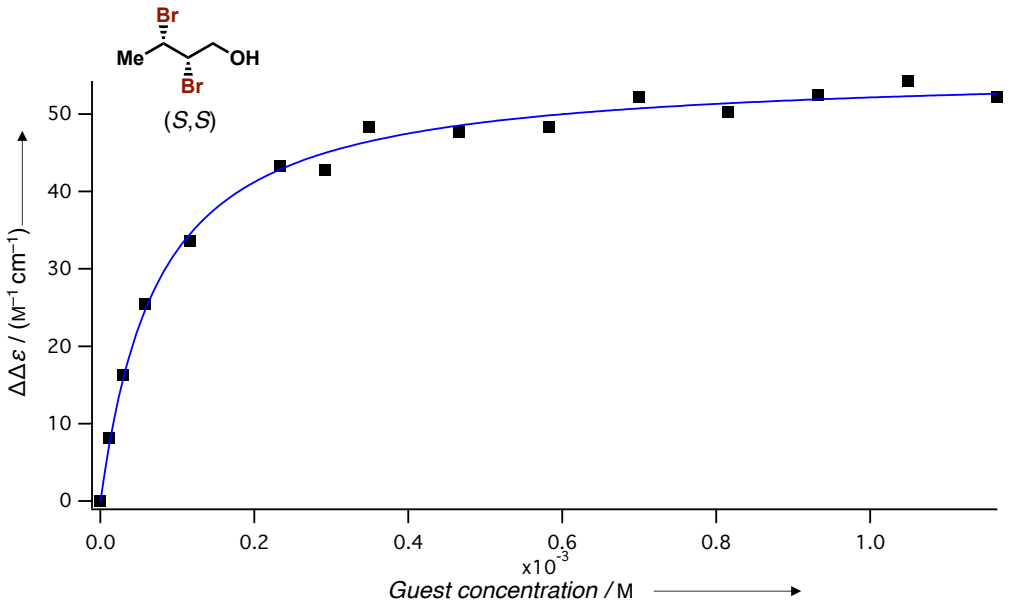

Figure S14. ECD binding isotherm of AAC $(P)_4$-**1** with (–)-(2*S*,3*S*)-2,3-dibromobutan-1-ol (*S*,*S*)-**8** in *n*-octane at 293 K. $K_a = 2.80 \cdot 10^5 \pm 0.37 \cdot 10^5$, $\Delta\Delta\varepsilon_{max} = 65.3$ M^{-1} cm^{-1}, $\Delta\Delta\varepsilon_{sat} = 74.9 \pm 2.0$ M^{-1} cm^{-1}.

(±)-(2*S**,3*R**)-2,3-Dibromo-2-methylbutan-1-ol (*R**,*S**)-**10**

Table S15. Experimental values for the determination of the association constant K_a of AAC $(P)_4$-**1** with (±)-(2*S**,3*R**)-2,3-dibromo-2-methylbutan-1-ol (*R**,*S**)-**10** in *n*-octane at 293 K.

	K_a	AAC $(P)_4$-**1**	$[\text{guest}]_{max}$	guest	$\Delta\Delta\varepsilon_{max}$	$\Delta\Delta\varepsilon_{sat}$
	M^{-1}	(μM)	(mM)	equiv._{max}	(M^{-1} cm^{-1})	(M^{-1} cm^{-1})
ECD	$1.2 \cdot 10^5$	9.7	0.03	26.2	87.2	92.2

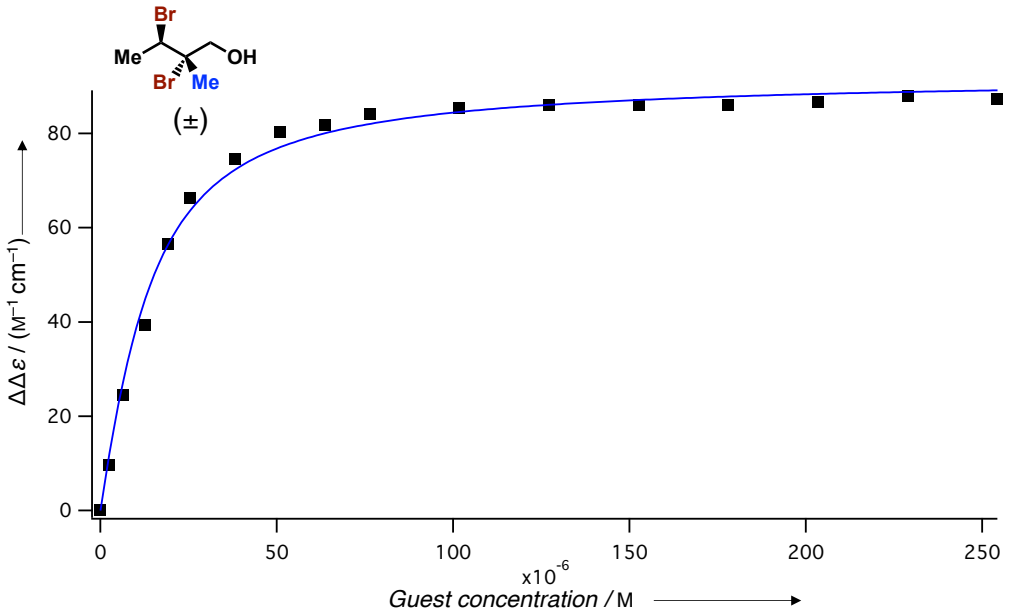

Figure S15. ECD binding isotherm of AAC $(P)_4$-**1** with (±)-(2*S**,3*R**)-2,3-dibromo-2-methylbutan-1-ol (*R**,*S**)-**10** in *n*-octane at 293 K. $K_a = 1.19 \cdot 10^5 \pm 0.10 \cdot 10^5$, $\Delta\Delta\varepsilon_{max} = 87.2$ M^{-1} cm^{-1}, $\Delta\Delta\varepsilon_{sat} = 92.2 \pm 1.1$ M^{-1} cm^{-1}.

(±)-(2*R**,3*R**)-2,3-Dibromo-2-methylbutan-1-ol (*R**,*R**)-**10**

Table S16. Experimental values for the determination of the association constant K_a of AAC $(P)_4$-**1** with (±)-(2*R**,3*R**)-2,3-dibromo-2-methylbutan-1-ol (*R**,*R**)-**10** in *n*-octane at 293 K.

	K_a	AAC $(P)_4$-**1**	$[\text{guest}]_{max}$	guest	$\Delta\Delta\varepsilon_{max}$	$\Delta\Delta\varepsilon_{sat}$
	M^{-1}	(μM)	(mM)	equiv._{max}	(M^{-1} cm^{-1})	(M^{-1} cm^{-1})
ECD	$3.8 \cdot 10^5$	4.9	0.02	4.8	94.9	92.3

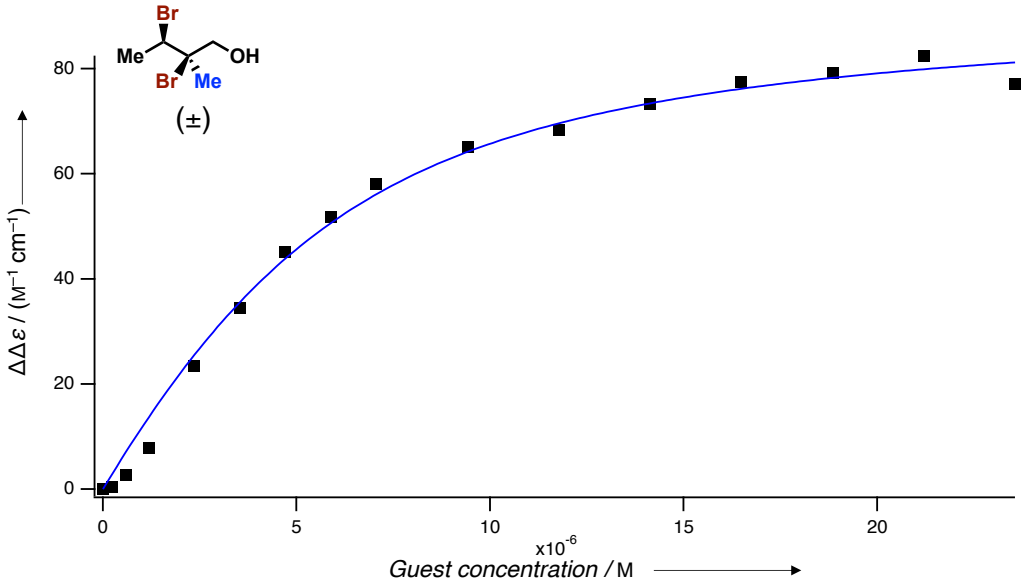

Figure S16. ECD binding isotherm of AAC $(P)_4$-**1** with (±)-(2*R**,3*R**)-2,3-dibromo-2-methylbutan-1-ol (*R**,*R**)-**10** in *n*-octane at 293 K. $K_a = 3.79 \cdot 10^5 \pm 0.59 \cdot 10^5$, $\Delta\Delta\varepsilon_{max} = 94.9$ M^{-1} cm^{-1}, $\Delta\Delta\varepsilon_{sat} = 92.3 \pm 3.1$ M^{-1} cm^{-1}.

(+)-(2*R*,3*R*)-2,3-Dibromo-2-methylbutan-1-ol (*R*,*R*)-10

Table S17. Experimental values for the determination of the association constant K_a of AAC $(P)_4$-**1** with (+)-(2*R*,3*R*)-2,3-dibromo-2-methylbutan-1-ol (*R*,*R*)-**10** in *n*-octane at 293 K.

	K_a	AAC $(P)_4$-**1**	$[\text{guest}]_{max}$	guest	$\Delta\Delta\varepsilon_{max}$	$\Delta\Delta\varepsilon_{sat}$
	M^{-1}	(μM)	(mM)	equiv._{max}	(M^{-1} cm^{-1})	(M^{-1} cm^{-1})
ECD	$1.0 \cdot 10^6$	4.7	0.03	5.3	83.0	87.0

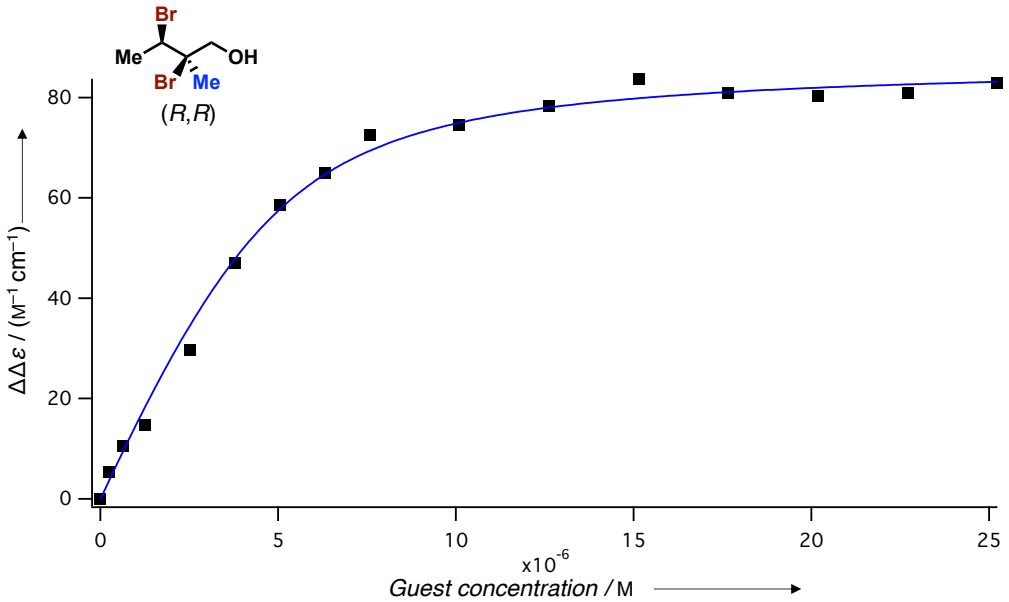

Figure S17. ECD binding isotherm of AAC $(P)_4$-**1** with (+)-(2*R*,3*R*)-2,3-dibromo-2-methylbutan-1 (*R*,*R*)-**10** in *n*-octane at 293 K. $K_a = 1.04 \cdot 10^6 \pm 0.16 \cdot 10^6$, $\Delta\Delta\varepsilon_{max} = 83.0$ M^{-1} cm^{-1}, $\Delta\Delta\varepsilon_{sat} = 87.0 \pm 1.6$ M^{-1} cm^{-1}.

(–)-(2*S*,3*S*)-2,3-Dibromo-2-methylbutan-1-ol (*S*,*S*)-10

Table S18. Experimental values for the determination of the association constant K_a of AAC $(P)_4$-**1** with (–)-(2*S*,3*S*)-2,3-dibromo-2-methylbutan-1-ol (*S*,*S*)-**10** in *n*-octane at 293 K.

	K_a	AAC $(P)_4$-**1**	$[\text{guest}]_{max}$	guest	$\Delta\Delta\varepsilon_{max}$	$\Delta\Delta\varepsilon_{sat}$
	M^{-1}	(μM)	(mM)	equiv._{max}	(M^{-1} cm^{-1})	(M^{-1} cm^{-1})
ECD	$1.3 \cdot 10^6$	9.6	0.1	13.6	64.3	64.0

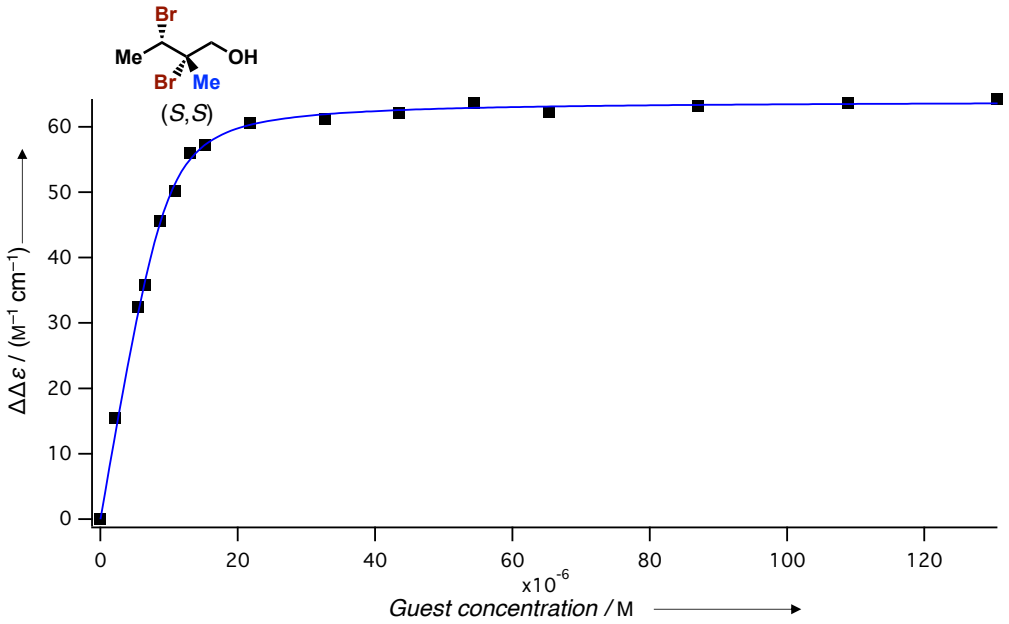

Figure S18. ECD binding isotherm of AAC $(P)_4$-**1** with (–)-(2*S*,3*S*)-2,3-dibromo-2-methylbutan-1-ol (*S*,*S*)-**10** in *n*-octane at 293 K. $K_a = 1.28 \cdot 10^6 \pm 0.12 \cdot 10^6$, $\Delta\Delta\varepsilon_{max} = 64.3$ M^{-1} cm^{-1}, $\Delta\Delta\varepsilon_{sat} = 64.0 \pm 0.4$ M^{-1} cm^{-1}.

(±)-(2*S**,3*R**)-2,3-Dibromo-4,4,4-trifluorobutan-1-ol (*R**,*S**)-11

Table S19. Experimental values for the determination of the association constant K_a of AAC $(P)_4$-**1** with (±)-(2*S**,3*R**)-2,3-dibromo-4,4,4-trifluorobutan-1-ol (*R**,*S**)-**11** in *n*-octane at 293 K.

	K_a	AAC $(P)_4$-**1**	$[\text{guest}]_{max}$	guest	$\Delta\Delta\varepsilon_{max}$	$\Delta\Delta\varepsilon_{sat}$
	M^{-1}	(μM)	(mM)	equiv._{max}	(M^{-1} cm^{-1})	(M^{-1} cm^{-1})
ECD	$1.3 \cdot 10^4$	8.6	0.7	82.7	57.4	59.3

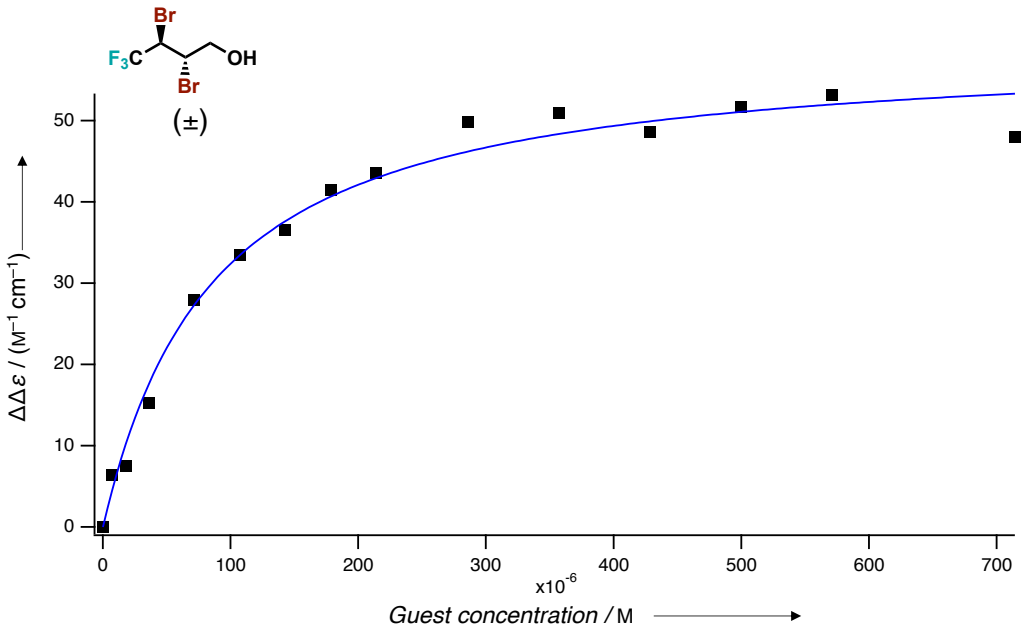

Figure S19. ECD binding isotherm of AAC $(P)_4$-**1** with (±)-(2*S**,3*R**)-2,3-dibromo-4,4,4-trifluorobutan-1-ol (*R**,*S**)-**11** in *n*-octane at 293 K. $K_a = 1.27 \cdot 10^4 \pm 0.16 \cdot 10^4$, $\Delta\Delta\varepsilon_{max} = 57.4$ M^{-1} cm^{-1}, $\Delta\Delta\varepsilon_{sat} = 59.3 \pm 1.9$ M^{-1} cm^{-1}.

(±)-((2*R**,3*R**)-2,3-Dibromo-4,4,4-trifluoro-2-methylbutan-1-ol (*R**,*S**)-12

Table S20. Experimental values for the determination of the association constant K_a of AAC $(P)_4$-**1** with (±)-(2*R**,3*R**)-2,3-Dibromo-4,4,4-trifluoro-2-methylbutan-1-ol (*R**,*S**)-**12** in *n*-octane at 293 K.

	K_a	AAC $(P)_4$-**1**	$[\text{guest}]_{max}$	guest	$\Delta\Delta\varepsilon_{max}$	$\Delta\Delta\varepsilon_{sat}$
	M^{-1}	(μM)	(mM)	equiv.$_{max}$	(M^{-1} cm^{-1})	(M^{-1} cm^{-1})
ECD	$1.2 \cdot 10^4$	9.1	0.8	87.7	71.1	78.5

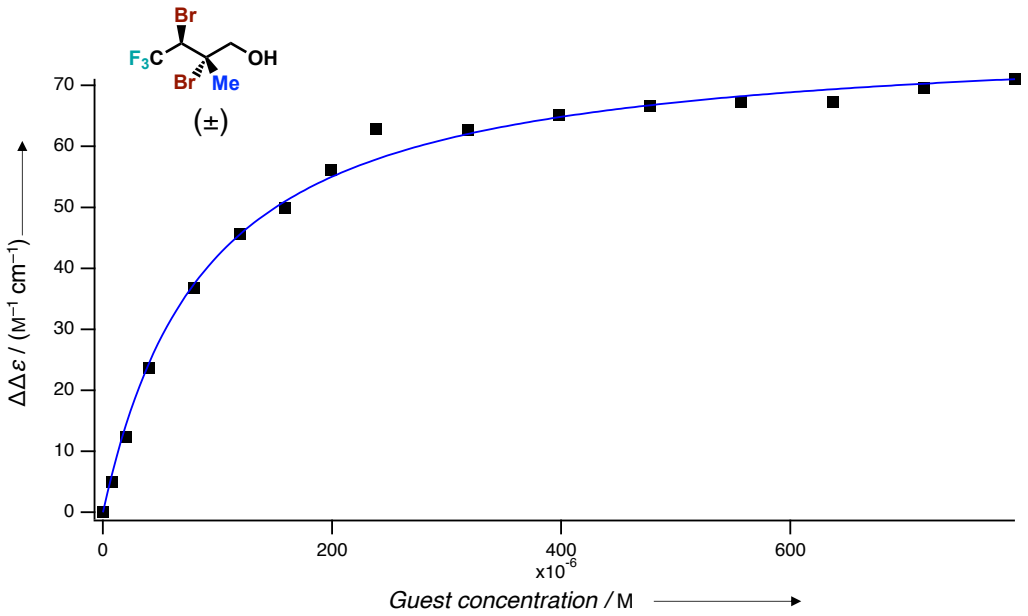

Figure S20. ECD binding isotherm of AAC $(P)_4$-**1** with (±)-(2*R**,3*R**)-2,3-Dibromo-4,4,4-trifluoro-2-methylbutan-1-ol in (*R**,*S**)-**12** *n*-octane at 293 K. $K_a = 1.21 \cdot 10^4 \pm 0.08 \cdot 10^4$, $\Delta\Delta\varepsilon_{max} = 71.1$ M^{-1} cm^{-1}, $\Delta\Delta\varepsilon_{sat} = 78.5 \pm 1.2$ M^{-1} cm^{-1}.

S5. Titration Data and Binding Isotherms Obtained by ITC

3-Methylbutan-1-ol 3

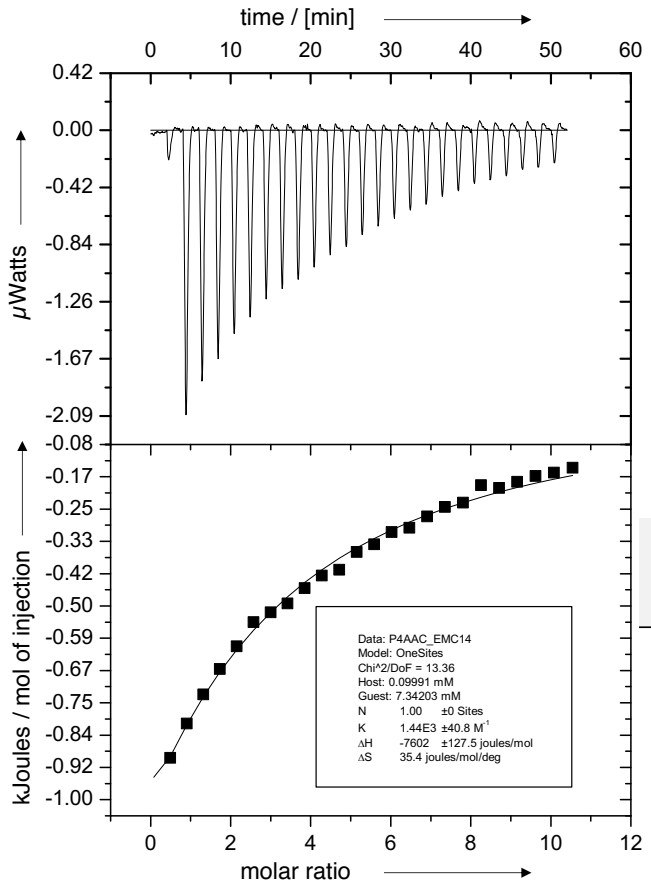

$(P)_4$-AAC ⊃ 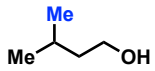

3-Methylbutan-1-ol

Host [mM]	Guest [mM]	$K_{a\ 303\ K}$ [M^{-1}]	ΔH [J mol^{-1}]	ΔS [J mol^{-1} K^{-1}]
0.1	7.3	$1.4 \cdot 10^3$	$-7.6 \cdot 10^3$	35.4

In *n*-octane at 303 K

Figure S21. ITC binding isotherm of AAC $(P)_4$-**1** with 3-methylbutan-1-ol **3** in *n*-octane at 303 K. $K_a = 1.44 \cdot 10^3 \pm 0.04 \cdot 10^3$ M^{-1}.

Table S21. Experimental values obtained from ITC titrations of AAC $(P)_4$-**1** with 3-methylbutan-1-ol **3** in *n*-octane calculated for 293 K.

K_a	$\Delta G_{293\ K}$	ΔH	$-T\Delta S_{293\ K}$
M^{-1}	[kcal mol^{-1}]	[kcal mol^{-1}]	[kcal mol^{-1}]
$1.6 \cdot 10^3$	–4.3	–1.8	–2.5

(±)-2-Methylbutan-1-ol (*R*/*S*)-**4**

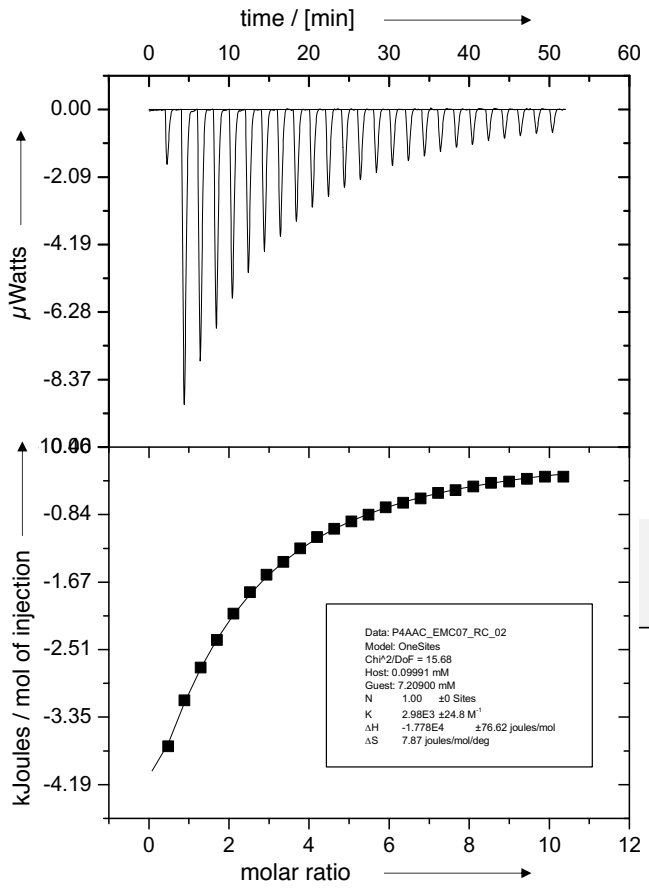

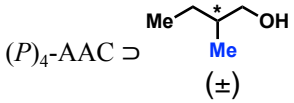

(±)-2-Methylbutan-1-ol

Host [mM]	Guest [mM]	$K_{a\ 303\ K}$ [M^{-1}]	ΔH [J mol^{-1}]	ΔS [J mol^{-1} K^{-1}]
0.1	7.2	$3.0 \cdot 10^3$	$-1.8 \cdot 10^4$	7.9

In *n*-octane at 303 K

Figure S22. ITC binding isotherm of AAC (*P*)$_4$-**1** with (±)-2-methylbutan-1-ol (*R*/*S*)-**4** in *n*-octane at 303 K. $K_a = 2.98 \cdot 10^3 \pm 0.03 \cdot 10^3\ M^{-1}$.

Table S22. Experimental values obtained from ITC titrations of AAC (*P*)$_4$-**1** with (±)-2-methylbutan-1-ol (*R*/*S*)-**4** in *n*-octane calculated for 293 K.

K_a	$\Delta G_{293\ K}$	ΔH	$-T\Delta S_{293\ K}$
M^{-1}	[kcal mol^{-1}]	[kcal mol^{-1}]	[kcal mol^{-1}]
$4.6 \cdot 10^3$	–4.90	–4.3	–0.6

2,2-Dimethylbutan-1-ol 5

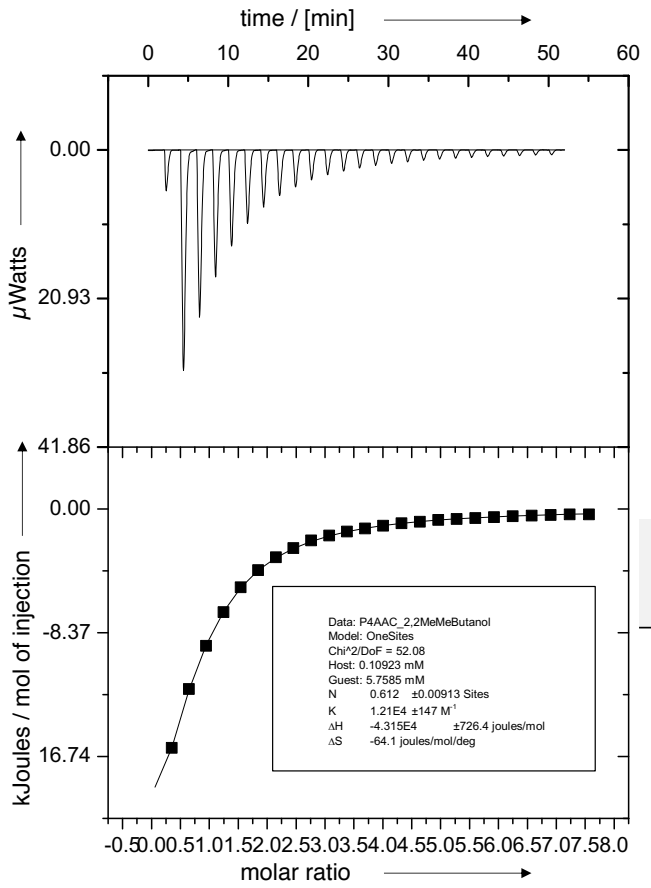

$(P)_4$-AAC ⊃ 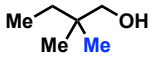

2,2-Dimethylbutan-1-ol

Host [mM]	Guest [mM]	$K_{a\ 303\ K}$ [M^{-1}]	ΔH [J mol^{-1}]	ΔS [J mol^{-1} K^{-1}]
0.1	5.8	$1.2 \cdot 10^4$	$-4.3 \cdot 10^4$	–64.1

In *n*-octane at 303 K

Figure S23. ITC binding isotherm of AAC $(P)_4$-**1** with 2,2-dimethylbutan-1-ol **5** in *n*-octane at 303 K. $K_a = 1.21 \cdot 10^4 \pm 0.02 \cdot 10^4\ M^{-1}$.

Table S23. Experimental values obtained from ITC titrations of AAC $(P)_4$-**1** with 2,2-dimethylbutan-1-ol **5** in *n*-octane calculated for 293 K.

K_a	$\Delta G_{293\ K}$	ΔH	$-T\Delta S_{293\ K}$
M^{-1}	[kcal mol^{-1}]	[kcal mol^{-1}]	[kcal mol^{-1}]
$1.7 \cdot 10^4$	–5.8	–10.3	+4.5

(±)-2,3-Methylbutan-1-ol (*R*/*S*)-**6**

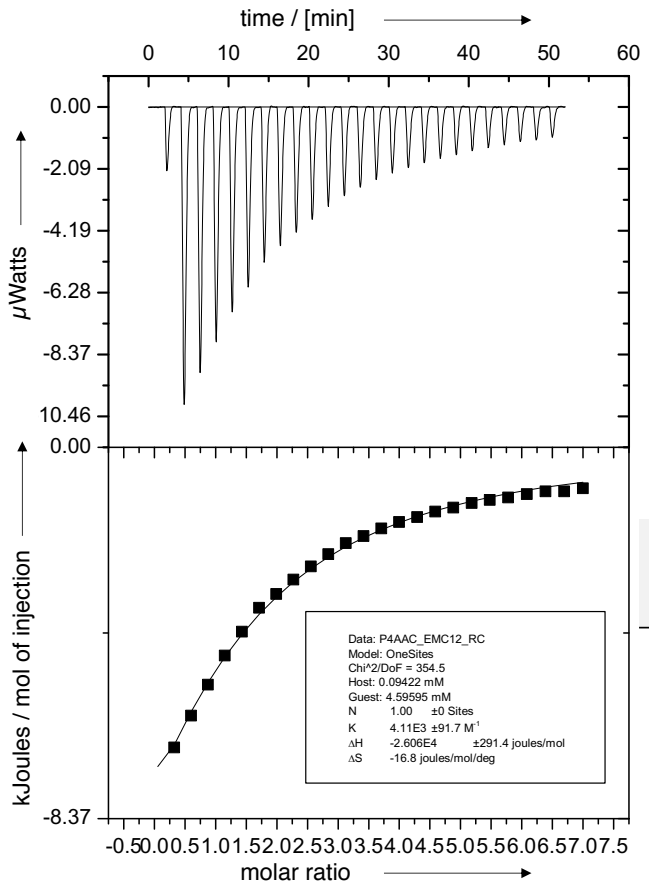

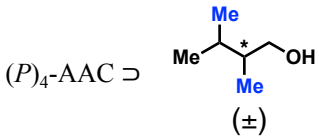

(±)-2,3-Methylbutan-1-ol

Host [mM]	Guest [mM]	$K_{a\ 303\ K}$ [M^{-1}]	ΔH [J mol^{-1}]	ΔS [J mol^{-1} K^{-1}]
0.1	4.6	$4.1 \cdot 10^3$	$-2.6 \cdot 10^4$	–16.8

In *n*-octane at 303 K

Figure S24. ITC binding isotherm of AAC $(P)_4$-**1** with (±)-2,3-methylbutan-1-ol (*R*/*S*)-**6** in *n*-octane at 303 K. $K_a = 4.11 \cdot 10^3 \pm 0.09 \cdot 10^3$ M^{-1}.

Table S24. Experimental values obtained from ITC titrations of AAC $(P)_4$-**1** with (±)-2,3-Methylbutan-1-ol (*R*/*S*)-**6** in *n*-octane calculated for 293 K.

K_a	$\Delta G_{293\ K}$	ΔH	$-T\Delta S_{293\ K}$
M^{-1}	[kcal mol^{-1}]	[kcal mol^{-1}]	[kcal mol^{-1}]
$5.9 \cdot 10^3$	–5.1	–6.2	+1.1

2,2,3-Trimethylbutan-1-ol 9

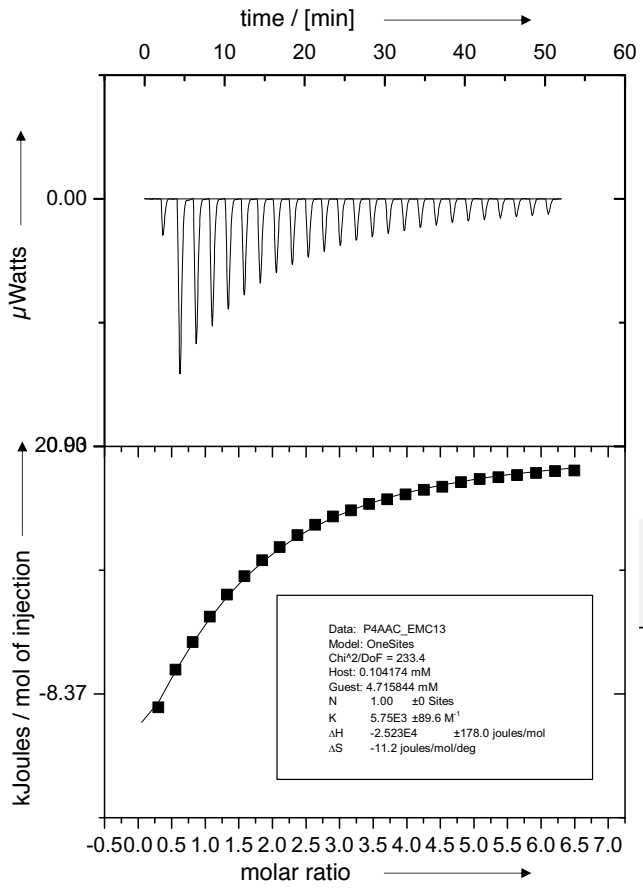

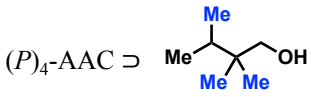

2,2,3-Trimethylbutan-1-ol

Host [mM]	Guest [mM]	$K_{a\ 303\ K}$ [M^{-1}]	ΔH [J mol^{-1}]	ΔS [J mol^{-1} K^{-1}]
0.1	4.7	$5.8 \cdot 10^3$	$-2.5 \cdot 10^4$	–11.2

In *n*-octane at 303 K

Figure S25. ITC binding isotherm of AAC $(P)_4$-**1** with 2,2,3-trimethylbutan-1-ol **9** in *n*-octane at 303 K. $K_a = 5.75 \cdot 10^3 \pm 0.09 \cdot 10^3\ M^{-1}$.

Table S25. Experimental values obtained from ITC titrations of AAC $(P)_4$-**1** with 2,2,3-trimethylbutan-1-ol **9** in *n*-octane calculated for 293 K.

K_a	$\Delta G_{293\ K}$	ΔH	$-T\Delta S_{293\ K}$
M^{-1}	[kcal mol^{-1}]	[kcal mol^{-1}]	[kcal mol^{-1}]
$8.2 \cdot 10^3$	–5.3	–6.0	+0.7

(±)-(2*S,3*R**)-2,3-Dichlorobutan-1-ol** (*R**,*S**)-**7**

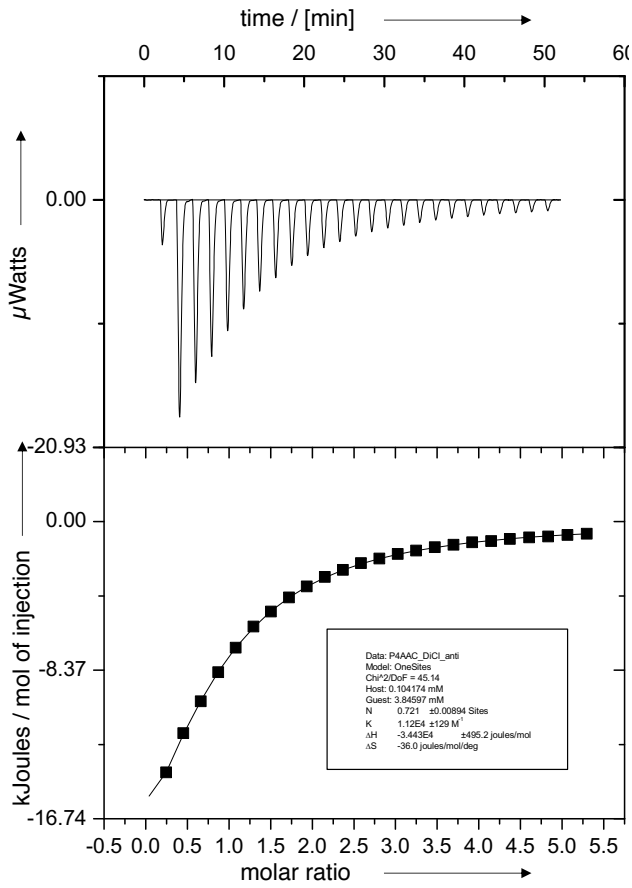

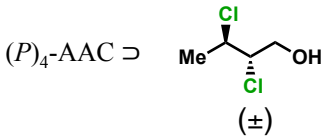

(±)-(2*S,3*R**)-2,3-Dichlorobutan-1-ol**

Host [mM]	Guest [mM]	$K_{a\ 303\ K}$ [M^{-1}]	ΔH [J mol^{-1}]	ΔS [J mol^{-1} K^{-1}]
0.1	3.9	$1.1 \cdot 10^4$	$-3.4 \cdot 10^4$	–36.0

In *n*-octane at 303 K

Figure S26. ITC binding isotherm of AAC $(P)_4$-**1** with (±)-(2*S**,3*R**)-2,3-dichlorobutan-1-ol (*R**,*S**)-**7** in *n*-octane at 303 K. $K_a = 1.12 \cdot 10^4 \pm 0.01 \cdot 10^4$ M^{-1}.

Table S26. Experimental values obtained from ITC titrations of AAC $(P)_4$-**1** with (±)-(2*S**,3*R**)-2,3-dichlorobutan-1-ol (*R**,*S**)-**7** in *n*-octane calculated for 293 K.

K_a	$\Delta G_{293\ K}$	ΔH	$-T\Delta S_{293\ K}$
M^{-1}	[kcal mol^{-1}]	[kcal mol^{-1}]	[kcal mol^{-1}]
$1.8 \cdot 10^4$	–5.7	–8.2	+2.5

(±)-(2*R,3*R**)-2,3-Dichlorobutan-1-ol** (*R**,*R**)-**7**

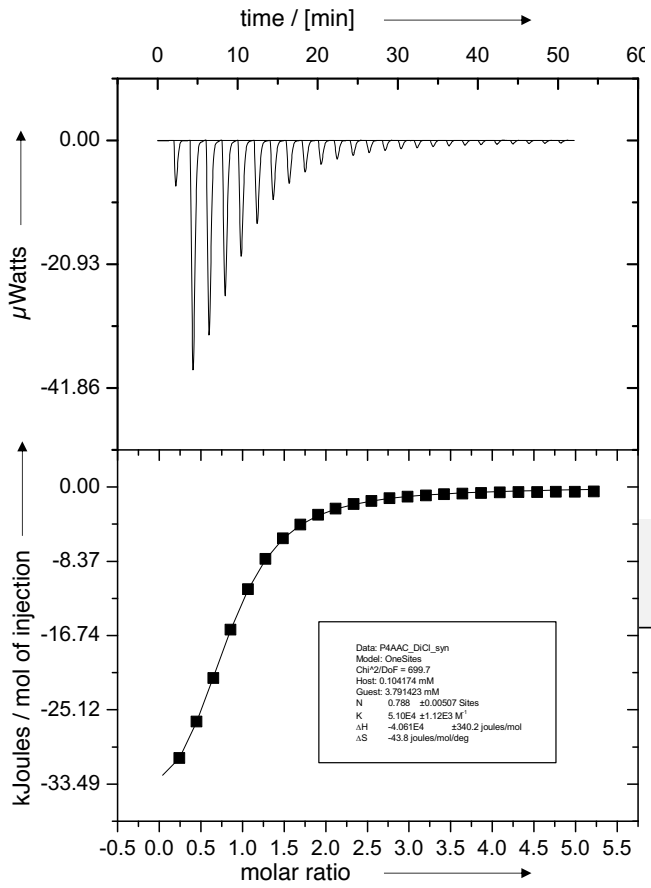

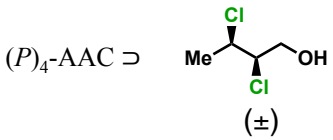

(±)-(2*R,3*R**)-2,3-Dichlorobutan-1-ol**

Host [mM]	Guest [mM]	$K_{a\ 303\ K}$ [M^{-1}]	ΔH [J mol^{-1}]	ΔS [J mol^{-1} K^{-1}]
0.1	3.8	$5.1 \cdot 10^4$	$-4.1 \cdot 10^4$	–43.8

In *n*-octane at 303 K

Figure S27. ITC binding isotherm of AAC (*P*)$_4$-**1** with (±)-(2*R**,3*R**)-2,3-dichlorobutan-1-ol (*R**,*R**)-**7** in *n*-octane at 303 K. $K_a = 5.10 \cdot 10^4 \pm 0.11 \cdot 10^4$ M^{-1}.

Table S27. Experimental values obtained from ITC titrations of AAC (*P*)$_4$-**1** with (±)-(2*R**,3*R**)-2,3-dichlorobutan-1-ol (*R**,*R**)-**7** in *n*-octane calculated for 293 K.

K_a	$\Delta G_{293\ K}$	ΔH	$-T\Delta S_{293\ K}$
M^{-1}	[kcal mol^{-1}]	[kcal mol^{-1}]	[kcal mol^{-1}]
$9.0 \cdot 10^4$	–6.6	–9.7	+3.1

(±)-(2*S,3*R**)-2,3-Dibromobutan-1-ol** (*R**,*S**)-**8**

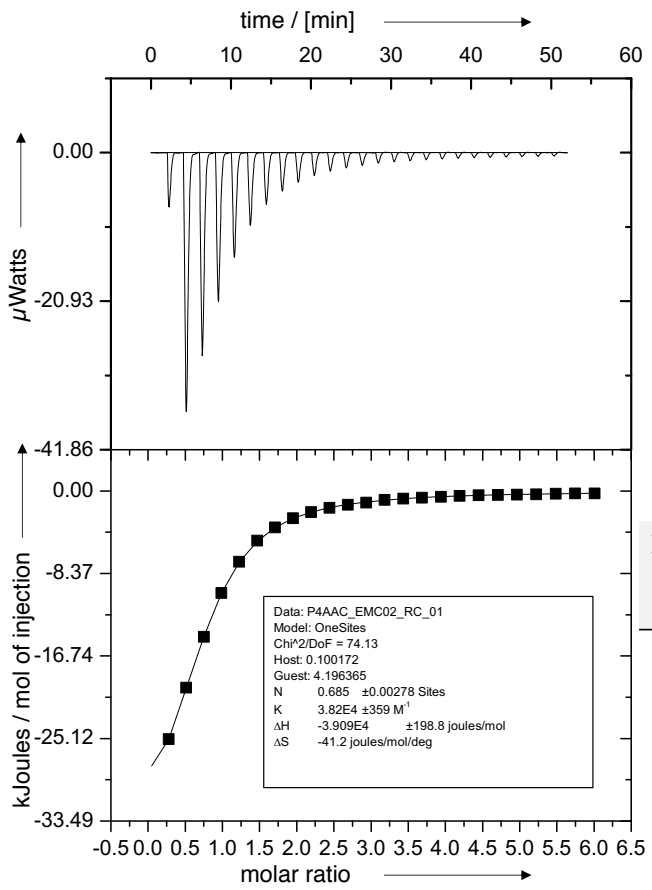

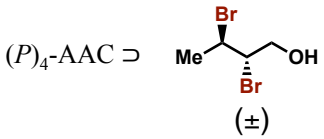

(±)

(±)-(2*S,3*R**)-2,3-Dibromobutan-1-ol**

Host [mM]	Guest [mM]	$K_{a\ 303\ K}$ [M^{-1}]	ΔH [J mol^{-1}]	ΔS [J mol^{-1} K^{-1}]
0.1	4.2	$3.8 \cdot 10^4$	$-3.9 \cdot 10^4$	–41.2

In *n*-octane at 303 K

Figure S28. ITC binding isotherm of AAC (*P*)$_4$-**1** with (±)-(2*S**,3*R**)-2,3-dibromobutan-1-ol (*R**,*S**)-**8** in *n*-octane at 303 K. $K_a = 3.82 \cdot 10^4 \pm 0.04 \cdot 10^4$ M^{-1}.

Table S28. Experimental values obtained from ITC titrations of AAC (*P*)$_4$-**1** with (±)-(2*S**,3*R**)-2,3-dibromobutan-1-ol (*R**,*S**)-**8** in *n*-octane calculated for 293 K.

K_a	$\Delta G_{293\ K}$	ΔH	$-T\Delta S_{293\ K}$
M^{-1}	[kcal mol^{-1}]	[kcal mol^{-1}]	[kcal mol^{-1}]
$6.6 \cdot 10^4$	–6.5	–9.4	+2.9

(–)-(2*R*,3*S*)-2,3-Dibromobutan-1-ol (*R*,*S*)-**8**

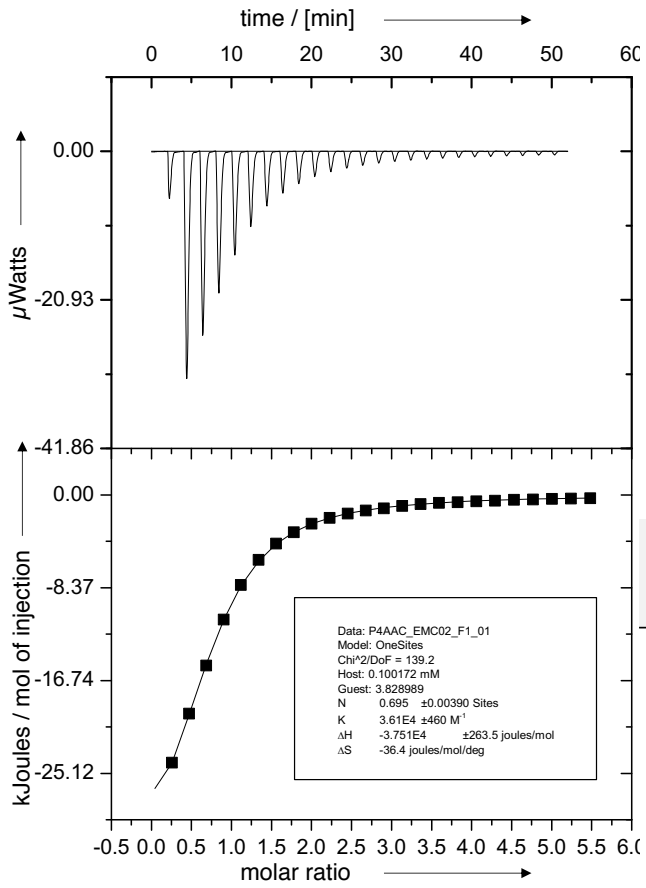

$(P)_4$-AAC ⊃

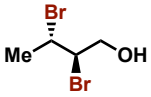

(*R*,*S*)

(–)-(2*R*,3*S*)-2,3-Dibromobutan-1-ol

Host [mM]	Guest [mM]	$K_{a\ 303\ K}$ [M^{-1}]	ΔH [J mol^{-1}]	ΔS [J mol^{-1} K^{-1}]
0.1	3.8	$3.6 \cdot 10^4$	$-3.8 \cdot 10^4$	–36.4

In *n*-octane at 303 K

Figure S29. ITC binding isotherm of AAC $(P)_4$-**1** with (–)-(2*R*,3*S*)-2,3-dibromobutan-1-ol (*R*,*S*)-**8** in *n*-octane at 303 K. $K_a = 3.61 \cdot 10^4 \pm 0.05 \cdot 10^4$ M^{-1}.

Table S29. Experimental values obtained from ITC titrations of AAC $(P)_4$-**1** with (–)-(2*R*,3*S*)-2,3-dibromobutan-1-ol (*R*,*S*)-**8** in *n*-octane calculated for 293 K.

K_a	$\Delta G_{293\ K}$	ΔH	$-T\Delta S_{293\ K}$
M^{-1}	[kcal mol^{-1}]	[kcal mol^{-1}]	[kcal mol^{-1}]
$6.1 \cdot 10^4$	–6.4	–8.9	+2.5

(+)-(2*S*,3*R*)-2,3-Dibromobutan-1-ol (*S*,*R*)-**8**

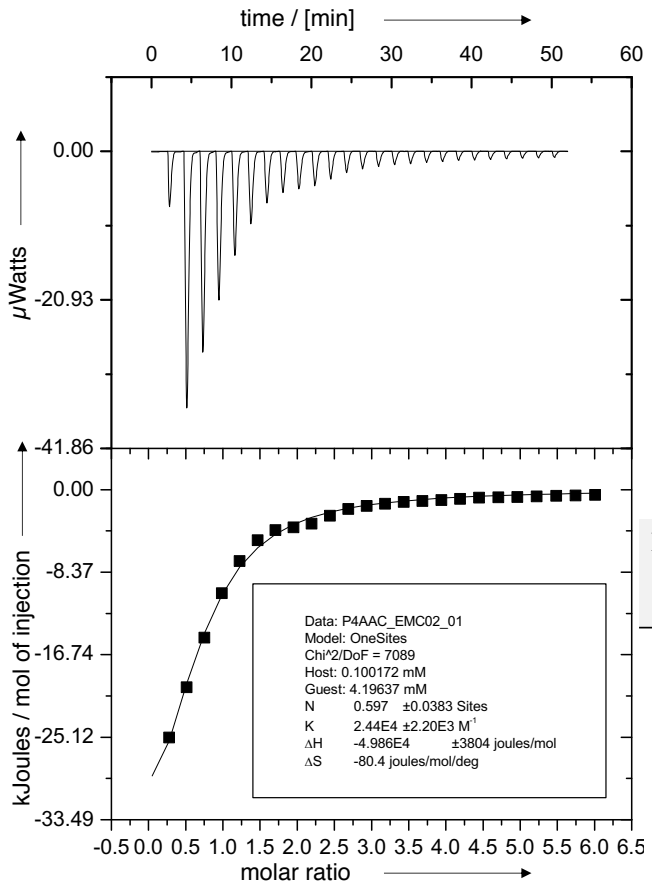

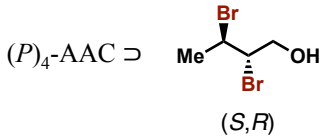

(+)-(2*S*,3*R*)-2,3-Dibromobutan-1-ol

Host [mM]	Guest [mM]	$K_{a\ 303\ K}$ [M^{-1}]	ΔH [J mol^{-1}]	ΔS [J mol^{-1} K^{-1}]
0.1	4.2	$2.4 \cdot 10^4$	$-5.0 \cdot 10^4$	–80.4

In *n*-octane at 303 K

Figure S30. ITC binding isotherm of AAC (*P*)$_4$-**1** with (+)-(2*S*,3*R*)-2,3-dibromobutan-1-ol (*S*,*R*)-**8** in *n*-octane at 303 K. $K_a = 2.44 \cdot 10^4 \pm 0.22 \cdot 10^4$ M^{-1}.

Table S30. Experimental values obtained from ITC titrations of AAC (*P*)$_4$-**1** with (+)-(2*S*,3*R*)-2,3-dibromobutan-1-ol (*S*,*R*)-**8** in *n*-octane calculated for 293 K.

K_a	$\Delta G_{293\ K}$	ΔH	$-T\Delta S_{293\ K}$
M^{-1}	[kcal mol^{-1}]	[kcal mol^{-1}]	[kcal mol^{-1}]
$4.9 \cdot 10^4$	–6.3	–11.9	+5.6

(±)-(2*R,3*R**)-2,3-Dibromobutan-1-ol** (*R**,*R**)-**8**

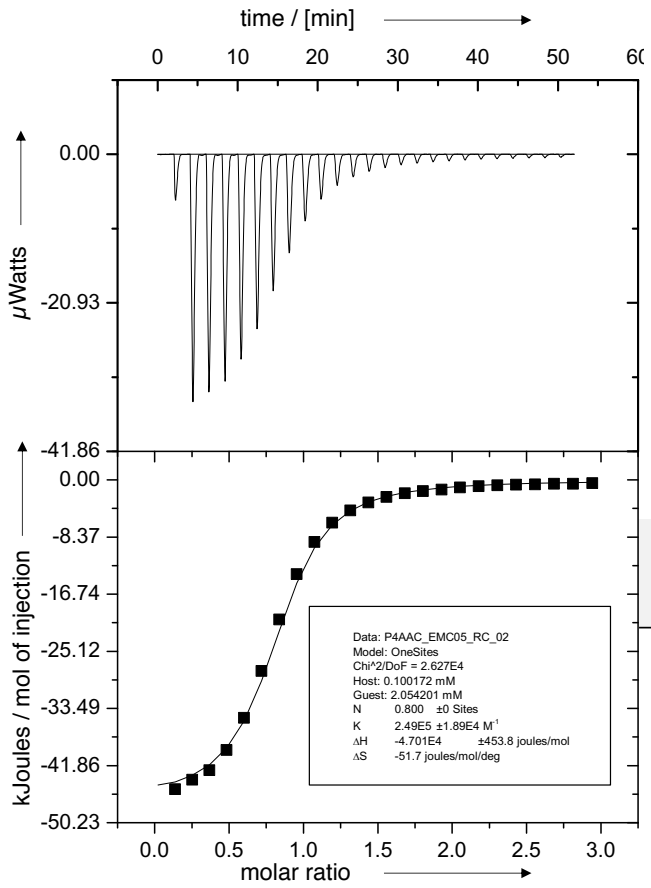

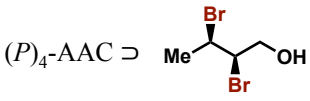

(±)

(±)-(2*R,3*R**)-2,3-Dibromobutan-1-ol**

Host [mM]	Guest [mM]	$K_{a\ 303\ K}$ [M^{-1}]	ΔH [J mol^{-1}]	ΔS [J mol^{-1} K^{-1}]
0.1	2.5	$2.5 \cdot 10^5$	$-4.7 \cdot 10^4$	–51.7

In *n*-octane at 303 K

Figure S31. ITC binding isotherm of AAC $(P)_4$-**1** with (±)-(2*R**,3*R**)-2,3-dibromobutan-1-ol (*R**,*R**)-**8** in *n*-octane at 303 K. $K_a = 2.49 \cdot 10^5 \pm 0.19 \cdot 10^5$ M^{-1}.

Table S31. Experimental values obtained from ITC titrations of AAC $(P)_4$-**1** with (±)-(2*R**,3*R**)-2,3-dibromobutan-1-ol (*R**,*R**)-**8** in *n*-octane calculated for 293 K.

K_a	$\Delta G_{293\ K}$	ΔH	$-T\Delta S_{293\ K}$
M^{-1}	[kcal mol^{-1}]	[kcal mol^{-1}]	[kcal mol^{-1}]
$4.8 \cdot 10^4$	–7.6	–11.2	+3.6

(+)-(2*R*,3*R*)-2,3-Dibromobutan-1-ol (*R*,*R*)-**8**

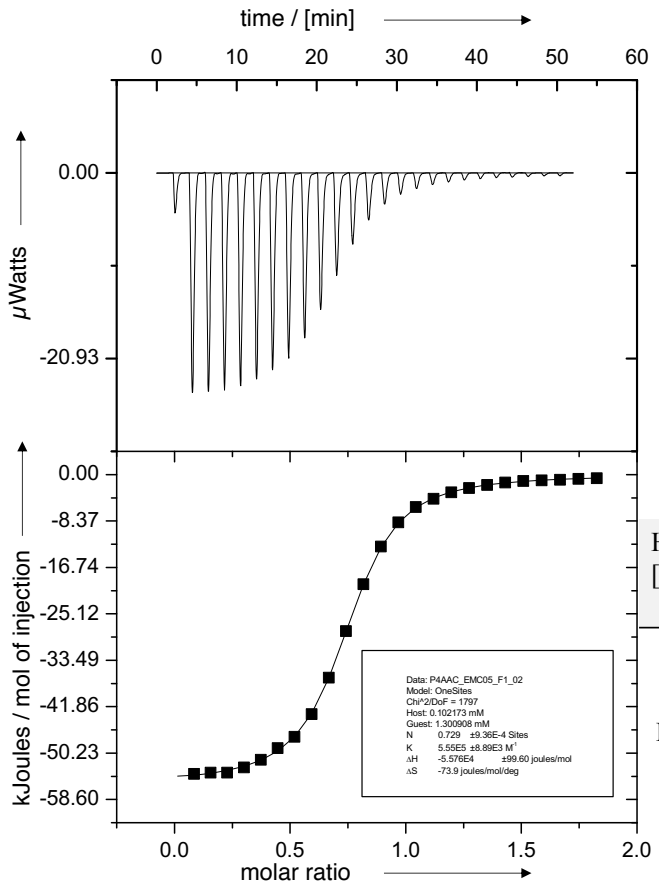

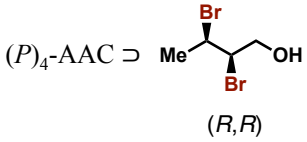

(+)-(2*R*,3*R*)-2,3-Dibromobutan-1-ol

Host [mM]	Guest [mM]	$K_{a\ 303\ K}$ [M^{-1}]	ΔH [J mol^{-1}]	ΔS [J mol^{-1} K^{-1}]
0.1	1.3	$5.6 \cdot 10^5$	$-5.6 \cdot 10^4$	–73.9

In *n*-octane at 303 K

Figure S32. ITC binding isotherm of AAC (*P*)$_4$-**1** with (+)-(2*R*,3*R*)-2,3-dibromobutan-1-ol (*R*,*R*)-**8** in *n*-octane at 303 K. $K_a = 5.55 \cdot 10^5 \pm 0.09 \cdot 10^5\ M^{-1}$.

Table S32. Experimental values obtained from ITC titrations of AAC (*P*)$_4$-**1** with (+)-(2*R*,3*R*)-2,3-dibromobutan-1-ol (*R*,*R*)-**8** in *n*-octane calculated for 293 K.

K_a	$\Delta G_{293\ K}$	ΔH	$-T\Delta S_{293\ K}$
M^{-1}	[kcal mol^{-1}]	[kcal mol^{-1}]	[kcal mol^{-1}]
$1.2 \cdot 10^6$	–8.1	–13.3	+5.2

(–)-(2*S*,3*S*)-2,3-Dibromobutan-1-ol (*S*,*S*)-**8**

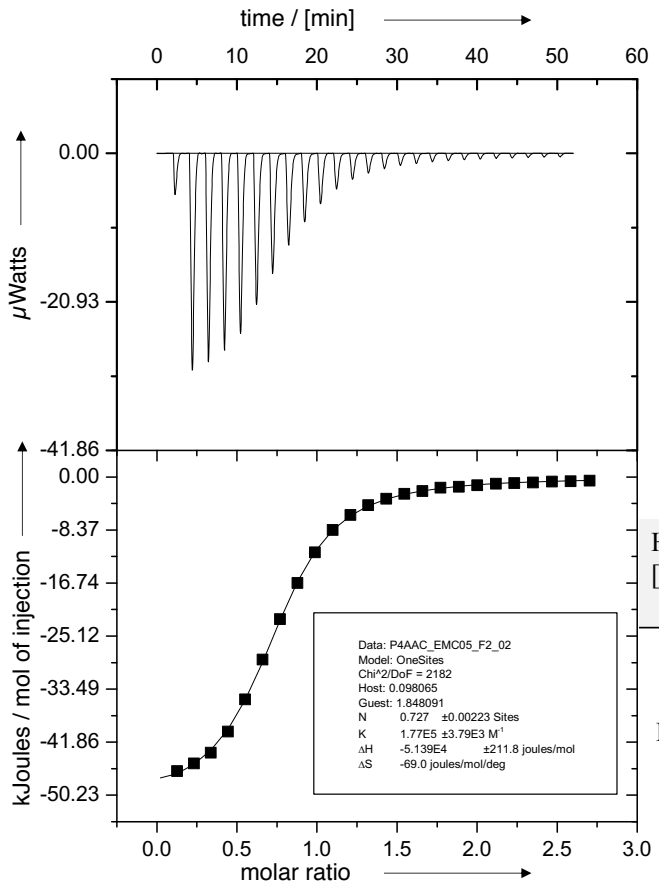

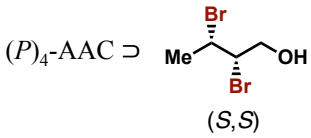

(–)-(2*S*,3*S*)-2,3-Dibromobutan-1-ol

Host [mM]	Guest [mM]	$K_{a\ 303\ K}$ [M^{-1}]	ΔH [J mol^{-1}]	ΔS [J mol^{-1} K^{-1}]
0.1	1.9	$1.8 \cdot 10^5$	$-5.1 \cdot 10^4$	–69.0

In *n*-octane at 303 K

Figure S33. ITC binding isotherm of AAC (*P*)$_4$-**1** with (–)-(2*S*,3*S*)-2,3-dibromobutan-1-ol (*S*,*S*)-**8** in *n*-octane at 303 K. $K_a = 1.77 \cdot 10^5 \pm 0.04 \cdot 10^5$ M^{-1}.

Table S33. Experimental values obtained from ITC titrations of AAC (*P*)$_4$-**1** with (–)-(2*S*,3*S*)-2,3-dibromobutan-1-ol (*S*,*S*)-**8** in *n*-octane calculated for 293 K.

K_a	$\Delta G_{293\ K}$	ΔH	$-T\Delta S_{293\ K}$
M^{-1}	[kcal mol^{-1}]	[kcal mol^{-1}]	[kcal mol^{-1}]
$3.6 \cdot 10^5$	–7.5	–12.3	+4.8

(±)-(2*S,3*R**)-2,3-Dibromo-2-methylbutan-1-ol** (*R**,*S**)-**10**

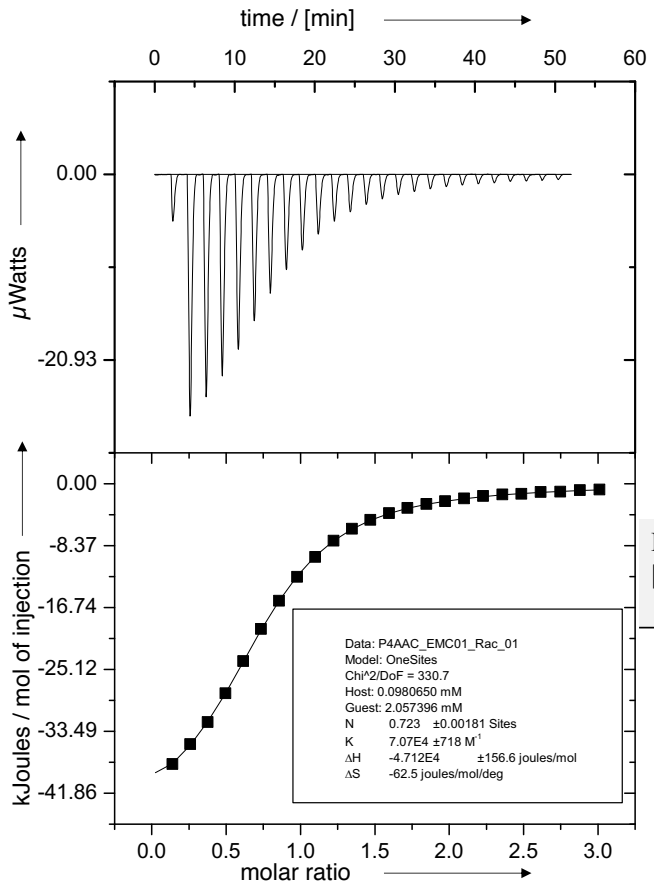

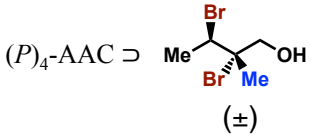

(±)-(2*S,3*R**)-2,3-Dibromo-2-methylbutan-1-ol**

Host [mM]	Guest [mM]	$K_{a\ 303\ K}$ [M^{-1}]	ΔH [J mol^{-1}]	ΔS [J mol^{-1} K^{-1}]
0.1	2.1	$7.1 \cdot 10^4$	$-4.7 \cdot 10^4$	–62.5

In *n*-octane at 303 K

Figure S34. ITC binding isotherm of AAC $(P)_4$-**1**C with (±)-(2*S**,3*R**)-2,3-dibromo-2-methylbutan-1-ol (*R**,*S**)-**10** in *n*-octane at 303 K. $K_a = 7.1 \cdot 10^4 \pm 0.07 \cdot 10^4$ M^{-1}.

Table S34. Experimental values obtained from ITC titrations of AAC $(P)_4$-**1** with (±)-(2*S**,3*R**)-2,3-dibromo-2-methylbutan-1-ol (*R**,*S**)-**10** in *n*-octane calculated for 293 K.

K_a	$\Delta G_{293\ K}$	ΔH	$-T\Delta S_{293\ K}$
M^{-1}	[kcal mol^{-1}]	[kcal mol^{-1}]	[kcal mol^{-1}]
$1.4 \cdot 10^5$	–6.9	–11.1	+4.2

(±)-(2*R,3*R**)-2,3-Dibromo-2-methylbutan-1-ol** (*R**,*R**)**-10**

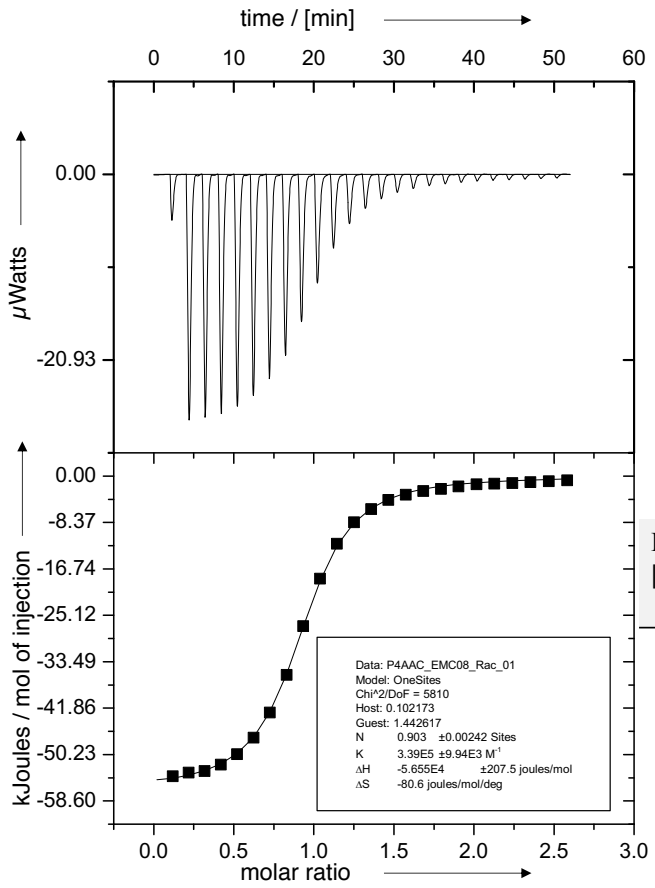

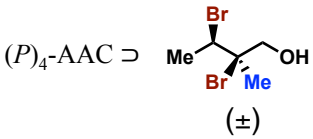

(±)-(2*R,3*R**)-2,3-Dibromo-2-methylbutan-1-ol**

Host [mM]	Guest [mM]	$K_{a\ 303\ K}$ [M^{-1}]	ΔH [J mol^{-1}]	ΔS [J mol^{-1} K^{-1}]
0.1	1.4	$3.4 \cdot 10^5$	$-5.7 \cdot 10^4$	–80.6

In *n*-octane at 303 K

Figure S35. ITC binding isotherm of AAC $(P)_4$-**1** with (±)-(2*R**,3*R**)-2,3-dibromo-2-methylbutan-1-ol (*R**,*R**)-**10** in *n*-octane at 303 K. $K_a = 3.39 \cdot 10^5 \pm 0.10 \cdot 10^5$ M^{-1}.

Table S35. Experimental values obtained from ITC titrations of AAC $(P)_4$-**1** with (±)-(2*R**,3*R**)-2,3-dibromo-2-methylbutan-1-ol (*R**,*R**)-**10** in *n*-octane calculated for 293 K.

K_a	$\Delta G_{293\ K}$	ΔH	$-T\Delta S_{293\ K}$
M^{-1}	[kcal mol^{-1}]	[kcal mol^{-1}]	[kcal mol^{-1}]
$7.4 \cdot 10^5$	–7.9	–13.5	+5.6

(+)-(2*R*,3*R*)-2,3-Dibromo-2-methylbutan-1-ol (*R*,*R*)**-10**

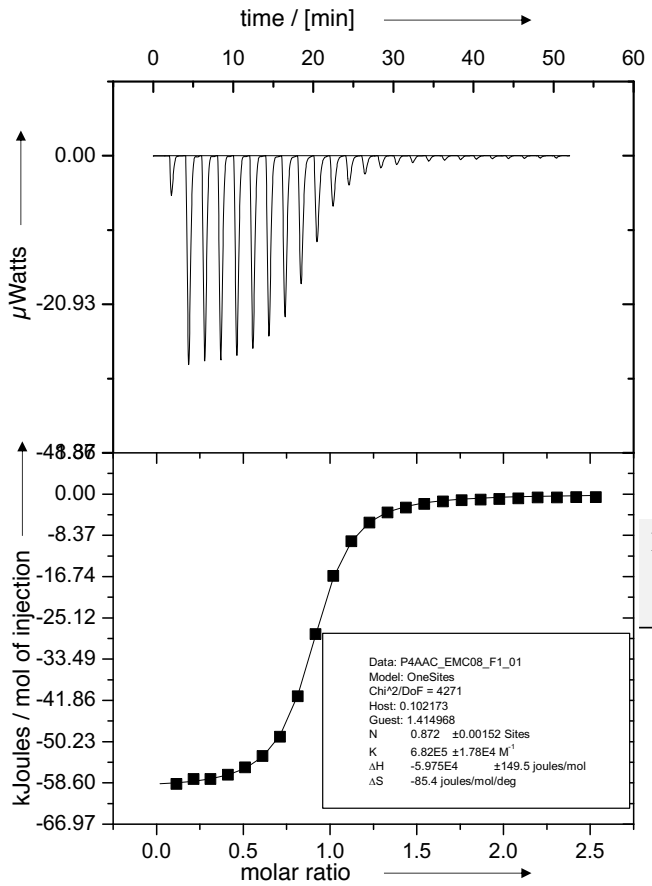

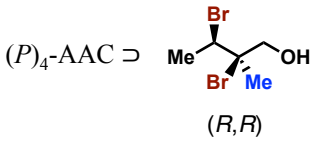

(+)-(2*R*,3*R*)-2,3-Dibromo-2-methylbutan-1-ol

Host [mM]	Guest [mM]	$K_{a\ 303\ K}$ [M^{-1}]	ΔH [J mol^{-1}]	ΔS [J mol^{-1} K^{-1}]
0.1	1.4	$6.8 \cdot 10^5$	$-6.0 \cdot 10^4$	–85.4

In *n*-octane at 303 K

Figure S36. ITC binding isotherm of AAC (*P*)$_4$-**1** with (+)-(2*R*,3*R*)-2,3-dibromo-2-methylbutan-1-ol (*R*,*R*)-**10** in *n*-octane at 303 K. $K_a = 6.82 \cdot 10^5 \pm 0.18 \cdot 10^5$ M^{-1}.

Table S36. Experimental values obtained from ITC titrations of AAC (*P*)$_4$-**1** with (+)-(2*R*,3*R*)-2,3-dibromo-2-methylbutan-1-ol (*R*,*R*)-**10** in *n*-octane calculated for 293 K.

K_a	$\Delta G_{293\ K}$	ΔH	$-T\Delta S_{293\ K}$
M^{-1}	[kcal mol^{-1}]	[kcal mol^{-1}]	[kcal mol^{-1}]
$1.6 \cdot 10^6$	–8.3	–14.3	+6.0

(–)-(2*S*,3*S*)-2,3-Dibromo-2-methylbutan-1-ol (*S*,*S*)-**10**

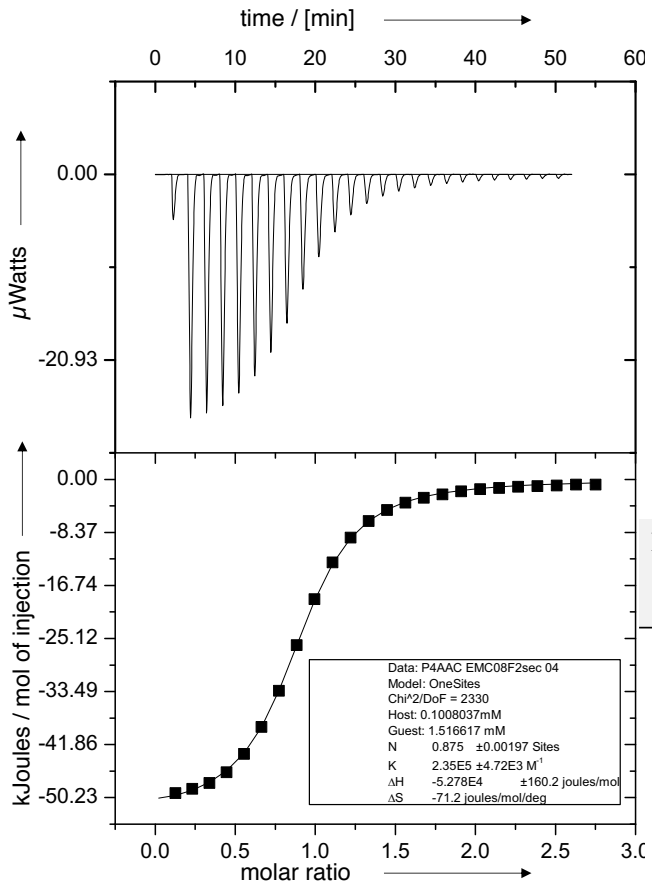

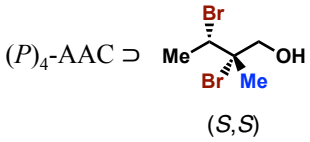

(*S*,*S*)

(–)-(2*S*,3*S*)-2,3-Dibromo-2-methylbutan-1-ol

Host [mM]	Guest [mM]	$K_{a\ 303\ K}$ [M^{-1}]	ΔH [J mol^{-1}]	ΔS [J mol^{-1} K^{-1}]
0.1	1.5	$2.4 \cdot 10^5$	$-5.3 \cdot 10^4$	–71.2

In *n*-octane at 303 K

Figure S37. ITC binding isotherm of AAC (*P*)$_4$-**1** with (–)-(2*S*,3*S*)-2,3-dibromo-2-methylbutan-1-ol (*S*,*S*)-**10** in *n*-octane at 303 K. $K_a = 2.35 \cdot 10^5 \pm 0.05 \cdot 10^5$ M^{-1}.

Table S37. Experimental values obtained from ITC titrations of AAC (*P*)$_4$-**1** with (–)-(2*S*,3*S*)-2,3-dibromo-2-methylbutan-1-ol (*S*,*S*)-**10** in *n*-octane calculated for 293 K.

K_a	$\Delta G_{293\ K}$	ΔH	$-T\Delta S_{293\ K}$
M^{-1}	[kcal mol^{-1}]	[kcal mol^{-1}]	[kcal mol^{-1}]
$4.9 \cdot 10^5$	–7.6	–12.6	+5.0

(±)-(2*S,3*R**)-2,3-Dibromo-4,4,4-trifluorobutan-1-ol** (*R**,*S**)-**11**

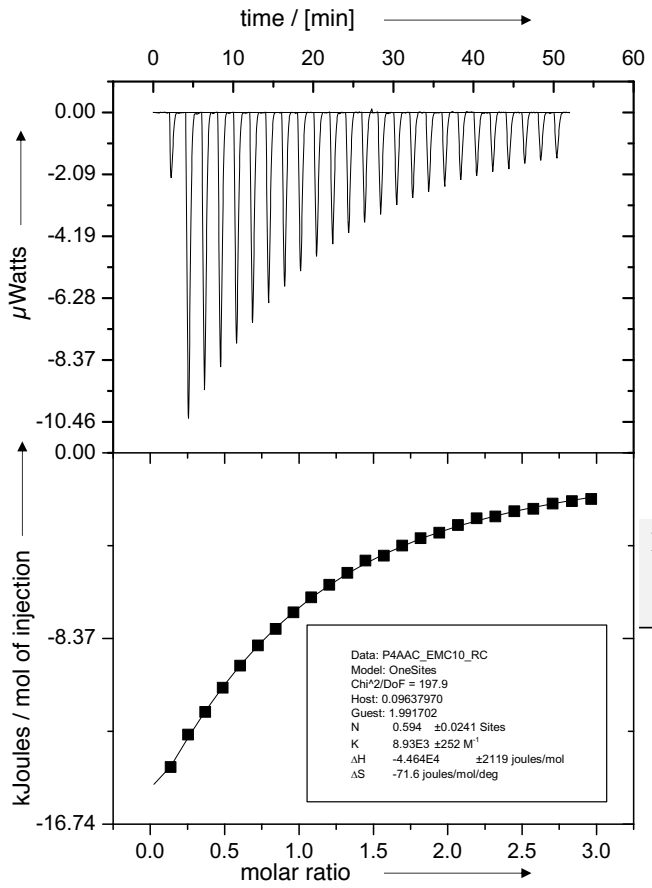

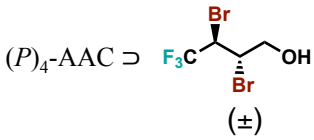

(±)-(2*S,3*R**)-2,3-Dibromo-4,4,4-trifluorobutan-1-ol**

Host [mM]	Guest [mM]	$K_{a\ 303\ K}$ [M^{-1}]	ΔH [J mol^{-1}]	ΔS [J mol^{-1} K^{-1}]
0.1	2.0	$8.9 \cdot 10^3$	$-4.5 \cdot 10^4$	–71.2

In *n*-octane at 303 K

Figure S38. ITC binding isotherm of AAC (*P*)$_4$-**1** with (±)-(2*S**,3*R**)-2,3-dibromo-4,4,4-trifluorobutan-1-ol (*R**,*S**)-**11** in *n*-octane at 303 K. $K_a = 8.93 \cdot 10^3 \pm 0.25 \cdot 10^3$ M^{-1}.

Table S38. Experimental values obtained from ITC titrations of AAC (*P*)$_4$-**1** with (±)-(2*S**,3*R**)-2,3-dibromo-4,4,4-trifluorobutan-1-ol (*R**,*S**)-**11** in *n*-octane calculated for 293 K.

K_a	$\Delta G_{293\ K}$	ΔH	$-T\Delta S_{293\ K}$
M^{-1}	[kcal mol^{-1}]	[kcal mol^{-1}]	[kcal mol^{-1}]
$1.7 \cdot 10^4$	–5.7	–10.7	+5.0

(±)-((2*R,3*R**)-2,3-Dibromo-4,4,4-trifluoro-2-methylbutan-1-ol** (*R**,*S**)-**12**

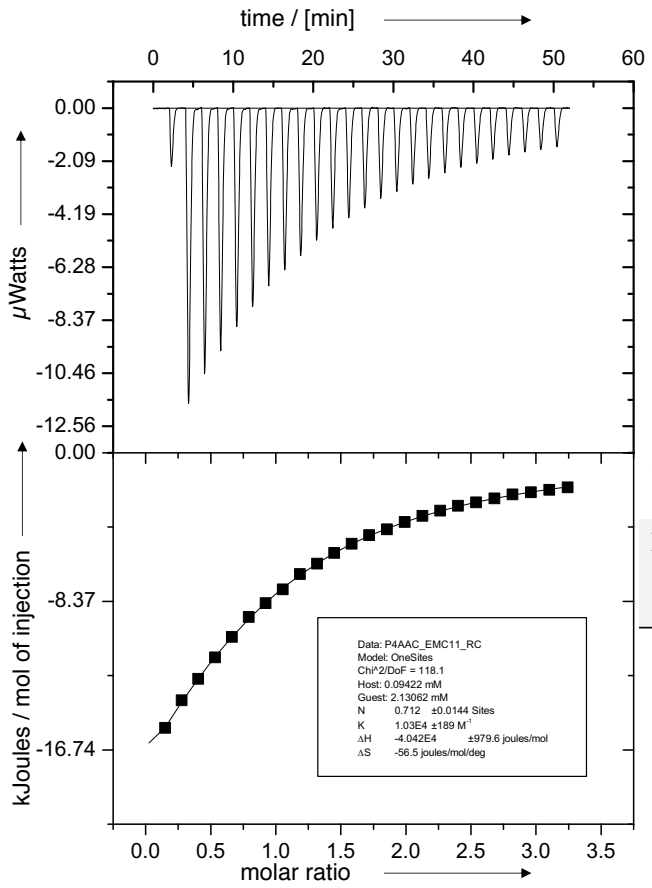

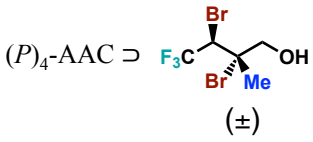

(±)

(±)-((2*R,3*R**)-2,3-Dibromo-4,4,4-trifluoro-2-methylbutan-1-ol**

Host [mM]	Guest [mM]	$K_{a\ 303\ K}$ [M^{-1}]	ΔH [J mol^{-1}]	ΔS [J mol^{-1} K^{-1}]
0.1	2.1	$1.0 \cdot 10^4$	$-4.0 \cdot 10^4$	–56.5

In *n*-octane at 303 K

Figure S39. ITC binding isotherm of AAC (*P*)$_4$-**1** with (±)-((2*R**,3*R**)-2,3-dibromo-4,4,4-trifluoro-2-methylbutan-1-ol (*R**,*S**)-**12** in *n*-octane at 303 K. $K_a = 1.03 \cdot 10^4 \pm 0.02 \cdot 10^4$ M^{-1}.

Table S39. Experimental values obtained from ITC titrations of AAC (*P*)$_4$-**1** with (±)-(2*R**,3*R**)-2,3-dibromo-4,4,4-trifluoro-2-methylbutan-1-ol (*R**,*S**)-**12** in *n*-octane calculated for 293 K.

K_a	$\Delta G_{293\ K}$	ΔH	$-T\Delta S_{293\ K}$
M^{-1}	[kcal mol^{-1}]	[kcal mol^{-1}]	[kcal mol^{-1}]
$1.8 \cdot 10^4$	–5.7	–9.7	+4.0

S6. Summary of Association Constants Obtained from ECD Spectroscopic and ITC Titrations

Table S40. Summary of association constants K_a as determined by ECD titrations in *n*-octane. $\Delta G_{293\ K}$ was calculated from K_a at 293 K. Errors in K_a are estimated to be in the range of ±20%.

Host: AAC $(P)_4$-**1** Entry	Guest	ITC K_a [M^{-1}]	ECD K_a [M^{-1}]	ITC $\Delta G_{293\ K}$ [kcal mol^{-1}]	ECD $\Delta G_{293\ K}$ [kcal mol^{-1}]
1	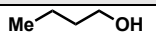	–	<1	–	–
2	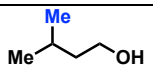	$(1.6 \pm 0.3) \cdot 10^3$	$(1.5 \pm 0.3) \cdot 10^3$	–4.3 ± 0.2	–4.3 ± 0.2
3	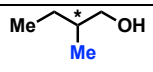 (±)	$(4.6 \pm 0.9) \cdot 10^3$	$(2.3 \pm 0.5) \cdot 10^3$	–4.9 ± 0.2	–4.5 ± 0.2
4		$(2.0 \pm 0.4) \cdot 10^4$	$(1.7 \pm 0.3) \cdot 10^4$	–5.8 ± 0.2	–5.7 ± 0.2
5	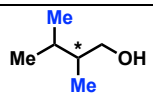 (±)	$(9.9 \pm 2.0) \cdot 10^3$	$(5.9 \pm 1.2) \cdot 10^3$	–5.1 ± 0.2	–5.4 ± 0.2
6	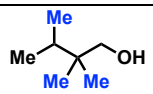	$(6.9 \pm 1.4) \cdot 10^3$	$(8.2 \pm 1.6) \cdot 10^3$	–5.1 ± 0.2	–5.2 ± 0.2
7	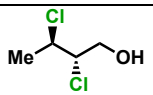 (±)	$(1.1 \pm 0.2) \cdot 10^4$	$(1.8 \pm 0.4) \cdot 10^4$	–5.7 ± 0.2	–5.4 ± 0.2
8	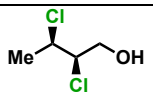 (±)	$(9.0 \pm 1.8) \cdot 10^4$	$(7.0 \pm 1.4) \cdot 10^4$	–6.5 ± 0.2	–6.6 ± 0.2
9	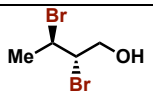 (±)	$(6.6 \pm 1.3) \cdot 10^4$	$(7.6 \pm 1.5) \cdot 10^4$	–6.5 ± 0.2	–6.5 ± 0.2
10	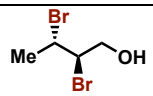 (*R*,*S*)	$(6.1 \pm 1.2) \cdot 10^4$	$(6.1 \pm 1.2) \cdot 10^4$	–6.4 ± 0.2	–6.4 ± 0.2
11	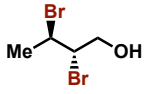 (*S*,*R*)	$(4.9 \pm 1.0) \cdot 10^4$	$(6.0 \pm 1.2) \cdot 10^4$	–6.3 ± 0.2	–6.4 ± 0.2
12	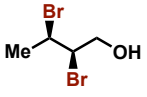 (±)	$(4.8 \pm 1.0) \cdot 10^5$	$(3.8 \pm 0.8) \cdot 10^5$	–7.6 ± 0.2	–7.5 ± 0.2

13	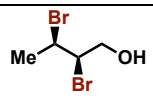 (*R*,*R*)	$(1.2 \pm 0.2)\cdot 10^6$	$(1.2 \pm 0.2)\cdot 10^6$	-8.2 ± 0.2	-8.1 ± 0.2
14	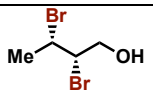 (*S*,*S*)	$(1.8 \pm 0.4)\cdot 10^5$	$(2.8 \pm 0.6)\cdot 10^5$	-7.5 ± 0.2	-7.3 ± 0.2
15	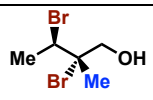 (±)	$(1.4 \pm 0.3)\cdot 10^5$	$(1.2 \pm 0.2)\cdot 10^5$	-6.9 ± 0.2	-6.8 ± 0.2
16	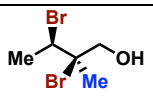 (±)	$(3.8 \pm 0.8)\cdot 10^5$	$(7.4 \pm 1.5)\cdot 10^5$	-7.9 ± 0.2	-7.5 ± 0.2
17	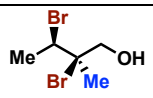 (*R*,*R*)	$(1.6 \pm 0.3)\cdot 10^6$	$(1.0 \pm 0.2)\cdot 10^6$	-8.3 ± 0.2	-8.1 ± 0.2
18	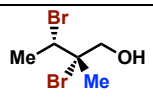 (*S*,*S*)	$(4.9 \pm 1.0)\cdot 10^5$	$(1.3 \pm 0.3)\cdot 10^6$	-7.6 ± 0.2	-8.2 ± 0.2
19	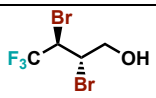 (±)	$(1.7 \pm 0.3)\cdot 10^4$	$(1.3 \pm 0.3)\cdot 10^4$	-5.7 ± 0.2	-5.5 ± 0.2
20	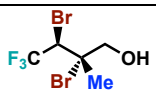 (±)	$(1.8 \pm 0.4)\cdot 10^4$	$(1.2 \pm 0.2)\cdot 10^4$	-5.7 ± 0.2	-5.5 ± 0.2

S7. Comparison of the Gibbs Binding Energies for Selected Methyl- and Bromo-Containing Alcohols

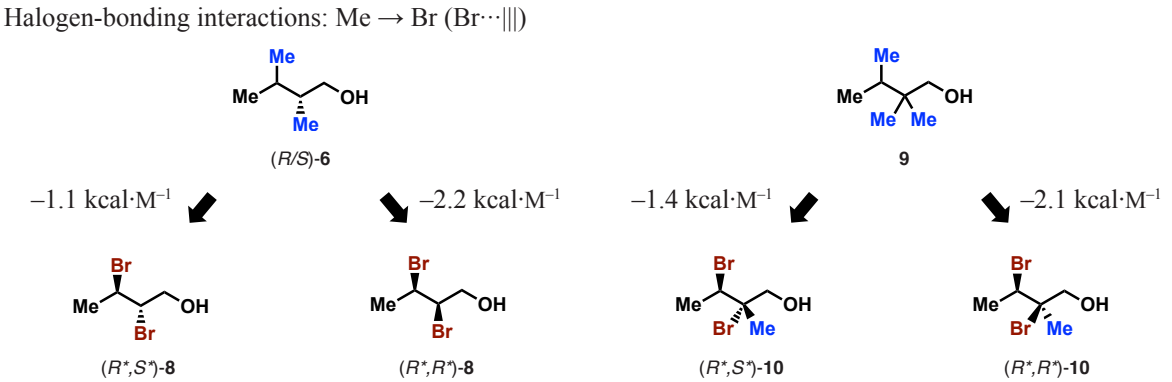

Figure S40. Comparison of the differences in Gibbs binding energies of binding $\Delta\Delta G_{293\ K}$ in kcal mol^{-1} obtained from ECD spectroscopic titrations of the 2,3-dimethylbutanol (*R*/S)-**6** (left) and 2,2,3-trimethylbutanol **9** bound to AAC (*P*)$_4$-**1** with their *anti*- and *syn*-configured bromo analogues **8** and **10**.[7]

S8. NMR Spectra of (*P*)$_4$-Configured AAC with Guest Molecules

Figure S41 displays the protons which were monitored during guest addition to a solution of AAC (*P*)$_4$-**1** in [D$_{18}$]*n*-octane. 1D and 2D NMR spectra of the host–guest complexes were recorded on a Bruker AVIII 600 Ultra Shell spectrometer equipped with a Prodigy Cryo Probe (600 MHz for ^{1}H; 150 MHz for ^{13}C). Low temperature 1D NMR spectroscopic measurements were conducted on a Bruker spectrometer equipped with a Prodigy Cryo Probe (500 MHz for ^{1}H).

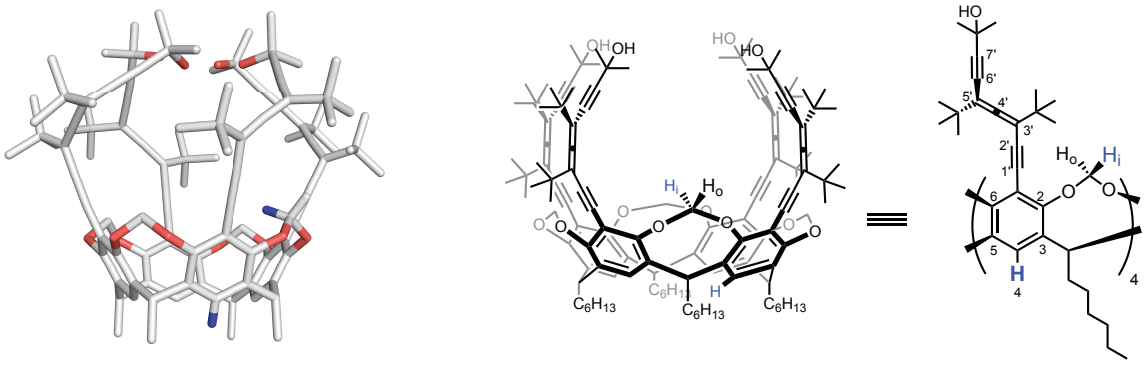

Figure S41. Protons, which were monitored during the binding studies, are highlighted in blue.

Preparation of solutions for NMR spectroscopic experiments (1D and 2D): A solution of the AAC (*P*)$_4$-**1** or (*M*)$_4$-**1**, referred to as "host", was prepared gravimetrically (~10 mM) in [D$_{18}$]*n*-octane. A second solution of the "guest" (**2**–**12**) was prepared gravimetrically in [D$_{18}$]*n*-octane and subsequently added to the host-solution. Slow exchange of the guests on the NMR timescale allowed for full characterization of the host–guest complexes. In ROESY NMR

studies, significant correlation of the guests with the inward pointing H_i of the host was observed. ROESY NMR spectra are shown for selected host–guest complexes.

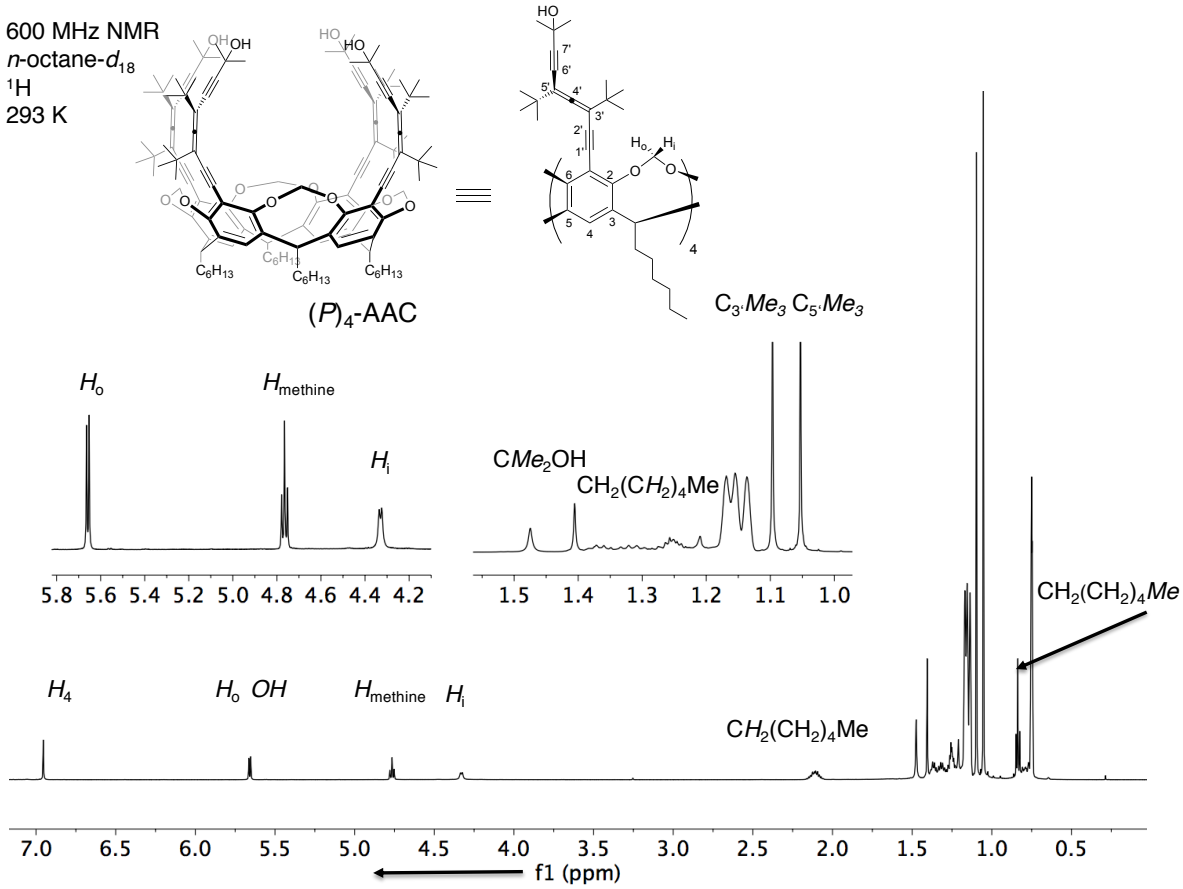

Figure S42. ^{1}H NMR (600 MHz) traces of AAC $(P)_4$-**1** (6 mM) in [D_{18}]*n*-octane at 293 K. Host-resonances: H_i = inside protons and H_o = outside protons of the methylene bridge; H_4 = aromatic protons, highlighted in Figure S41.

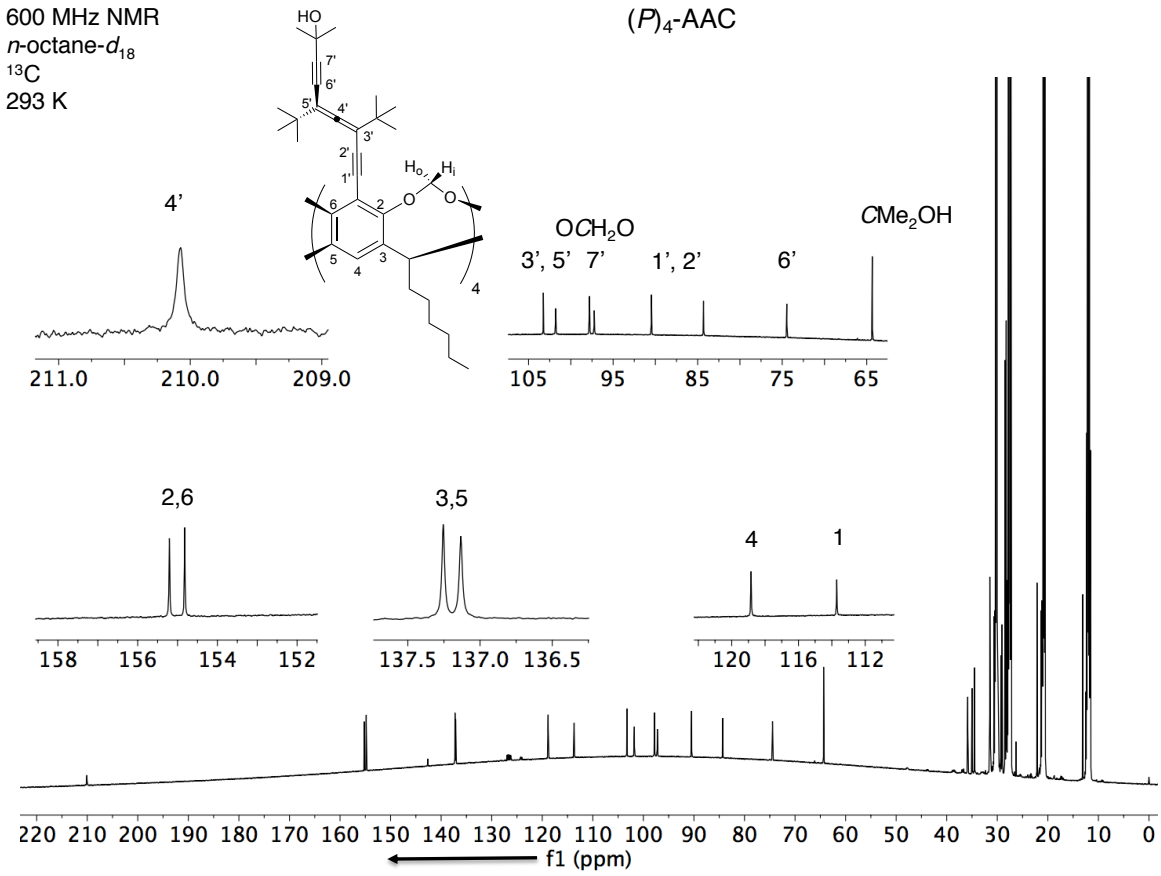

Figure S43. ^{13}C NMR (150 MHz) traces of AAC (*P*)$_4$-**1** (6 mM) in [D$_{18}$]*n*-octane at 293 K. Corresponding host-resonances are highlighted in Figure S41.

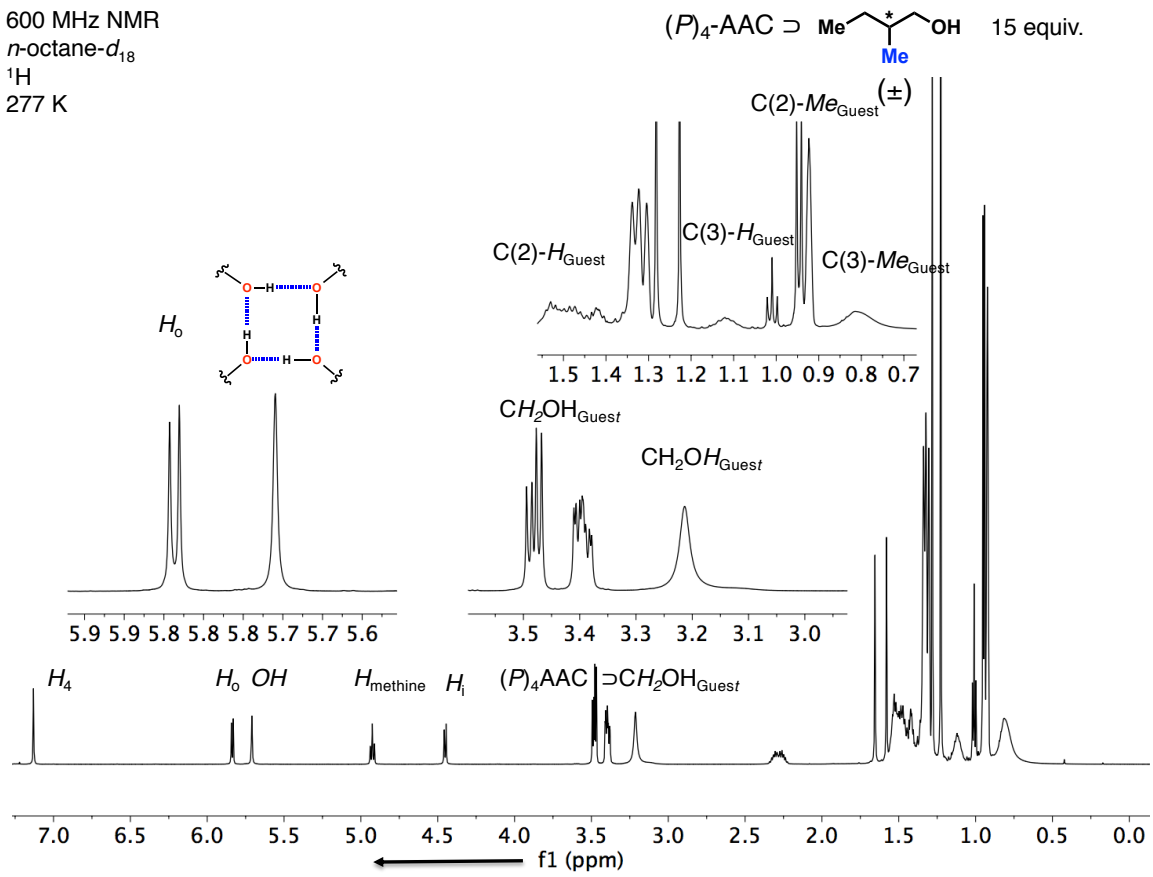

Figure S44. ^{1}H NMR (600 MHz) traces of AAC (*P*)$_4$-**1** (7.0 mM) in [D$_{18}$]*n*-octane at 277 K with 15 equiv. of (*R*/*S*)-**4**.. Host-resonances: H$_i$ = inside protons and H$_o$ = outside protons of the methylene bridge; H$_4$ = aromatic protons, highlighted in Figure S41.

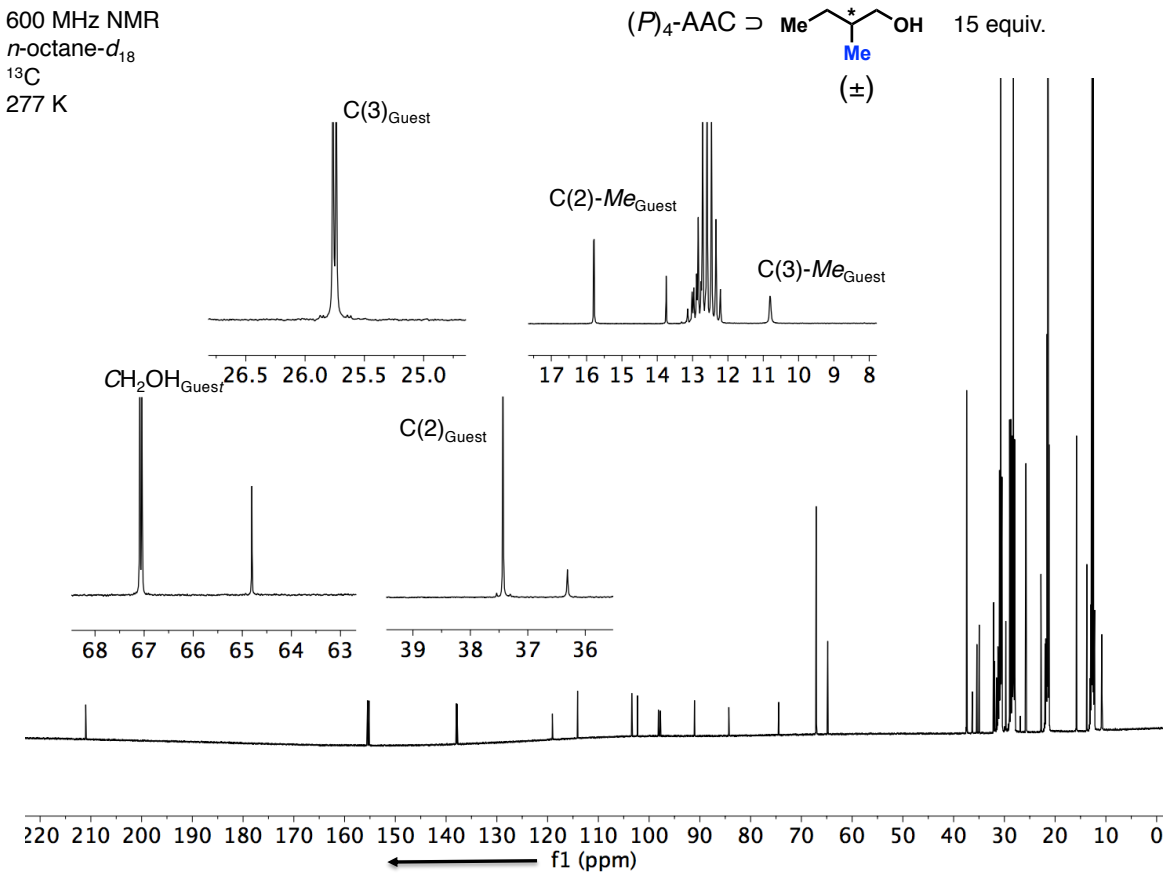

Figure S45. ^{13}C NMR (150 MHz) traces of AAC (*P*)$_4$-**1** (7.0 mM) in [D$_{18}$]*n*-octane at 277 K with 15 equiv. of (*R*/*S*)-**4**.

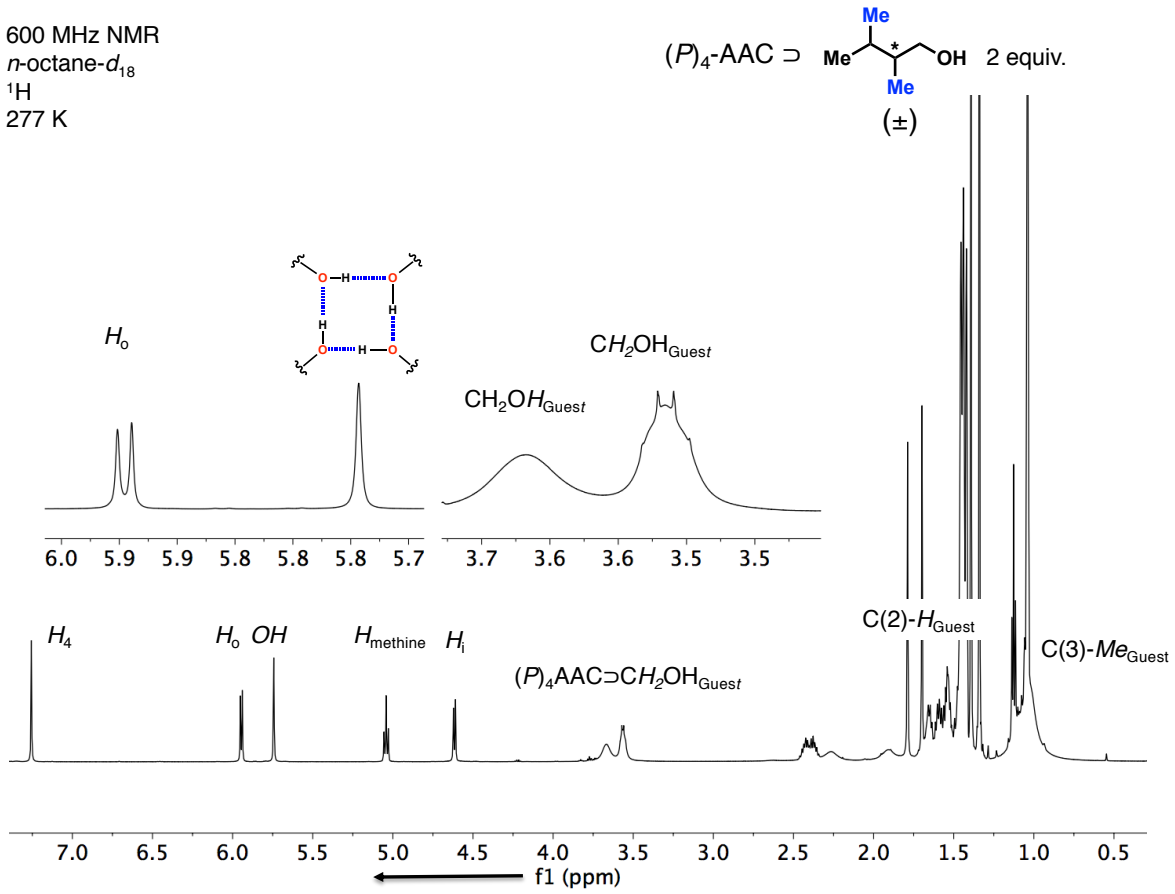

Figure S46. ^{1}H NMR (600 MHz) traces of AAC $(P)_4$-**1** (7.0 mM) in [D_{18}]*n*-octane at 277 K with 2 equiv. of (*R*/*S*)-**6**. Host-resonances: H_i = inside protons and H_o = outside protons of the methylene bridge; H_4 = aromatic protons, highlighted in Figure S41.

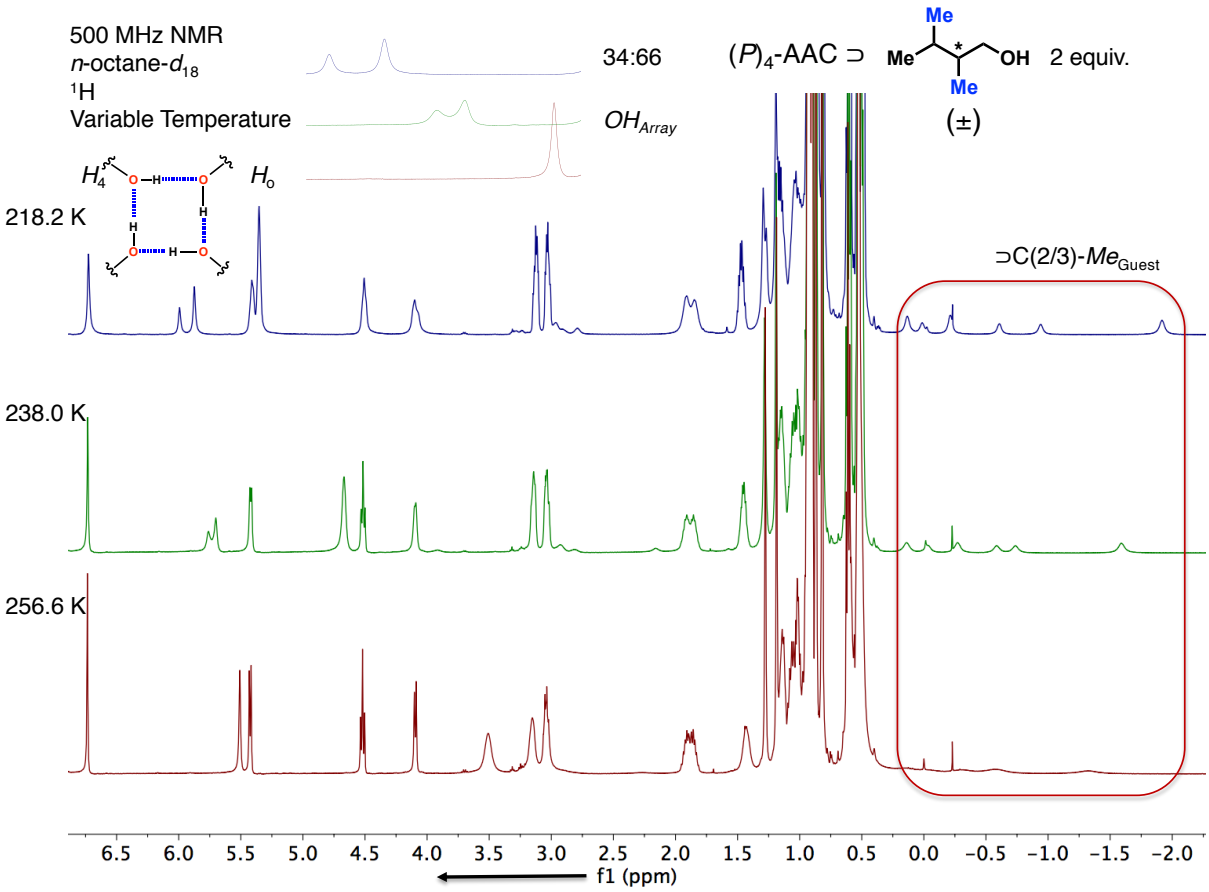

Figure S47. VT-^{1}H NMR (500 MHz) traces of AAC $(P)_4$-**1** (7.0 mM) in [D_{18}]*n*-octane at 277 K with 2 equiv. of (*R*/*S*)-**6**. Host-resonances: H_i = inside protons and H_o = outside protons of the methylene bridge; H_4 = aromatic protons, highlighted in Figure S41. Splitting of the Host-OH-resonances correspond to the diastereoisomeric complexes of the host–guest complexes.

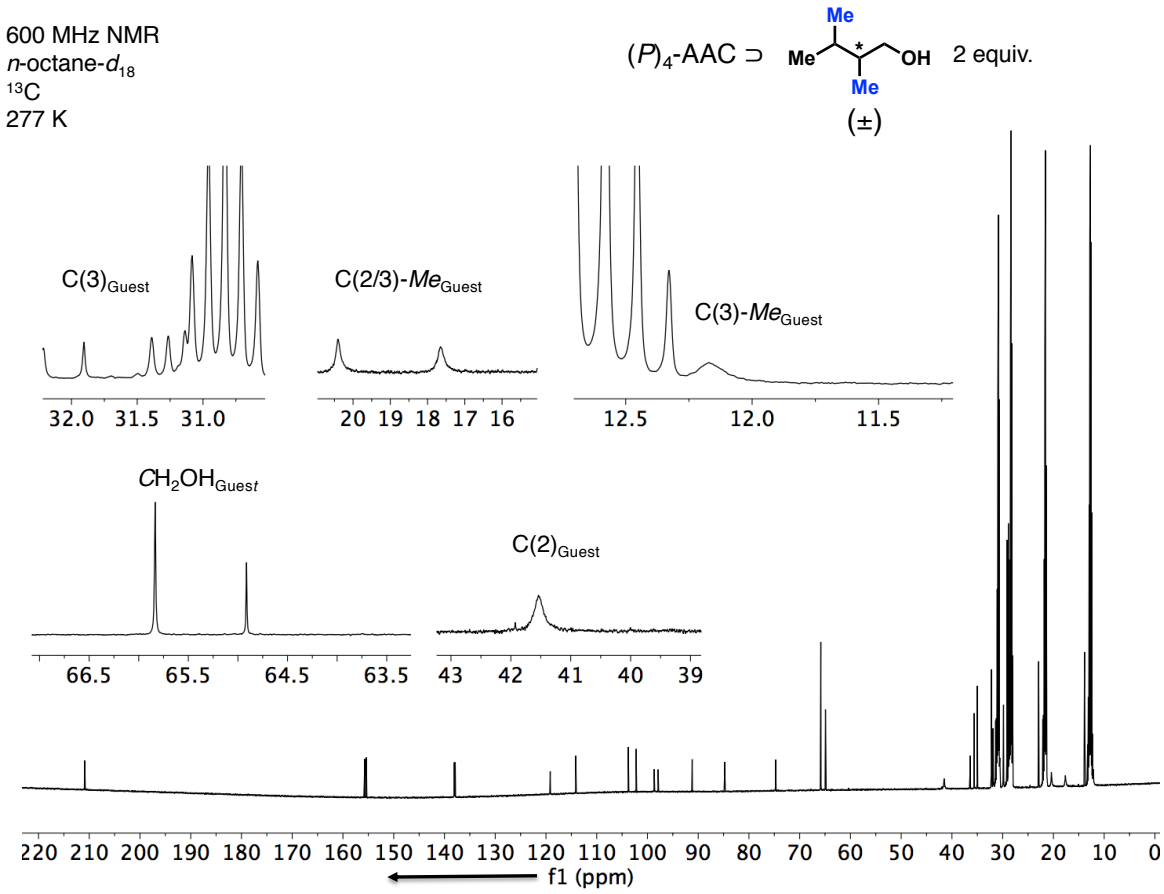

Figure S48. ^{13}C NMR (150 MHz) traces of AAC $(P)_4$-**1** (7.0 mM) in [D_{18}]*n*-octane at 277 K with 2 equiv. of (*R*/*S*)-**6**.

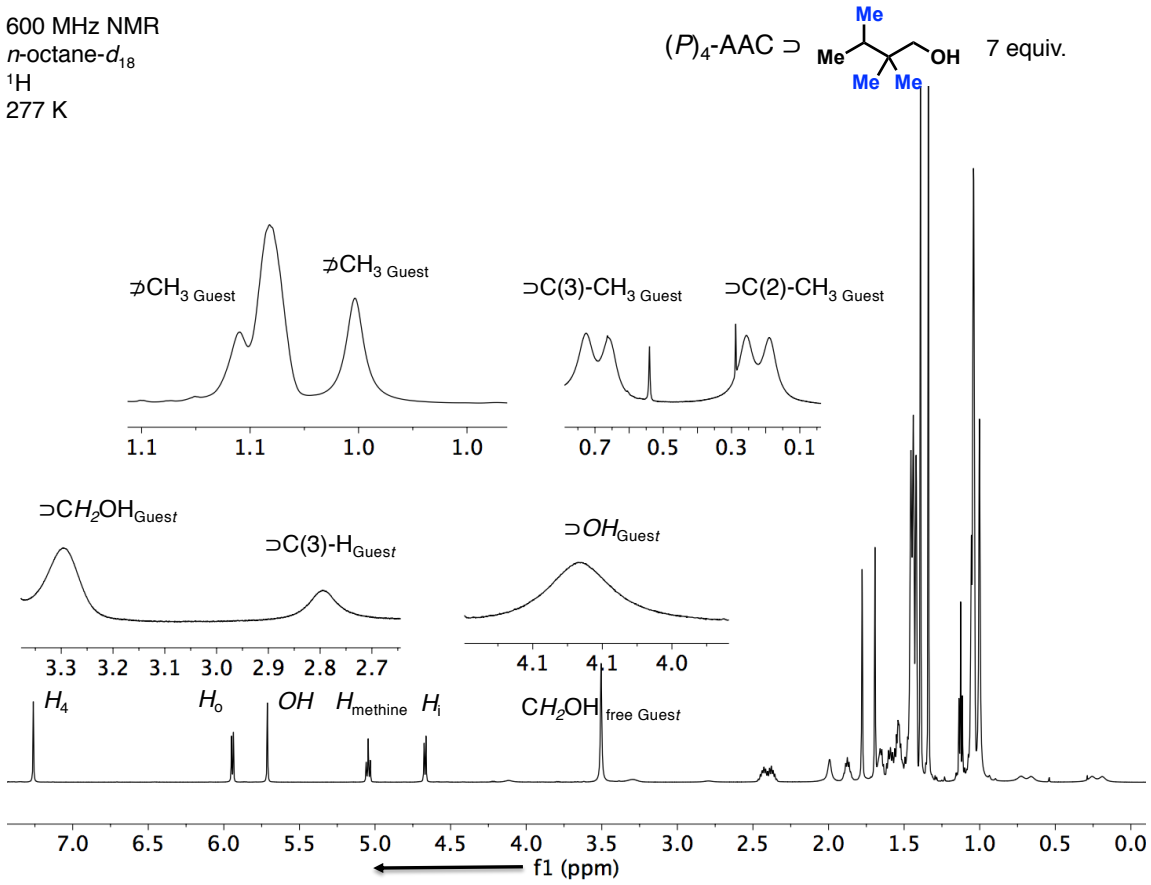

Figure S49. ^{1}H NMR (600 MHz) traces of AAC (*P*)$_4$-**1** (7.0 mM) in [D$_{18}$]*n*-octane at 277 K with 7 equiv. of **9**. The ⊃ denotes the complexed guest and ⊅ signifies the unbound guest molecule. Host-resonances: H$_i$ = inside protons and H$_o$ = outside protons of the methylene bridge; H$_4$ = aromatic protons, highlighted in Figure S41.

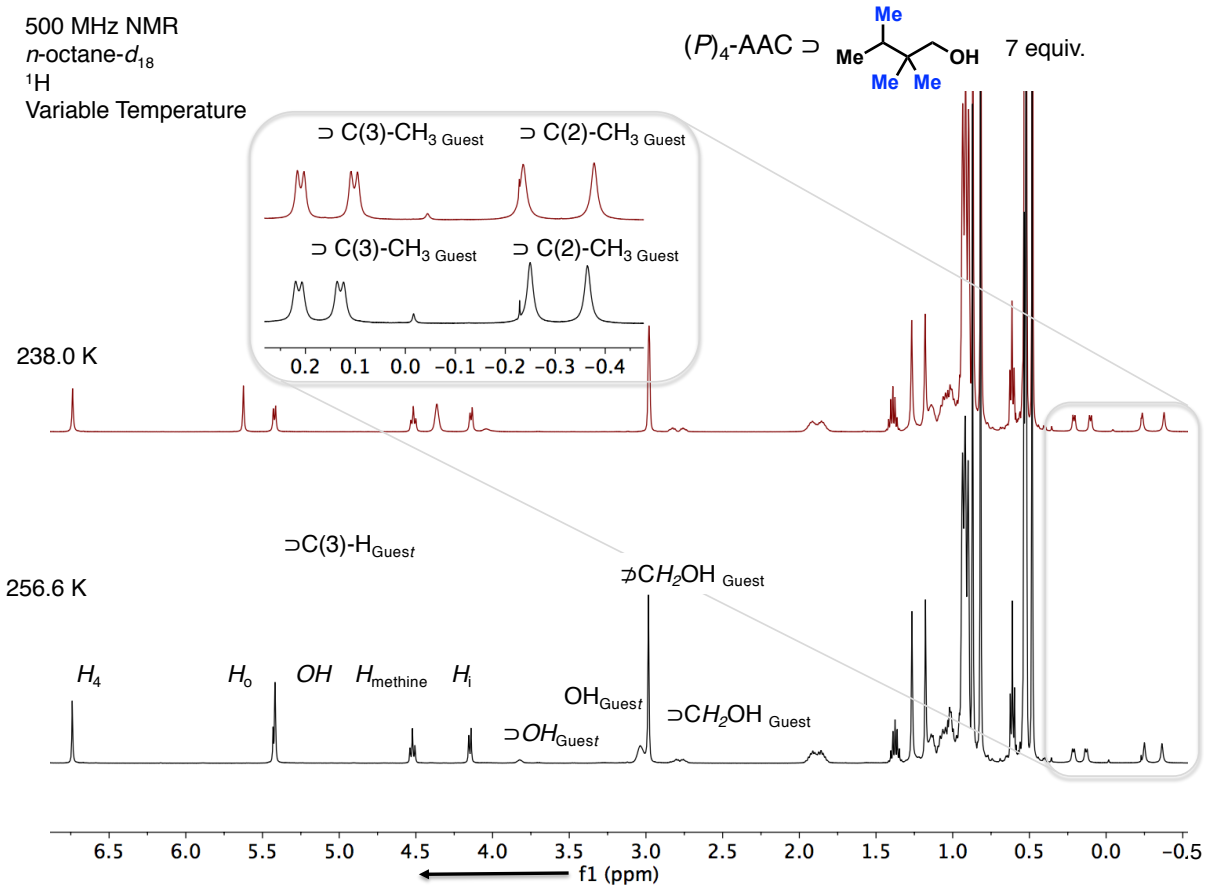

Figure S50. VT-^{1}H NMR (500 MHz) traces of AAC $(P)_4$-**1** (7.0 mM) in [D_{18}]*n*-octane at 277 K with 7 equiv. of **9**. Host-resonances: H_i = inside protons and H_o = outside protons of the methylene bridge; H_4 = aromatic protons, highlighted in Figure S41.

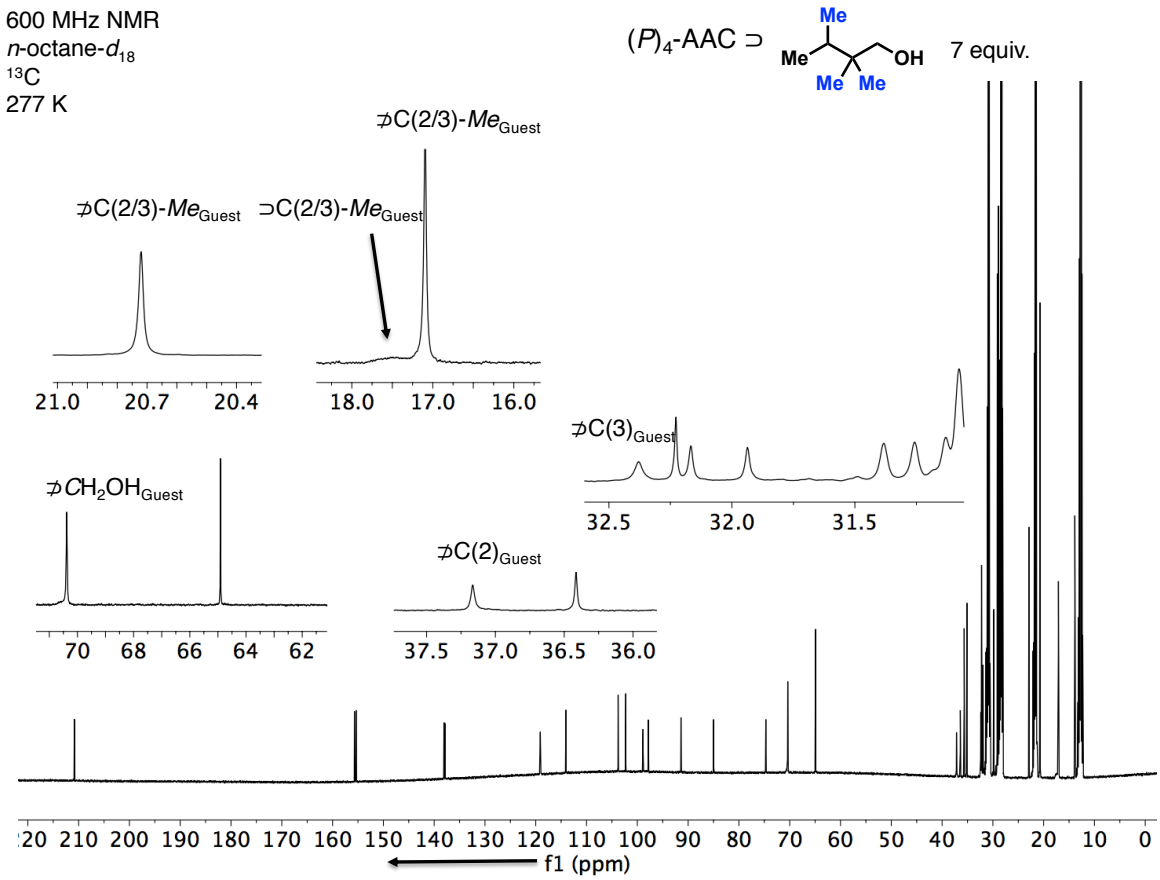

Figure S51. ^{13}C NMR (150 MHz) traces of AAC $(P)_4$-**1** (7.0 mM) in [D_{18}]*n*-octane at 277 K with 7 equiv. of **9**.

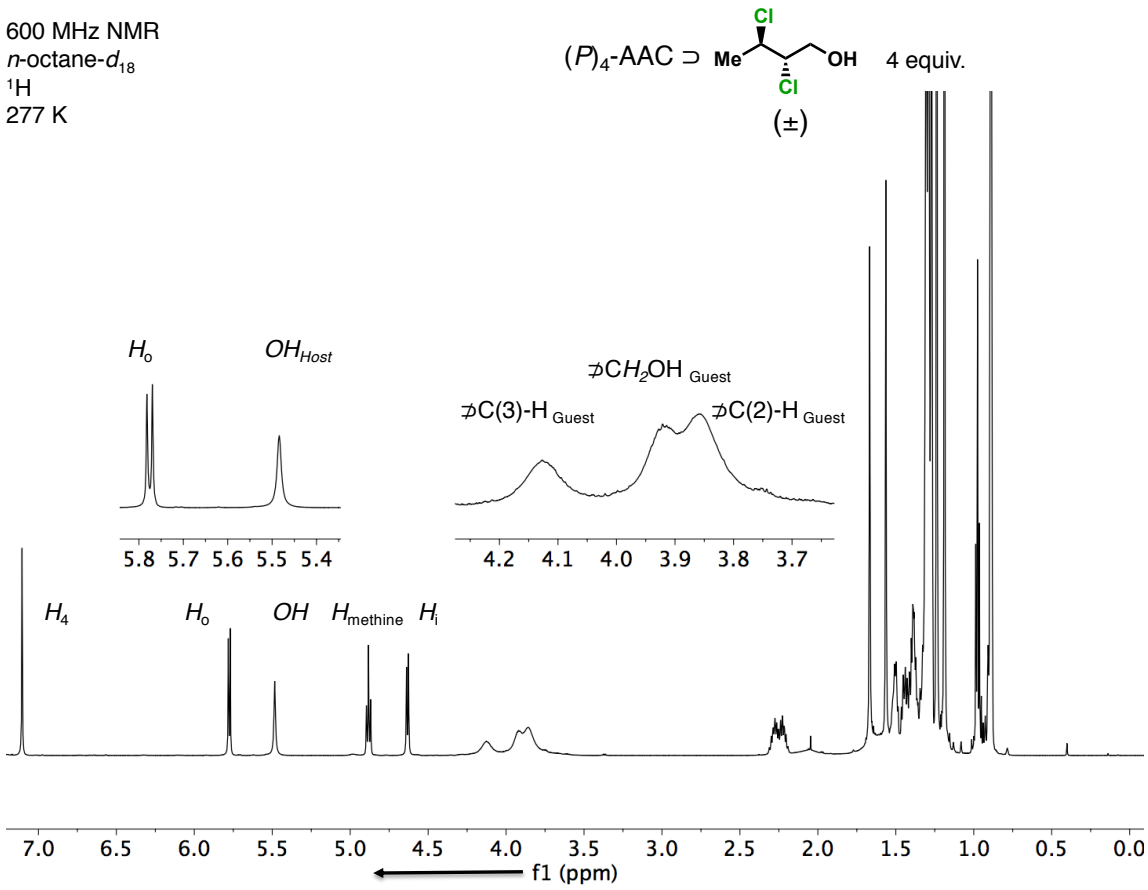

Figure S52. ^{1}H NMR (600 MHz) traces of AAC (*P*)$_4$-**1** (7.0 mM) in [D$_{18}$]*n*-octane at 277 K with 4 equiv. of (*R**,*S**)-**7**. The ⊅ signifies the unbound guest molecule at fast exchange on the NMR-timescale. Host-resonances: H$_i$ = inside protons and H$_o$ = outside protons of the methylene bridge; H$_4$ = aromatic protons, highlighted in Figure S41.

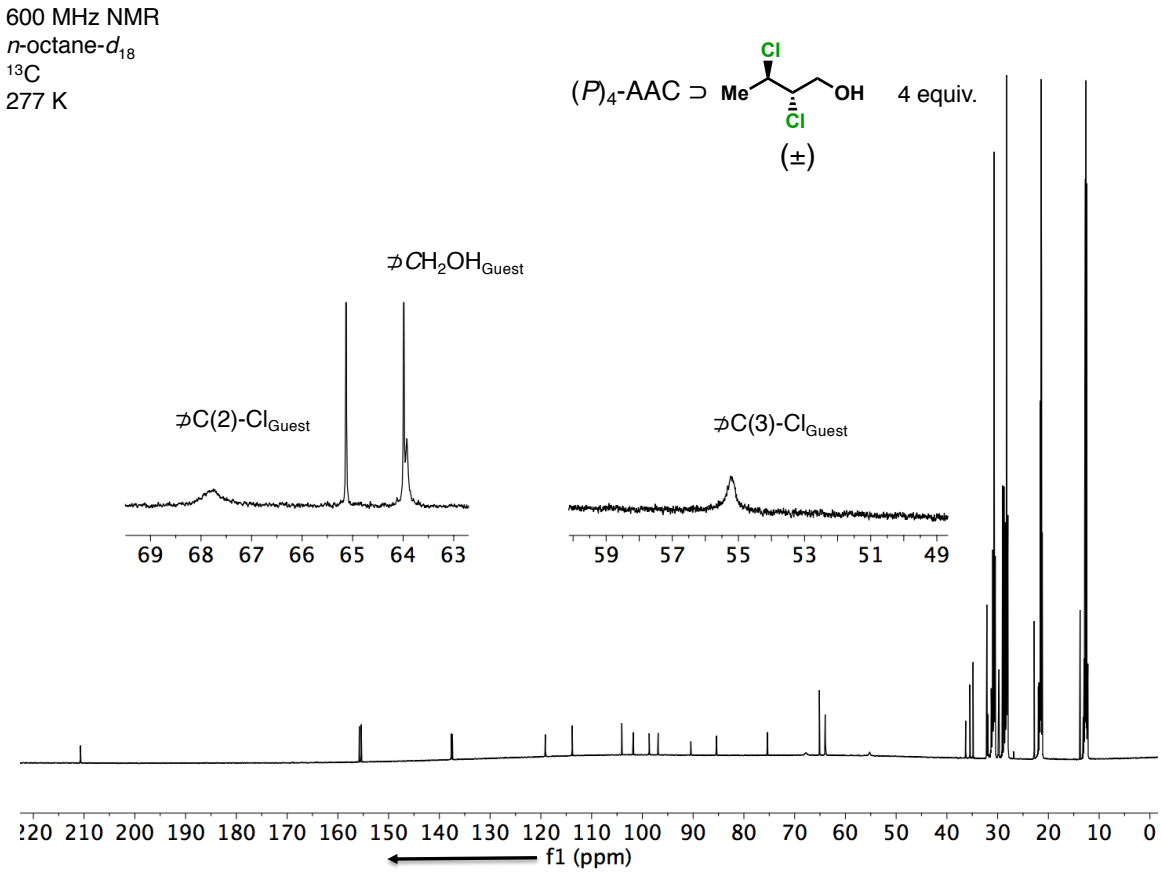

Figure S53. ^{13}C NMR (150 MHz) traces of AAC $(P)_4$-**1** (7.0 mM) in [D_{18}]*n*-octane at 277 K with 4 equiv. of (*R**,*S**)-**7**. The ⊅ signifies the unbound guest molecule at fast exchange on the NMR-timescale.

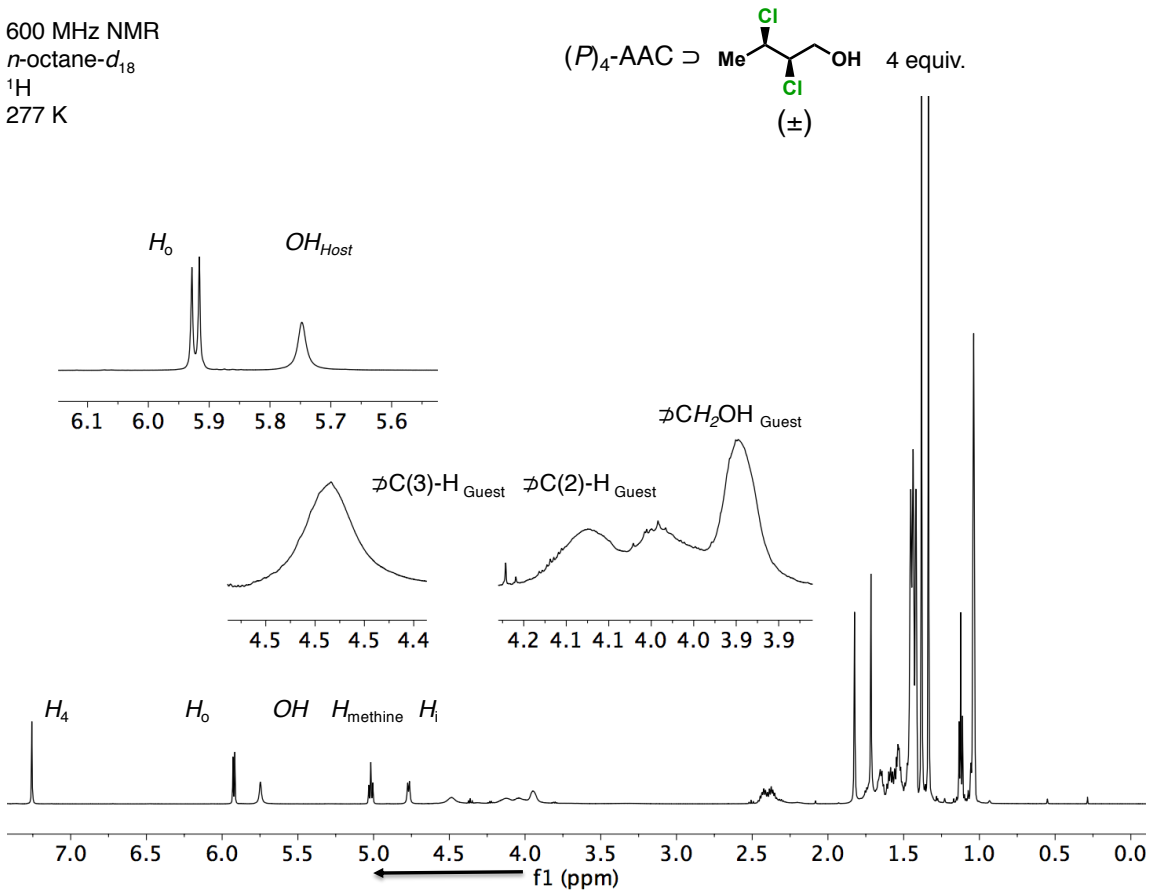

Figure S54. ^{1}H NMR (600 MHz) traces of AAC $(P)_4$-**1** (7.0 mM) in [D_{18}]*n*-octane at 277 K with 4 equiv. of (*R**,*R**)-**7**. The ⊅ signifies the unbound guest molecule at fast exchange on the NMR-timescale. Host-resonances: H_i = inside protons and H_o = outside protons of the methylene bridge; H_4 = aromatic protons, highlighted in Figure S41.

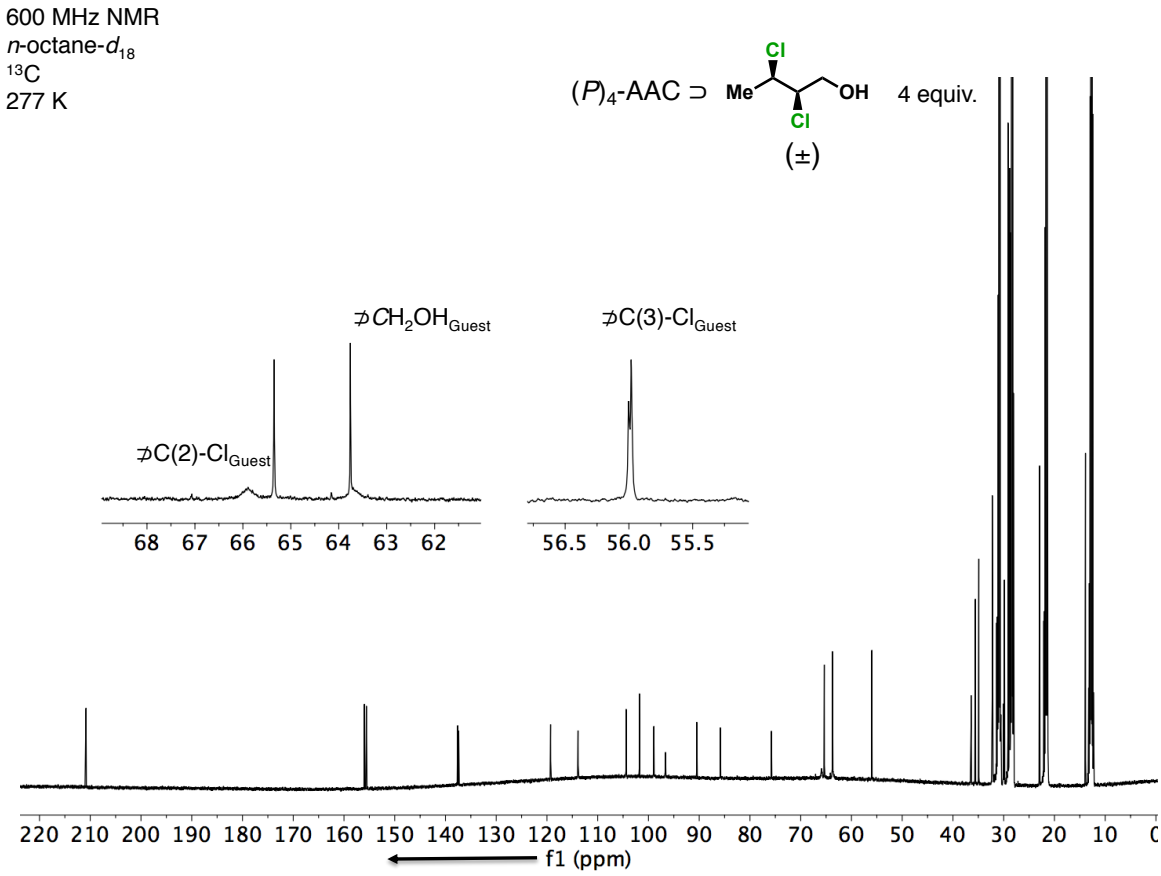

Figure S55. ^{13}C NMR (150 MHz) traces of AAC $(P)_4$-**1** (7.0 mM) in [D_{18}]*n*-octane at 277 K with 4 equiv. of (*R**,*R**)-**7**. The ⊅ signifies the unbound guest molecule at fast exchange on the NMR-timescale.

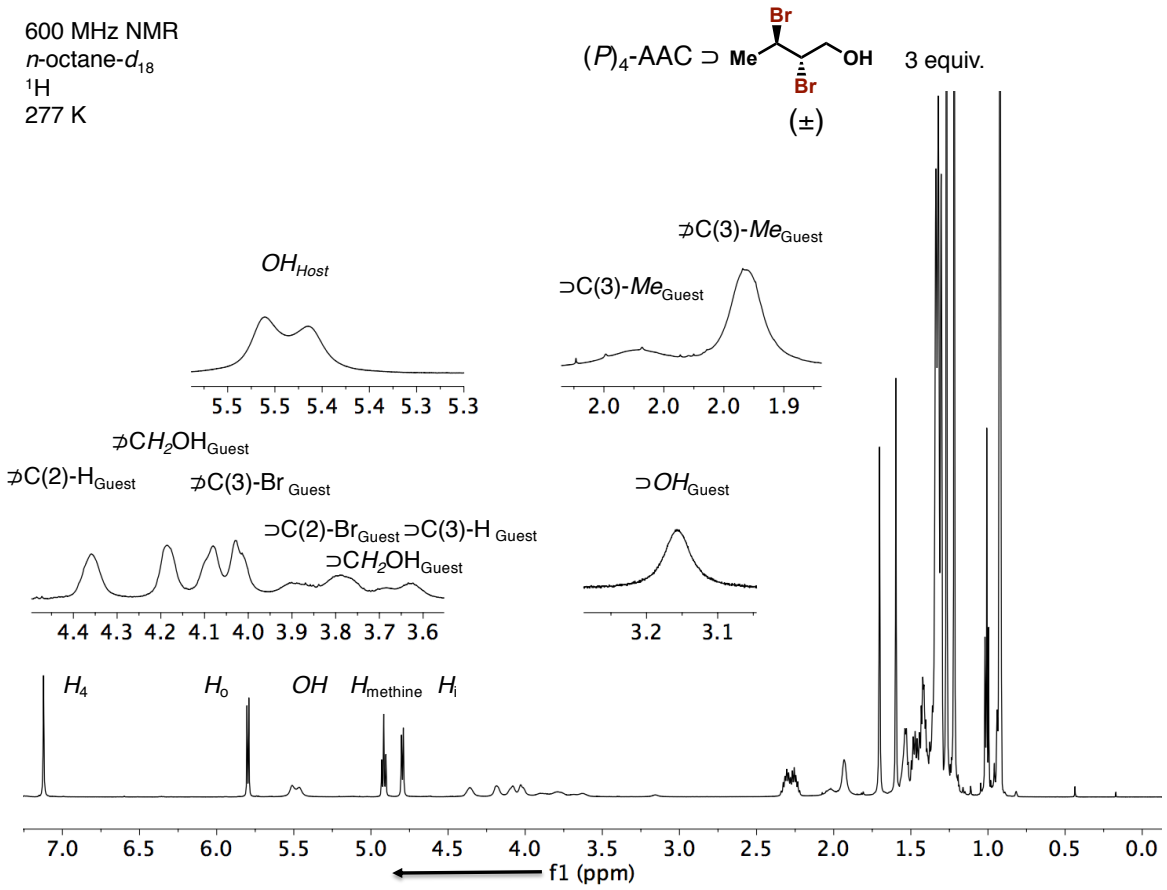

Figure S56. ^{1}H NMR (600 MHz) traces of AAC (*P*)$_4$-**1** (7.0 mM) in [D$_{18}$]*n*-octane at 277 K with 3 equiv. of (*R**,*S**)-**8**. The ⊃ denotes the complexed guest and ⊅ signifies the unbound at slow exchange on the NMR-timescale. Host-resonances: H$_i$ = inside protons and H$_o$ = outside protons of the methylene bridge; H$_4$ = aromatic protons, highlighted in Figure S41.

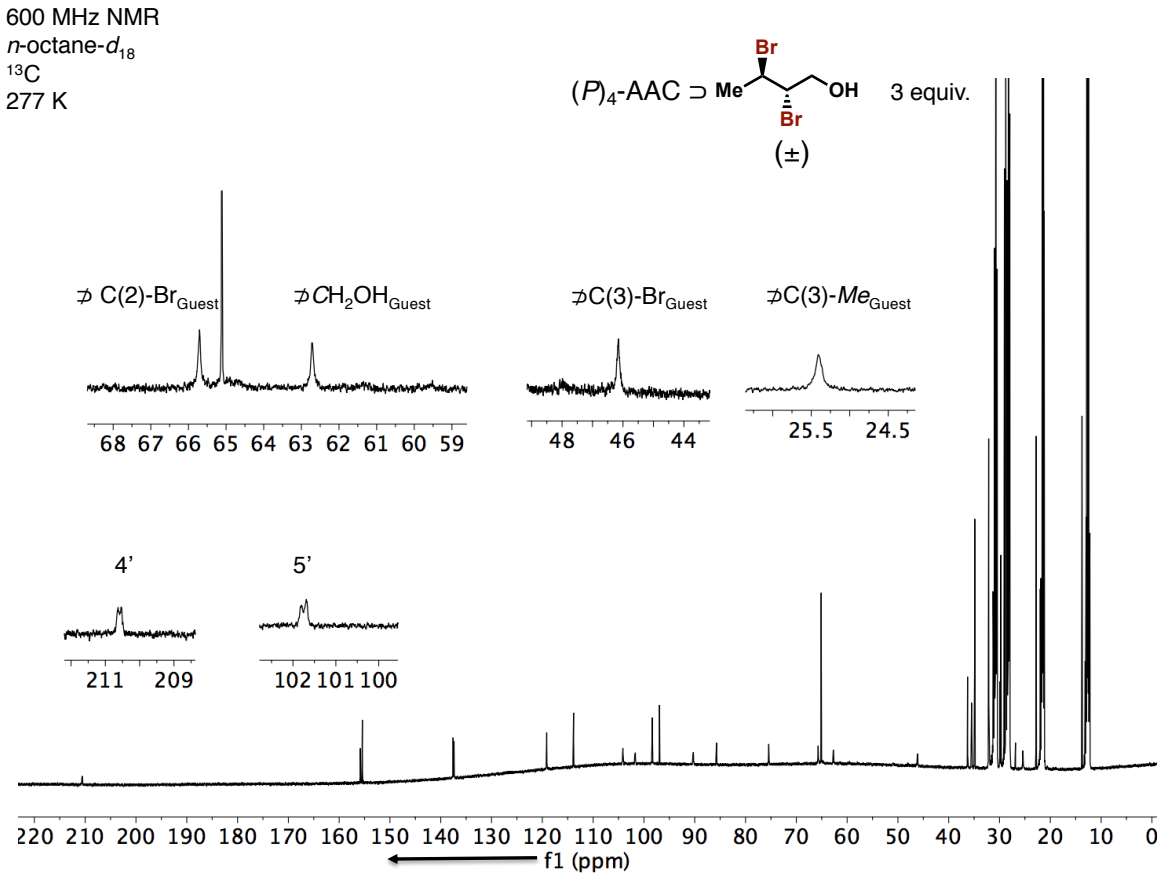

Figure S57. ^{13}C NMR (150 MHz) traces of AAC $(P)_4$-**1** (7.0 mM) in [D_{18}]*n*-octane at 277 K with 3 equiv. of (*R**,*S**)-**8**. The ⊅ signifies the unbound guest molecule.

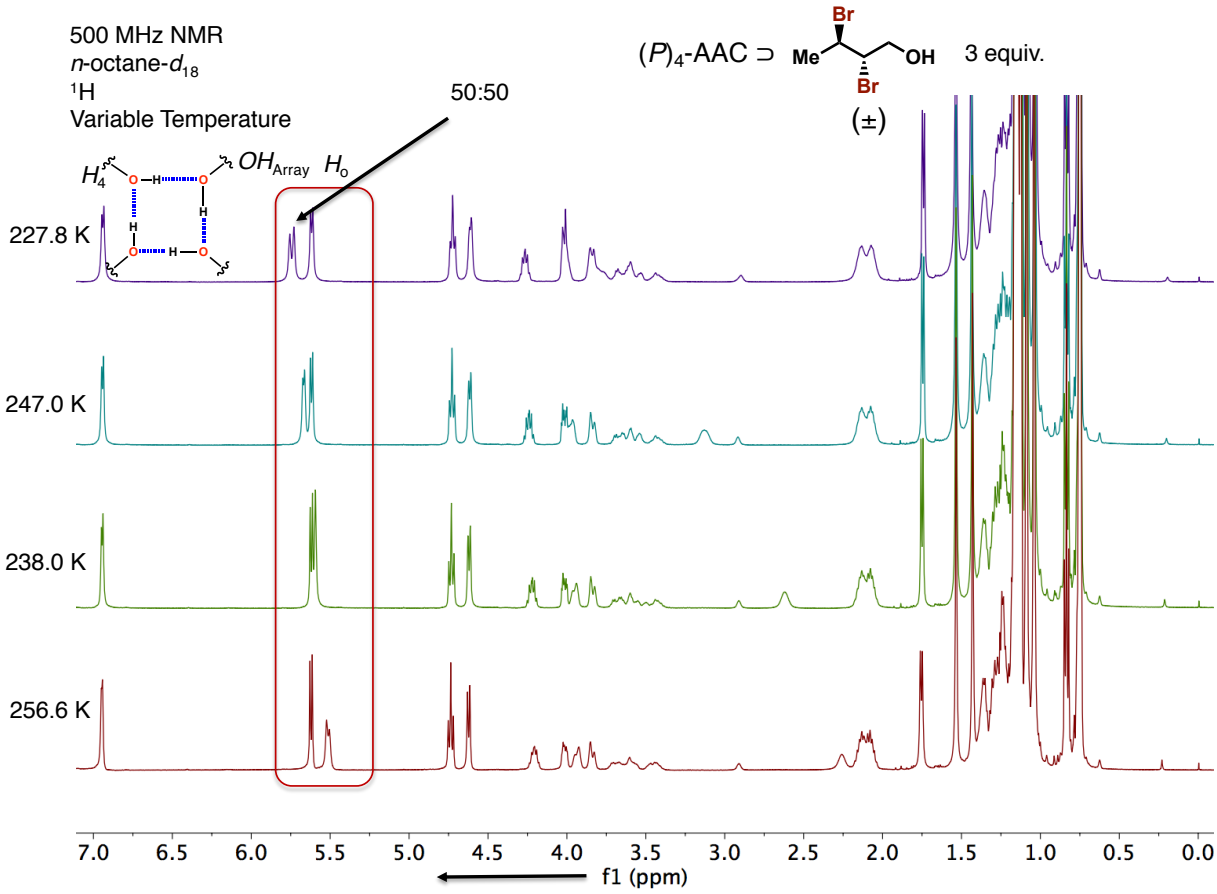

Figure S58. VT-^{1}H NMR (500 MHz) traces of AAC $(P)_4$-**1** (7.0 mM) in [D_{18}]*n*-octane at 277 K with 3 equiv. of (*R**,*S**)-**8**. Host-resonances: H_i = inside protons and H_o = outside protons of the methylene bridge; H_4 = aromatic protons, highlighted in Figure S41. Splitting of the Host-OH-resonances correspond to the diastereoisomeric complexes of the host–guest complexes.

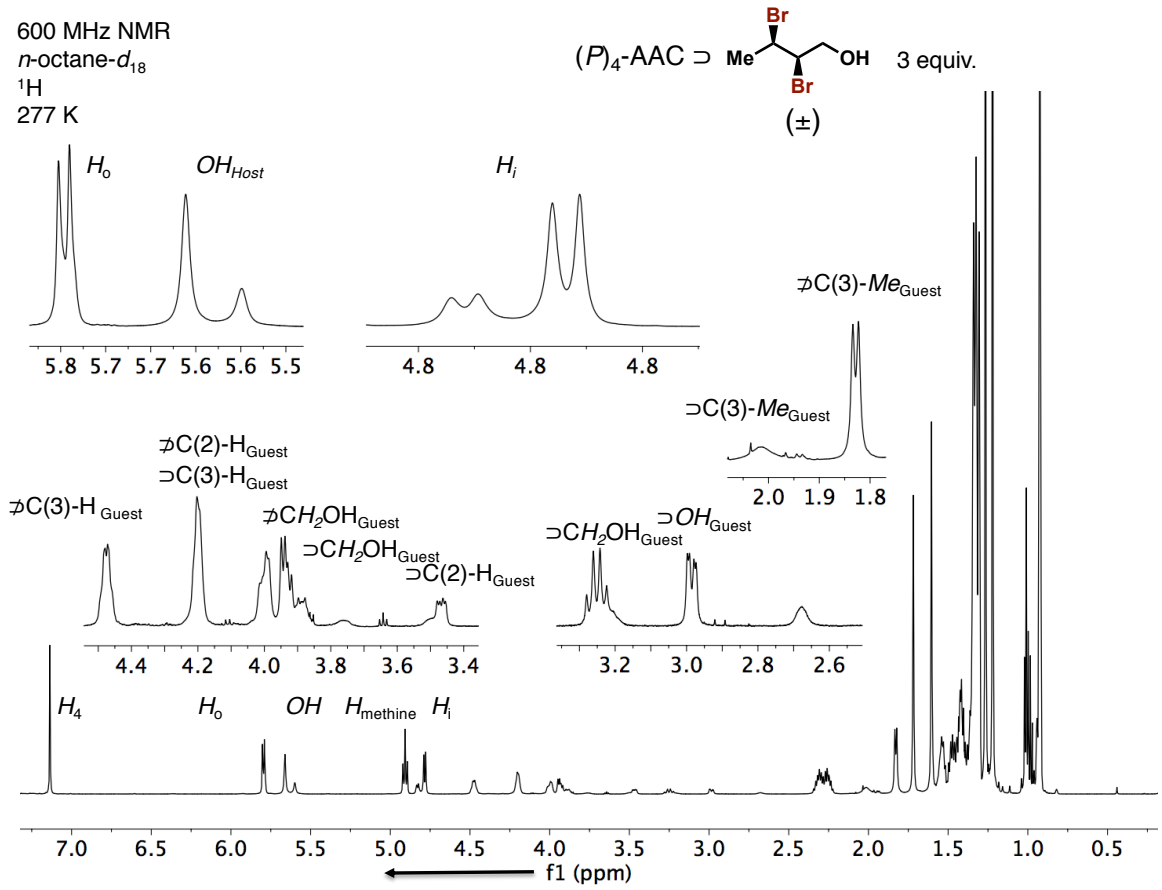

Figure S59. ^{1}H NMR (600 MHz) traces of AAC $(P)_4$-**1** (7.0 mM) in [D_{18}]*n*-octane at 277 K with 3 equiv. of (*R**,*R**)-**8**. The ⊃ denotes the complexed guest and ⊅ signifies the unbound at slow exchange on the NMR-timescale. Host-resonances: H_i = inside protons and H_o = outside protons of the methylene bridge; H_4 = aromatic protons, highlighted in Figure S41.

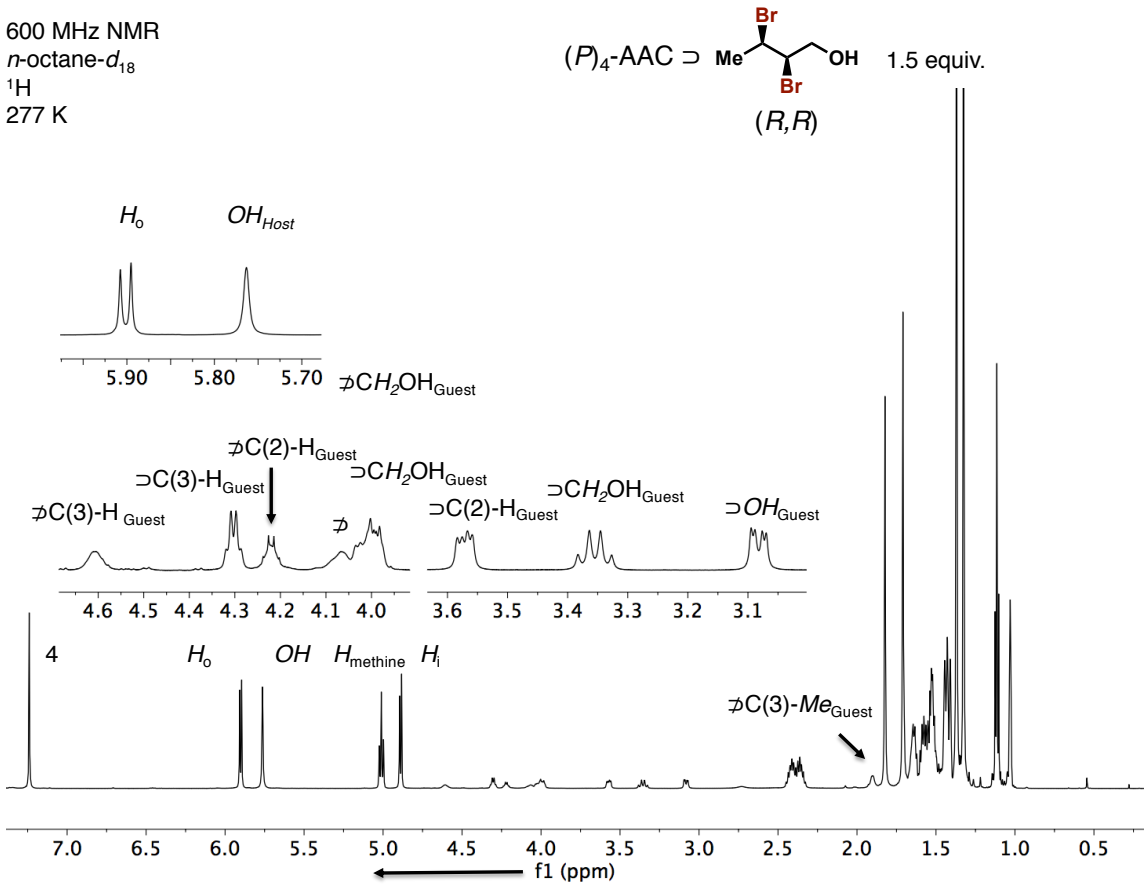

Figure S60. ^{1}H NMR (600 MHz) traces of AAC $(P)_4$-**1** (20.0 mM) in [D_{18}]*n*-octane at 277 K with 1.5 equiv. of the enantiopure (*R*,*R*)-**8**. The ⊃ denotes the complexed guest and ⊅ signifies the unbound at slow exchange on the NMR-timescale. Host-resonances: H_i = inside protons and H_o = outside protons of the methylene bridge; H_4 = aromatic protons, highlighted in Figure S41.

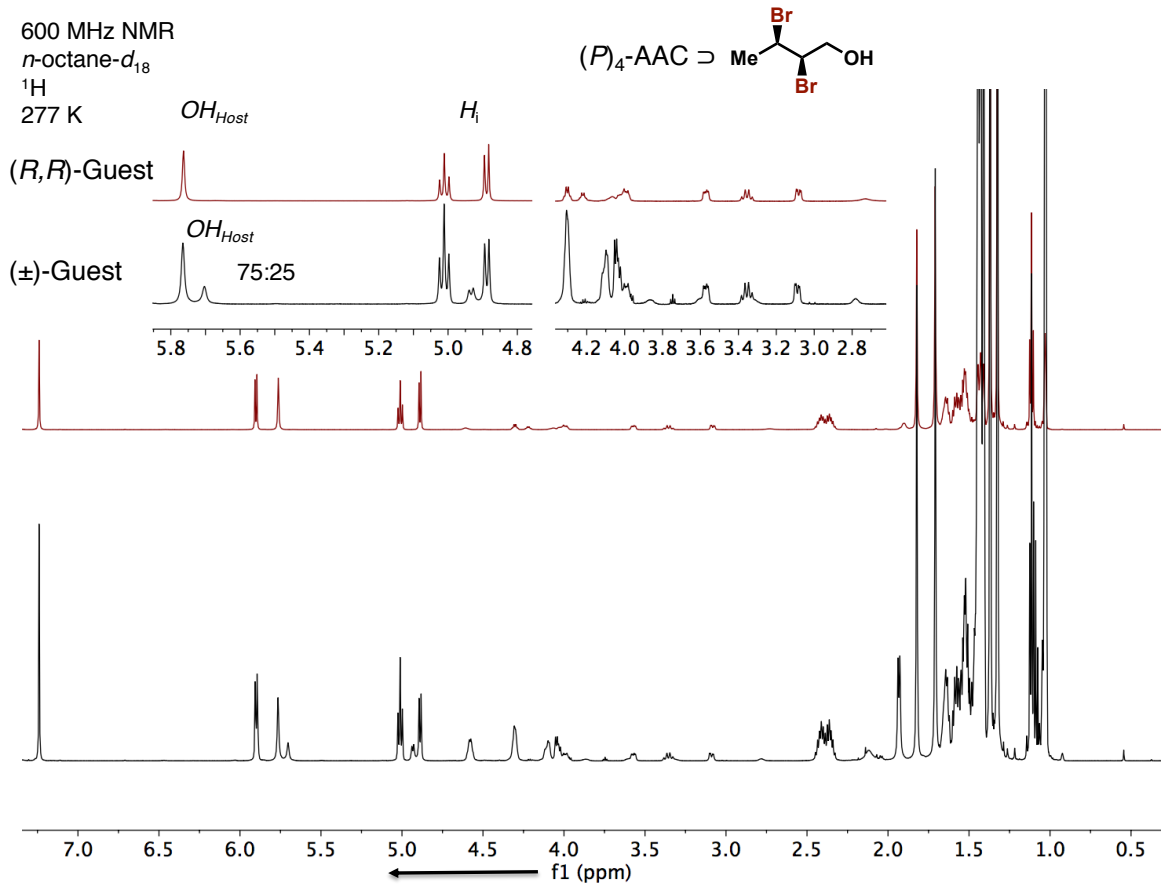

Figure S61. Overlay of the ^{1}H NMR (600 MHz) traces of AAC (*P*)$_4$-**1** in [D$_{18}$]*n*-octane at 277 K with the enantiopure (*R*,*R*)-**8** (top) and the racemic (*R**,*R**)-**8** (bottom). Splitting of the OH-Host-resonances is observed only for the racemic (±)-guest (*R**,*R**)-**8**.

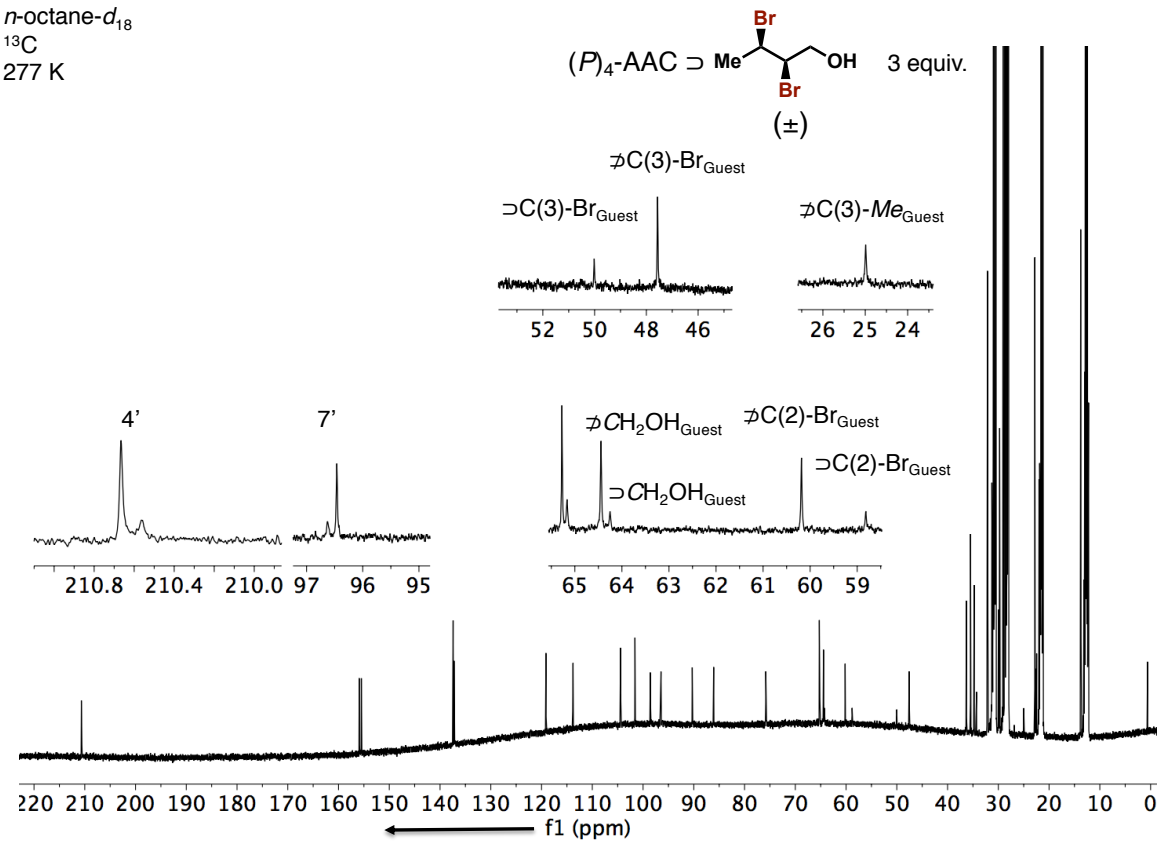

Figure S62. ^{13}C NMR (150 MHz) traces of AAC $(P)_4$-**1** (7.0 mM) in [D_{18}]*n*-octane at 277 K with 3 equiv. of (*R**,*R**)-**8**. The ⊃ denotes the complexed guest and ⊅ signifies the unbound at slow exchange on the NMR-timescale.

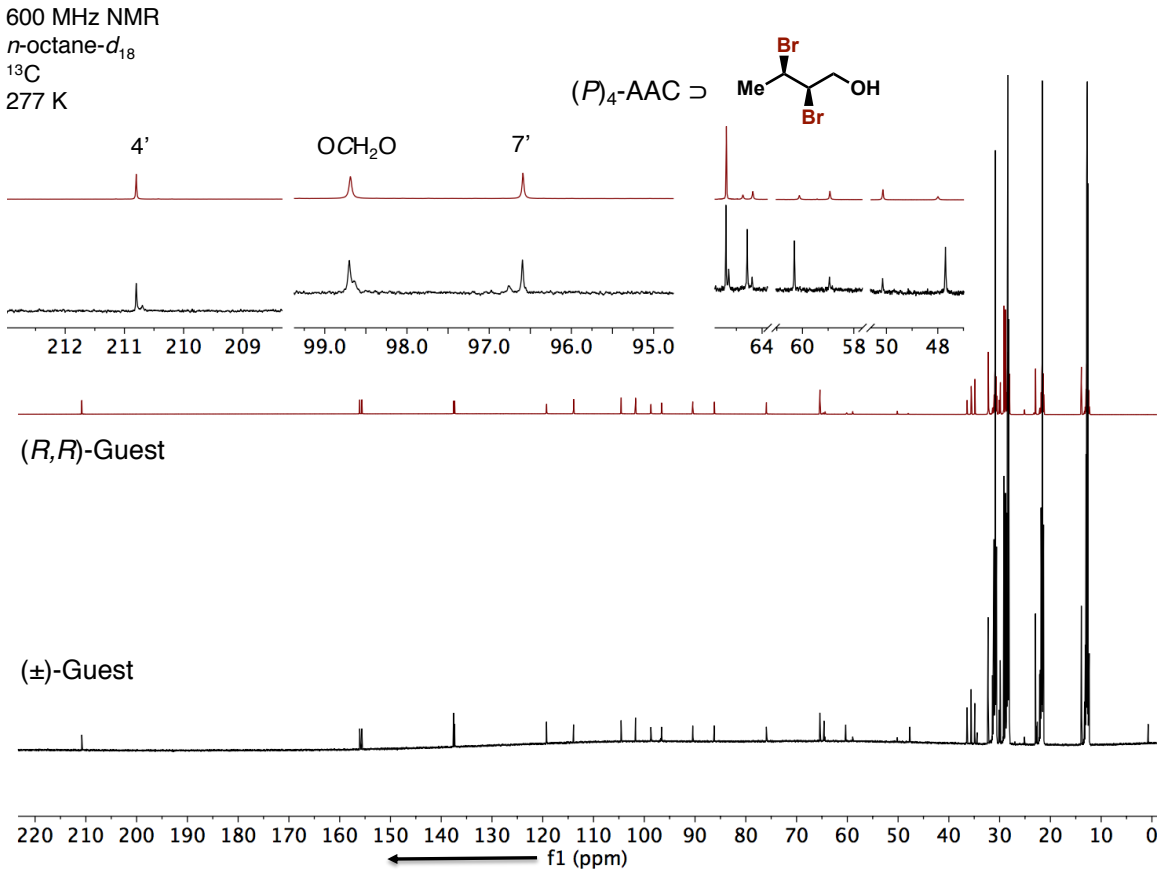

Figure S63. Overlay of the ^{13}C NMR (150 MHz) traces of AAC $(P)_4$-**1** in [D_{18}]*n*-octane at 277 K with the enantiopure (*R*,*R*)-**8** (top) and the racemic (*R**,*R**)-**8** (bottom). Splitting of the Host-resonances is observed only for the racemic (±)-guest (*R**,*R**)-**8**.

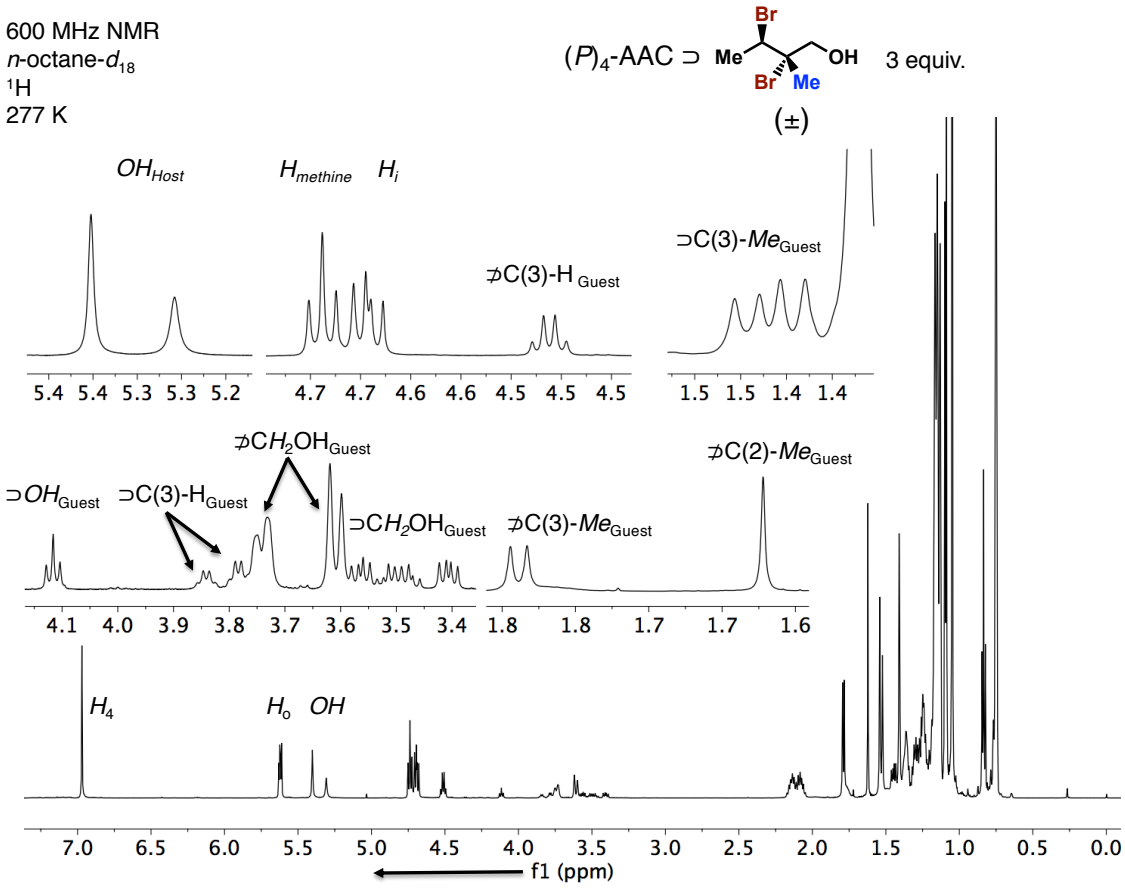

Figure S64. ^{1}H NMR (600 MHz) traces of AAC $(P)_4$-**1** (7.0 mM) in [D_{18}]*n*-octane at 277 K with 3 equiv. of the (*R**,*S**)-**10**. The ⊃ denotes the complexed guest and ⊅ signifies the unbound at slow exchange on the NMR-timescale. Host-resonances: H_i = inside protons and H_o = outside protons of the methylene bridge; H_4 = aromatic protons, highlighted in Figure S41.

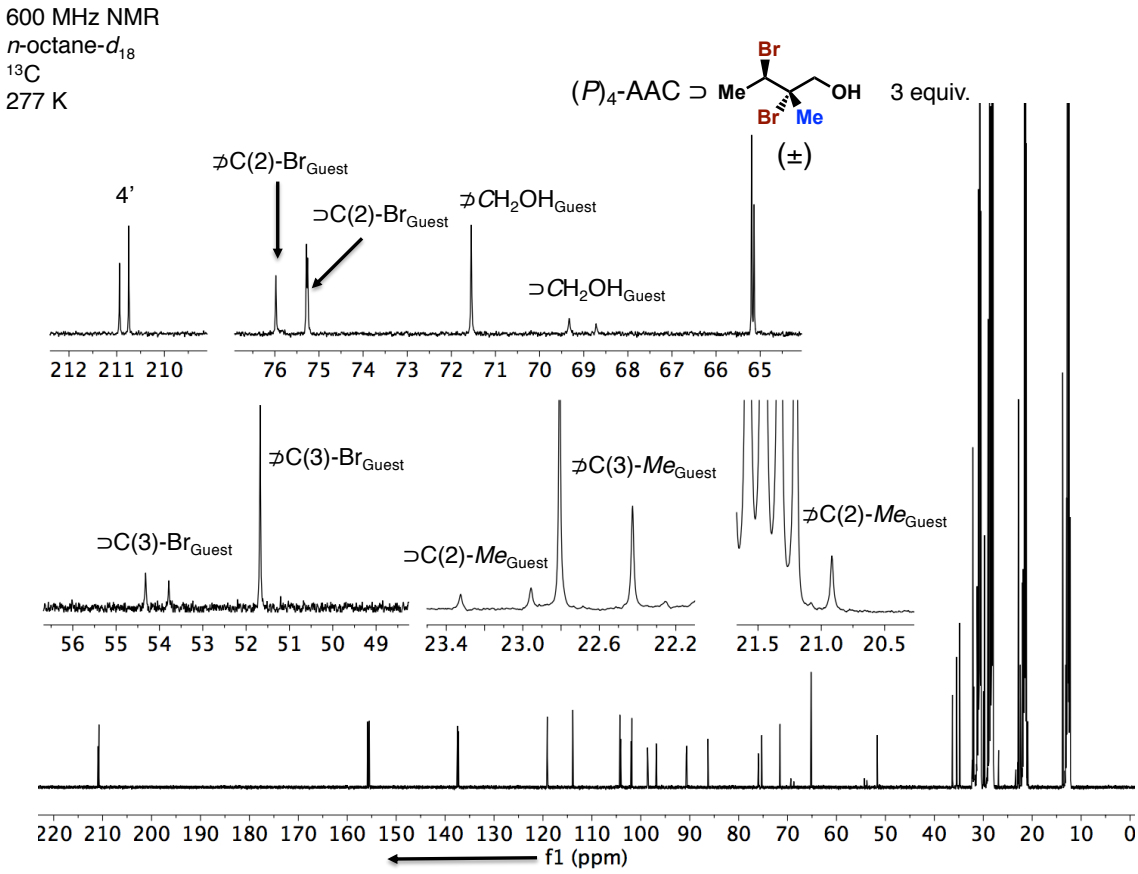

Figure S65. ^{13}C NMR (150 MHz) traces of AAC $(P)_4$-**1** (7.0 mM) in [D_{18}]*n*-octane at 277 K with 3 equiv. of (*R**,*S**)-**10**. The ⊃ denotes the complexed guest and ⊅ signifies the unbound at slow exchange on the NMR-timescale.

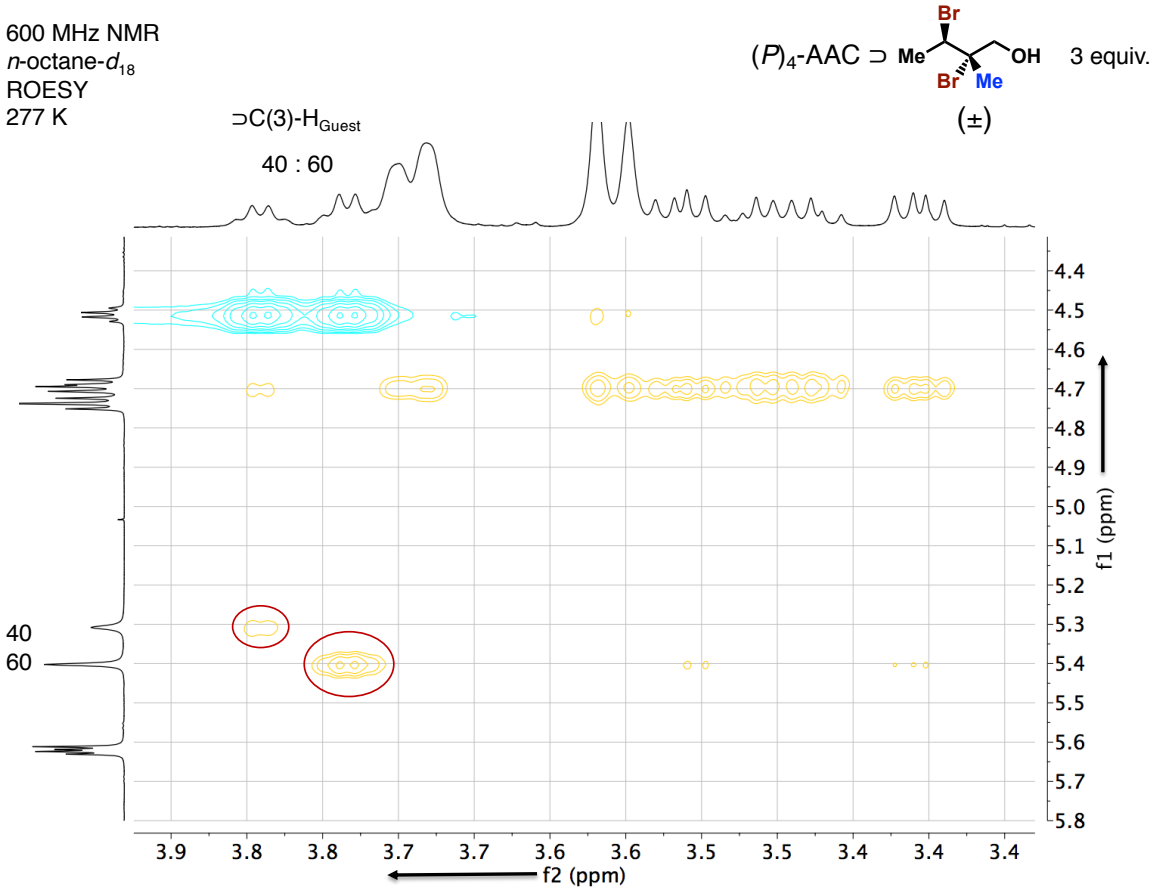

Figure S66. 2D ROESY NMR traces of AAC $(P)_4$-**1** (7.0 mM) in [D_{18}]*n*-octane at 277 K with 3 equiv. of (*R**,*S**)-**10**. One equivalent of the guest is complexed to the interior of the host, while the second equivalent remains unbound in solution. The diastereoisomeric ratio of the host–guest complexes matches with the ratio of the splitting of the OH-host-resonance (60:40).

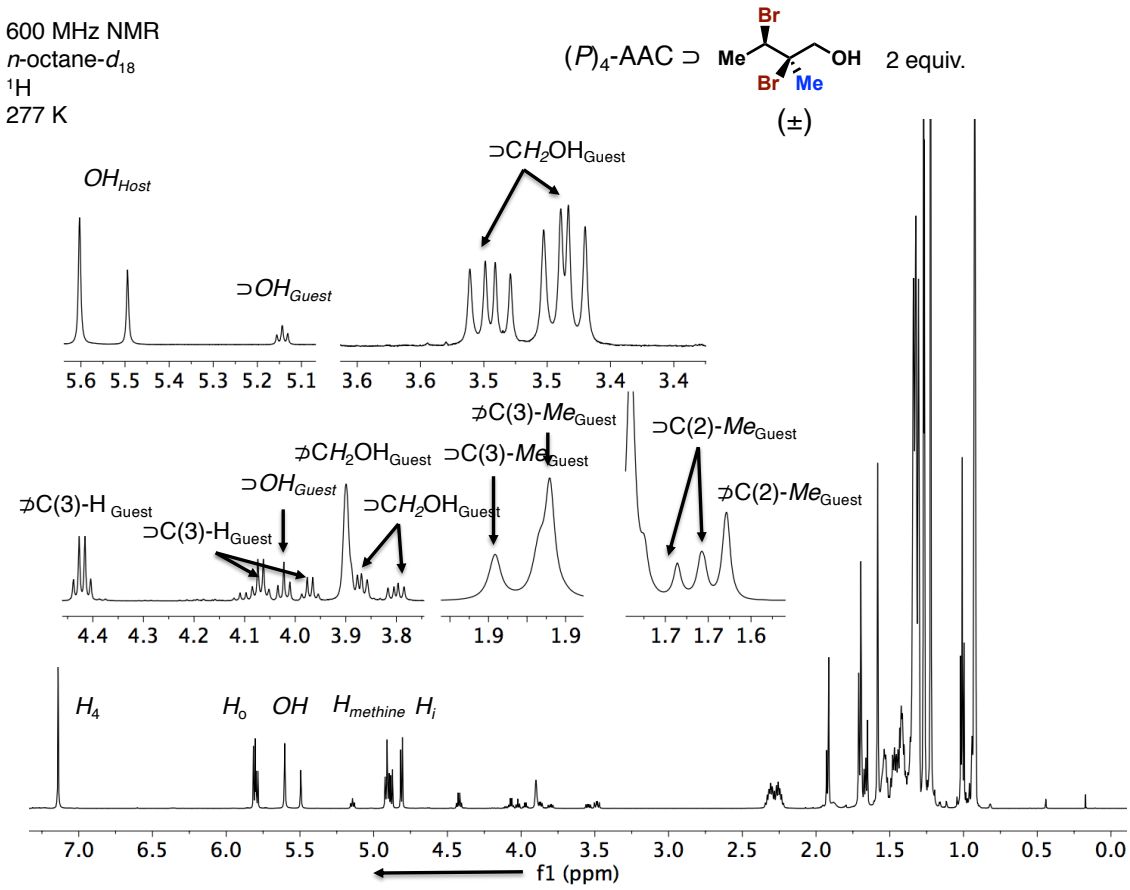

Figure S67. ^{1}H NMR (600 MHz) traces of AAC (*P*)$_4$-**1** (7.0 mM) in [D$_{18}$]*n*-octane at 277 K with 2 equiv. of the (*R**,*R**)-**10**. The ⊃ denotes the complexed guest and ⊅ signifies the unbound at slow exchange on the NMR-timescale. Host-resonances: H$_i$ = inside protons and H$_o$ = outside protons of the methylene bridge; H$_4$ = aromatic protons, highlighted in Figure S41.

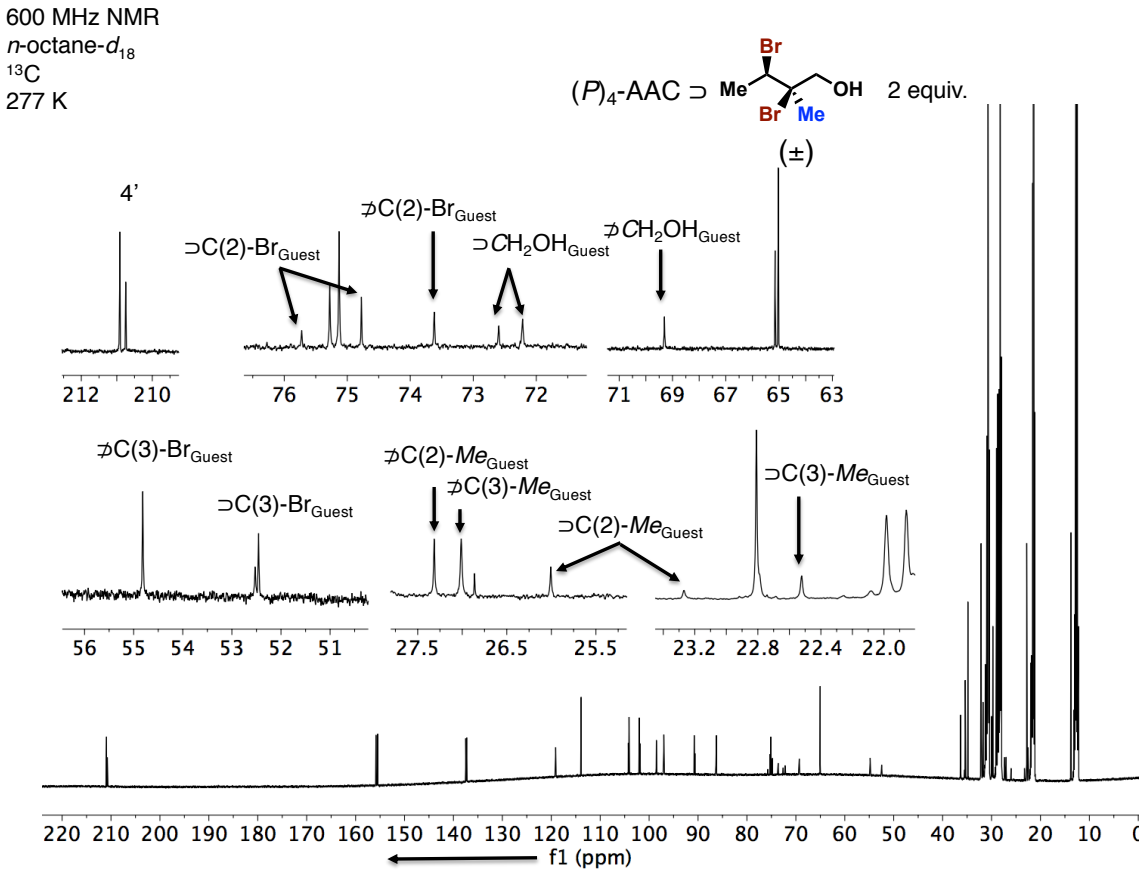

Figure S68. ^{13}C NMR (150 MHz) traces of AAC (*P*)$_4$-**1** (7.0 mM) in [D$_{18}$]*n*-octane at 277 K with 3 equiv. of (*R**,*R**)-**10**. The ⊃ denotes the complexed guest and ⊅ signifies the unbound at slow exchange on the NMR-timescale.

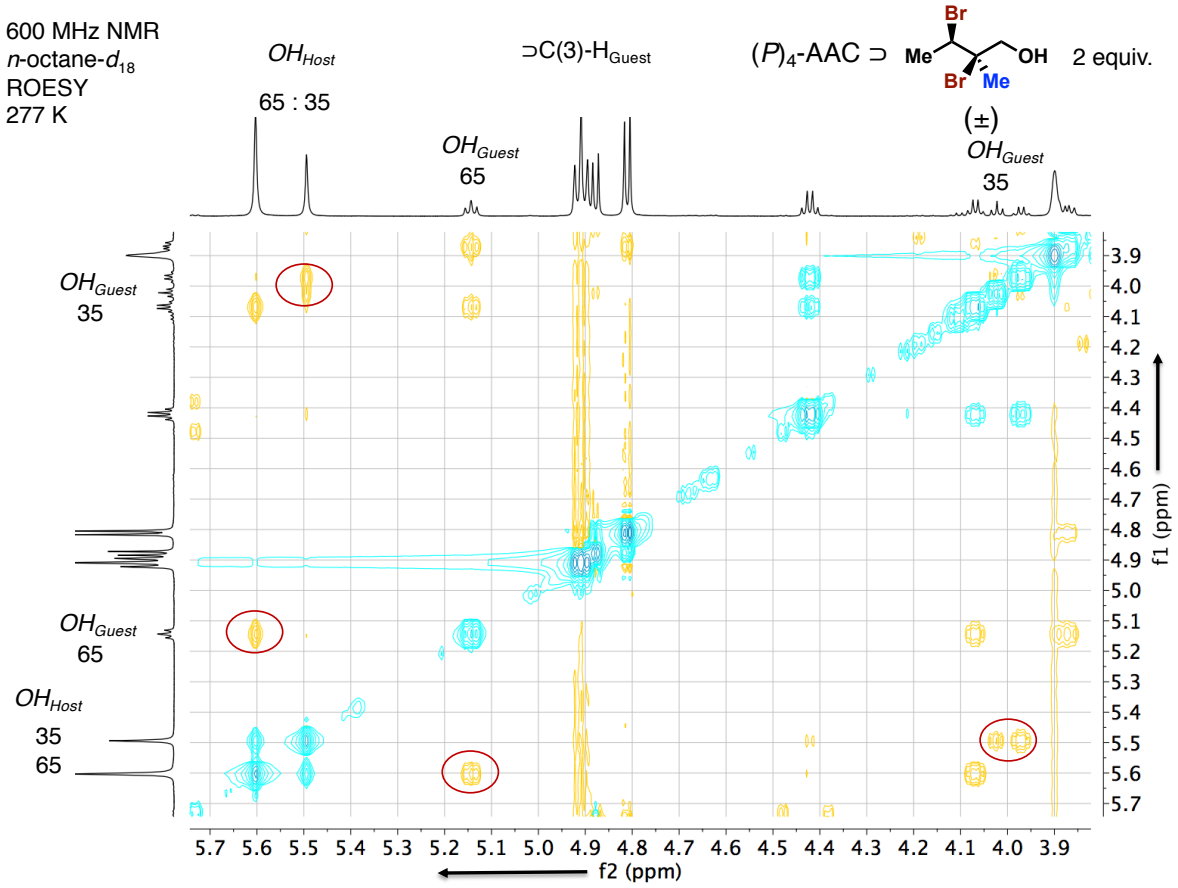

Figure S69. 2D ROESY NMR traces of AAC $(P)_4$-**1** (7.0 mM) in [D_{18}]*n*-octane at 277 K with 3 equiv. of (*R**,*R**)-**10**. One equivalent of the guest is complexed to the interior of the host, while the second equivalent remains unbound in solution. The diastereoisomeric ratio of the host–guest complexes matches with the ratio of the splitting of the OH-host-resonance (65:35).

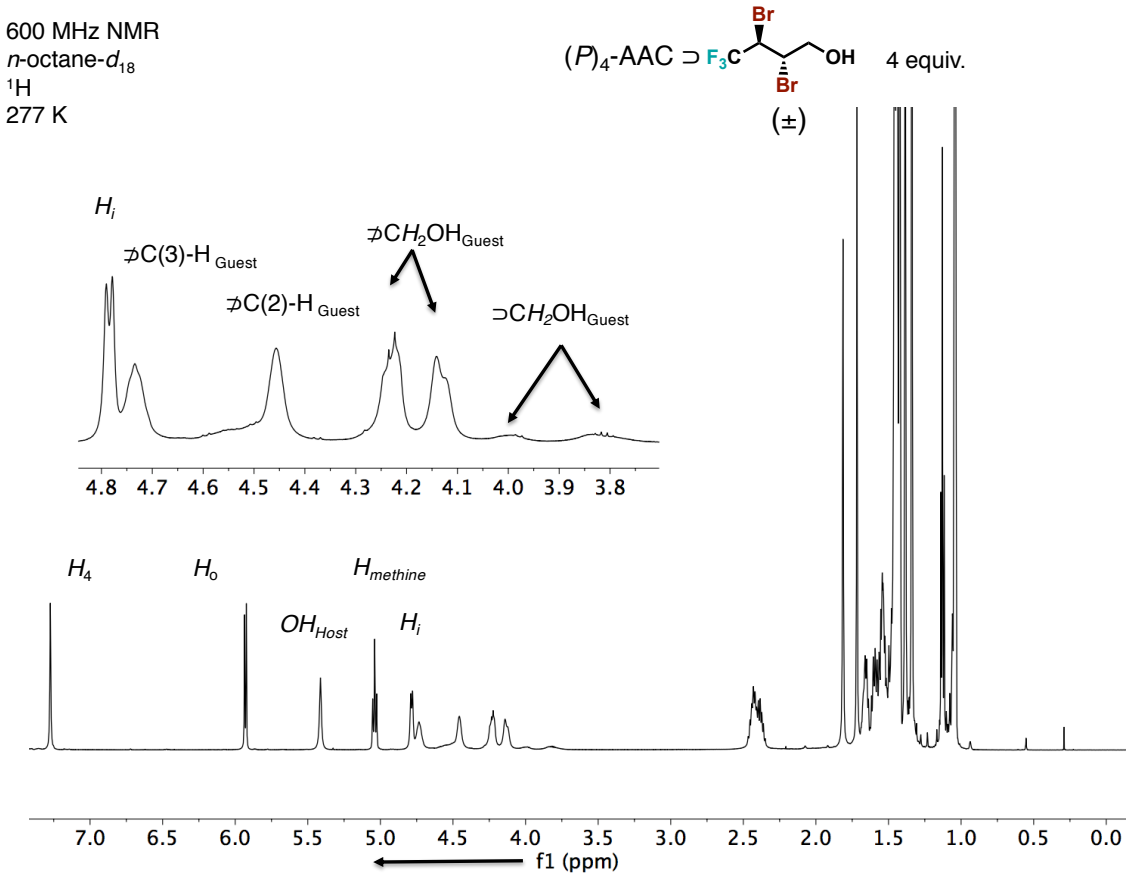

Figure S70. ^{1}H NMR (600 MHz) traces of AAC $(P)_4$-**1** (7.0 mM) in [D_{18}]*n*-octane at 277 K with 4 equiv. of the (*R**,*S**)-**11**. The ⊃ denotes the complexed guest and ⊅ signifies the unbound at slow exchange on the NMR-timescale. Host-resonances: H_i = inside protons and H_o = outside protons of the methylene bridge; H_4 = aromatic protons, highlighted in Figure S41.

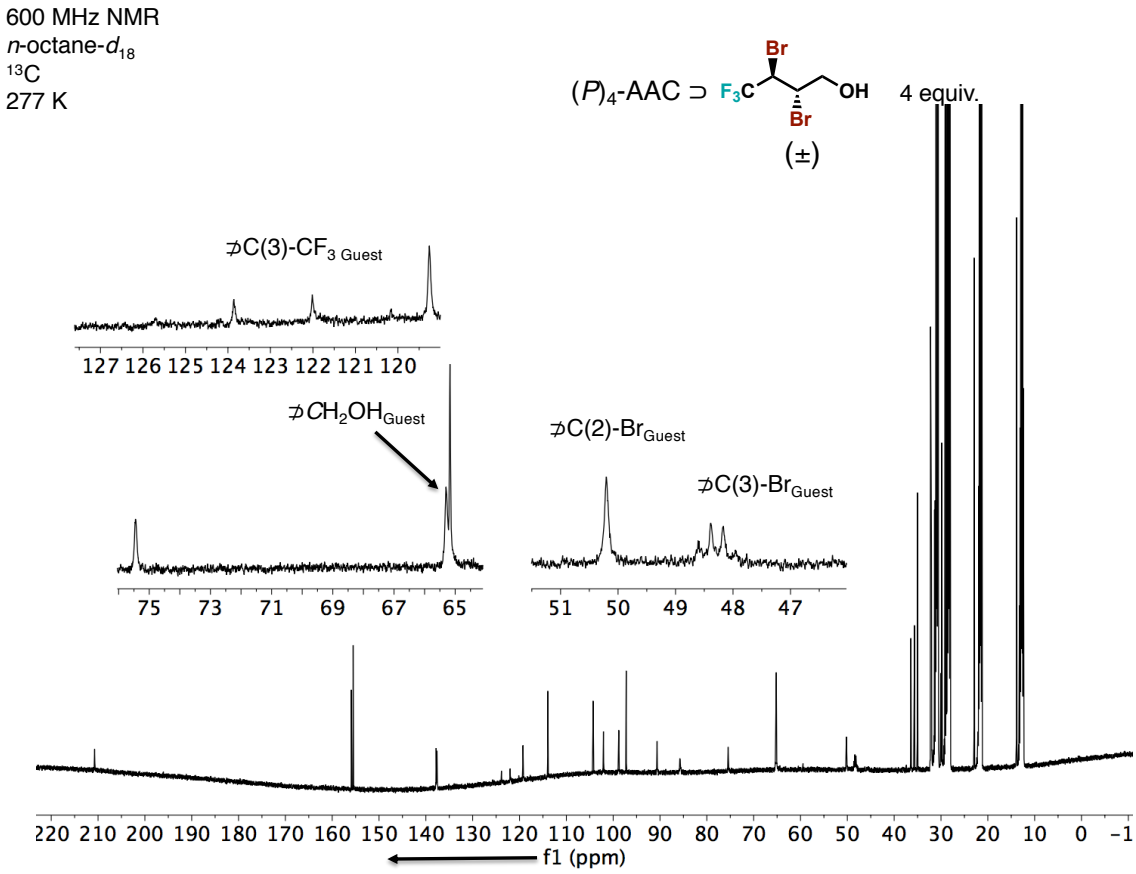

Figure S71. ^{13}C NMR (150 MHz) traces of AAC $(P)_4$-**1** (7.0 mM) in [D_{18}]*n*-octane at 277 K with 4 equiv. of (*R**,*S**)-**11**. The ⊅ signifies the unbound guest.

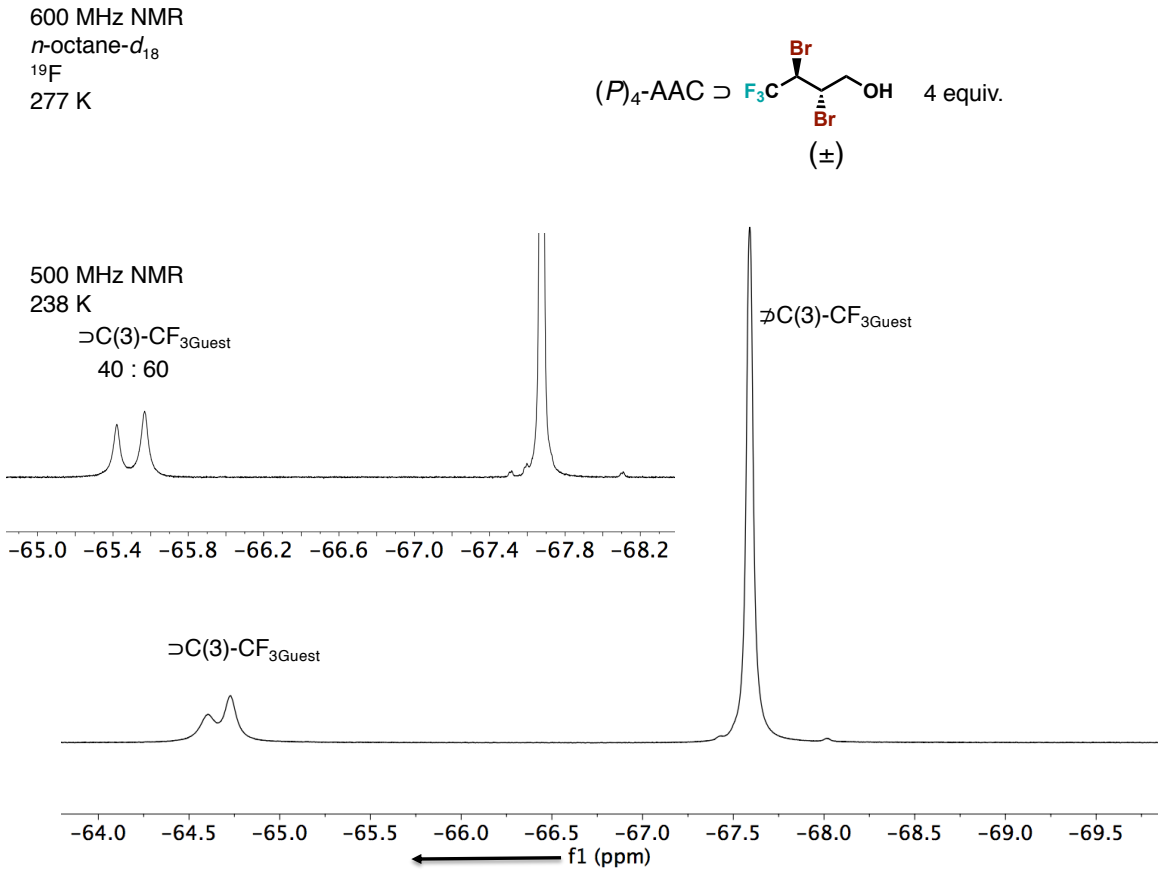

Figure S72. ^{19}F NMR traces of AAC $(P)_4$-**1** (7.0 mM) in [D_{18}]*n*-octane at 277 K with 4 equiv. of (*R**,*S**)-**11**. The ⊃ denotes the complexed guest and ⊅ signifies the unbound at slow exchange on the NMR-timescale. VT-^{1}H NMR traces of $(P)_4$-AAC (7.0 mM) in [D_{18}]*n*-octane at 238 K with 3 equiv. of guest are added to the spectra.

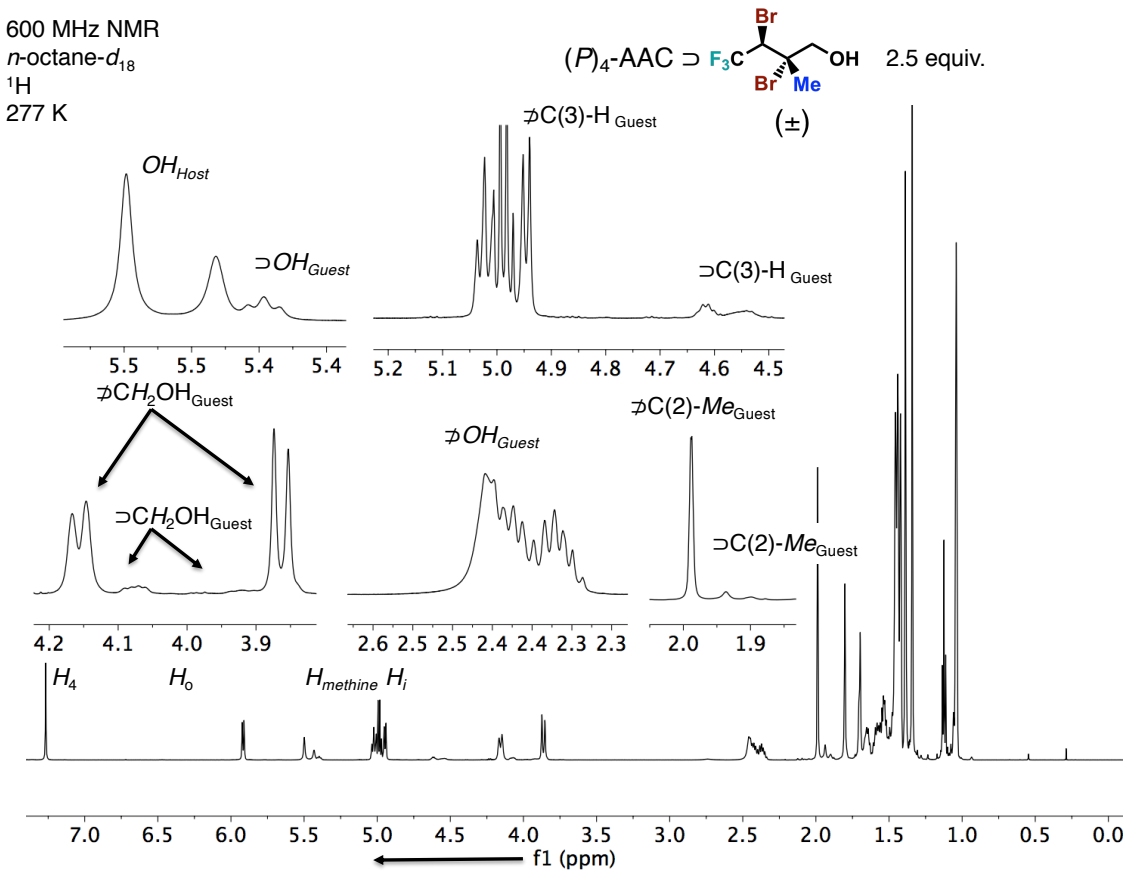

Figure S73. ^{1}H NMR (600 MHz) traces of AAC $(P)_4$-**1** (7.0 mM) in [D_{18}]*n*-octane at 277 K with 2.5 equiv. of the (*R**,*S**)-**12**. The ⊃ denotes the complexed guest and ⊅ signifies the unbound at slow exchange on the NMR-timescale. Host-resonances: H_i = inside protons and H_o = outside protons of the methylene bridge; H_4 = aromatic protons, highlighted in Figure S41.

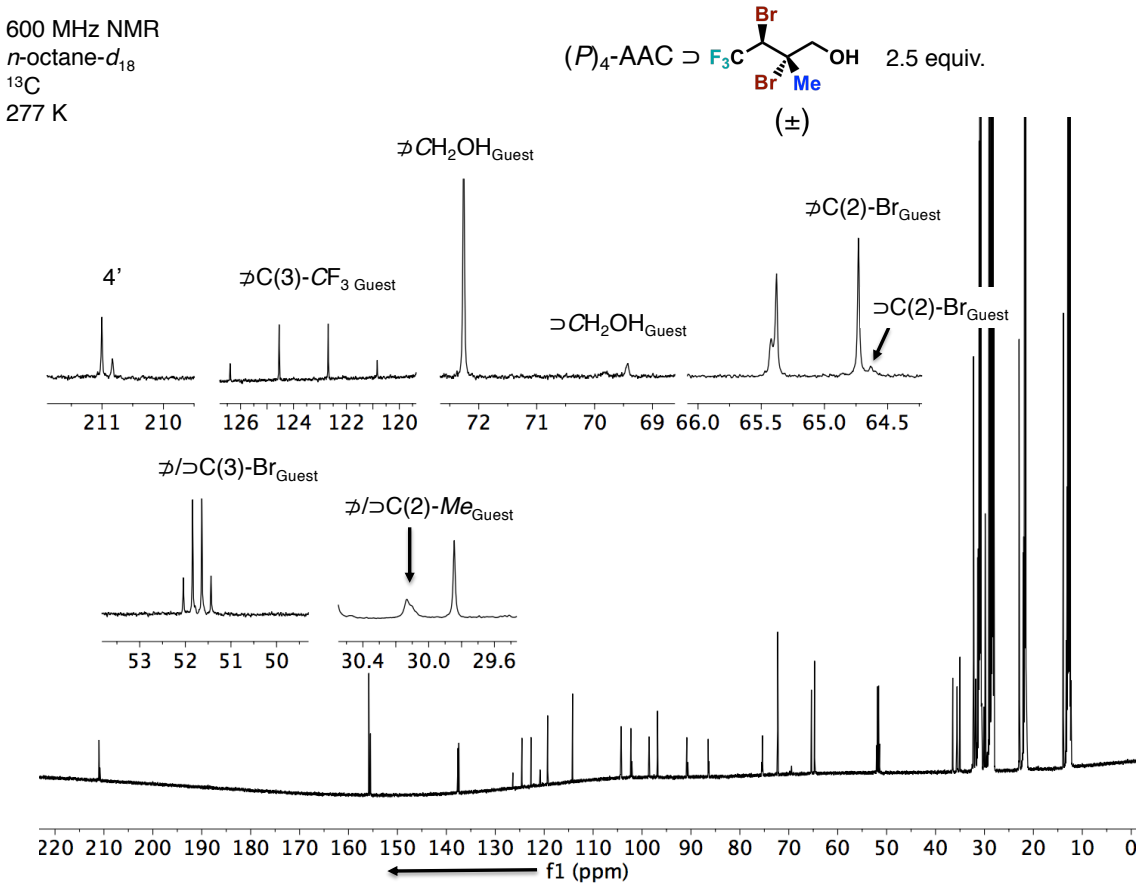

Figure S74. ^{13}C NMR (150 MHz) traces of AAC (*P*)$_4$-**1** (7.0 mM) in [D$_{18}$]*n*-octane at 277 K with 2.5 equiv. of (*R**,*S**)-**12**. The ⊃ denotes the complexed guest and ⊅ signifies the unbound at slow exchange on the NMR-timescale.

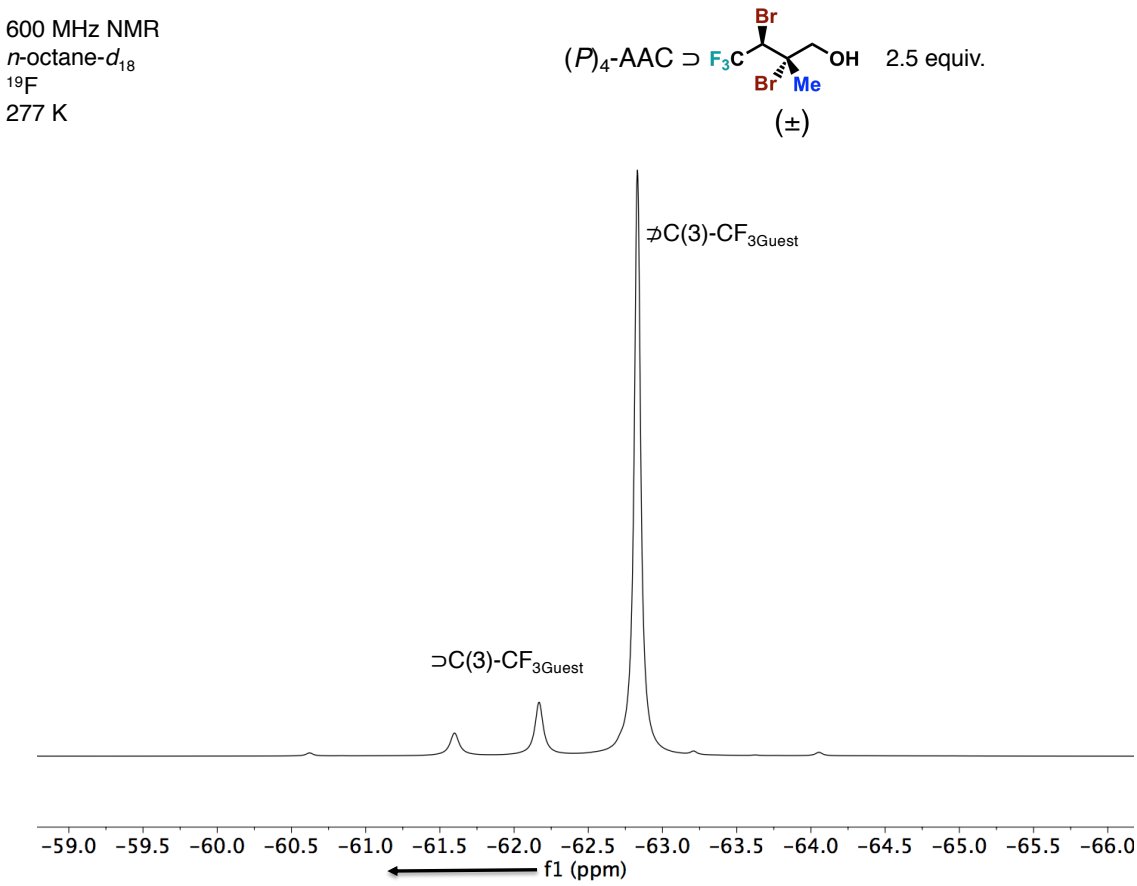

Figure S75. ^{19}F NMR traces of AAC $(P)_4$-**1** (7.0 mM) in [D_{18}]*n*-octane at 277 K with 2.5 equiv. of (*R**,*S**)-**12**. The ⊃ denotes the complexed guest and ⊅ signifies the unbound at slow exchange on the NMR-timescale.

S9. Splitting of the Host-OH-Bonding Array upon Complexation of Guests

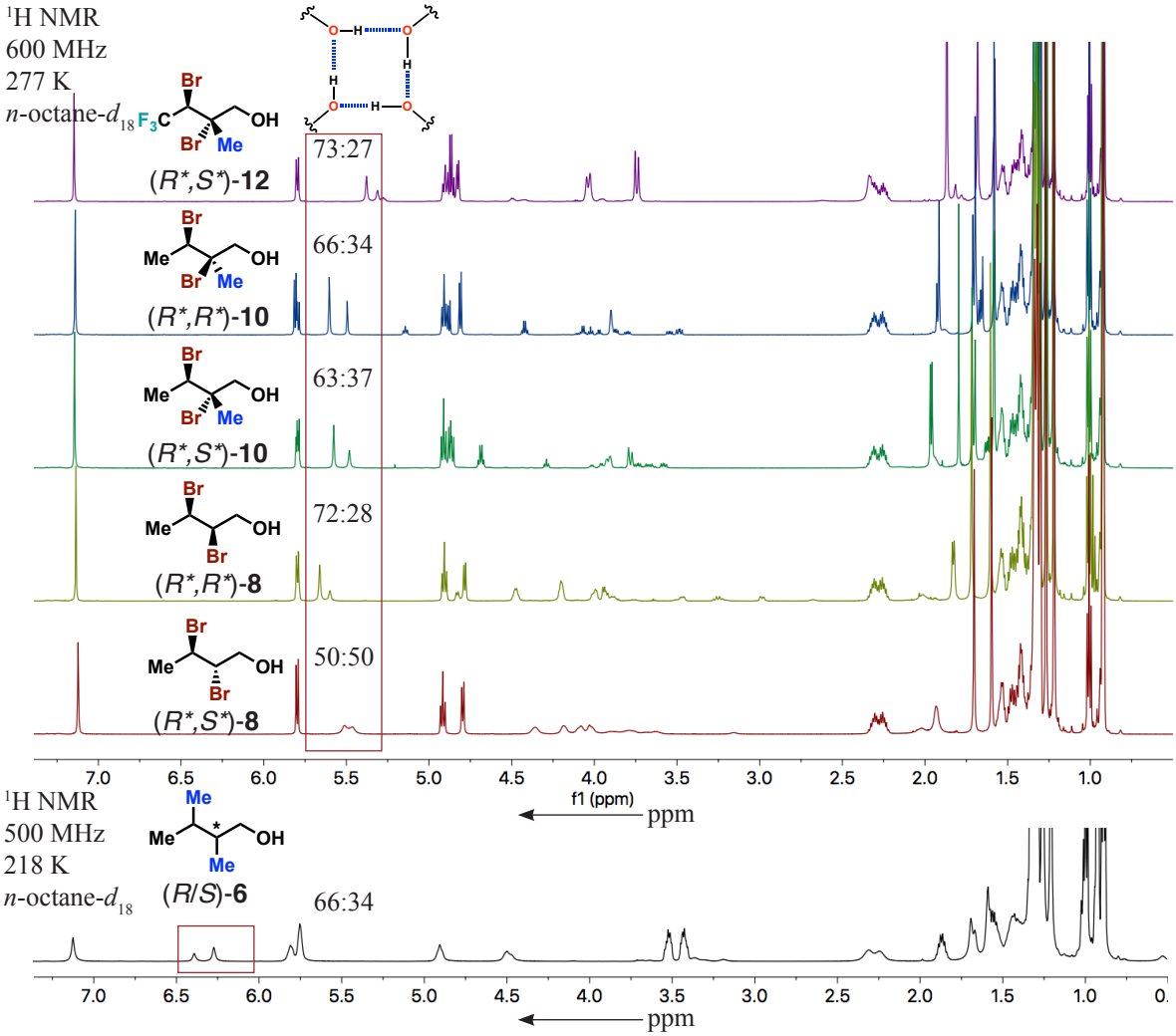

Figure S76. Splitting of the host-OH-bonding array of AAC $(P)_4$-**1** upon complexation of the racemic guests, as observed in the ^{1}H NMR spectroscopic traces.[8]

S10. *J*-Based Conformational Analysis of Guests 7 and 8 in Acetonitrile

Homo- and hetero-nuclear coupling constants were extracted from ^{1}H-NMR and HSQC-HECADE spectra.[9] Individual peak assignments are based on ^{1}H, ^{13}C, HSQC, HMBC and COSY spectra.

A summary of the conformational analysis of alcohols (*R**,*S**)-, (*R**,*R**)-**7** and (*R**,*S**)-, (*R**,*R**)-**8** is given in Figure S77.

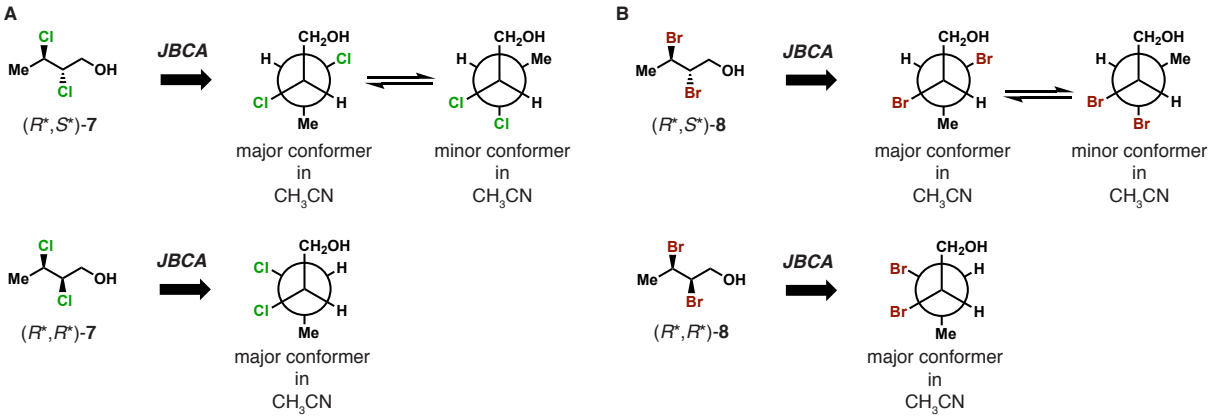

Figure S77. Conformational analysis of guests (*R**,*S**)- and (*R**,*R**)-**7**, and (*R**,*S**)- and (*R**,*R**)-**8** in CD_3CN at 298 K through 1 and 2D NMR spectroscopic experiments.

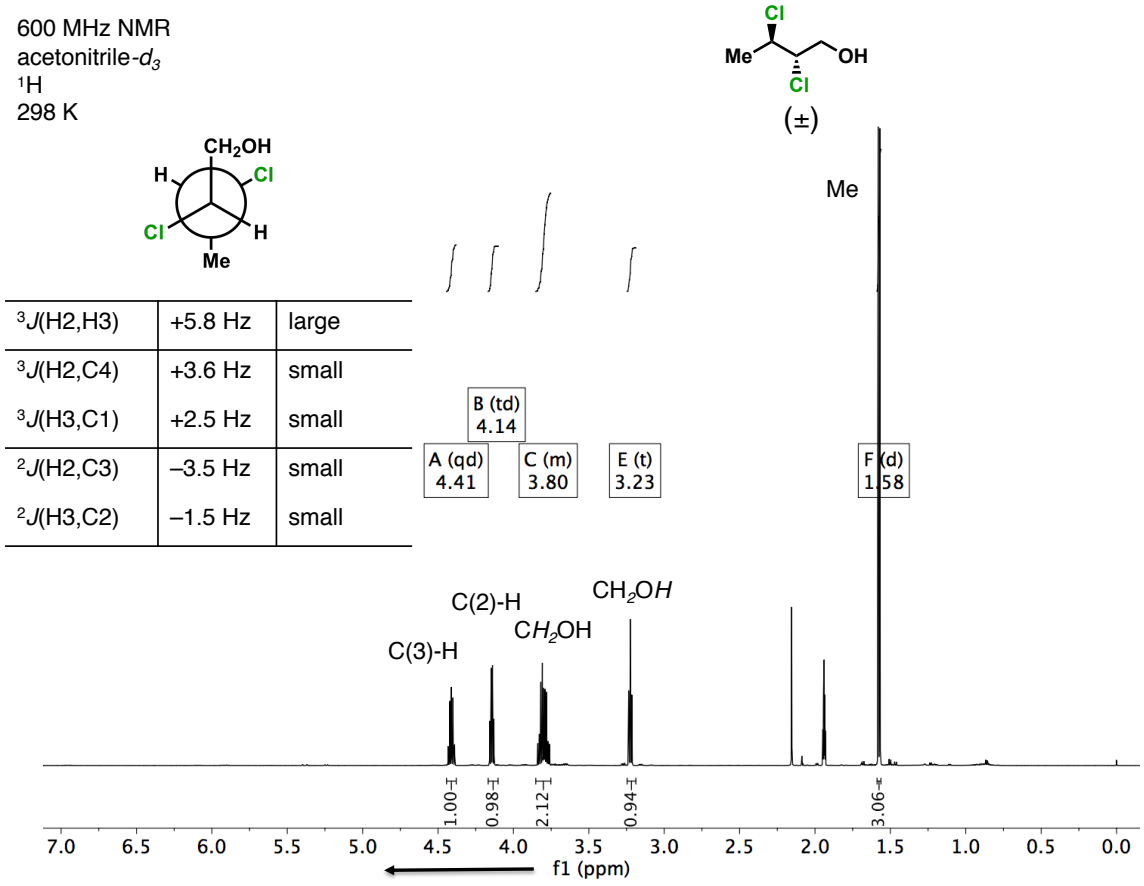

^3J(H2,H3)	+5.8 Hz	large
^3J(H2,C4)	+3.6 Hz	small
^3J(H3,C1)	+2.5 Hz	small
^2J(H2,C3)	–3.5 Hz	small
^2J(H3,C2)	–1.5 Hz	small

Figure S78. ^{1}H NMR (600 MHz) traces of (*R**,*S**)-**7** in acetonitrile-d_3 at 298 K. *J*-based coupling constants are assigned and given in the table.

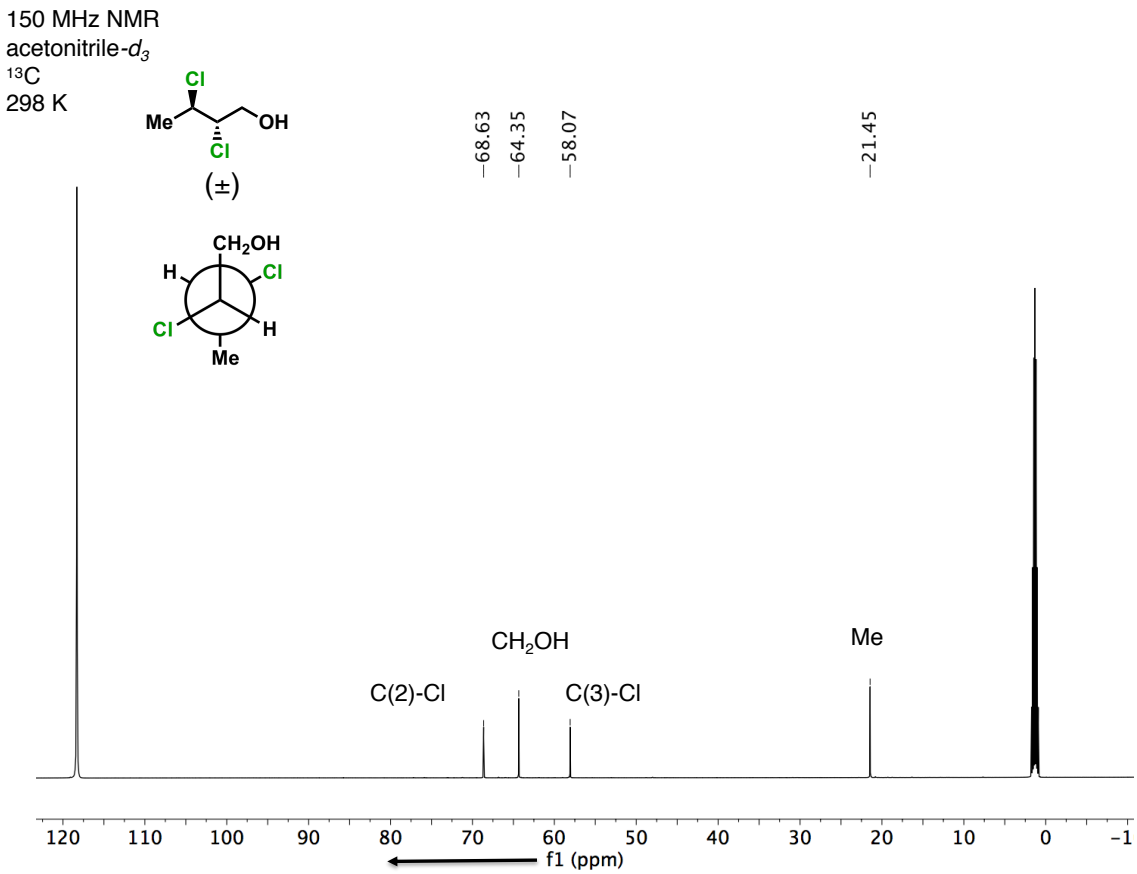

Figure S79. ^{13}C NMR (150 MHz) traces of (*R**,*S**)-**7** in acetonitrile-d_3 at 298 K.

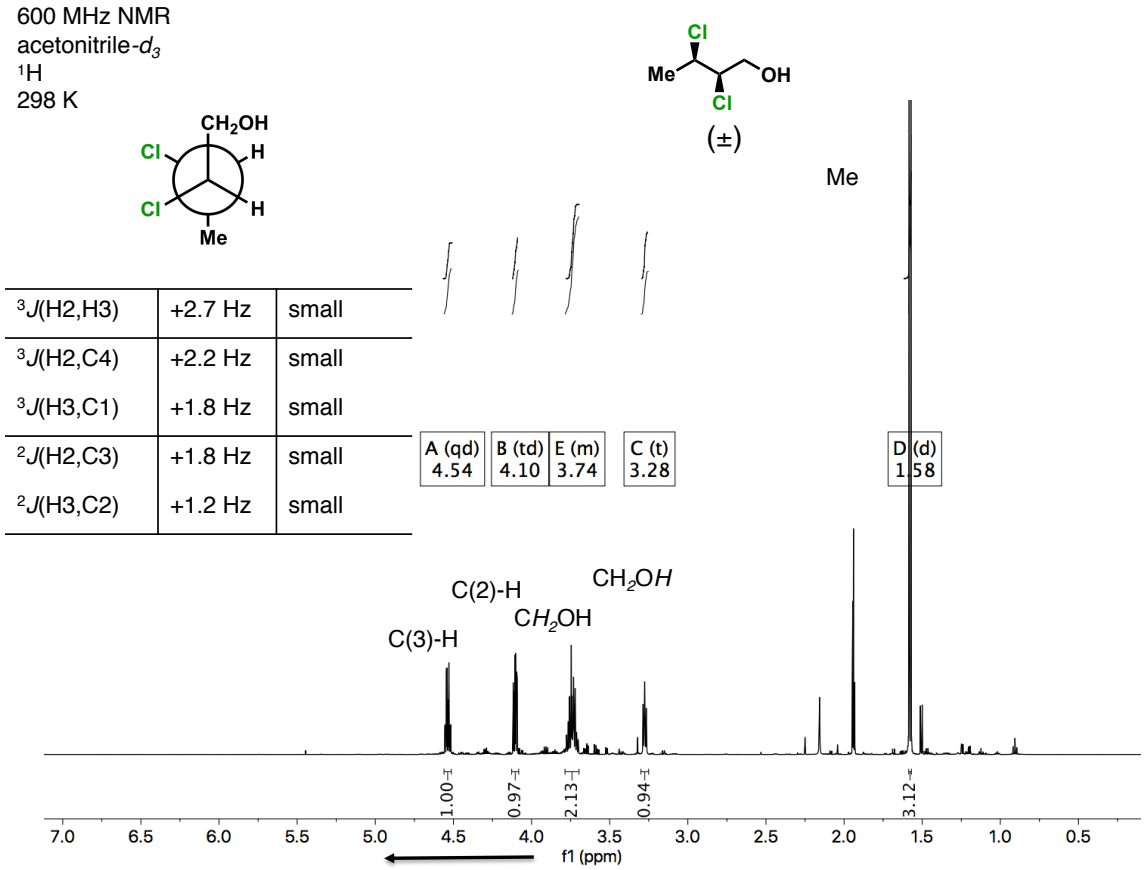

^3J(H2,H3)	+2.7 Hz	small
^3J(H2,C4)	+2.2 Hz	small
^3J(H3,C1)	+1.8 Hz	small
^2J(H2,C3)	+1.8 Hz	small
^2J(H3,C2)	+1.2 Hz	small

Figure S80. ^{1}H NMR (600 MHz) traces of (*R**,*R**)-**7** in acetonitrile-d_3 at 298 K. *J*-based coupling constants are assigned and given in the table.

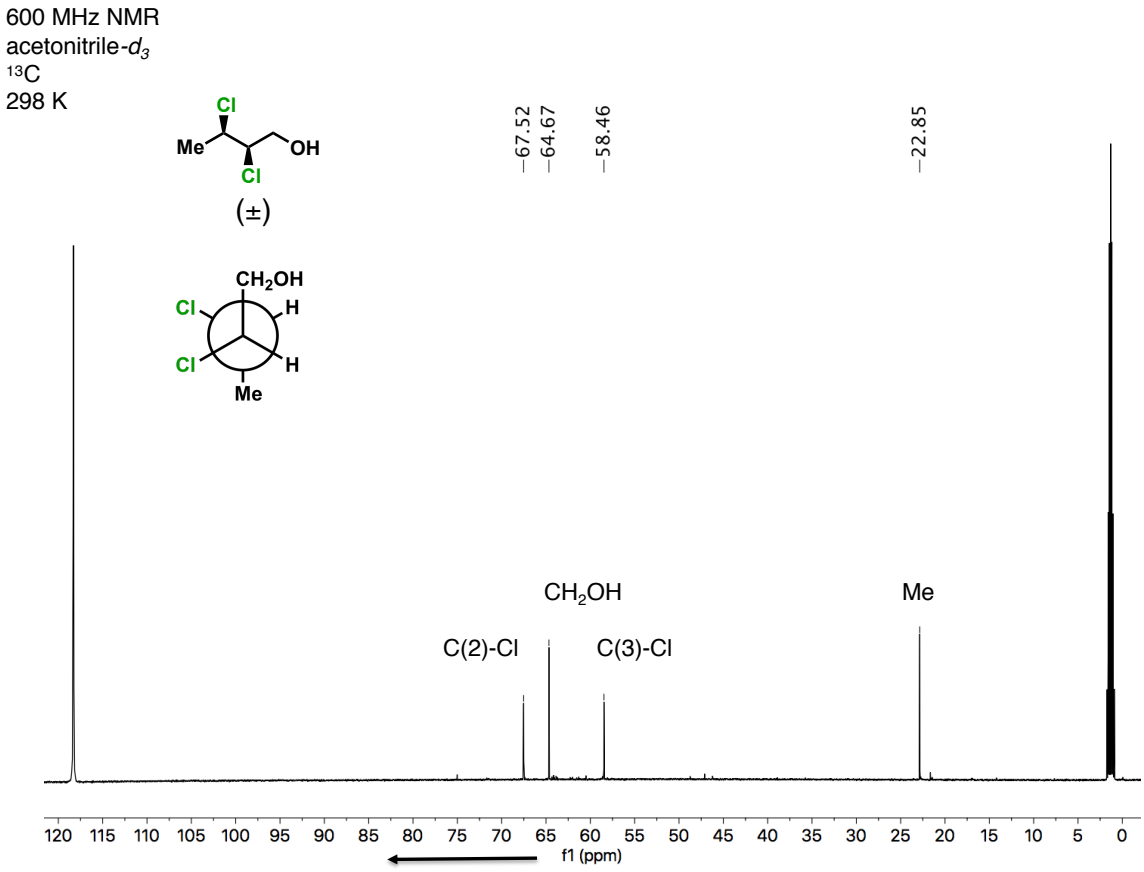

Figure S81. ^{13}C NMR (150 MHz) traces of (*R**,*R**)-**7** in acetonitrile-d_3 at 298 K.

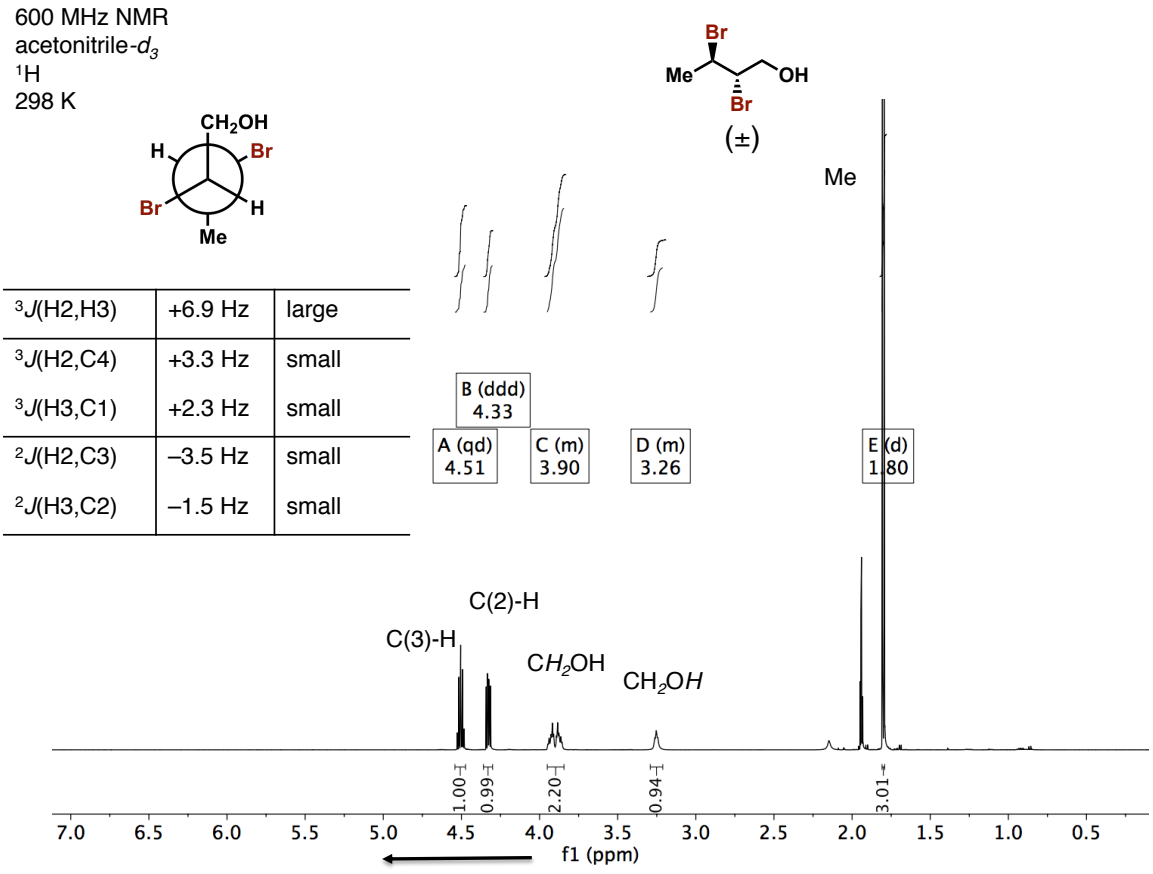

^{3}J(H2,H3)	+6.9 Hz	large
^{3}J(H2,C4)	+3.3 Hz	small
^{3}J(H3,C1)	+2.3 Hz	small
^{2}J(H2,C3)	–3.5 Hz	small
^{2}J(H3,C2)	–1.5 Hz	small

Figure S82. ^{1}H NMR (600 MHz) traces of (*R**,*S**)-**8** in acetonitrile-d_3 at 298 K. *J*-based coupling constants are assigned and given in the table.

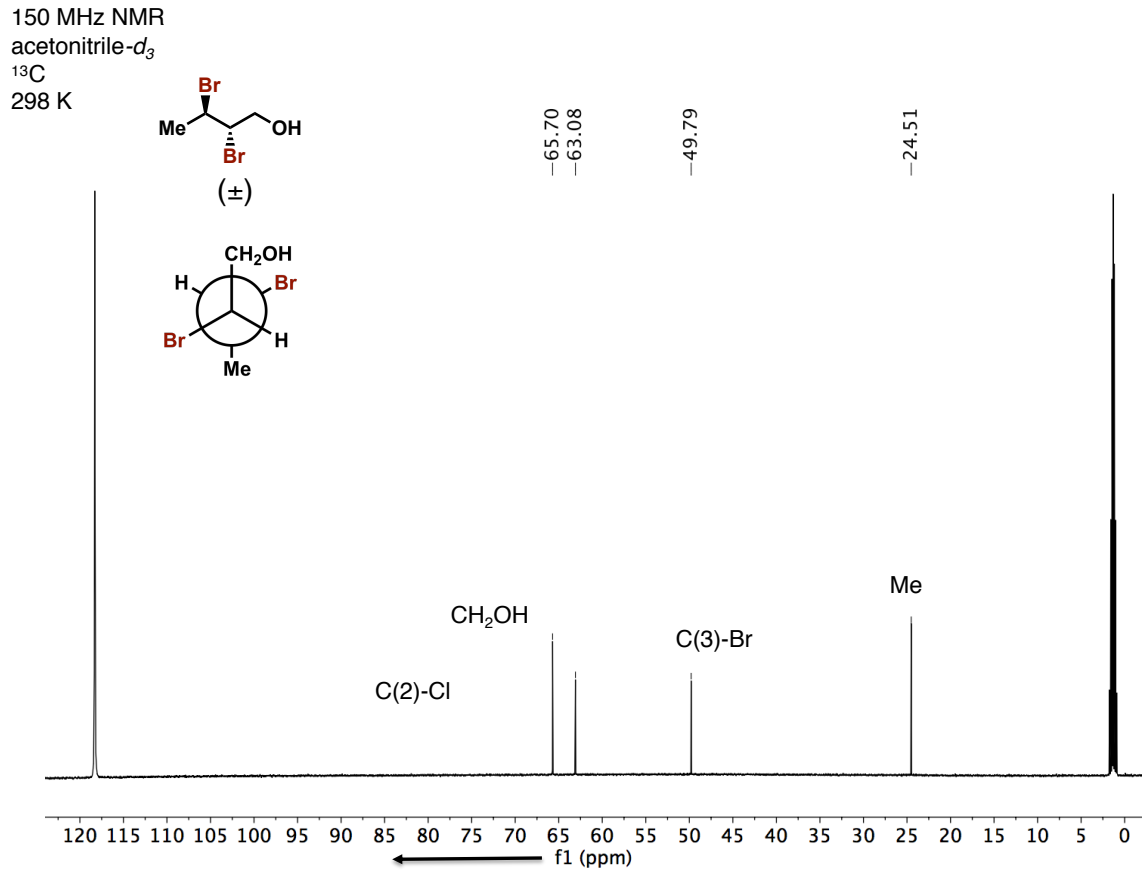

Figure S83. ^{13}C NMR (150 MHz) traces of (*R**,*S**)-**7** in acetonitrile-d_3 at 298 K.

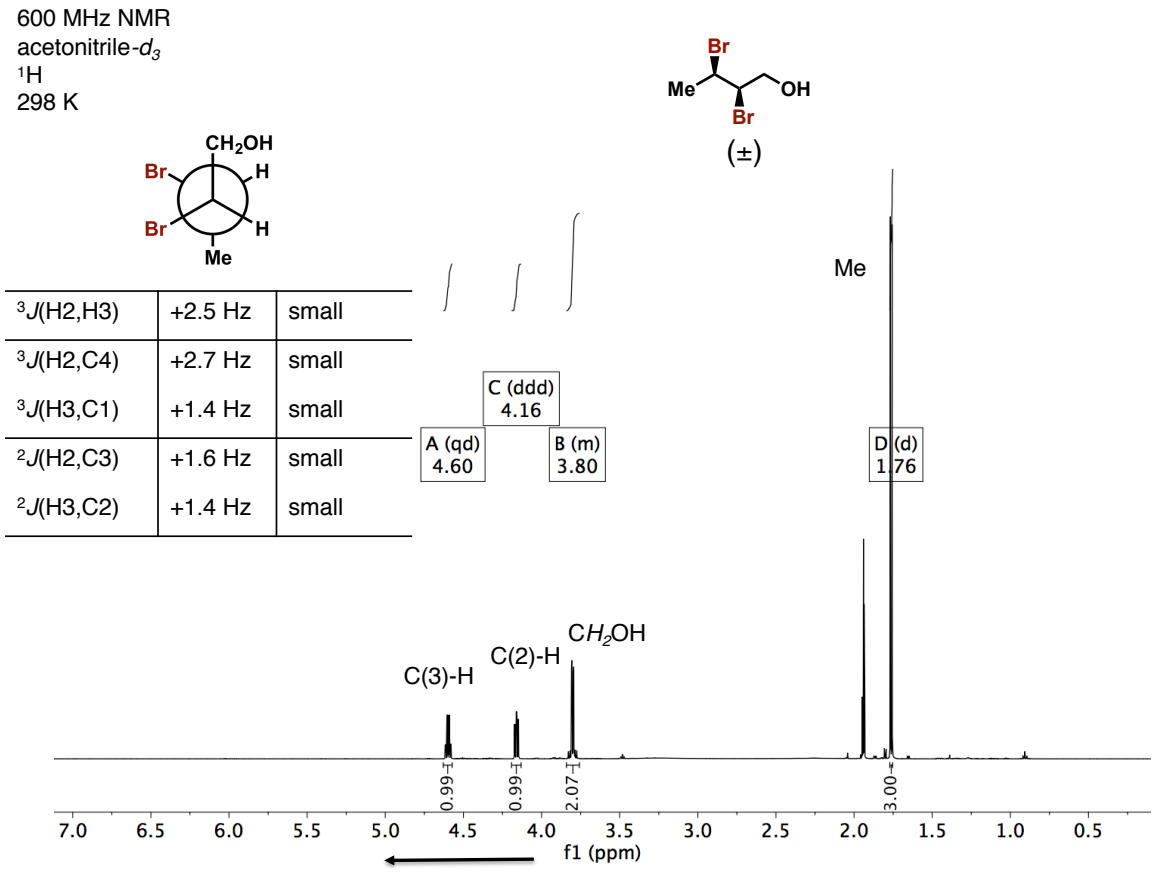

^3J(H2,H3)	+2.5 Hz	small
^3J(H2,C4)	+2.7 Hz	small
^3J(H3,C1)	+1.4 Hz	small
^2J(H2,C3)	+1.6 Hz	small
^2J(H3,C2)	+1.4 Hz	small

Figure S84. ^{1}H NMR (600 MHz) traces of (*R**,*R**)-**8** in acetonitrile-d_3 at 298 K. *J*-based coupling constants are assigned and given in the table.

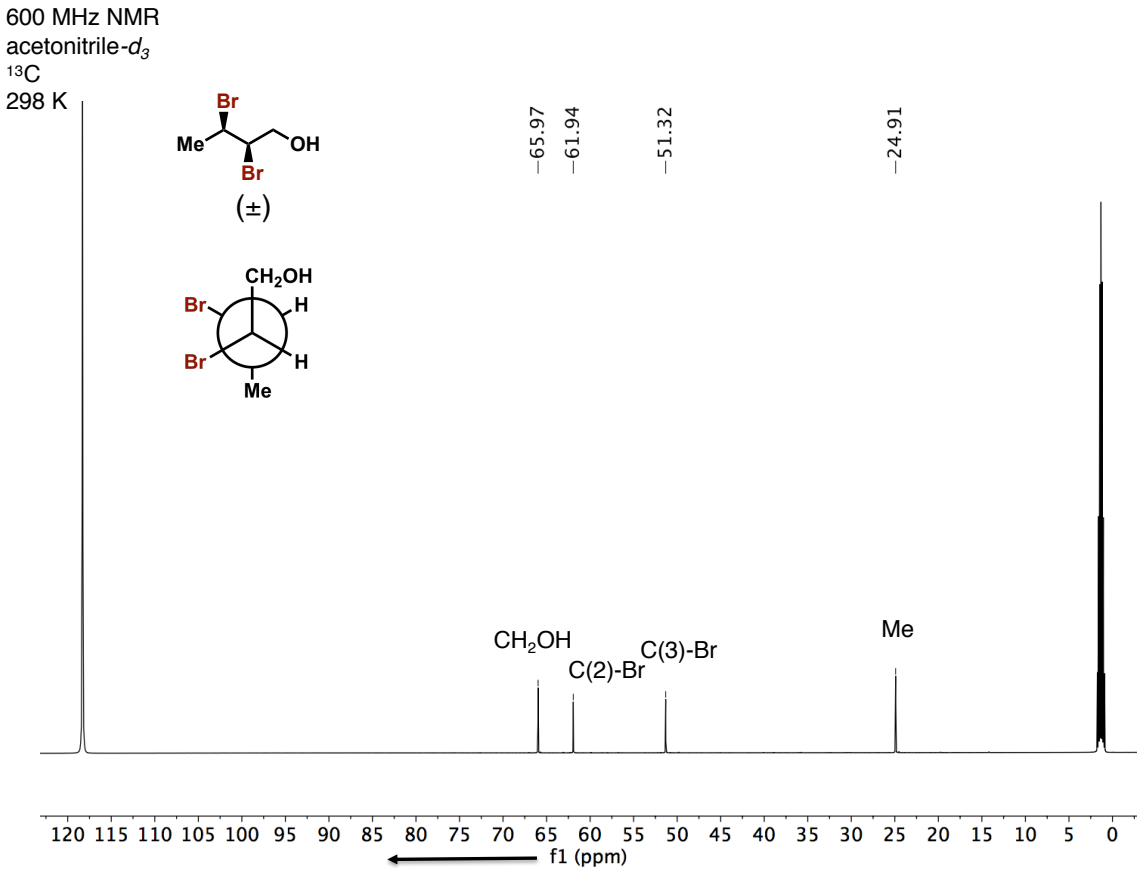

Figure S85. ^{13}C NMR (150 MHz) traces of (*R**,*R**)-**8** in acetonitrile-d_3 at 298 K.

S11. Structures Obtained from Single Crystal X-ray Diffraction

General Crystallization Protocol:

Enantiopure AAC $(P)_4$-**1** or $(M)_4$-**1** (~1 mg) were dissolved in dry acetonitrile (1mL) in a conical vials (1.5 mL) and the non-crystalline guest was added (~1–2 mg). The vial was sealed and cooled from 20 °C to 0 °C over 72–100 h using a PID controller to establish a linear profile. The single crystals were subsequently submerged in perfluoroalkylether oil and left for ca. 48 h (to allow for phase transition into the orthorhombic polymorph). Suitable single crystals were then studied by single crystal X-ray diffraction.

All X-ray co-crystal structures presented herein (CCDC 1914836-1914859) crystallized in space group $P2_12_12_1$ or $P2_1$. These usually exhibited only one cavity occupied by a guest molecule. Occasionally, they showed disorder in the top hydrogen-bonding array and alkyl periphery, corresponding with overall decreasing structure quality. Occasionally, monoclinic structures were found, but these crystals reliably and irreversibly relaxed into the orthorhombic polymorph. For this compound class, the presented X-ray co-crystal structures show comparatively high resolution and low *R* values, meeting generally accepted small molecule

crystal structure publication standards. In the following images, only the donor hydrogen atoms are shown for clarity.

Comparison of X-ray Co-crystal structures of AAC (P)$_4$-1 with Aliphatic Alcohols

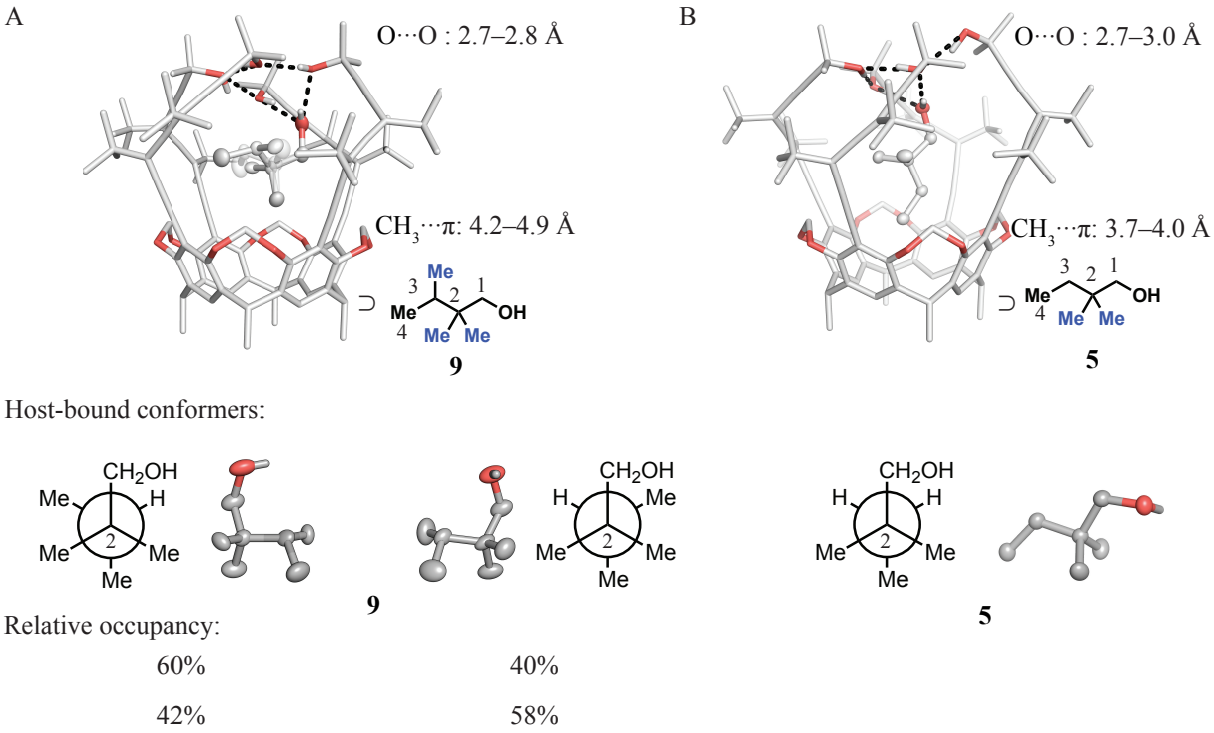

Figure S86. X-ray co-crystal structure of AAC (*P*)$_4$-**1** with 2,2,3-trimethylbutanol **9** (**A**); the guest is bound in two enantiomeric conformations. X-ray co-crystal structure of AAC (*P*)$_4$-**1** with 2,2-dimethylbutanol **5** (**B**). Distances are given in Å. *n*-Hexyl chains of the receptor are omitted for clarity. Guests are shown in their ellipsoid representation (50% probability).

Summary and Overlay of Obtained X-ray Co-crystal structures of AAC $(P)_4$-1 with Racemic Alcohols

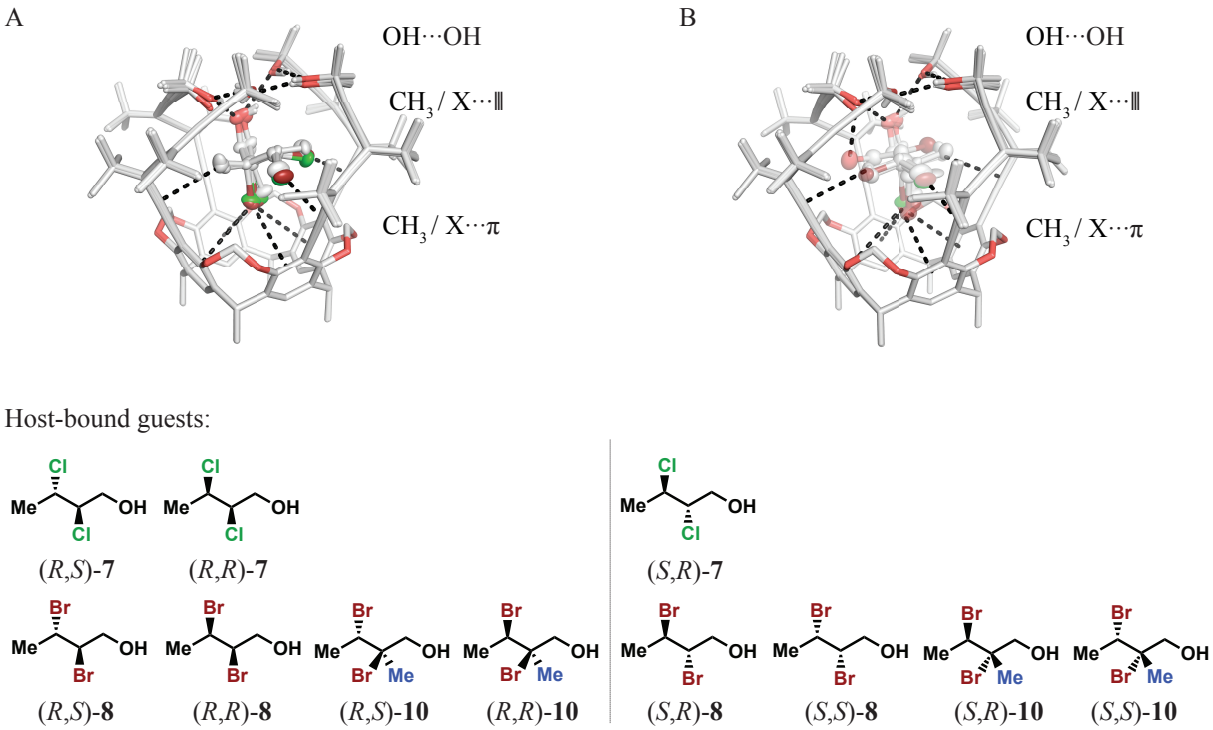

Figure S87. Overlay of X-ray co-crystal structures obtained from AAC $(P)_4$-**1** with the selected series of racemic guest molecules. Preferential complexation of the guest enantiomers was observed: The stronger binding guest enantiomers (higher occupancy) are depicted in **A**, while the weaker binding (lower occupancy) are depicted in **B** with decreased transparency of the ellipsoids. *n*-Hexyl chains of the receptor are omitted for clarity. Guests are shown in their ellipsoid representation (50% probability).

X-ray Co-Crystal Structure as Determined by Single Crystal X-Ray Diffraction: $(P)_4$-AAC⊃2,2-Dimethylbutan-1-ol 5: CCDC-1914838

Single crystals were grown following the general crystallization protocol. All protons were detected crystallographically. The H-bonding array shows a clockwise orientation.

Empirical formula	$C_{134}H_{182}O_{13}$
Formula weight	2000.79
Temperature/K	100.0(1)
Crystal system	orthorhombic
Space group	$P2_12_12_1$
a/Å	15.41030(10)
b/Å	18.60230(10)
c/Å	44.9029(2)
α/°	90
β/°	90
γ/°	90
Volume/Å^3	12872.18(12)
Z	4
ρ_{calc}g/cm^3	1.032
μ/mm^{-1}	0.501
F(000)	4360.0
Crystal size/mm^3	0.173 × 0.134 × 0.106
Radiation	CuKα (λ = 1.54184)
2Θ range for data collection/°	6.064 to 160.426
Index ranges	-16 ≤ h ≤ 19, -23 ≤ k ≤ 23, -56 ≤ l ≤ 57
Reflections collected	264846
Independent reflections	27814 [R_{int} = 0.0400, R_{sigma} = 0.0170]
Data/restraints/parameters	27814/105/1389
Goodness-of-fit on F^2	1.065
Final R indexes [I>=2σ (I)]	R_1 = 0.0366, wR_2 = 0.0997
Final R indexes [all data]	R_1 = 0.0381, wR_2 = 0.1011
Flack parameter	0.03(3)

(*P*)$_4$-AAC

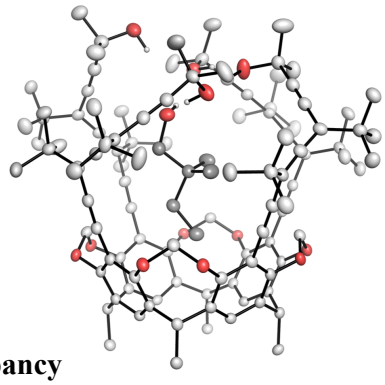

100% occupancy

Guest in cavity:

- **2,2-dimethylbutan-1-ol**

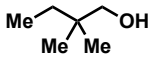

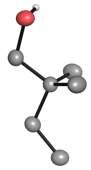

Figure S88. Crystallographic data and ORTEP representation of (*P*)$_4$-AAC⊃2,2-dimethylbutan-1-ol **5**. Ellipsoids are shown at 50% probability. *n*-Hexyl chains are omitted for clarity.

X-ray Co-Crystal Structure as Determined by Single Crystal X-Ray Diffraction: (*P*)$_4$-AAC⊃2,2,3-Trimethylbutan-1-ol 9: CCDC-1914840

Single crystals were grown following the general crystallization protocol. The guest **9** is disordered over two positions with major and minor occupancies of 60% and 40%. The different occupancy of the guest molecule corresponds to the two enantiomeric conformers depicted below. The sample was twinned, but the domains could be cleanly separated during raw data integration. HKLF5 format structure factor data was employed during final refinement. Absolute structure could not be determined from diffraction data in this case, which is of no consequence since the absolute configuration of the AAC is known.

Empirical formula	$C_{135}H_{184}O_{13}$
Formula weight	2014.81
Temperature/K	100.0(1)
Crystal system	orthorhombic
Space group	$P2_12_12_1$
a/Å	15.5129(4)
b/Å	18.7006(6)
c/Å	44.5116(19)
α/°	90
β/°	90
γ/°	90
Volume/Å^3	12912.8(8)
Z	4
ρ_{calc}g/cm^3	1.036
μ/mm^{-1}	0.502
F(000)	4392.0
Crystal size/mm^3	0.124 × 0.072 × 0.025
Radiation	CuKα (λ = 1.54184)
2Θ range for data collection/°	6.034 to 163.006
Index ranges	-19 ≤ h ≤ 19, -23 ≤ k ≤ 23, -56 ≤ l ≤ 56
Reflections collected	45980
Independent reflections	45980 [R_{int} = 0.1700, R_{sigma} = 0.1333]
Data/restraints/parameters	45980/361/1458
Goodness-of-fit on F^2	1.068
Final R indexes [I>=2σ (I)]	R_1 = 0.1270, wR_2 = 0.3004
Final R indexes [all data]	R_1 = 0.1757, wR_2 = 0.3374
Flack parameter	-0.1(5)

$(P)_4$-AAC

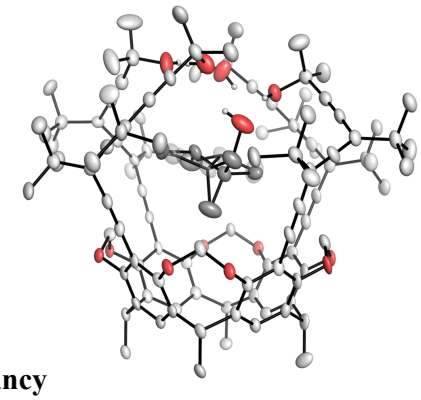

100% occupancy

Guest in cavity:

- **2,2,3-trimethylbutan-1-ol**

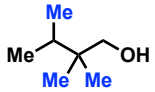

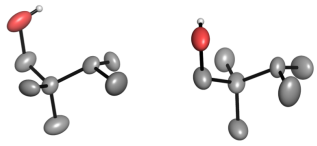

60 : 40

Figure S89. Crystallographic data and ORTEP representation of $(P)_4$-AAC⊃2,2,3-trimethylbutan-1-ol **9**. Ellipsoids are shown at 50% probability. *n*-Hexyl chains are omitted for clarity.

X-ray Co-Crystal Structure as Determined by Single Crystal X-Ray Diffraction: $(M)_4$-AAC⊃2,2,3-Trimethylbutan-1-ol 9: CCDC-1914836

Single crystals were grown following the general crystallization protocol. All protons were detected crystallographically. The H-bonding array shows a counter-clockwise orientation. The guest **9** is disordered over two positions with major and minor occupancies of 58% and 42%. The different occupancy of the guest molecule corresponds to the two enantiomeric conformers depicted below. Traces of solvent encapsulation in the AAC are visible in the difference density map, but proved too insignificant to refine in a stable convergent model.

Empirical formula	$C_{135}H_{184}O_{13}$
Formula weight	2014.81
Temperature/K	100.0(1)
Crystal system	orthorhombic
Space group	$P2_12_12_1$
a/Å	15.51930(10)
b/Å	18.67160(10)
c/Å	44.6387(6)
α/°	90
β/°	90
γ/°	90
Volume/Å^3	12935.0(2)
Z	4
ρ_{calc}g/cm^3	1.035
μ/mm^{-1}	0.501
F(000)	4392.0
Crystal size/mm^3	0.117 × 0.058 × 0.051
Radiation	CuKα (λ = 1.54184)
2Θ range for data collection/°	6.03 to 161.466
Index ranges	-19 ≤ h ≤ 19, -17 ≤ k ≤ 23, -56 ≤ l ≤ 56
Reflections collected	268363
Independent reflections	27902 [R_{int} = 0.0701, R_{sigma} = 0.0326]
Data/restraints/parameters	27902/355/1484
Goodness-of-fit on F^2	1.032
Final *R* indexes [I>=2σ (I)]	R_1 = 0.0525, wR_2 = 0.1366
Final *R* indexes [all data]	R_1 = 0.0668, wR_2 = 0.1473
Flack parameter	0.03(5)

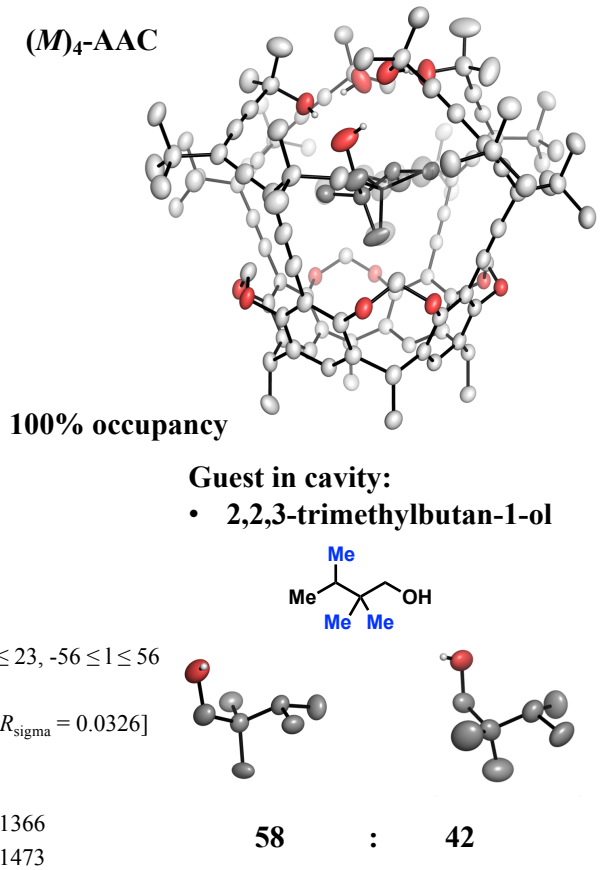

Figure S90. Crystallographic data and ORTEP representation of (*M*)$_4$-AAC⊃2,2,3-trimethylbutan-1-ol **9**. Ellipsoids are shown at 50% probability. *n*-Hexyl chains are omitted for clarity.

X-ray Co-Crystal Structure as Determined by Single Crystal X-Ray Diffraction: (*P*)$_4$-AAC⊃(±)-(2*S,3*R**)-2,3-Dichlorobutan-1-ol** (*R**,*S**)**-7:** CCDC-1914858

Single crystals were grown following the general crystallization protocol. The guest (*R**,*S**)-**7** is disordered over two positions with major and minor occupancies of 58% and 42%. The different occupancy of the guest molecule corresponds to the two enantiomers depicted below.

Empirical formula	$C_{132}H_{176}Cl_2O_{13}$
Formula weight	2041.62
Temperature/K	100.0(1)
Crystal system	orthorhombic
Space group	$P2_12_12_1$
a/Å	15.61350(10)
b/Å	18.75150(10)
c/Å	43.6512(2)
α/°	90
β/°	90
γ/°	90
Volume/Å^3	12780.05(12)
Z	4
ρ_{calc}g/cm^3	1.061
μ/mm^{-1}	0.889
F(000)	4424.0
Crystal size/mm^3	0.154 × 0.112 × 0.076
Radiation	CuKα (λ = 1.54184)
2Θ range for data collection/°	6.012 to 159.476
Index ranges	-15 ≤ h ≤ 19, -23 ≤ k ≤ 23, -55 ≤ l ≤ 55
Reflections collected	210898
Independent reflections	27582 [R_{int} = 0.0432, R_{sigma} = 0.0227]
Data/restraints/parameters	27582/366/1442
Goodness-of-fit on F^2	1.028
Final R indexes [I>=2σ (I)]	R_1 = 0.0718, wR_2 = 0.2119
Final R indexes [all data]	R_1 = 0.0757, wR_2 = 0.2171
Flack parameter	0.066(4)

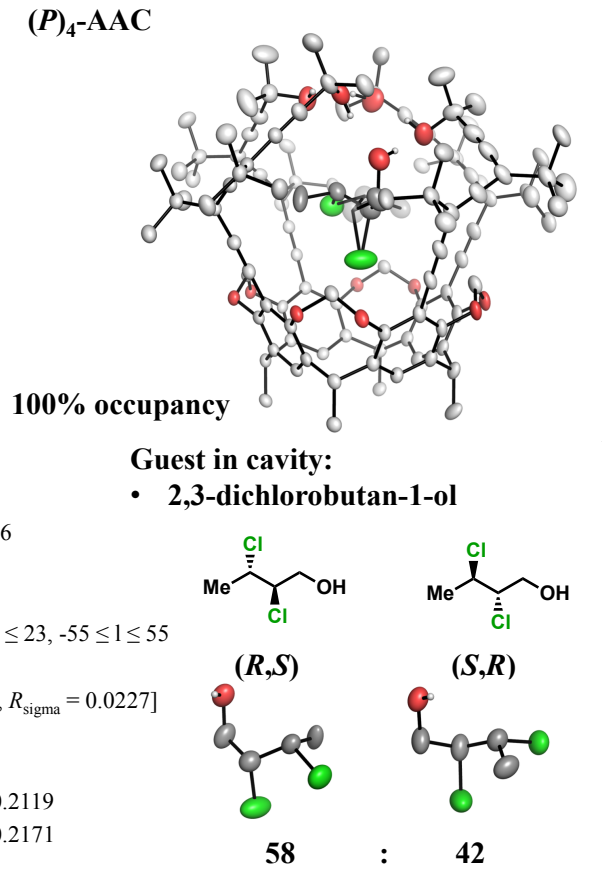

Figure S91. Crystallographic data and ORTEP representation of $(P)_4$-AAC⊃(±)-(2*S**,3*R**)-2,3-dichlorobutan-1-ol (*R**,*S**)-**7**. Ellipsoids are shown at 50% probability. *n*-Hexyl chains are omitted for clarity.

X-ray Co-Crystal Structure as Determined by Single Crystal X-Ray Diffraction: $(M)_4$-AAC⊃(±)-(2*S,3*R**)-2,3-Dichlorobutan-1-ol** (*R**,*S**)**-7:** CCDC-1914853

Single crystals were grown following the general crystallization protocol. All protons were detected crystallographically. The guest (*R**,*S**)-**7** is disordered over two positions with major and minor occupancies of 53% and 47%. The different occupancy of the guest molecule corresponds to the two enantiomers depicted below.

Empirical formula	$C_{132}H_{176}Cl_2O_{13}$
Formula weight	2041.62
Temperature/K	100.0(1)
Crystal system	orthorhombic
Space group	$P2_12_12_1$
a/Å	15.59180(10)
b/Å	18.73920(10)
c/Å	43.8114(2)
α/°	90
β/°	90
γ/°	90
Volume/Å^3	12800.72(12)
Z	4
ρ_{calc}g/cm^3	1.059
μ/mm^{-1}	0.888
F(000)	4424.0
Crystal size/mm^3	0.187 × 0.096 × 0.036
Radiation	CuKα (λ = 1.54184)
2Θ range for data collection/°	6.206 to 159.38
Index ranges	-19 ≤ h ≤ 18, -23 ≤ k ≤ 23, -55 ≤ l ≤ 54
Reflections collected	212369
Independent reflections	27540 [R_{int} = 0.0447, R_{sigma} = 0.0236]
Data/restraints/parameters	27540/270/1446
Goodness-of-fit on F^2	1.028
Final R indexes [I>=2σ (I)]	R_1 = 0.0506, wR_2 = 0.1463
Final R indexes [all data]	R_1 = 0.0542, wR_2 = 0.1504
Flack parameter	0.025(4)

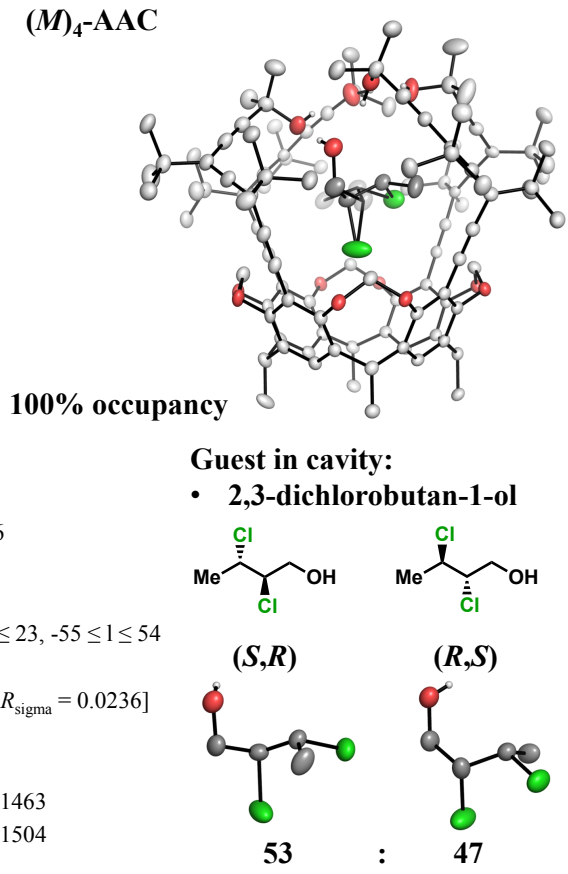

Figure S92. Crystallographic data and ORTEP representation of $(M)_4$-AAC⊃(±)-(2*S**,3*R**)-2,3-dichlorobutan-1-ol (*R**,*S**)-**7**. Ellipsoids are shown at 50% probability. *n*-Hexyl chains are omitted for clarity.

X-ray Co-Crystal Structure as Determined by Single Crystal X-Ray Diffraction: $(P)_4$-AAC⊃(±)-(2*R,3*R**)-2,3-Dichlorobutan-1-ol** (*R**,*R**)-**7:** CCDC-1914852

Single crystals were grown following the general crystallization protocol. The guest (*R**,*R**)-**7** shows 50% occupancy, with some indications in the difference density that the remaining occupancy consists of DCM. However, this could not be modelled.

Empirical formula	$C_{130.0}H_{173.0}Cl_{1.0}O_{12.5}$
Formula weight	1969.44
Temperature/K	100.0(1)
Crystal system	orthorhombic
Space group	$P2_12_12_1$
a/Å	15.60340(10)
b/Å	18.7470(2)
c/Å	43.6221(4)
α/°	90
β/°	90
γ/°	90
Volume/Å^3	12760.2(2)
Z	4
ρ_{calc}g/cm^3	1.025
μ/mm^{-1}	0.683
F(000)	4275.0
Crystal size/mm^3	0.122 × 0.11 × 0.044
Radiation	CuKα (λ = 1.54184)
2Θ range for data collection/°	6.016 to 160.042
Index ranges	-19 ≤ h ≤ 17, -21 ≤ k ≤ 23, -55 ≤ l ≤ 55
Reflections collected	210282
Independent reflections	27516 [R_{int} = 0.0678, R_{sigma} = 0.0368]
Data/restraints/parameters	27516/263/1419
Goodness-of-fit on F^2	1.036
Final *R* indexes [I>=2σ (I)]	R_1 = 0.0713, wR_2 = 0.1983
Final *R* indexes [all data]	R_1 = 0.0837, wR_2 = 0.2112
Flack parameter	0.029(8)

(*P*)$_4$-AAC

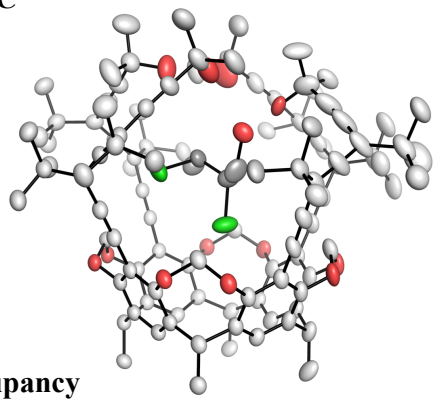

50% occupancy

Guest in cavity:

- **2,3-dichlorobutan-1-ol**

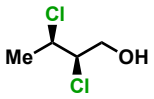

(*R*,*R*)

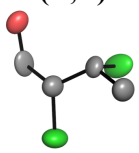

Figure S93. Crystallographic data and ORTEP representation of (*P*)$_4$-AAC⊃(±)-(2*R**,3*R**)-2,3-dichlorobutan-1-ol (*R**,*R**)-**7**. Ellipsoids are shown at 50% probability. *n*-Hexyl chains are omitted for clarity.

X-ray Co-Crystal Structure as Determined by Single Crystal X-Ray Diffraction: (*M*)$_4$-AAC⊃(±)-(2*R,3*R**)-2,3-Dichlorobutan-1-ol** (*R**,*R**)**-7:** CCDC-1914855

Single crystals were grown following the general crystallization protocol. The guest (*R**,*R**)-**7** shows 70% occupancy. The remaining cavities are occupied by an alternate conformation of the guest molecule with the hydroxyl group pointing toward the cage walls, but this species could not be refined within a stable and convergent model.

Empirical formula	$C_{130.8}H_{173.5}Cl_{1.4}O_{12.7}$
Formula weight	1997.16
Temperature/K	100.0(1)
Crystal system	orthorhombic
Space group	$P2_12_12_1$
a/Å	15.55690(10)
b/Å	18.73900(10)
c/Å	43.9862(3)
α/°	90
β/°	90
γ/°	90
Volume/Å^3	12822.89(14)
Z	4
ρ_{calc}g/cm^3	1.035
μ/mm^{-1}	0.759
F(000)	4332.0
Crystal size/mm^3	0.165 × 0.113 × 0.029
Radiation	CuKα (λ = 1.54184)
2Θ range for data collection/°	6.196 to 159.444
Index ranges	-18 ≤ h ≤ 19, -18 ≤ k ≤ 23, -55 ≤ l ≤ 55
Reflections collected	212820
Independent reflections	27663 [R_{int} = 0.0437, R_{sigma} = 0.0225]
Data/restraints/parameters	27663/249/1411
Goodness-of-fit on F^2	1.031
Final *R* indexes [I>=2σ (I)]	R_1 = 0.0625, wR_2 = 0.1783
Final *R* indexes [all data]	R_1 = 0.0686, wR_2 = 0.1853
Flack parameter	0.021(4)

(*M*)$_4$-AAC

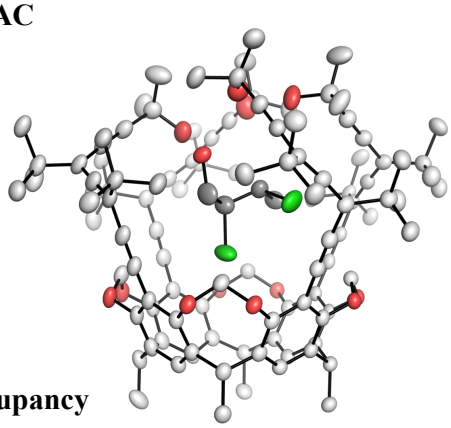

70% occupancy

Guest in cavity:

- **2,3-dichlorobutan-1-ol**

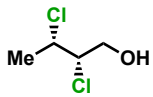

(*S*,*S*)

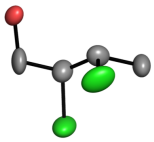

Figure S94. Crystallographic data and ORTEP representation of (*M*)$_4$-AAC⊃(±)-(2*R**,3*R**)-2,3-dichlorobutan-1-ol (*R**,*R**)-**7**. Ellipsoids are shown at 50% probability. *n*-Hexyl chains are omitted for clarity.

X-ray Co-Crystal Structure as Determined by Single Crystal X-Ray Diffraction: (*P*)$_4$-AAC⊃(±)-(2*S,3*R**)-2,3-Dibromobutan-1-ol** (*R**,*S**)**-8:** CCDC-1914857

Single crystals were grown following the general crystallization protocol. The guest (*R**,*S**)-**8** is disordered over two positions with occupancies of 50%. The different occupancy of the guest molecule corresponds to the two enantiomers depicted below. Hydrogen bonding pattern direction was chosen arbitrarily as residual peaks for protons were not detected. There are weak residual peaks clearly matching an alternate rotamer or different guest. Other possible reasons such as twinning or poor data could be excluded. In this alternate structure the hydrogen bonding array is clearly fully closed (only one host hydroxyl group is affected), equidistant and planar, i.e. no hydroxyl group of the guest impurity points towards the array. However, since the contribution is weak (5% or less), all refinement attempts failed and the alternate orientations were omitted from the model. An additional structure, in which two orientations of the guest molecule amount to only 60% occupancy (with residual electron density too diffuse to identify) is deposited under CCDC-1914843.

Empirical formula	$C_{132}H_{176}Br_2O_{13}$
Formula weight	2130.54
Temperature/K	100.0(1)
Crystal system	orthorhombic
Space group	$P2_12_12_1$
a/Å	43.9781(5)
b/Å	18.7317(2)
c/Å	15.60869(16)
α/°	90
β/°	90
γ/°	90
Volume/Å^3	12858.2(2)
Z	4
ρ_{calc}g/cm^3	1.101
μ/mm^{-1}	1.230
F(000)	4568.0
Crystal size/mm^3	0.156 × 0.077 × 0.042
Radiation	CuKα (λ = 1.54184)
2Θ range for data collection/°	6.008 to 159.788
Index ranges	-55 ≤ h ≤ 54, -17 ≤ k ≤ 23, -19 ≤ l ≤ 17
Reflections collected	95618
Independent reflections	26585 [R_{int} = 0.0700, R_{sigma} = 0.0515]
Data/restraints/parameters	26585/257/1442
Goodness-of-fit on F^2	1.022
Final R indexes [I>=2σ (I)]	R_1 = 0.0819, wR_2 = 0.2392
Final R indexes [all data]	R_1 = 0.0890, wR_2 = 0.2469
Flack parameter	-0.013(9)

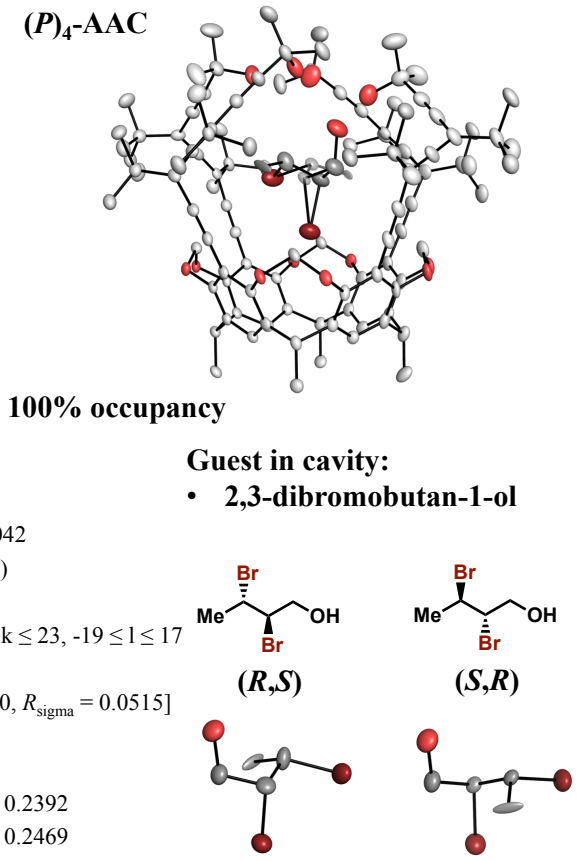

Figure S95. Crystallographic data and ORTEP representation of $(P)_4$-AAC⊃(±)-(2*S**,3*R**)-2,3-dibromobutan-1-ol (*R**,*S**)-**8**. Ellipsoids are shown at 50% probability. *n*-Hexyl chains are omitted for clarity.

X-ray Co-Crystal Structure as Determined by Single Crystal X-Ray Diffraction: (*M*)$_4$-AAC⊃(±)-(2*S,3*R**)-2,3-Dibromobutan-1-ol** (*R**,*S**)**-8:** CCDC-1914841

Single crystals were grown following the general crystallization protocol. The guest (*R**,*S**)-**8** is disordered over two positions with major and minor occupancies of 56% and 44%. The different occupancy of the guest molecule corresponds to the two enantiomers depicted below. All hydrogen positions were detected crystallographically. There are weak residual peaks clearly matching two alternate guest rotamers or different guest species. Other possible reasons such as twinning or poor data could be excluded. However, since the contribution is weak (5% or less), all refinement attempts failed and the alternate orientations were omitted from the model.

Empirical formula	$C_{132}H_{176}Br_2O_{13}$
Formula weight	2130.54
Temperature/K	100.0(1)
Crystal system	orthorhombic
Space group	$P2_12_12_1$
a/Å	15.60580(10)
b/Å	18.73660(10)
c/Å	43.8709(3)
α/°	90
β/°	90
γ/°	90
Volume/Å^3	12827.84(14)
Z	4
ρ_{calc}g/cm^3	1.103
μ/mm^{-1}	1.233
F(000)	4568.0
Crystal size/mm^3	0.226 × 0.111 × 0.075
Radiation	CuKα (λ = 1.54184)
2Θ range for data collection/°	6.012 to 159.616
Index ranges	-19 ≤ h ≤ 16, -23 ≤ k ≤ 22, -55 ≤ l ≤ 55
Reflections collected	210855
Independent reflections	27662 [R_{int} = 0.0481, R_{sigma} = 0.0256]
Data/restraints/parameters	27662/287/1453
Goodness-of-fit on F^2	1.036
Final R indexes [I>=2σ (I)]	R_1 = 0.0821, wR_2 = 0.2409
Final R indexes [all data]	R_1 = 0.0865, wR_2 = 0.2481
Flack parameter	0.014(4)

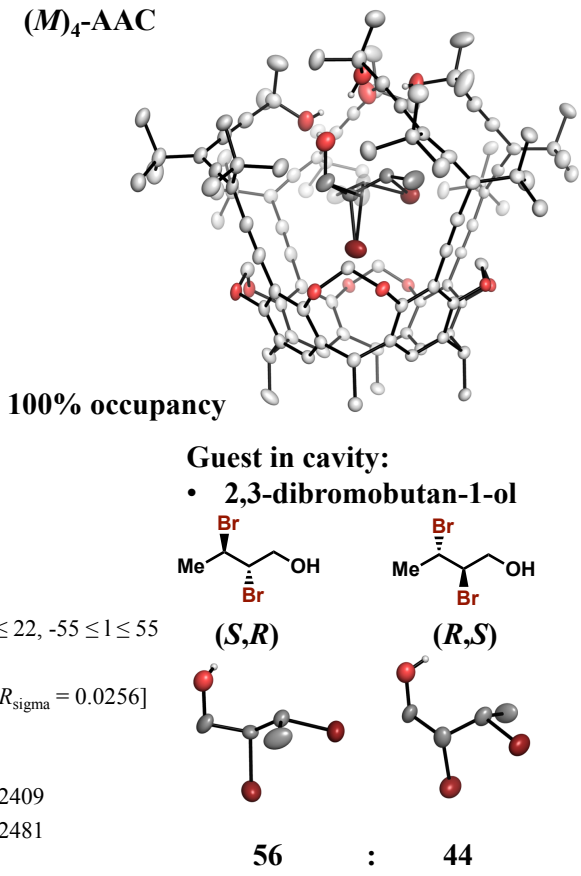

Figure S96. Crystallographic data and ORTEP representation of (*M*)$_4$-AAC⊃(±)-(2*S**,3*R**)-2,3-dibromobutan-1-ol (*R**,*S**)-**8**. Ellipsoids are shown at 50% probability. *n*-Hexyl chains are omitted for clarity.

X-ray Co-Crystal Structure as Determined by Single Crystal X-Ray Diffraction: (*P*)$_4$-AAC⊃(±)-(2*R,3*R**)-2,3-Dibromobutan-1-ol** (*R**,*R**)-**8:** CCDC-1914842

Single crystals were grown following the general crystallization protocol. The guest (*R**,*R**)-**8** is disordered over three positions with major and minor occupancies of 68%, 24% and 8%. The different occupancy of the guest molecule corresponds to the two enantiomers depicted below.

Empirical formula	$C_{132}H_{176}Br_2O_{13}$
Formula weight	2130.51
Temperature/K	100.0(1)
Crystal system	orthorhombic
Space group	$P2_12_12_1$
a/Å	15.55780(10)
b/Å	18.75530(10)
c/Å	43.8495(3)
α/°	90
β/°	90
γ/°	90
Volume/Å^3	12794.90(14)
Z	4
ρ_{calc}g/cm^3	1.106
μ/mm^{-1}	1.236
F(000)	4568.0
Crystal size/mm^3	0.149 × 0.126 × 0.031
Radiation	CuKα (λ = 1.54184)
2Θ range for data collection/°	6.202 to 160.242
Index ranges	-18 ≤ h ≤ 19, -23 ≤ k ≤ 23, -55 ≤ l ≤ 55
Reflections collected	212525
Independent reflections	27576 [R_{int} = 0.0505, R_{sigma} = 0.0266]
Data/restraints/parameters	27576/303/1507
Goodness-of-fit on F^2	1.034
Final R indexes [I>=2σ (I)]	R_1 = 0.0536, wR_2 = 0.1493
Final R indexes [all data]	R_1 = 0.0601, wR_2 = 0.1554
Flack parameter	-0.007(3)

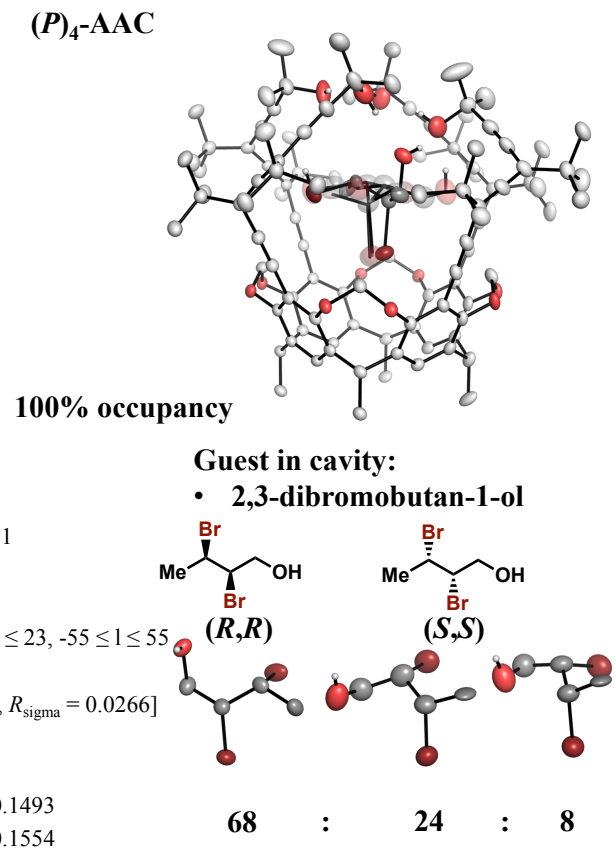

Figure S97. Crystallographic data and ORTEP representation of $(P)_4$-AAC⊃(±)-(2*R**,3*R**)-2,3-dibromobutan-1-ol (*R**,*R**)-**8**. Ellipsoids are shown at 50% probability. *n*-Hexyl chains are omitted for clarity.

X-ray Co-Crystal Structure as Determined by Single Crystal X-Ray Diffraction: $(M)_4$-AAC⊃(±)-(2*R,3*R**)-2,3-Dibromobutan-1-ol** (*R**,*R**)**-8:** CCDC-1914837

Single crystals were grown following the general crystallization protocol. The guest (*R**,*R**)-**8** shows 66% occupancy. The residual density was too diffuse to discern the remaining content.

Empirical formula	$C_{130.7}H_{173.3}Br_{1.3}O_{12.7}$
Formula weight	2051.95
Temperature/K	100.0(1)
Crystal system	orthorhombic
Space group	$P2_12_12_1$
a/Å	15.56520(10)
b/Å	18.75780(10)
c/Å	43.9214(3)
α/°	90
β/°	90
γ/°	90
Volume/Å^3	12823.68(14)
Z	4
ρ_{calc}g/cm^3	1.063
μ/mm^{-1}	0.977
F(000)	4419.0
Crystal size/mm^3	0.14 × 0.067 × 0.03
Radiation	CuKα (λ = 1.54184)
2Θ range for data collection/°	6.024 to 159.704
Index ranges	-19 ≤ h ≤ 16, -23 ≤ k ≤ 23, -55 ≤ l ≤ 55
Reflections collected	265365
Independent reflections	27728 [R_{int} = 0.0771, R_{sigma} = 0.0357]
Data/restraints/parameters	27728/157/1395
Goodness-of-fit on F^2	1.022
Final R indexes [I>=2σ (I)]	R_1 = 0.0890, wR_2 = 0.2560
Final R indexes [all data]	R_1 = 0.0963, wR_2 = 0.2664
Flack parameter	0.009(4)

(*M*)$_4$-AAC

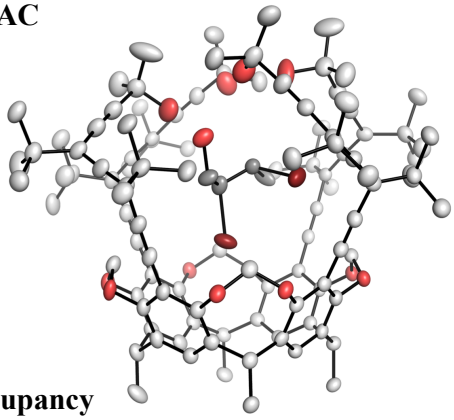

66% occupancy

Guest in cavity:

- **2,3-dibromobutan-1-ol**

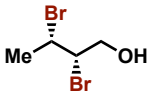

(*S*,*S*)

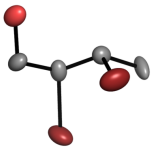

Figure S98. Crystallographic data and ORTEP representation of (*M*)$_4$-AAC⊃(±)-(2*R**,3*R**)-2,3-dibromobutan-1-ol (*R**,*R**)-**8**. Ellipsoids are shown at 50% probability. *n*-Hexyl chains are omitted for clarity.

X-ray Co-Crystal Structure as Determined by Single Crystal X-Ray Diffraction: (*P*)$_4$-AAC⊃(±)-(2*S,3*R**)-2,3-Dibromo-2-methylbutan-1-ol** (*R**,*S**)**-10:** CCDC-1914839

Single crystals were grown following the general crystallization protocol. The guest (*R**,*S**)-**10** is disordered over two positions with occupancies of 50%. The different occupancy of the guest molecule corresponds to the two enantiomers depicted below. 15% of the host cavity is occupied by acetonitrile. This description does not incorporate a partial occupancy with acetonitrile in the host cavity, which is clearly visible in the difference density map and amounts to approximately 15%. However, it was not possible to obtain a stable and convergent model including this contribution without over-constraining.

Empirical formula	$C_{133}H_{178}Br_2O_{13}$
Formula weight	2144.56
Temperature/K	100.0(1)
Crystal system	orthorhombic
Space group	$P2_12_12_1$
a/Å	43.9914(3)
b/Å	18.74020(10)
c/Å	15.61220(10)
α/°	90
β/°	90
γ/°	90
Volume/Å^3	12870.82(14)
Z	4
ρ_{calc}g/cm^3	1.107
μ/mm^{-1}	1.231
F(000)	4600.0
Crystal size/mm^3	0.187 × 0.125 × 0.027
Radiation	CuKα (λ = 1.54184)
2Θ range for data collection/°	6.006 to 160.13
Index ranges	-55 ≤ h ≤ 56, -18 ≤ k ≤ 23, -19 ≤ l ≤ 19
Reflections collected	273849
Independent reflections	27806 [R_{int} = 0.0648, R_{sigma} = 0.0264]
Data/restraints/parameters	27806/320/1470
Goodness-of-fit on F^2	1.286
Final R indexes [I>=2σ (I)]	R_1 = 0.0902, wR_2 = 0.2706
Final R indexes [all data]	R_1 = 0.0933, wR_2 = 0.2754
Flack parameter	0.022(4)

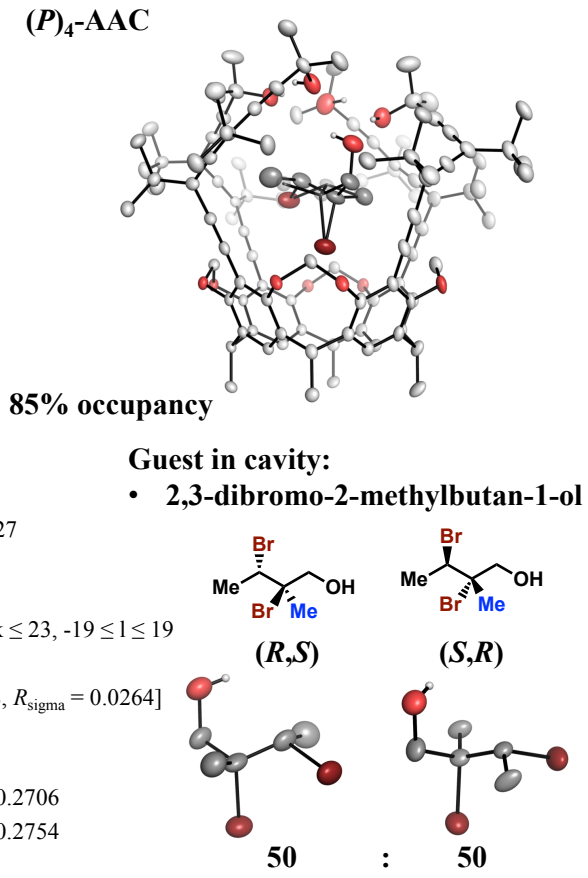

Figure S99. Crystallographic data and ORTEP representation of $(P)_4$-AAC⊃(±)-(2*S**,3*R**)-2,3-Dibromo-2-methylbutan-1-ol (*R**,*S**)-**10**. Ellipsoids are shown at 50% probability. *n*-Hexyl chains are omitted for clarity.

X-ray Co-Crystal Structure as Determined by Single Crystal X-Ray Diffraction: $(M)_4$-AAC⊃(±)-(2*S,3*R**)-2,3-Dibromo-2-methylbutan-1-ol** (*R**,*S**)**-10:** CCDC-1914856

Single crystals were grown following the general crystallization protocol. The sample was twinned, but the domains could be cleanly separated during raw data integration. HKLF5 format structure factor data was employed during final refinement. The H-bonding array shows a clockwise orientation. The guest (*R**,*S**)-**10** is disordered over two positions with major and minor occupancies of 56% and 44%. The different occupancy of the guest molecule corresponds to the two enantiomeric conformers depicted below.

Empirical formula	$C_{133}H_{178}Br_2O_{13}$
Formula weight	2144.56
Temperature/K	100.0(1)
Crystal system	orthorhombic
Space group	$P2_12_12_1$
a/Å	15.60920(10)
b/Å	18.73600(10)
c/Å	44.0628(3)
α/°	90
β/°	90
γ/°	90
Volume/Å^3	12886.34(14)
Z	4
ρ_{calc}g/cm^3	1.105
μ/mm^{-1}	1.230
F(000)	4600.0
Crystal size/mm^3	0.254 × 0.155 × 0.102
Radiation	CuKα (λ = 1.54184)
2Θ range for data collection/°	6.192 to 160.286
Index ranges	-16 ≤ h ≤ 19, -23 ≤ k ≤ 23, -55 ≤ l ≤ 55
Reflections collected	44246
Independent reflections	44246 [R_{int} = 0.0280, R_{sigma} = 0.0206]
Data/restraints/parameters	44246/315/1461
Goodness-of-fit on F^2	1.024
Final *R* indexes [I>=2σ (I)]	R_1 = 0.0653, wR_2 = 0.1875
Final *R* indexes [all data]	R_1 = 0.0679, wR_2 = 0.1912
Flack parameter	-0.024(7)

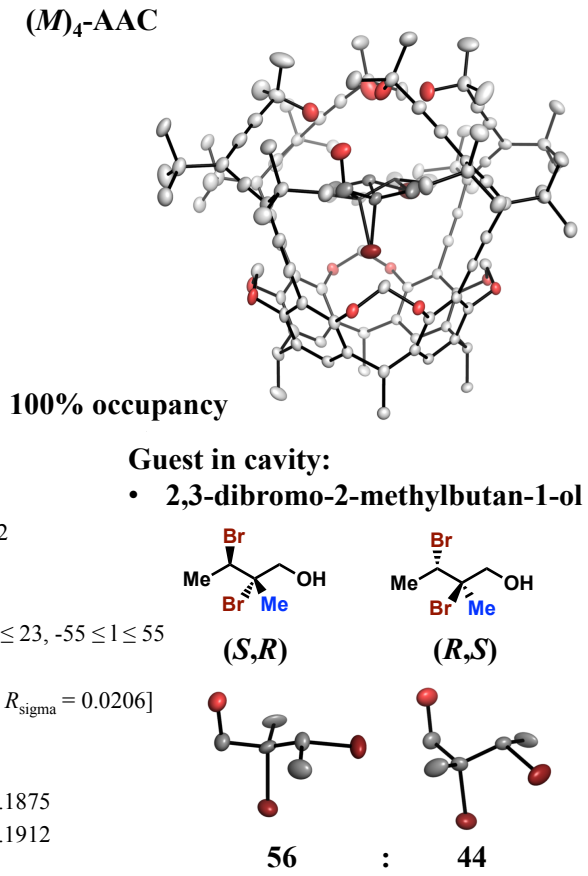

Figure S100. Crystallographic data and ORTEP representation of (*M*)$_4$-AAC⊃(±)-(2*S**,3*R**)-2,3-Dibromo-2-methylbutan-1-ol (*R**,*S**)-**10**. Ellipsoids are shown at 50% probability. *n*-Hexyl chains are omitted for clarity.

X-ray Co-Crystal Structure as Determined by Single Crystal X-Ray Diffraction: (*P*)$_4$-AAC⊃(±)-(2*R,3*R**)-2,3-Dibromo-2-methylbutan-1-ol** (*R**,*R**)-**10:** CCDC-1914854

Single crystals were grown following the general crystallization protocol. All protons were detected crystallographically. The H-bonding array shows a clockwise orientation. The guest (*R**,*R**)-**10** is disordered over two positions with major and minor occupancies of 65% and 35%. The different occupancy of the guest molecule corresponds to the two enantiomeric conformers depicted below.

Empirical formula	$C_{133}H_{178}Br_2O_{13}$
Formula weight	2144.56
Temperature/K	100.0(1)
Crystal system	orthorhombic
Space group	$P2_12_12_1$
a/Å	15.54830(10)
b/Å	18.78360(10)
c/Å	44.2547(3)
α/°	90
β/°	90
γ/°	90
Volume/Å^3	12924.72(14)
Z	4
ρ_{calc}g/cm^3	1.102
μ/mm^{-1}	1.226
F(000)	4600.0
Crystal size/mm^3	0.127 × 0.066 × 0.034
Radiation	CuKα (λ = 1.54184)
2Θ range for data collection/°	6.024 to 159.49
Index ranges	-19 ≤ h ≤ 19, -23 ≤ k ≤ 23, -55 ≤ l ≤ 56
Reflections collected	210259
Independent reflections	27875 [R_{int} = 0.0708, R_{sigma} = 0.0385]
Data/restraints/parameters	27875/317/1464
Goodness-of-fit on F^2	1.027
Final *R* indexes [I>=2σ (I)]	R_1 = 0.0515, wR_2 = 0.1339
Final *R* indexes [all data]	R_1 = 0.0647, wR_2 = 0.1432
Flack parameter	-0.014(5)

(*P*)$_4$-AAC

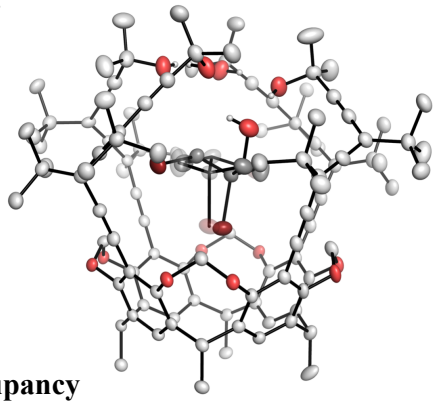

100% occupancy

Guest in cavity:

- **2,3-dibromo-2-methylbutan-1-ol**

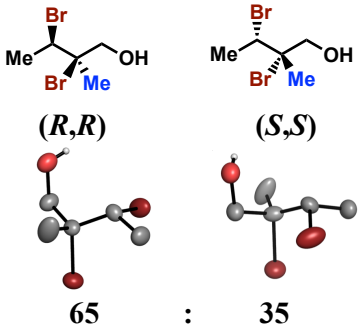

Figure S101. Crystallographic data and ORTEP representation of (*P*)$_4$-AAC⊃(±)-(2*R**,3*R**)-2,3-Dibromo-2-methylbutan-1-ol (*R**,*R**)-**10**. Ellipsoids are shown at 50% probability. *n*-Hexyl chains are omitted for clarity.

X-ray Co-Crystal Structure as Determined by Single Crystal X-Ray Diffraction: (*M*)$_4$-AAC⊃(±)-(2*R,3*R**)-2,3-Dibromo-2-methylbutan-1-ol** (*R**,*R**)-**10:** CCDC-1914859

Single crystals were grown following the general crystallization protocol. All protons were detected crystallographically. The H-bonding array shows a counter-clockwise orientation. The guest (*R**,*R**)-**10** is disordered over two positions with major and minor occupancies of 65% and 35%. The different occupancy of the guest molecule corresponds to the two enantiomeric conformers depicted below.

Empirical formula	$C_{133}H_{178}Br_2O_{13}$
Formula weight	2144.56
Temperature/K	100.0(1)
Crystal system	orthorhombic
Space group	$P2_12_12_1$
a/Å	44.1945(2)
b/Å	18.78150(10)
c/Å	15.55630(10)
α/°	90
β/°	90
γ/°	90
Volume/Å^3	12912.34(12)
Z	4
ρ_{calc}g/cm^3	1.103
μ/mm^{-1}	1.228
F(000)	4600.0
Crystal size/mm^3	0.123 × 0.08 × 0.042
Radiation	CuKα (λ = 1.54184)
2Θ range for data collection/°	6.024 to 159.608
Index ranges	-56 ≤ h ≤ 55, -23 ≤ k ≤ 19, -19 ≤ l ≤ 18
Reflections collected	215132
Independent reflections	27917 [R_{int} = 0.0575, R_{sigma} = 0.0302]
Data/restraints/parameters	27917/353/1436
Goodness-of-fit on F^2	1.024
Final R indexes [I>=2σ (I)]	R_1 = 0.0528, wR_2 = 0.1485
Final R indexes [all data]	R_1 = 0.0570, wR_2 = 0.1522
Flack parameter	-0.005(4)

(*M*)$_4$-AAC

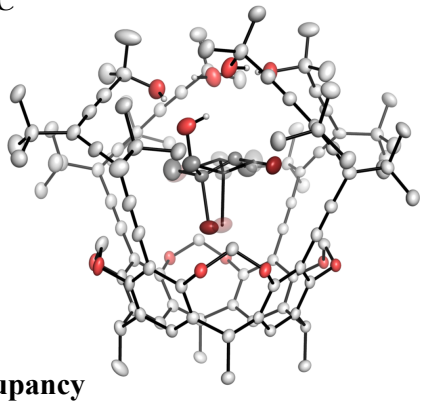

100% occupancy

Guest in cavity:

- **2,3-dibromo-2-methylbutan-1-ol**

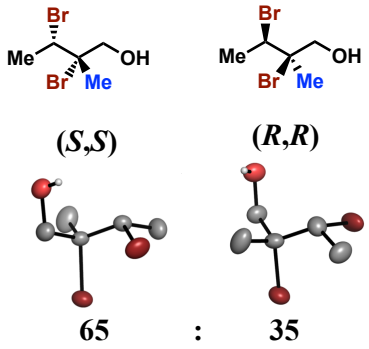

Figure S102. Crystallographic data and ORTEP representation of (*M*)$_4$-AAC⊃(±)-(2*R**,3*R**)-2,3-Dibromo-2-methylbutan-1-ol (*R**,*R**)-**10**. Ellipsoids are shown at 50% probability. *n*-Hexyl chains are omitted for clarity.

S12. NMR Spectra of $(P)_4$-Configured AAC and Guest Compounds

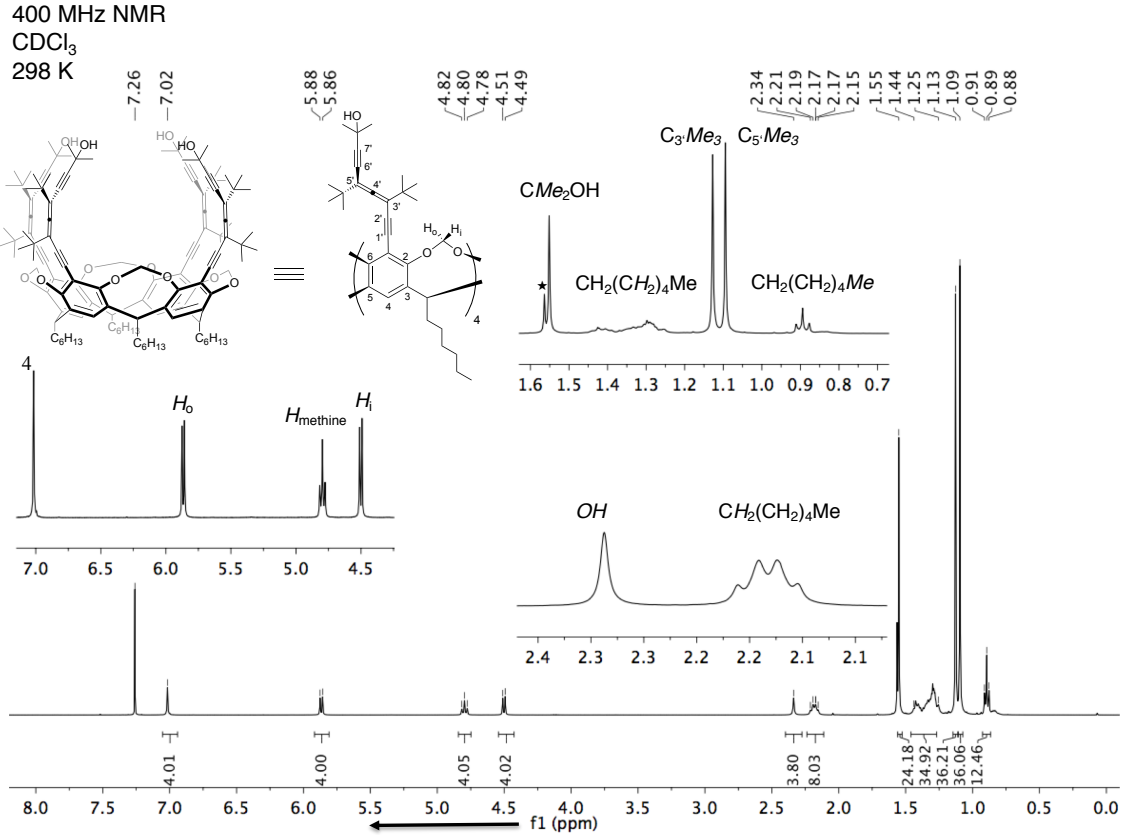

Figure S103. ^{1}H NMR (400 MHz) spectrum of AAC (*P*)-**1** in $CDCl_3$.[1]

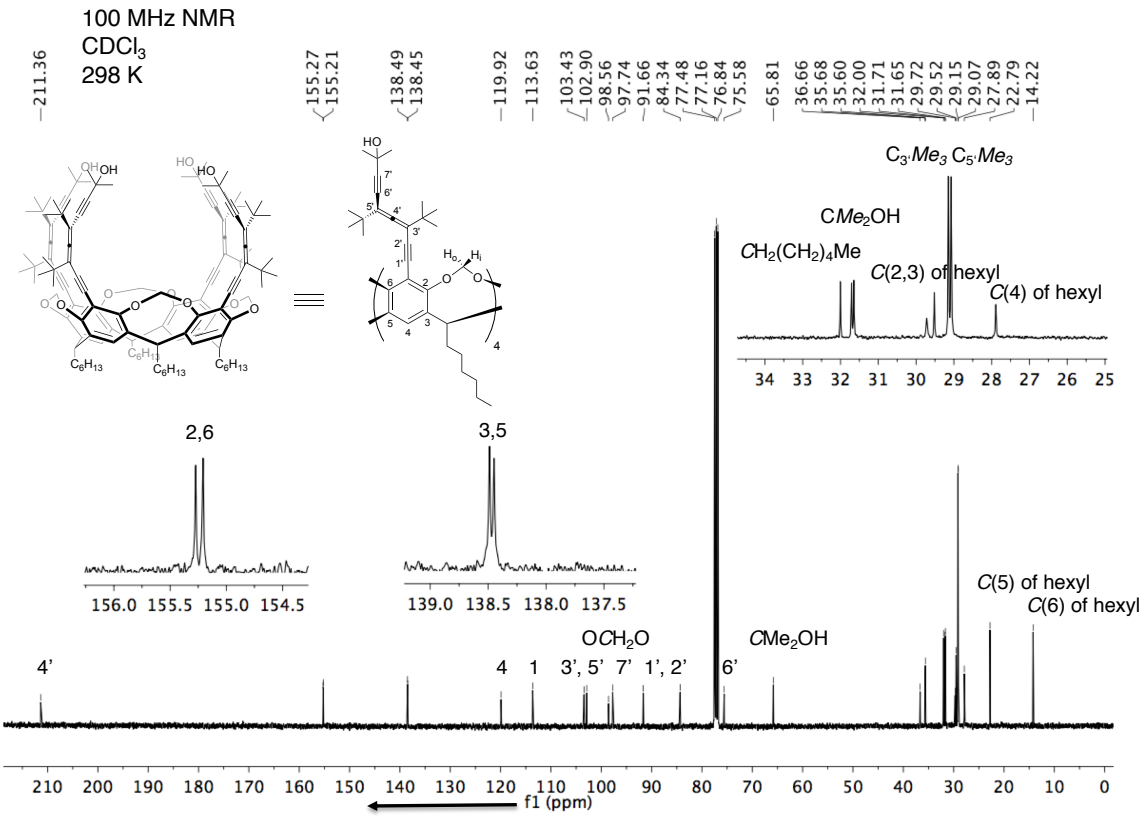

Figure S104. ^{13}C NMR (100 MHz) spectrum of AAC (*P*)-**1** in $CDCl_3$.[1]

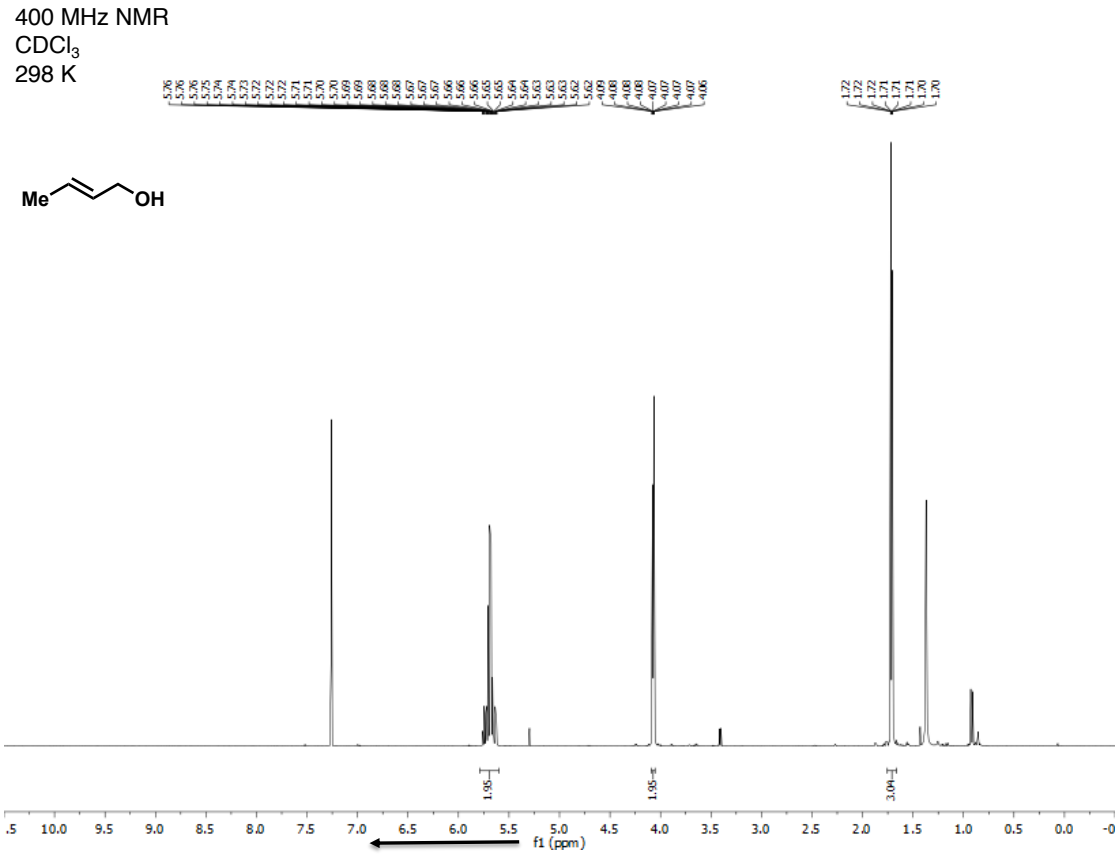

Figure S105. ^{1}H NMR (400 MHz) spectrum of **14** in $CDCl_3$.

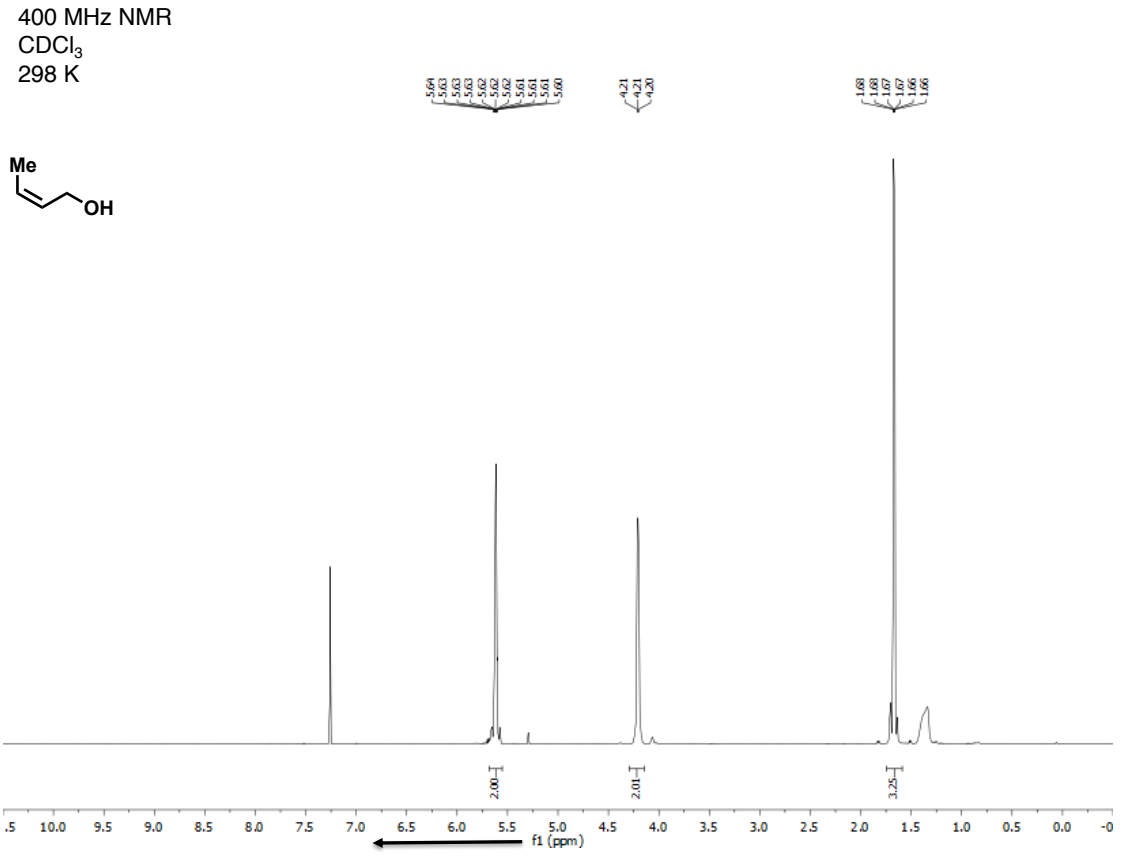

Figure S106. ^{1}H NMR (400 MHz) spectrum of **16** in $CDCl_3$.

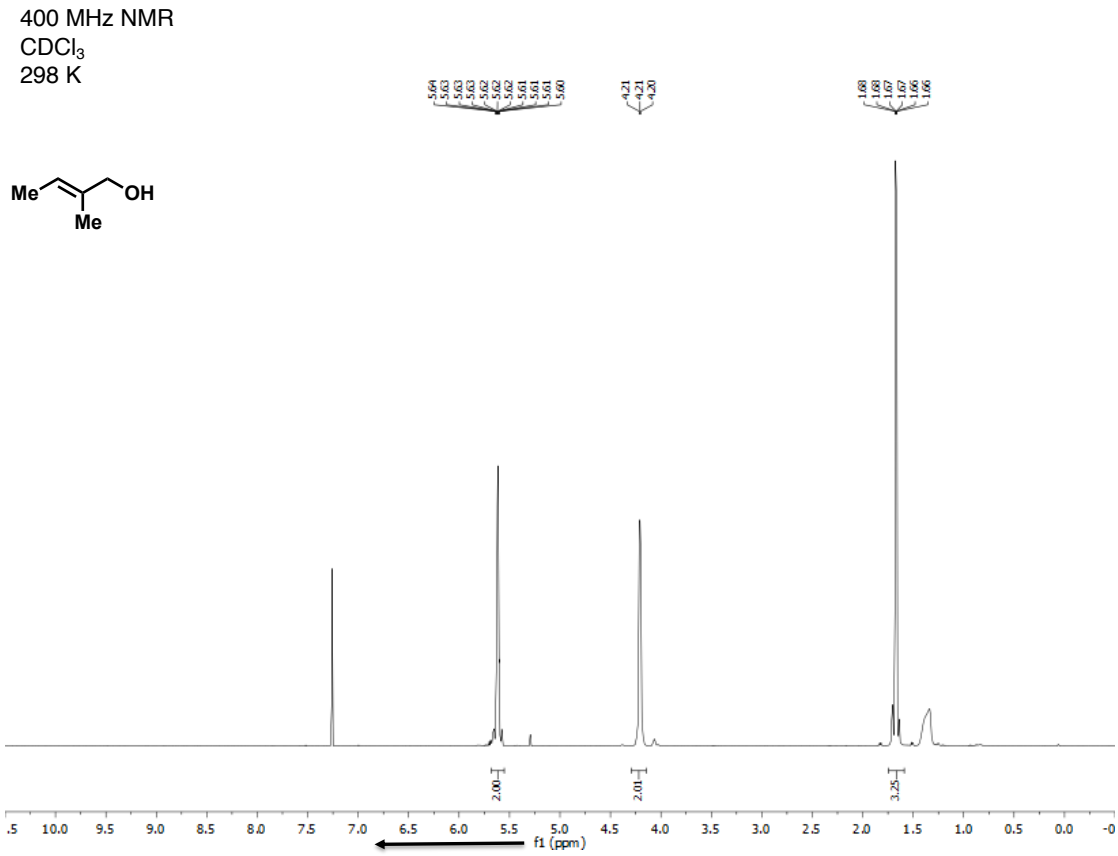

Figure S107. ^{1}H NMR (400 MHz) spectrum of **18** in $CDCl_3$.

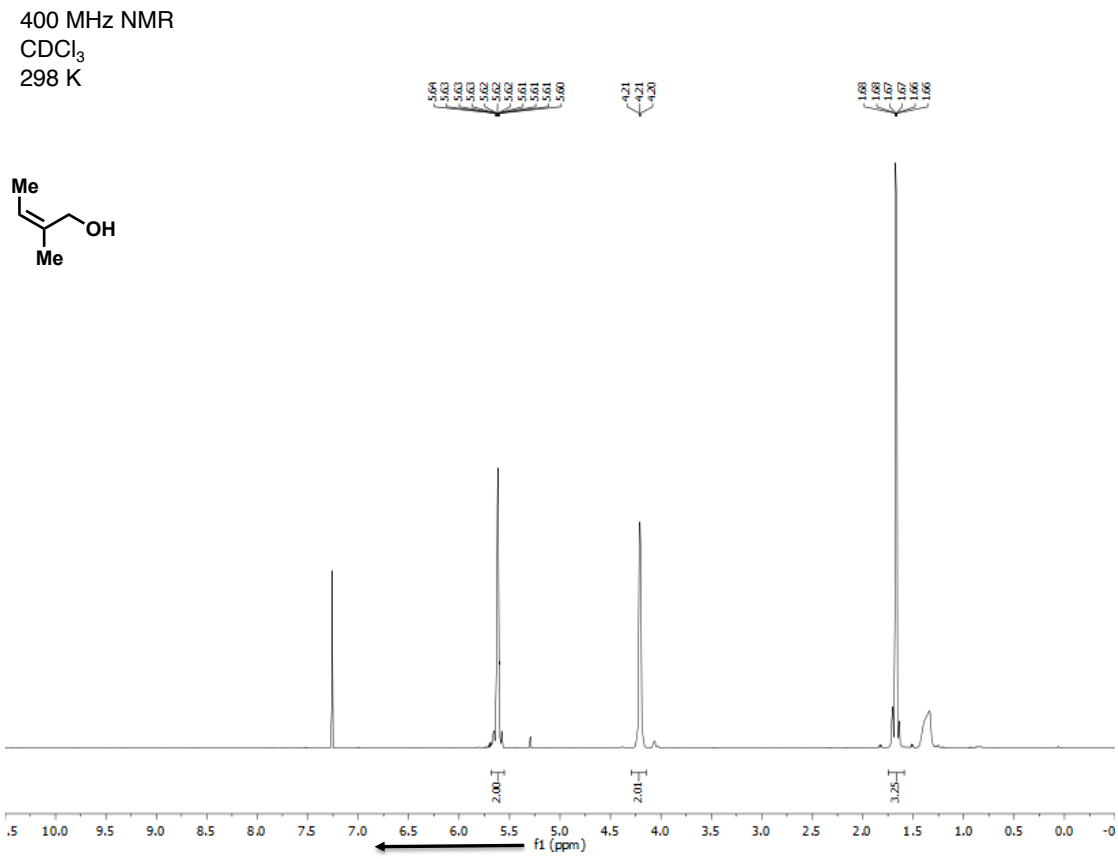

Figure S108. ^{1}H NMR (400 MHz) spectrum of **20** in $CDCl_3$.

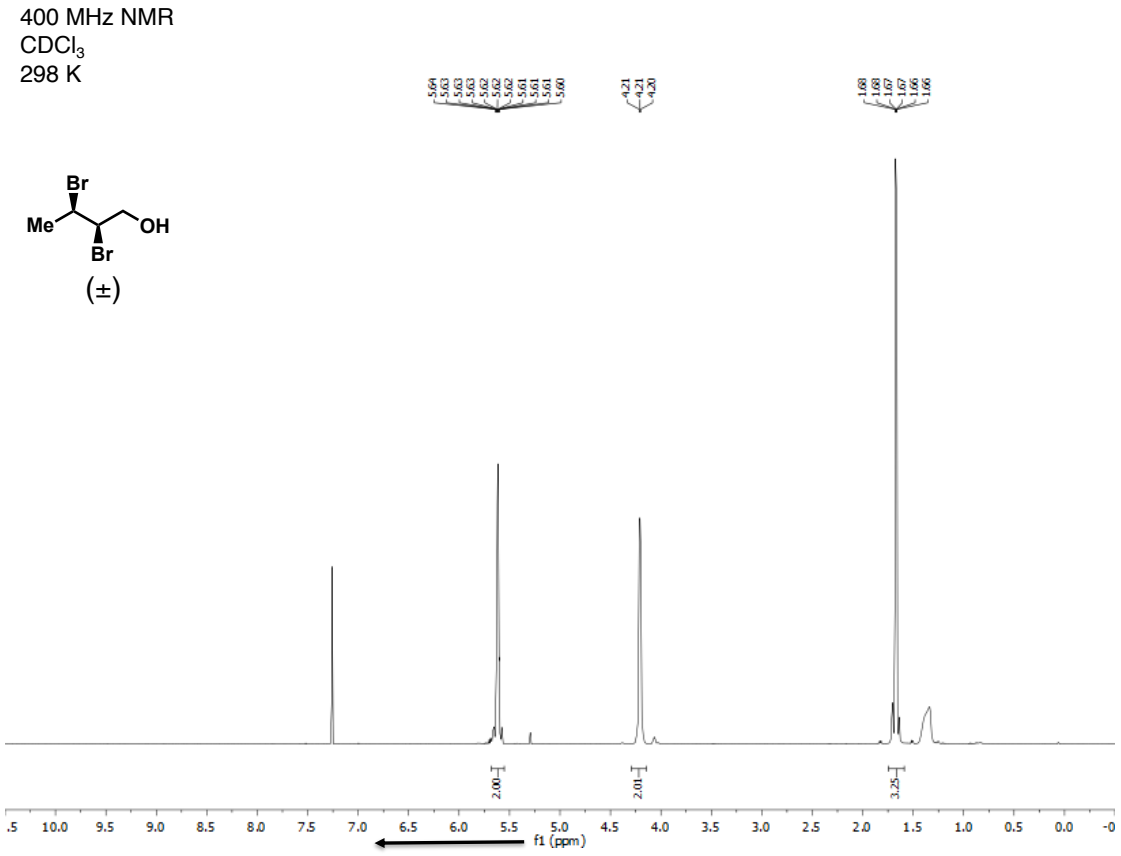

Figure S109. ^{1}H NMR (400 MHz) spectrum of (*R**,*R**)-**8** in $CDCl_3$.

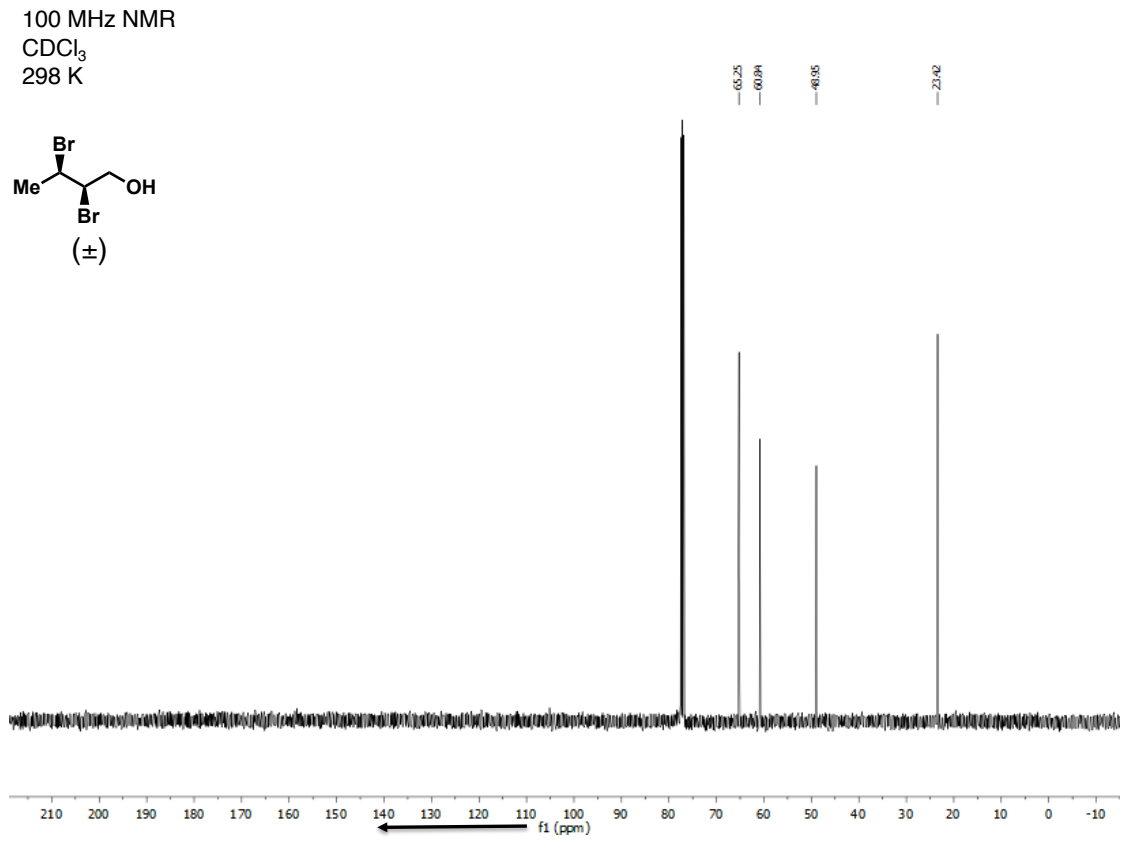

Figure S110. ^{13}C NMR (400 MHz) spectrum of (*R**,*R**)-**8** in $CDCl_3$.

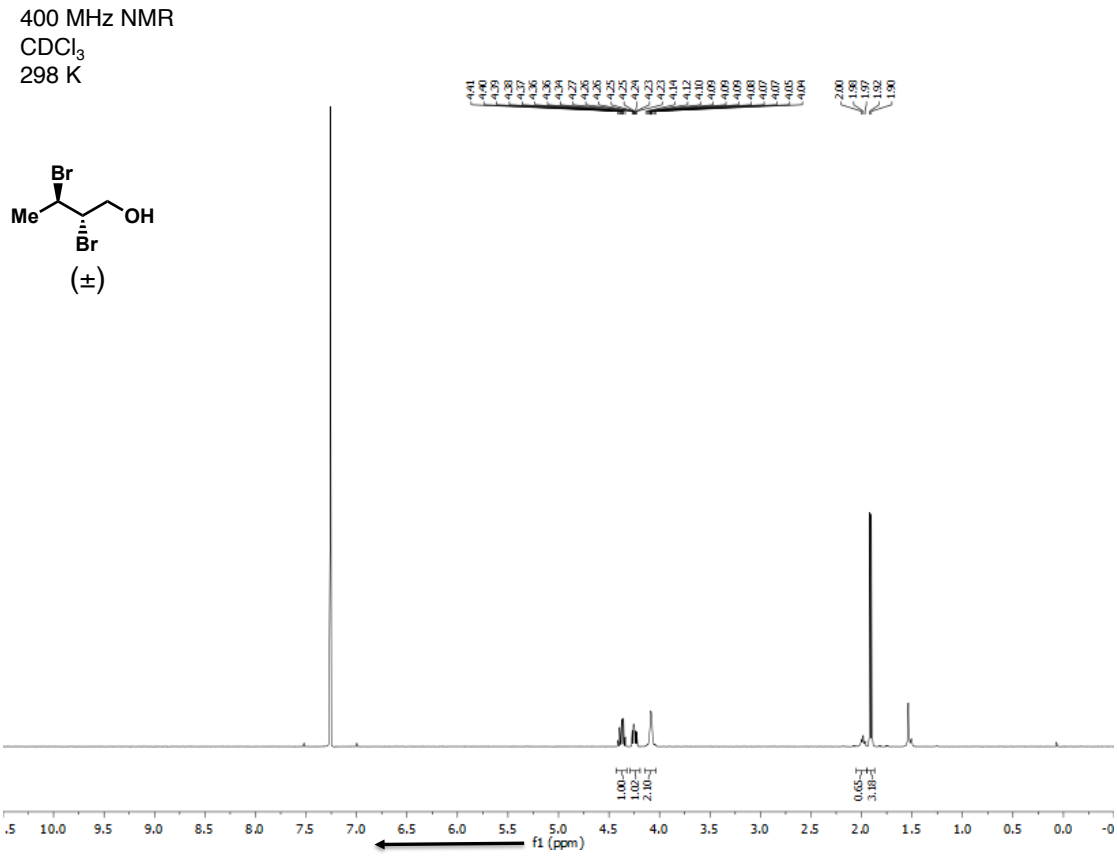

Figure S111. ^{1}H NMR (400 MHz) spectrum of (*R**,*S**)-**8** in $CDCl_3$.

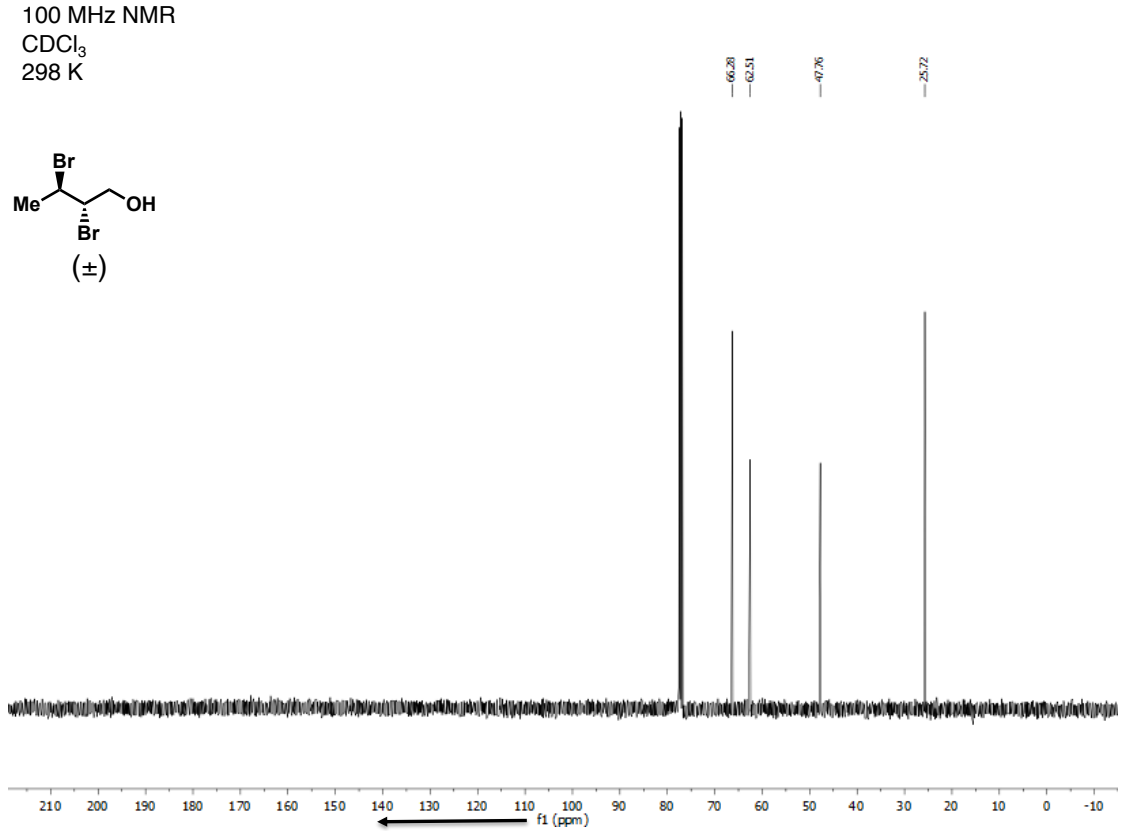

Figure S112. ^{13}C NMR (400 MHz) spectrum of (*R**,*S**)-**8** in $CDCl_3$.

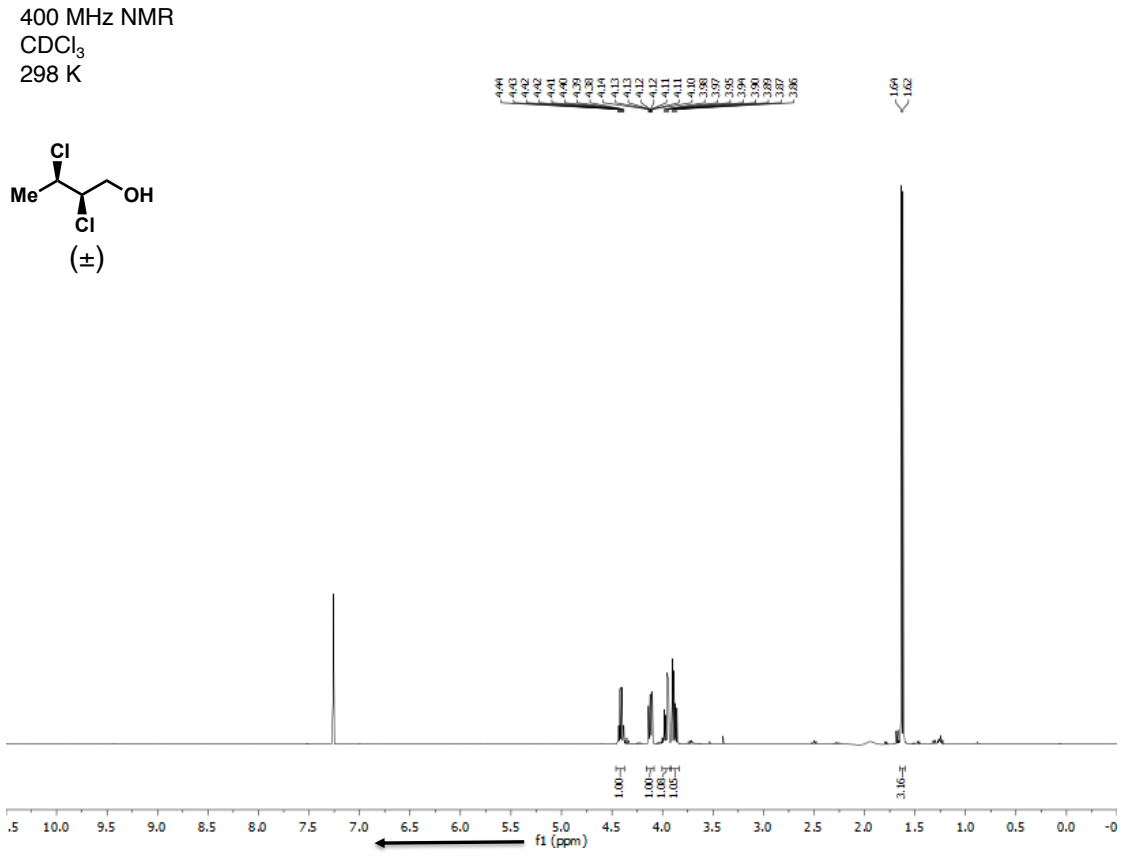

Figure S113. ^{1}H NMR (400 MHz) spectrum of (*R**,*R**)-**7** in $CDCl_3$.

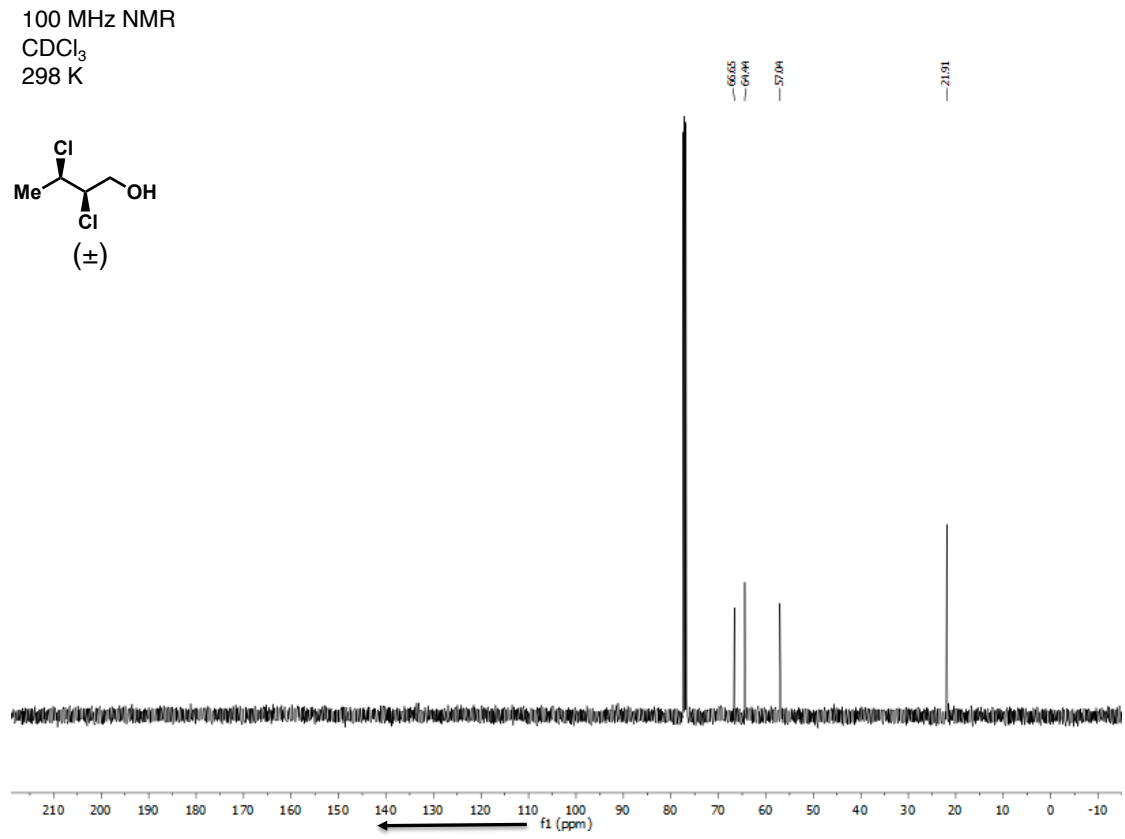

Figure S114. ^{13}C NMR (400 MHz) spectrum of (*R**,*R**)-**7** in $CDCl_3$.

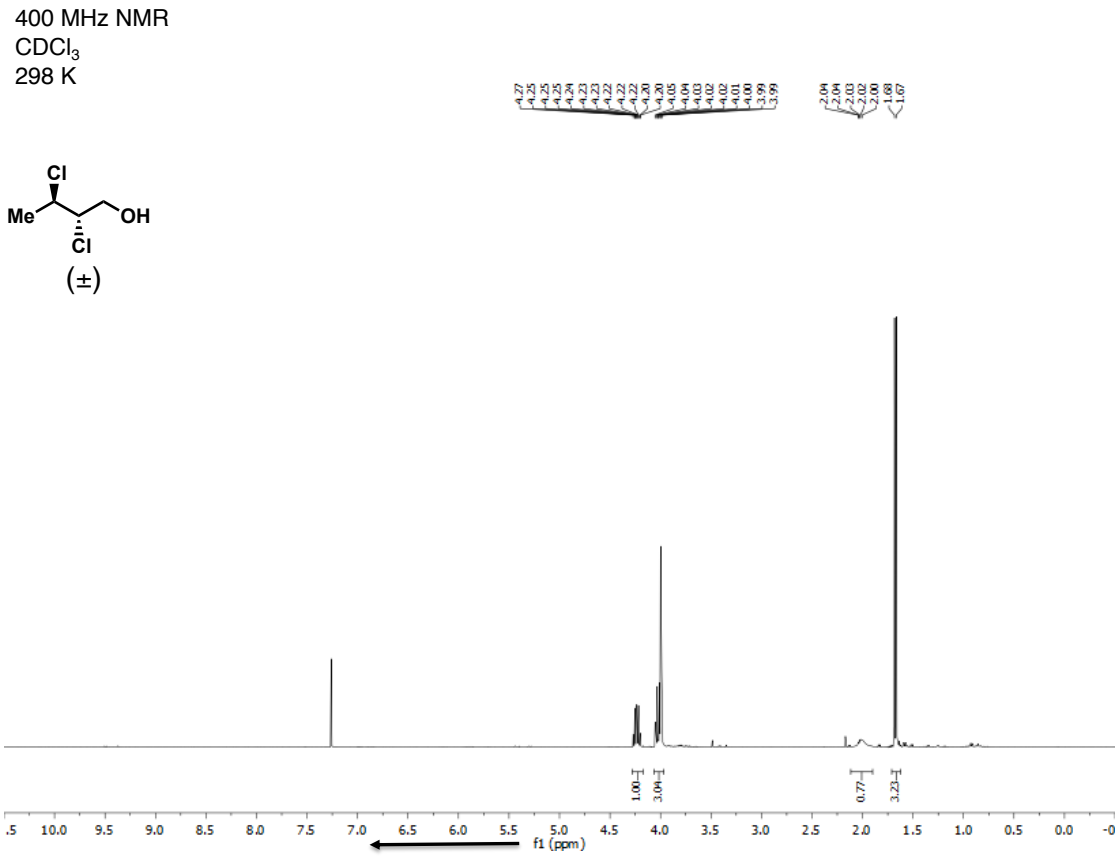

Figure S115. ^{1}H NMR (400 MHz) spectrum of (*R**,*S**)-**7** in $CDCl_3$.

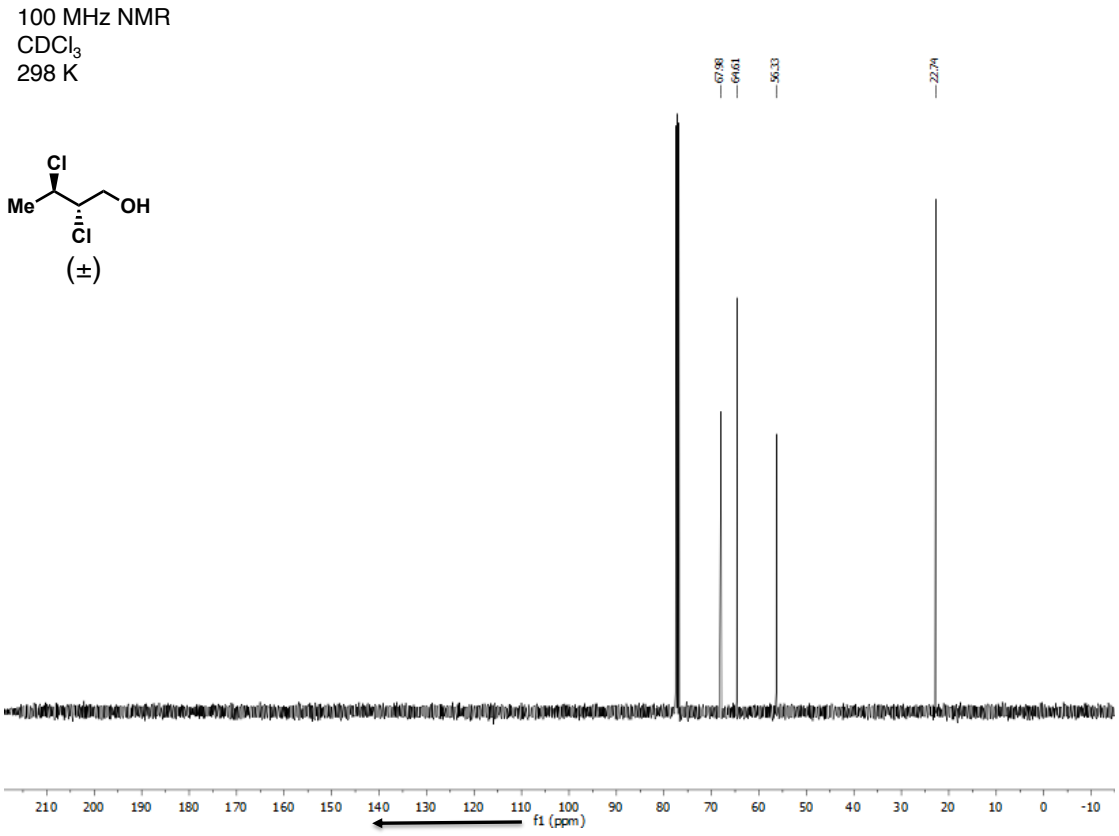

Figure S116. ^{13}C NMR (400 MHz) spectrum of (*R**,*S**)-**7** in $CDCl_3$.

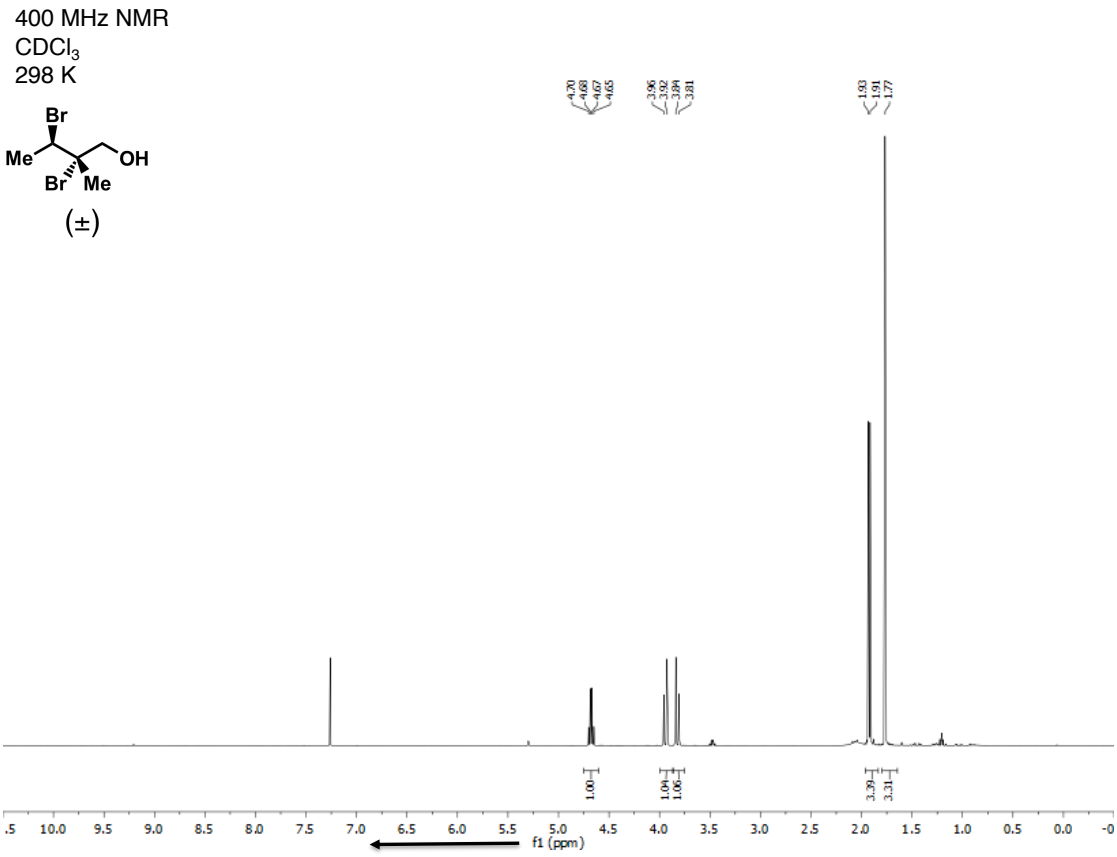

Figure S117. ^{1}H NMR (400 MHz) spectrum of (*R**,*S**)-**10** in $CDCl_3$.

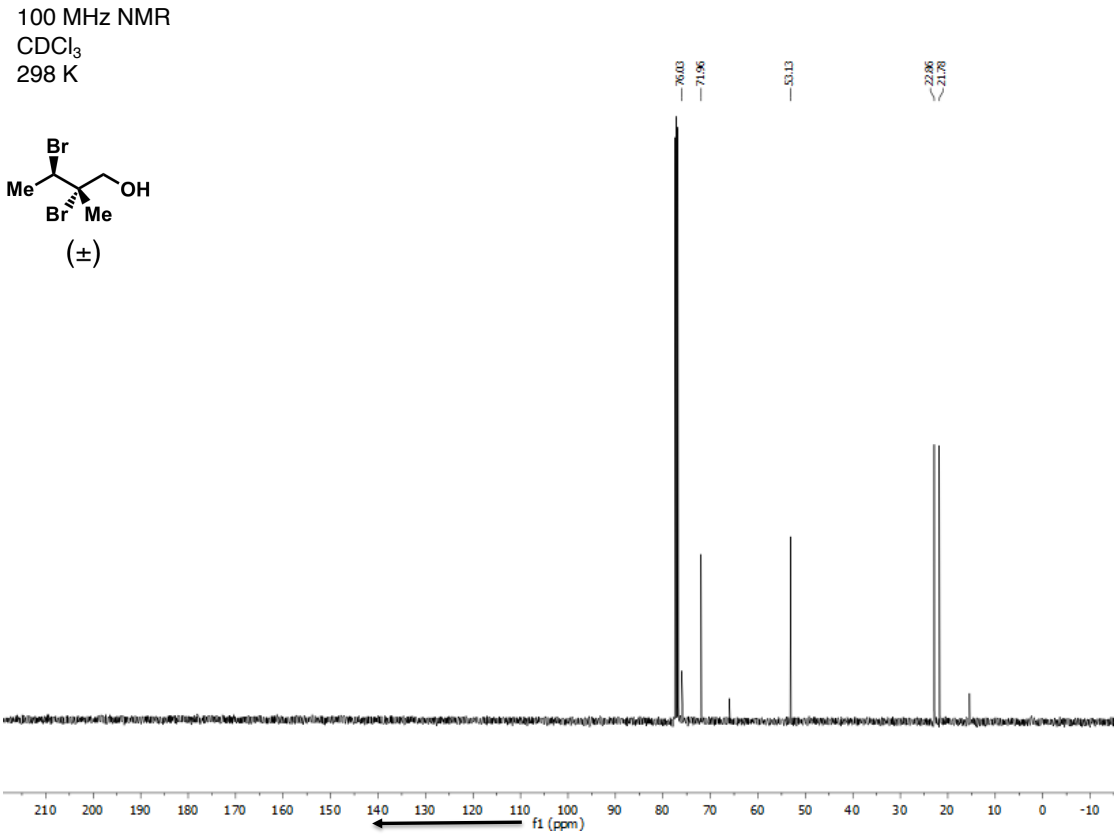

Figure S118. ^{13}C NMR (400 MHz) spectrum of (*R**,*S**)-**10** in $CDCl_3$.

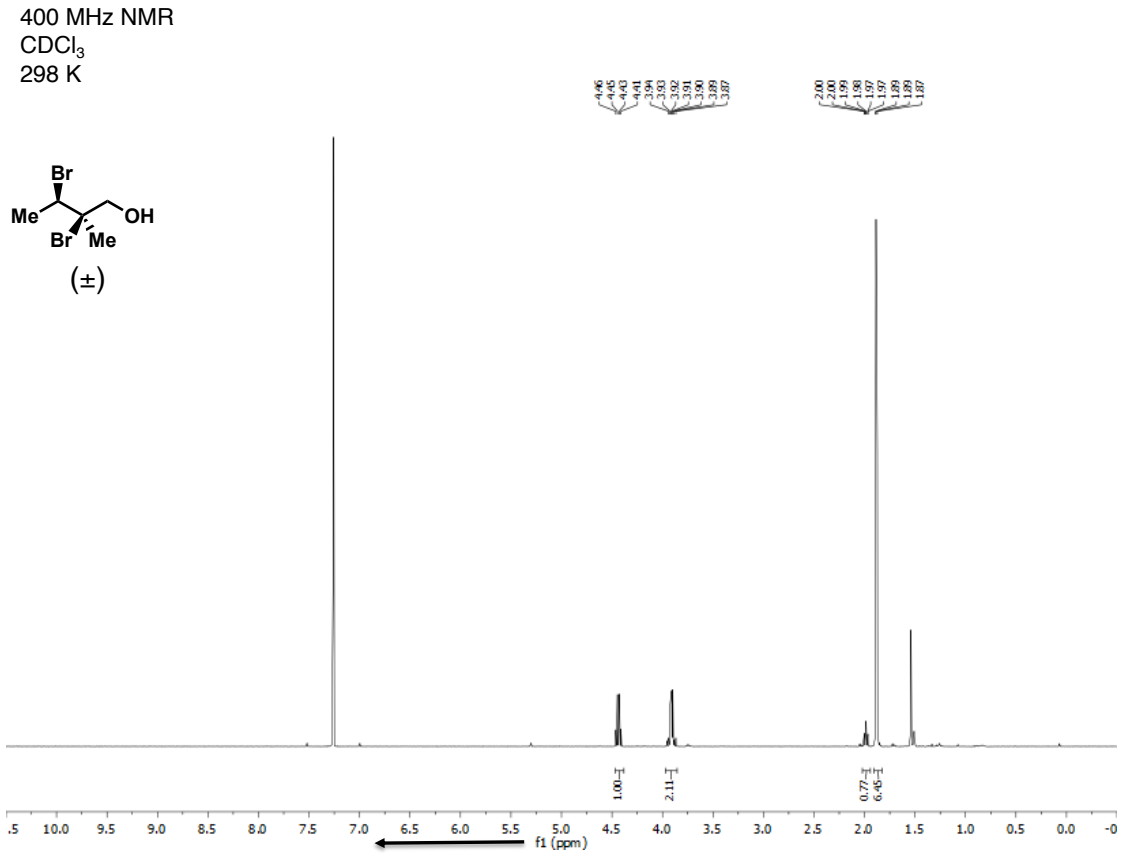

Figure S119. ^{1}H NMR (400 MHz) spectrum of (*R**,*R**)-**10** in $CDCl_3$.

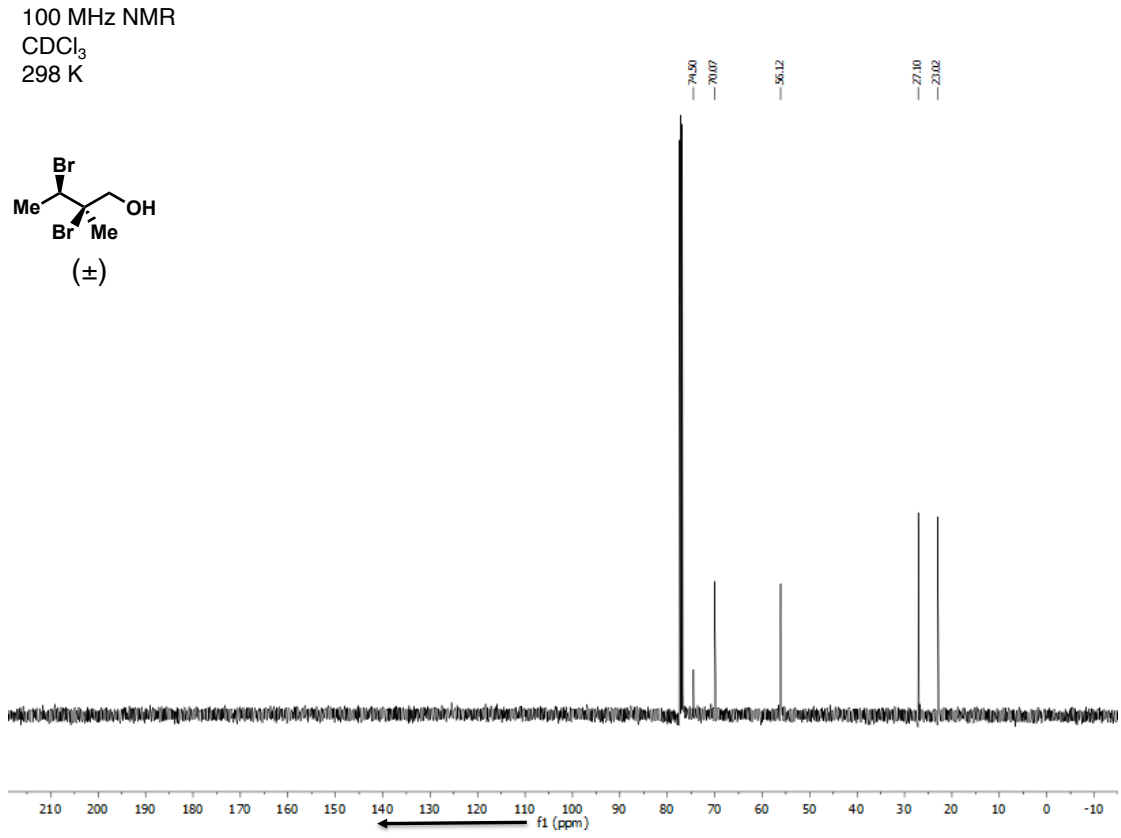

Figure S120. ^{13}C NMR (400 MHz) spectrum of (*R**,*R**)-**10** in $CDCl_3$.

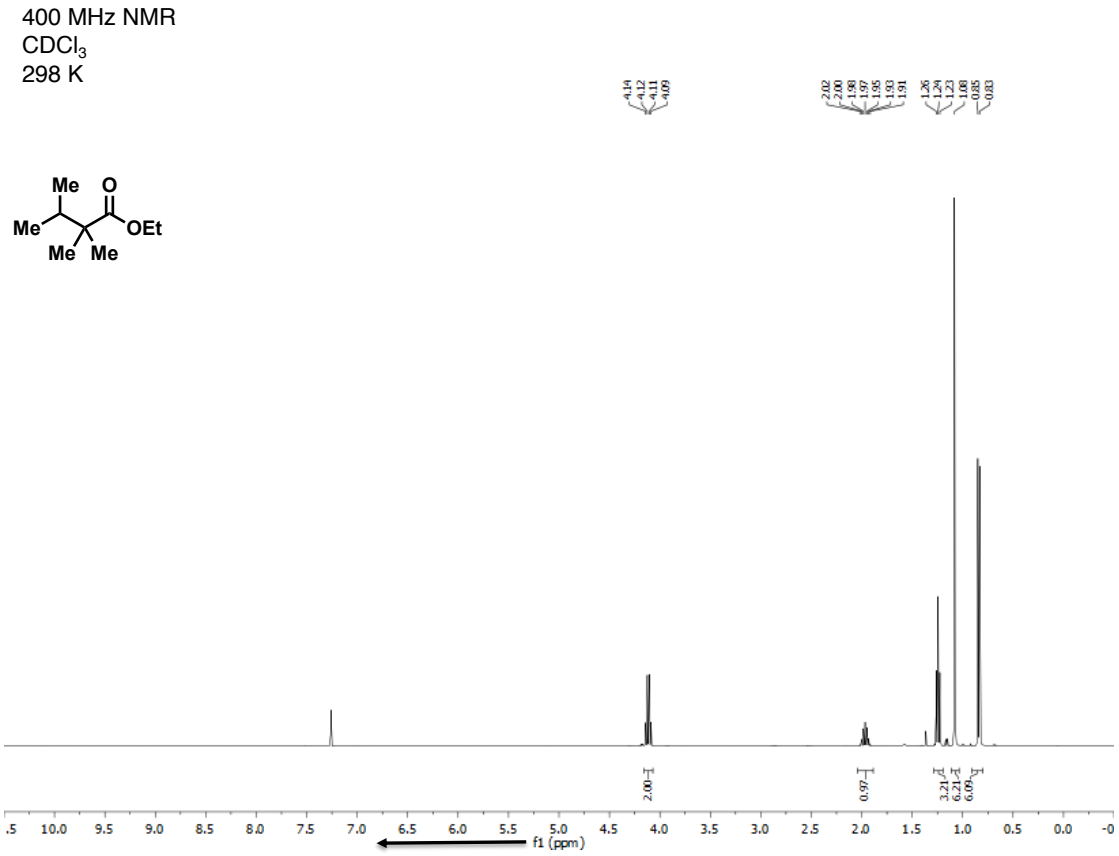

Figure S121. ^{1}H NMR (400 MHz) spectrum of **23** in $CDCl_3$.

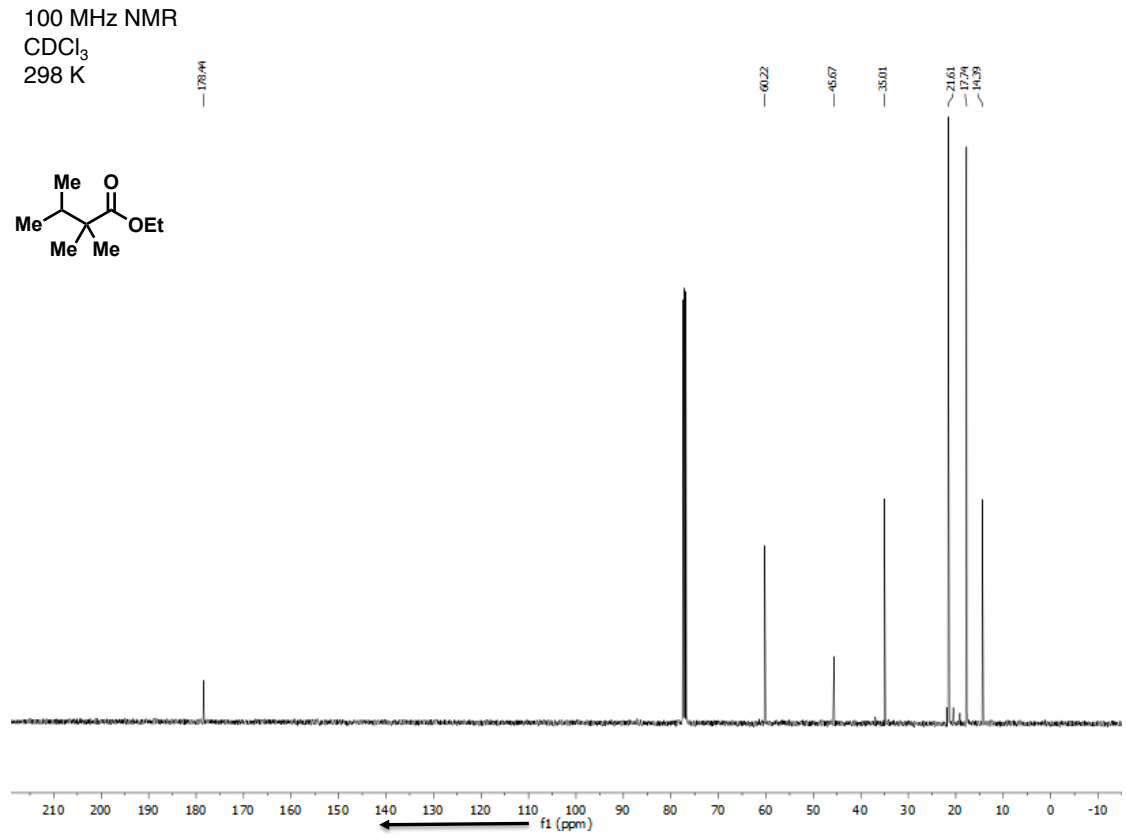

Figure S122. ^{13}C NMR (400 MHz) spectrum of **23** in $CDCl_3$.

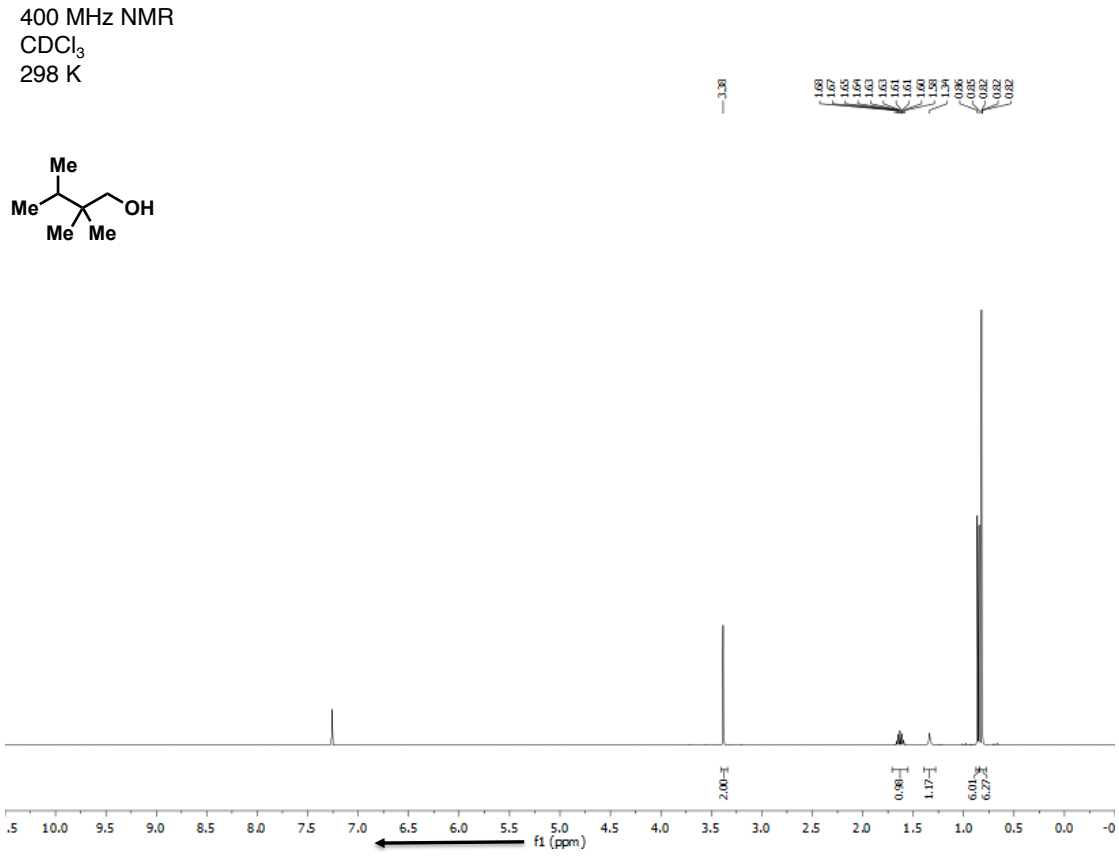

Figure S123. ^{1}H NMR (400 MHz) spectrum of **9** in $CDCl_3$.

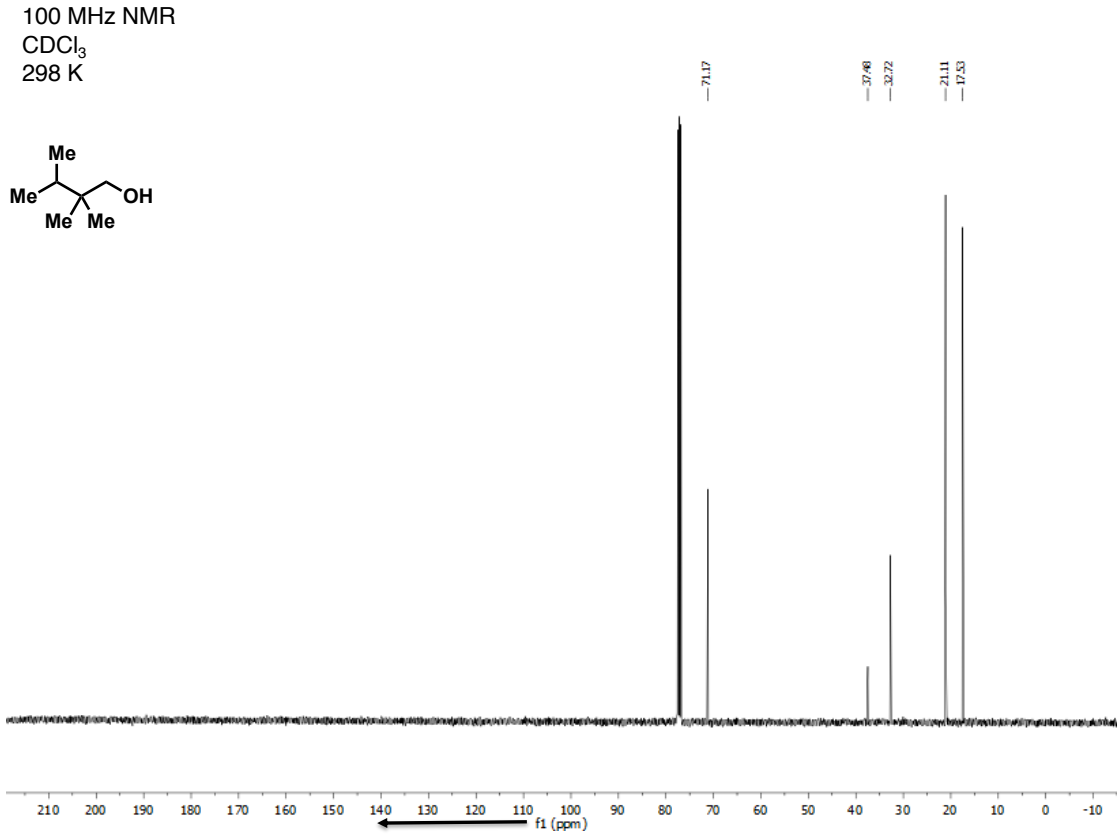

Figure S124. ^{13}C NMR (400 MHz) spectrum of **9** in $CDCl_3$.

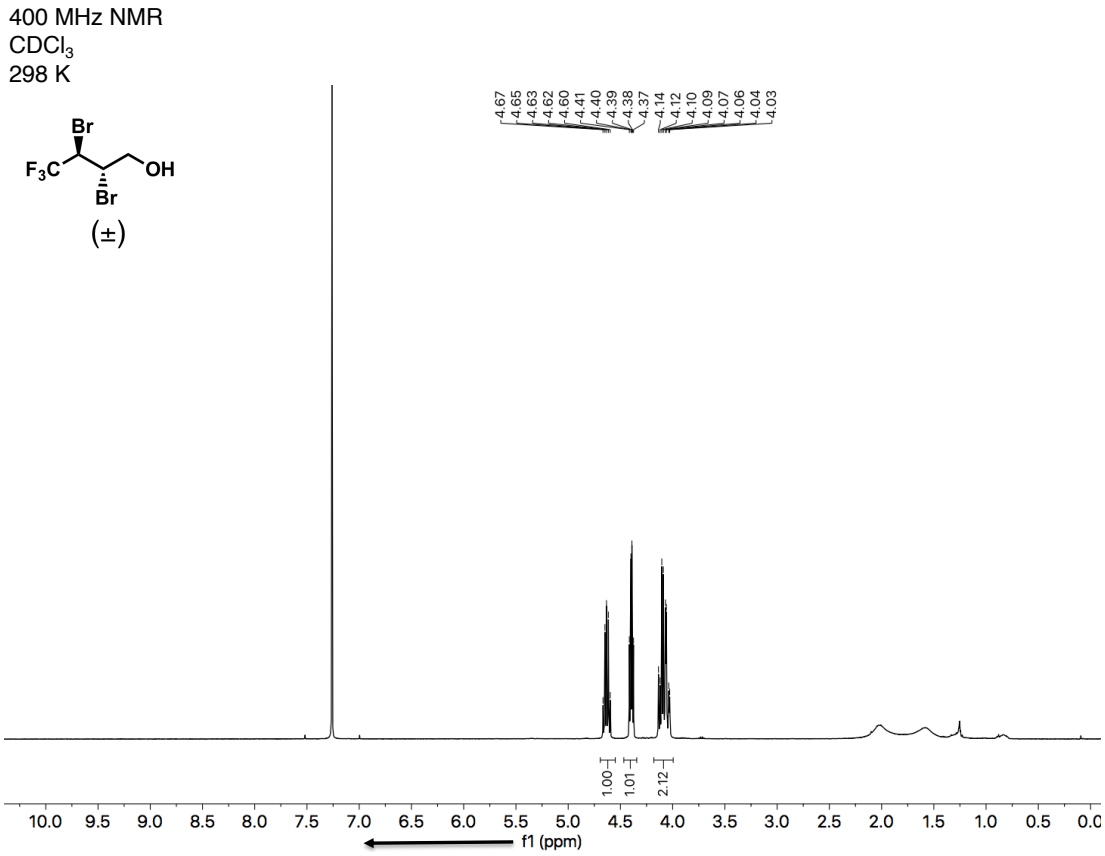

Figure S125. ^{1}H NMR (400 MHz) spectrum of (*R**,*S**)-**11** in $CDCl_3$.

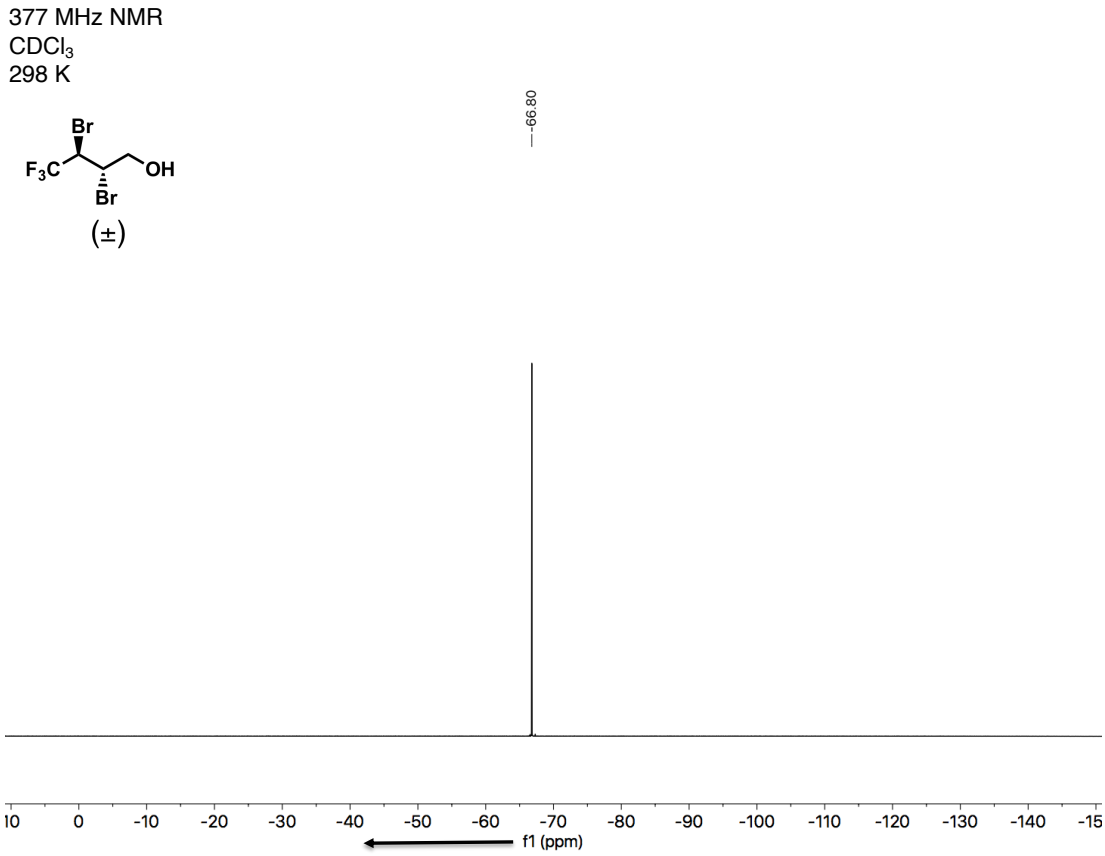

Figure S126. ^{19}F NMR (377 MHz) spectrum of (*R**,*S**)-**11** in $CDCl_3$.

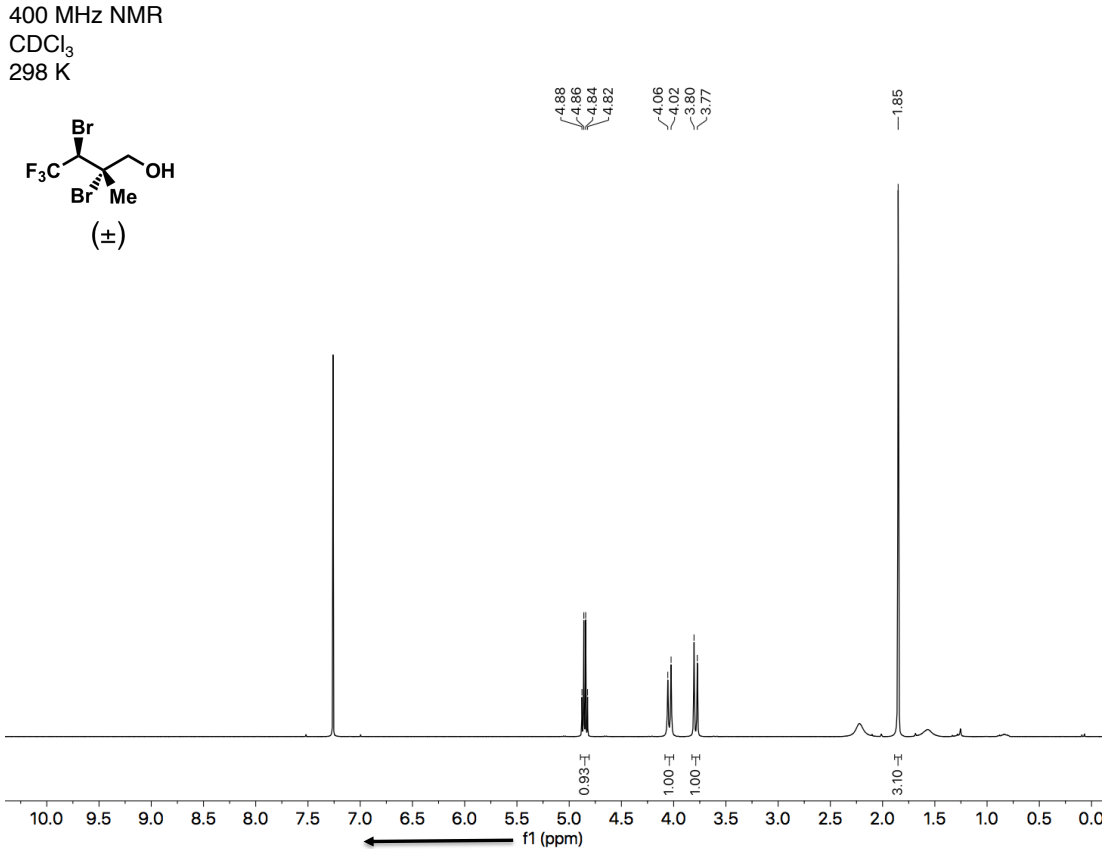

Figure S127. ^{1}H NMR (400 MHz) spectrum of (*R**,*S**)-**12** in $CDCl_3$.

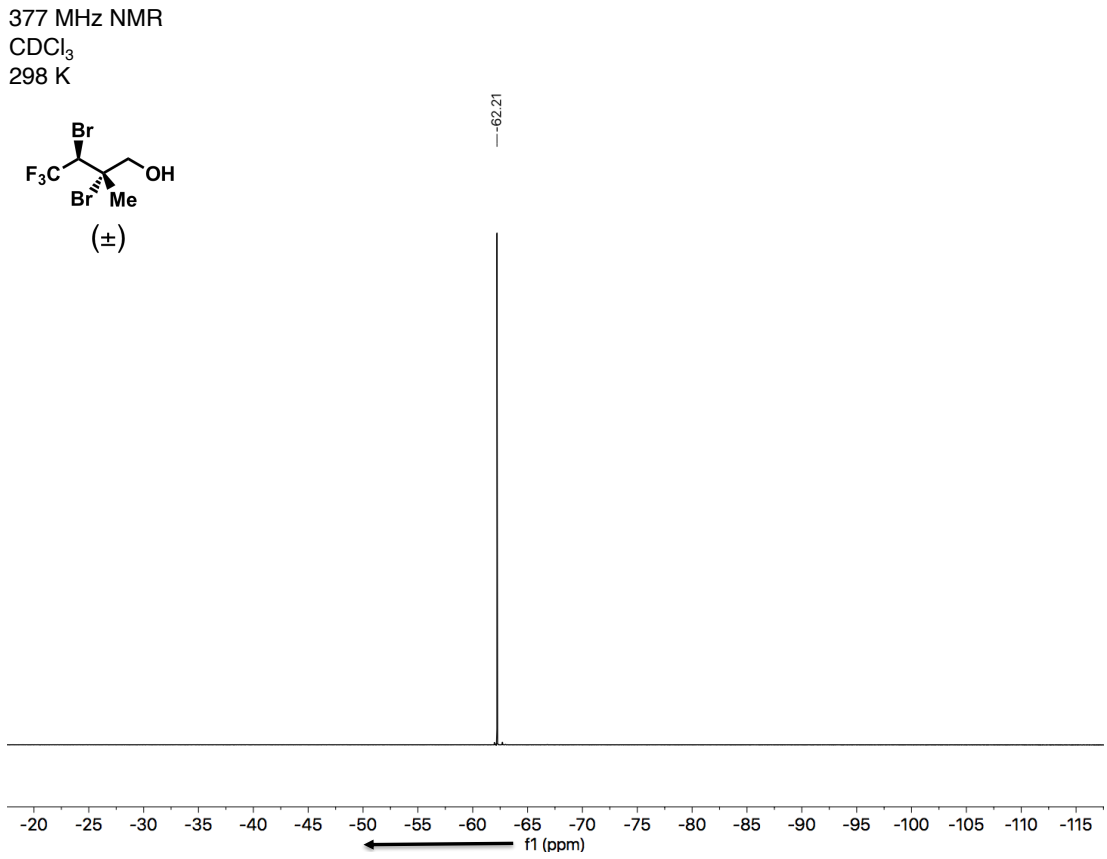

Figure S128. ^{19}F NMR (377 MHz) spectrum of (*R**,*S**)-**12** in $CDCl_3$.

Theoretical Section

S1. Computational Methodology

We generate the structures for the guest molecules **2**–**12** with the exhaustive conformer generator CONFAB[10] implemented in the Open Babel package.[11] All subsequent structure optimizations were carried out with ORCA (version 4.0.1).[12] We applied the PBE functional[13] including empirical dispersion corrections ("D3") with a Becke-Johnson damping function[14] for all structure optimizations. We chose the def2-TZVPP basis set[15] for all calculations and invoked the resolution-of-the-identity density fitting of the Coulomb integrals. For all molecules, we carried out structure optimizations in gas phase and in an implicit continuum solvent simulating acetonitrile[16] (CPCM(Acetonitrile) keyword). The maximum norm of the Cartesian structure gradient was converged to 10^{-3} Hartree bohr^{-1} in all cases.

We determined thermal corrections with the standard rigid-rotor-harmonic-oscillator (RRHO) model in the gas phase[17] based on frequencies calculated with PBE-D3(BJ)/def2-TZVPP.

Additionally, we carried out DLPNO-CCSD(T)[18] single-point energy evaluations with the ORCA program for the PBE/def2-TZVPP optimized gas-phase structures. We chose a def2-TZVPP basis set[15] and appropriate fitting bases. The single-point energies were converged to 10^{-8} Hartree (TightSCF).

A calculation of a single-point energy with one method (e.g., DLPNO-CCSD(T)) for a structure optimized with another method (e.g., PBE-D3(BJ)) is denoted by a combination of the two methods with a double slash (e.g., DLPNO-CCSD(T)/PBE-D3(BJ)).

The Cartesian coordinates of all optimized structures (in Ångstrom) are included as Supporting Material, the second line of each file contains the single-point energies obtained for the structure.

S2. Conformational Analysis

We determined the preferred conformations around the C(2)–C(3) bond in the isolated guest molecules where "C(2)" refers to the second carbon atom in the butan-1-ol backbone and the "C(3)" refers to the third carbon atom (see also Table S41). For each of the N conformers, we evaluate the respective Boltzmann weight P at room temperature (T = 295 K),

$$P_i = \frac{exp(-E_i/(k_B T))}{\sum_{j=1}^{N} exp(-E_j/(k_B T))}$$

where k_B is the Boltzmann constant and E_i the electronic energy of the i-th conformation of a molecule (see Table S41). Each structure **2**–**12** features a different substitution pattern for the

substituents R_1, R_2, R_3, and R_4 which is also specified in Table S41. For easier readability, we present the results additionally in Figure S129.

Table S41. Boltzmann populations P at 295 K for the three groups of conformers shown as Newman projections for **2**–**12**. The Boltzmann populations are based on PBE-D3(BJ)//PBE-D3(BJ) electronic energy differences in the gas phase (mimicking *n*-octane). We also provide Boltzmann populations based on PBE-D3(BJ)-CPCM//PBE-D3(BJ)-CPCM energy differences in the condensed phase (acetonitrile) in parenthesis. We specify the rests R_{1-4} on C(3) (in the foreground of the Newman projections) and C(2) (in the background of the Newman projections) for each structure.

	Substituent on C(3)	Substituent on C(2)	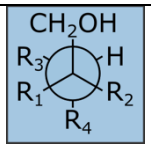	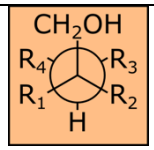	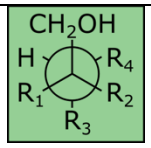
2	R_1, R_2=H	R_3=H, R_4=Me	0.58 (0.62)	0.25 (0.62)	0.18 (0.13)
3	R_1, R_2=H	R_3, R_4=Me	0.38 (0.35)	0.06 (0.06)	0.56 (0.59)
4	R_1=H, R_2=Me	R_3=H, R_4=Me	0.57 (0.60)	0.29 (0.26)	0.14 (0.14)
5	R_1,R_2=Me	R_3=H, R_4=Me	0.42 (0.45)	0.28 (0.29)	0.29 (0.27)
6	R_1=H, R_2=Me	R_3, R_4=Me	0.32 (0.27)	0.17 (0.18)	0.49 (0.54)
(*R*,S**)-**7**	R_1=H, R_2=Cl	R_3=Cl, R_4=Me	0.93 (0.65)	0.01 (0.09)	0.05 (0.27)
(*R*,R**)-**7**	R_1=Cl, R_2=H	R_3=Cl, R_4=Me	0.31 (0.74)	0.65 (0.15)	0.04 (0.10)
(*R*,S**)-**8**	R_1=H, R_2=Br	R_3=Br, R_4=Me	0.95 (0.74)	0.01 (0.07)	0.03 (0.19)
(*R*,R**)-**8**	R_1=Cl, R_2=H	R_3=Br, R_4=Me	0.20 (0.68)	0.80 (0.29)	0.01 (0.04)
9	R_1, R_2=Me	R_3, R_4=Me	0.44 (0.45)	0.14 (0.15)	0.42 (0.40)
(*R*,S**)-**10**	R_1=Me, R_2=Br	R_3=Br, R_4=Me	0.99 (0.94)	0.00 (0.0)	0.01 (0.06)
(*R*,R**)-**10**	R_1=Br, R_2=Me	R_3=Br, R_4=Me	0.16 (0.57)	0.78 (0.26)	0.06 (0.16)
11	R_1=H, R_2=Br	R_3=Br, R_4=CF_3	0.83 (0.82)	0.16 (0.11)	0.01 (0.07)
(*R*,S**)-**12**	R_1=Me, R_2=Br	R_3=Br, R_4=CF_3	0.97 (0.93)	0.01 (0.03)	0.01(0.04)

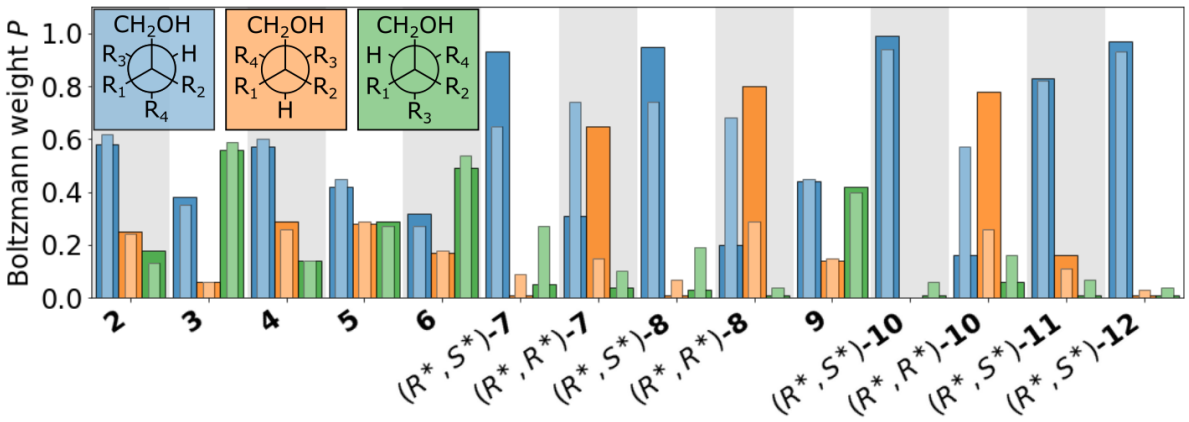

Figure S129. Boltzmann weights *P* at 295 K for three conformers displayed as Newman projections (colored blue, orange, and green) for **2**–**12** based on PBE-D3(BJ)//PBE-D3(BJ) electronic energy differences in the gas phase (solid, dark colored bars) and based on PBE-D3(BJ)-CPCM//PBE-D3(BJ)-CPCM electronic energy

differences in the condensed phase (translucent, light colored bars). The rests R_{1-4} for **2**–**12** are specified in Table S41.

The structures which do not feature halogen substituents (**2**, **3**, **4**, **5**, **6**, **9**) preferentially adopt a conformation in which the largest substituents on the C(2) and C(3) are *anti-periplanar* to each other (see Table S41). The *anti-periplanar* conformation is also the conformation which is experimentally observed for **5** encapsulated in the host. The encapsulated alcohol **9** adopts an *anti-periplanar* and a *gauche* structure of the terminal methyl groups relative to the CH_2OH group. This conformation is also the preferred conformation of **9** in the gas phase (Boltzmann population of 0.86, see Table S41). The Boltzmann weights of the conformers of **2**, **3**, **4**, **5**, **6**, and **9** change at most by 0.05 in a polar implicit solvent.

All halogen-substituted guests (**7**, **9**, **10**, **11**, and **12**) adopt a conformation in the host where the halogens are *gauche* to each other. The isolated (*R*,S**)-**7,** (*R*,S**)-**8**, and (*R*,S**)-**10** preferentially adopt a conformation in which the halogen groups are placed *anti-periplanar* to each other (Boltzmann weights of 0.93, 0.95, and 0.99, respectively; see Table S41). The *gauche* conformation is significantly populated in the gas phase for (*R*,R**)-**7, (***R*,R**)-**8**, and (*R*,R**)-**10** (Boltzmann weights of 0.65, 0.80, and 0.78, respectively; see Table S41). The higher association constants of (*R*,R**)-**7, (***R*,R**)-**8**, and (*R*,R**)-**10** may be partially rationalized by the observation that the *gauche* conformation, which the guests adopt in the host, is already significantly populated in the gas phase. By contrast, (*R*,S**)-**7,** (*R*,S**)-**8**, and (*R*,S**)-**10** strongly prefer the *anti-periplanar* conformation in the gas phase and, hence, they likely have to undergo a conformational change when being encapsulated in the host (see also main text).

In a polar solvent, such as acetonitrile, the conformation in which the halogen groups are *gauche* to each other becomes significantly populated for (*R*,S**)-**7,** (*R*,S**)-**8**, and (*R*,S**)-**10** (Boltzmann weights of 0.27, 0.19, and 0.06, respectively). Nevertheless, the *anti-periplanar* conformation is still the preferred one (0.65, 0.74, 0.94). (*R*,R**)-**7, (***R*,R**)-**8**, and (*R*,R**)-**10** generally favor the *anti-periplanar* conformation in acetonitrile (Boltzmann weights of 0.74, 0.68, and 0.57, respectively).

Replacing the terminal methyl group with a CF_3-group in (*R*,S**)-**8** and (*R*,S**)-**10** yields (*R*,S**)-**11** and (*R*,S**)-**12**. (*R*,S**)-**11** and (*R*,S**)-**12** preferentially adopt the anti-periplanar conformation in the gas phase (0.83 and 0.97, see Table S41) and in the polar solution phase (0.82 and 0.93, see Table S41). The population of the other conformations in the gas phase and in the polar solution phase is below 0.16.

S3. Effect of Computational Methodology

The conformational analysis in the Theoretical Section, S2 is based on Boltzmann distributions obtained from electronic energy differences calculated with PBE-D3(BJ) for the PBE-D3(BJ) optimized structures in the gas phase and with PBE-D3(BJ)-CPCM for the PBE-D3(BJ)-CPCM optimized structures in the condensed phase. The application of the implicit solvation model CPCM has a large effect on the electronic energy differences calculated for PBE-D3(BJ)-CPCM optimized structures (Figure S130, a). The difference between PBE-D3(BJ)-CPCM//PBE-D3(BJ)-CPCM and PBE-D3(BJ)//PBE-D3(BJ)-CPCM energies is on average 0.96 kcal mol^{-1}. The inclusion of electrostatic effects in a polar environment as in CPCM, hence, has a large effect on the predicted Boltzmann distributions. Structures optimized with PBE-D3(BJ) are similar to the ones optimized with PBE-D3(BJ)-CPCM as evidenced by the fact that DLPNO-CCSD(T) single-point energies evaluated for both structures differ on average difference by only 0.22 kcal mol^{-1}. (Figure S130, b). Furthermore, the DLPNO-CCSD(T)//PBE-D3(BJ) and DLPNO-CCSD(T)//PBE-D3(BJ)-CPCM energies are strongly correlated (Pearson correlation of 0.93). The PBE-D3(BJ) energies deviate on average by 0.31 kcal mol^{-1} from DLPNO-CCSD(T) energies for PBE-D3(BJ) optimized structures, and the two are strongly correlated with a Pearson correlation of 0.98 (Figure S130, c). We may take this as an indication that the density functional energies are reliable in this case. A calculation of the Boltzmann distributions based on the DLPNO-CCSD(T) energy leads to changes smaller than 0.04. The consideration of thermal effects calculated within the RRHO model changes the energy differences on average by 0.20 kcal mol^{-1}. Furthermore, the electronic energy differences and the gas-phase free energy differences are strongly correlated (R=0.99, Figure S130, d).

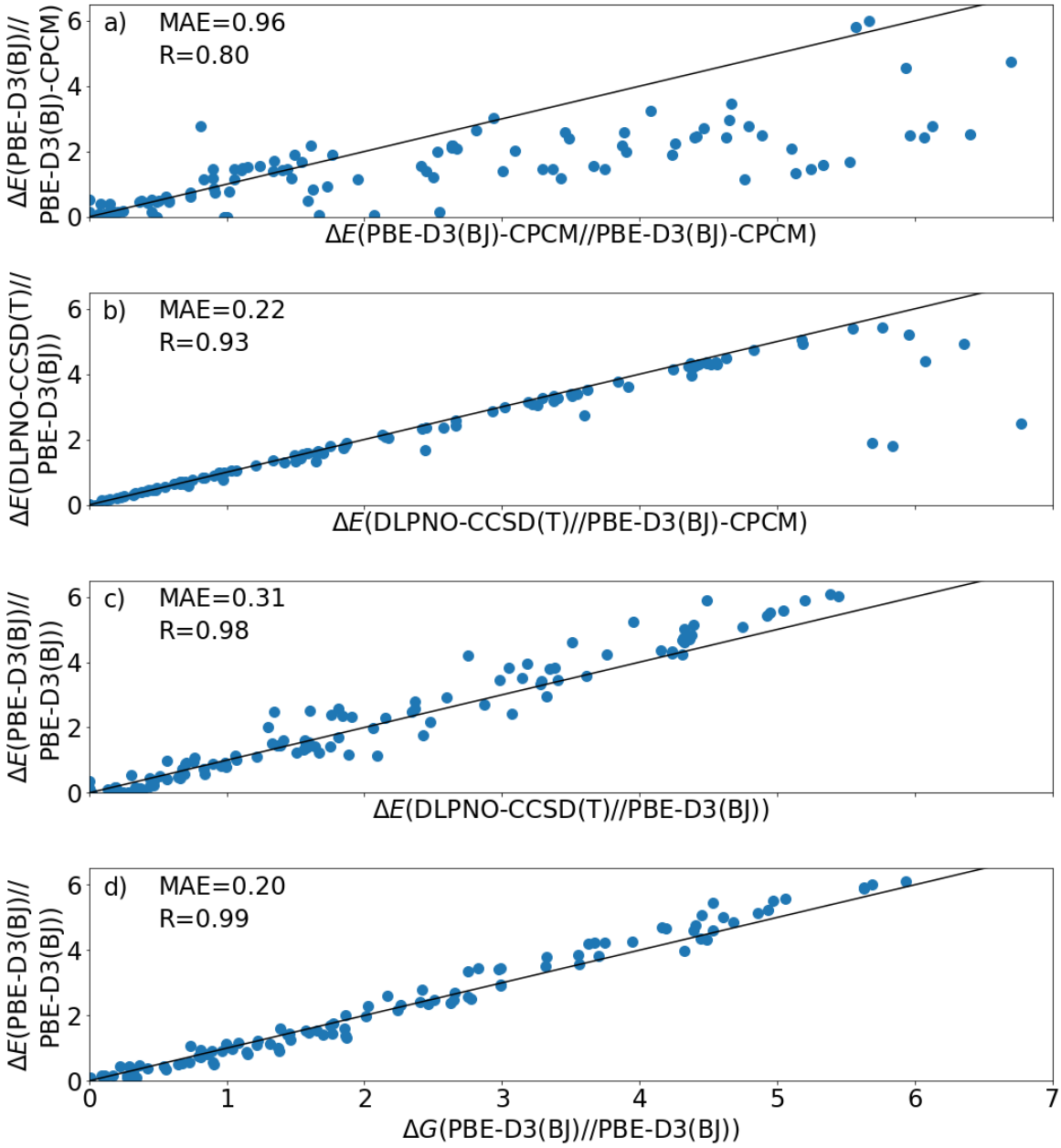

Figure S130. a) Comparison of the electronic energy differences *ΔE* obtained with PBE-D3(BJ) and PBE-D3(BJ)-CPCM for PBE-D3(BJ)-CPCM optimized structures. b) Comparison of *ΔE* obtained with DLPNO-CCSD(T) for PBE-D3(BJ) and for PBE-D3(BJ)-CPCM optimized structures. c) Comparison of *ΔE* obtained with DLPNO-CCSD(T) and PBE-D3(BJ) for PBE-D3(BJ) optimized structures. d) Comparison of Gibbs free energy differences at 295 K *ΔG* and *ΔE* obtained with PBE-D3(BJ) for PBE-D3(BJ) optimized structures. In each panel a–d, we indicate the mean absolute error (MAE) in kcal mol^{-1} of the compared data sets and their Pearson correlation (R). All energy differences are given in kcal mol^{-1}.

S4. Determination of Packing Coefficients

We determined the packing coefficients, which are defined as the ratio of the volume of the encapsulated guest molecule to the volume of the cavity formed by the host, for the obtained crystal structures in Tables S42 and S43. The volumes were determined with the program VOIDOO [19] with two different probe sizes as described in our previous work.[7] The obtained cavity volumes (215–234 Å^3 and 176–200 Å^3 for a probe radius of 1.0 Å and of 1.6 Å, respectively) are similar to the ones obtained in our previous work [7] (190–242 Å^3 and 154–191 Å^3 for a probe radius of 1.0 Å and of 1.4 Å, respectively). This leads to packing coefficients of 41–53% for a probe radius of 1.0 Å and of 48–61% for a probe radius of 1.6 Å (see also Tables S42 and S43). In this case, a probe radius of 1.6 Å leads to in better agreement with the Mecozzi-Rebek volume occupancy rule of 55% than a probe radius of 1.0 Å. [20a] For molecular baskets encapsulating heteroalicyclic guests undergoing polar interactions, the volume occupancies can increase to 63%.[20b]

Table S42. Guest volumes in Å^3, cavity volumes in Å^3 with a probe size of 1.0 Å and 1.6 Å, and packing coefficients in percent for co-crystal structures of AAC $(P)_4$-**1**.

Encapsulated guest	Guest volume [Å^3]	Cavity volume [Å^3] with probe size of 1.0 Å	Packing coefficient [%] with probe size of 1.0 Å	Cavity volume [Å^3] with probe size of 1.6 Å	Packing coefficient [%] with probe size of 1.6 Å
5	92	223	41	188	48
(*R**,*S**)-**7**	98	223	43	185	53
(*R**,*R**)-**7**	100	215	46	176	56
(*R**,*S**)-**8**	109	229	47	196	55
(*R**,*R**)-**8**	109	224	48	188	57
9	104	234	44	200	52
(*R**,*S**)-**10**	121	229	52	197	61
(*R**,*R**)-**10**	120	232	51	200	60

Table S43. Guest volumes in Å^3, cavity volumes in Å^3 with a probe size of 1.0 Å and 1.6 Å, and packing coefficients in percent for co-crystal structures of AAC (*M*)$_4$-**1**.

Encapsulated guest	Guest volume (Å^3)	Cavity volume (Å^3) Probe size of 1.0 Å	Packing coefficient [%] Probe size of 1.0 Å	Cavity volume (Å^3) Probe size of 1.6 Å	Packing coefficient [%] Probe size of 1.6 Å
(*S**,*R**)-**7**	99	226	43	184	53
(*S**,*S**)-**7**	97	226	42	187	52
(*S**,*R**)-**8**	108	227	47	177	60
(*S**,*S**)-**8**	109	222	48	183	59
9	104	234	44	200	52
(*S**,*R**)-**10**	122	230	53	193	62
(*S**,*S**)-**10**	120	233	51	198	60

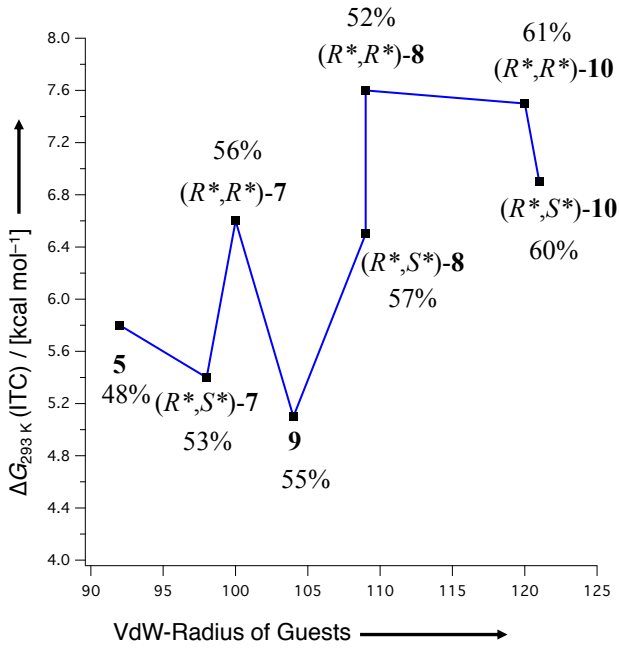

Guests	$\lvert\Delta G_{293\ K}\rvert$ (ITC) / [kcal mol^{-1}]	VdW-Radius / [Å^3]	*PC*s
5	5.8	92	48%
(*R**,*S**)-**7**	5.4	98	53%
(*R**,*R**)-**7**	6.6	100	56%
9	5.1	104	55%
(*R**,*S**)-**8**	6.5	109	57%
(*R**,*R**)-**8**	7.6	109	52%
(*R**,*R**)-**10**	7.5	120	61%
(*R**,*S**)-**10**	6.9	121	60%

Figure S131. Plot of the experimental values of the association constants of the guests in $\lvert\Delta G_{293\ K}\rvert$ (ITC) in kcal mol^{-1} against the Van-der-Waals-Radii of the guests as determined in Section S4 of the Theoretical Section. The packing coefficients (*PC*, *PC* = V_{vdW} (Guest)/ V_{vdW} (Host) x 100%), see Section S4 of the Theoretical Section. All *PC*-calculations are based on obtained X-ray co-crystal structures.

References

[1] Gropp, C.; Trapp, N.; Diederich, F. Alleno-Acetylenic Cage (AAC) Receptors: Chiroptical Switching and Enantioselective Complexation of *trans*-1,2-Dimethylcyclohexane in a Diaxial Conformation. *Angew. Chem. Int. Ed.* **2016**, *55*, 14444–14449.

[2] MicroCal Origin, Version 5.0, Northampton, USA, **1998**.

[3] CrysAlisPro, Rigaku Oxford Diffraction, **2015–2017**.

[4] Dolomanov, O. V.; Bourhis, L. J.; Gildea, R. J.; Howard, J. A. K.; Puschmann, H. OLEX2: A Complete Structure Solution, Refinement and Analysis Program. *J. Appl. Cryst.* **2009**, *42*, 339–341.

[5] G. M. Sheldrick, *Acta Cryst. A* **2008**, *64*, 112–122.

[6] IgorPro, Wavemetrics, Version 6.37, Portland, USA, **2009**.

[7] Gropp, C.; Husch, T.; Trapp, N.; Reiher, M.; Diederich, F. Dispersion and Halogen-Bonding Interactions: Binding of the Axial Conformers of Monohalo- and (±)-*trans*-1,2-Dihalocyclohexanes in Enantiopure Alleno-Acetylenic Cages. *J. Am. Chem. Soc.* **2017**, *139*, 12190–12200.

[8] Gropp, C.; Husch, T.; Trapp, N.; Reiher, M.; Diederich, F. Hydrogen-Bonded Networks: Molecular Recognition of Cyclic Alcohols in Enantiopure Alleno-Acetylenic Cage Receptors. *Angew. Chem. Int. Ed.* **2018**, *57*, 16296–16301.

[9] Koźmiński, W.; Nanz, D. HECADE: HMQC- and HSQC-Based 2D NMR Experiments for Accurate and Sensitive Determination of Heteronuclear Coupling Constants from E.COSY-Type Cross Peaks. *J. Magn. Res.* **1997**, *124*, 383–392.

[10] O'Boyle, N. M.; Vandermeersch, T.; Flynn, C. J.; Maguire, A. R.; Hutchison, G. R. Confab – Systematic Generation of Diverse Low-energy Conformers. *J. Cheminform.* **2011**, 3, 8.

[11] O'Boyle, N. M.; Banck, M.; James, C. A.; Morley, C.; Vandermeersch, T.; Hutchison, G. R Open Babel: An Open Chemical Toolbox. *J. Cheminform.* **2011**, 3, 33.

[12] Neese F. *WIREs Comput. Mol. Sci.* **2018**, 8, e1327.

[13] a) Perdew, J. P.; Wang, Y. Accurate and Simple Analytic Representation of the Electron-gas Correlation Energy. *Phys. Rev. B* **1992**, *45*, 13244–13249; b) Perdew, J. P.; Burke, K.; Ernzerhof, M. Generalized Gradient Approximation Made Simple. *Phys. Rev. Lett.* **1996**, *77*, 3865–3868.

[14] Grimme, S.; Antony, J.; Ehrlich, S.; Krieg, H. A Consistent and Accurate Ab Initio Parametrization of Density Functional Dispersion Correction (DFT-D) for the 94 Elements H-Pu. *J. Chem. Phys.* **2010**, *132*, 154104.

[15] Weigend, F.; Ahlrichs, R. Balanced Basis Sets of Split Valence, Triple Zeta Valence and Quadruple Zeta Valence Quality for H to Rn: Design and Assessment of Accuracy. *Phys. Chem. Chem. Phys.* **2005**, *7*, 3297–3305.

[16] Klamt, A.; Schüürmann, G. COSMO: A New Approach to Dielectric Screening in Solvents with Explicit Expressions for the Screening Energy and its Gradient. *J. Chem. Soc., Perkin Trans. 2*, **1993**, 799–805.

[17] McQuarrie, D. A. Statistical Mechanics; University Science Books: Sausalito, 2000.

[18] Riplinger, C.; Neese, F. An Efficient and Near Scaling Pair Natural Orbital Based Local Coupled Cluster Method. *J. Chem. Phys.* **2013**, 138, 034106.

[19] Kleywegt, G. J. VOIDOO, version 3.3.4, Uppsala Software Factory, Uppsala, **2007**.

[20] a) Mecozzi, S.; Rebek, J. Jr. The 55 % Solution: A Formula for Molecular Recognition in the Liquid State. *Chem. Eur. J.* **1998**, *4*, 1016–1022; b) Hornung, J.; Fankhauser, D.; Shirtcliff, L. D.; Praetorius, A.; Schweizer, W. B.; Diederich, F. Cycloalkane and Alicyclic Heterocycle Complexation by New Switchable Resorcin[4]arene-based Container Molecules: NMR and ITC Binding Studies. *Chem.–Eur. J.* **2011**, *17*, 12362–12371.